MORPHOLOGICAL RESPONSE OF HIGH-ENERGY MACROTIDAL BEACHES

by

TIMOTHY GEORGE POATE

A thesis submitted to the University of Plymouth
in partial fulfilment for the degree of

DOCTOR OF PHILOSOPHY

School of Marine Sciences and Engineering
Faculty of Science

October 2011

ABSTRACT

Name: Timothy Poate

Title: *Morphological response of high-energy macrotidal beaches*

Spatial data collected over 3 years is presented to assess the extent of morphological variability under seasonal and storm waves at four high-energy macrotidal beaches. A novel approach is adopted to identify and classify the beach response which is used to assess the relative stability of the system to changes in the dominant forcing conditions. Field measurements and modelling simulations using XBeach provide further support for a storm dominated system exhibiting relative stability.

Morphologically the beaches range from dissipative to intermediate and are characterised by low tide bar/rip morphology which plays a key role in the nearshore dynamics and beach safety. Located in the north coast of Cornwall the sites are exposed to high-energy waves that dominate the stability and behaviour of beaches in this region.

The growing need for marine renewable energy in the UK has led to the deployment of a Wave Hub on the seabed off the north coast of Cornwall, designed to provide grid connection for wave energy devices (WECs). As a unique development much has been done to address concerns over potential impacts cause by arrays of WECs during its construction and operational lifetime; these predicted impacts include changes in the quality of waves for surfing and effects on the beach dynamics which determines beach safety through the presence of bar/rip features.

In this thesis three years of monthly topographic surveys were collected from beaches in the proposed Wave Hub shadow zone to assess their morphodynamic variability. Real-time kinematic (RTK) GPS surveys were undertaken using an all-terrain vehicle to measure the three dimensional (3D) morphology at four beaches (Perranporth, Chapel Porth, Porthtowan and Gwithian) situated along a 23 km stretch of the north Cornish coast. In addition nearshore wave data, in-situ hydrodynamic measurements, local tide gauges and Argus video data allowed detailed analysis of process-response mechanisms for long term (yearly); seasonal (monthly); storm (weekly/daily); and tidal (hourly) morphological behaviour.

Of particular interest was the degree to which the beaches displayed bar/rip morphology, characterised by the three dimensionality (3D) of beach response, which determines wave breaking and affects beach safety. Using a combination of measured shoreline variability and empirical beach classification schemes, the response to changes in the wave conditions at each beach have been assessed. The sites exhibited net long term accretion derived from the intertidal beach volume. Throughout the survey period inter-site similarity in beach response was observed in response to storm waves, yet coupling between the seasonal wave climate and the beach morphology was not evident at any of the sites, due to the dominance of recovery phases following storm events. The role of increased wave conditions (exceeding H_s=4 m*)* during sustained storm events (> 50 hrs) led to offshore transport from the beach face to the subtidal bar region. Post-storm recovery was characterised by onshore transport and the development of substantial 3D low tide morphology. Under normal wave conditions (H_s=1.6 m) the dominant 3D

features smoothed out as channels in-filled and bars reduced over a period of 2-3 months. This cyclicity was observed on ~3 occasions at the northern sites, while Gwithian remained more stable throughout; reflecting the more sheltered position of the beach. Overall the beaches exhibited a significant storm dominated morphological response cycle, unlike the more familiar winter/summer seasonal response.

Nearshore bar behaviour at Perranporth and Porthtowan, assessed using ARGUS images, was dominated by offshore migration (ca.20 m/yr) following closely the net intertidal accretion, while bar shape exhibited changes over monthly periods. Intensive field studies of morphological change, nearshore current flows and surf zone wave conditions were undertaken at Porthtowan during small swell dominated waves and large energetic storm conditions in May and October 2010 respectively. The field data highlighted accretionary response under small swell dominated waves, and strong offshore directed undertow flows (0.5 m/s^{-1}) during erosive energetic conditions ($>H_s$ = 4m) which were then related to the monthly surveys. These results were applied to XBeach model simulations which helped further identify the importance of antecedent morphology and the complexities of intertidal geology in controlling beach response.

The study provides the longest continuous record of beach morphology dynamics for macrotidal energetic sites and provides a valuable addition to work in this field. The dominance of storm driven morphological response was clear with highly three-dimensional morphology developing under post storm conditions and continued beach evolution driven by the seasonal conditions. Antecedent morphology was found to be a key element of beach response with geological control an additional component. The projected reduction in wave conditions due to the Wave Hub and the natural variability observed indicates the sites are unlikely to shift significantly from their current dynamic state in response to the Wave Hub, and as such the potential impact on nearshore and beach dynamics is minimal.

AUTHORS DECLARATION

At no time during the registration for the degree of Doctor of Philosophy has the author been registered for any other University award without prior agreement of the Graduate Committee.

This study was partly financed by the Peninsular Research Institute for Marine Renewable Energy (PRIMaRE), through support from the South West Regional Development Agency, and the University of Plymouth. The author would also like to acknowledge the financial contribution provided by the Marine Institute Marine Education Fund (2010) and the Plymouth Marine Sciences Education Fund (2011) which provided support for overseas conference attendance.

Results presented in Chapter 2 were generated using data kindly provided by Guillaume Dodet as an extension to work which was presented in Dodet *et al.* (2010). The author acknowledges the technical support from Dr M. Austin of the University of Plymouth who provided instrument guidance during two field experiments (Chapter 5), and follow up support in the form of processing code for hydrodynamic data.

Relevant scientific conferences and symposiums were attended at which work was presented through oral and poster presentations. Conferences include the International Coastal Symposium, Lisbon 2009 and Coastal Sediments, Miami 2011.

Word count of main body of thesis: 55,800

Signed.....

Date.....

Publications:

Poate, T. G., Austin, M., Russell, P., Masselink, G. & Kingston, K. S. (2011) '3D Beach response to energetic wave climate, Cornwall, UK', Rosati, J.D., Wang, P. and Roberts, T.M. eds.). *The 7th Coastal Sediments*. Miami, Florida World Scientific, pp. 1893-1906.

Poate, T.G.; Kingston, K.S.; Masselink, G. and Russell, P., 2009. Response of high-energy, macrotidal beaches to seasonal changes in wave conditions: examples from North Cornwall, UK. Journal of Coastal Research, SI 56, pp. 747-751.

Other presented work:

Poate, T.G., *Wave Hub Impacts on Seabed and Shoreline Processes.*Oral presentation at PRIMaRE Annual Research Conference, Exeter. Janurary 2010.

Poate, T.G. *Application of Argus to 3D beaches*. Oral presentation at the 2009, Argus Workshop at the University of Plymouth.

Poate, T.G.; Kingston, K.S.; Masselink, G. and Russell, P., 2009. *Seasonal response of high-energy macrotidal beaches on the North coast of Cornwall,UK*. Poster presentation at Young Coastal Scientist and Engineers Conference, Lancaster.

Poate, T.G.; Kingston, K.S.; Masselink, G. and Russell, P., 2009. *Response of high-energy, macrotidal beaches to seasonal changes in wave conditions: examples from North Cornwall,UK.* Oral presentation atPMSP Symposium 2009: Marine Science for a Changing World.

TABLE OF CONTENTS

LIST OF FIGURES

LIST OF TABLES

ACKNOWLEDGEMENTS

Firstly I would like to give my thanks to Prof. Paul Russell and Prof. Gerd Masselink who have shown faith in me from the outset and provided a level of support throughout for which I am truly indebted. They have both been a continued source of positive enthusiasm and encouragement combined with critical feedback at all stages which has provided inspiration and shaped every aspect of this work. I would also like to thank Dr Ken Kingston for his support and guidance with all applications of the video monitoring and analysis.

I would also like to thank Dr Martin Austin for support with the monthly field surveys, guidance with instrument deployment and further expertise throughout many aspect of the data processing using Matlab. In addition Dr Tim Scott has also assisted with the various field campaigns and shared much of his knowledge on beach behaviour within this region. I am very grateful for the technical support and instrument assistance with the field deployments from Mr Peter Ganderton. I would like to thank Mr Robert McCall for this help and direction with setting up and problem solving the XBeach simulations, much of the work presented here would not have progressed without his input.

As the years have passed various colleagues have had the pleasure of enduring the hotbox that is A510; Dr. Iain Fairley, Dr Rob Schindler and Mr Saul Reynolds and Dr Dan Buscombe have all provided advice, distractions, constructive feedback and surf checks as necessary.

Beyond Plymouth I would like to thank the Unknown for support on finding the right balance, perspective and the odd wave; my former colleagues at the Channel Coastal Observatory, in particular Dr Travis Mason who is always keen to help however she can, and Mark who is less keen but eventually gives in to my beck and call.

While my friends have been amused by my “sand counting”, my parents have shown continued support with discussions of a real job carefully avoided. They have been a source of continued inspiration and I will always hope of achieving the high standard they set. Finally I would like to thank Cate who has endured the hours in the office and the worst of the moods, yet has remained by my side and the love of my life. Thank you for saying yes.

Next page: My Thesis “Word Cloud” which displays the more frequently used words with greater prominences.


tide
period
evident
presented
Section
undertaken
using
mean
observed
change
increased
became
channel
Argus
GWT
waves
rip
showing
subtidal
data
throughout
panel
flows
events
migration
peak
morphology
highly
face
area
bar
channels
identify
periods
dashed
longshore
beaches
calm
development
bar/rip
however
top
low
sites
lower
November
show
following
transport
MLWN
large
regions
rhythmic
state
beach
significant
high
across
planar
al
intertidal
volume
tidal
storm
system
four
present
CHP
loss
profile
surveys
CV
experienced
behaviour
level
net
indicate
removal
PTN
morphological
clear
wave
PX2
However
offshore
also
material
shoreline
conditions
site
north
well
region
Hs
January
sediment
first
lines
features
flow
shows
dynamics
PX1
cross-shore
resulted
increasingly
states
subsequent
alongshore
variability
model
et
survey
onshore
response
two
surface
MLWS
XBeach
energetic
nearshore
within
range
term
bars
images
right
line
position
energy
resulting
spatial
remained
relative
used
approach
dominant
velocity
upper
analysis
identified
bottom
height
systems
zone
coverage
increase
water
PPT
solid

1 INTRODUCTION

This chapter lays the foundation for the thesis and the work that is presented in the following sections. The framework of the thesis is introduced starting with a brief outline of the context of the research and the wider project it sits within; following this the thesis structure and the overriding aims and objectives are outlined defining the direction of the research; finally a summary of key research and relevant literature is provided, highlighting the principal areas relevant to the present study.

1.1 Project Overview

Increasingly the UK is looking to exploit more sustainable renewable sources for future energy demands. As an island nation the UK is well placed to take advantage of both tide and wave-power which are readily available within the territorial waters. However, a combination of financial constraints and the challenge of designing devices to cope with hostile environments have delayed the growth of this field. Recent investment has led to the deployment of a "Wave-Hub" sited off the north coast of Cornwall in the south west of the UK (Figure 1.1): which will allow wave energy converters (WECs) to be deployed and connected to the National Grid.

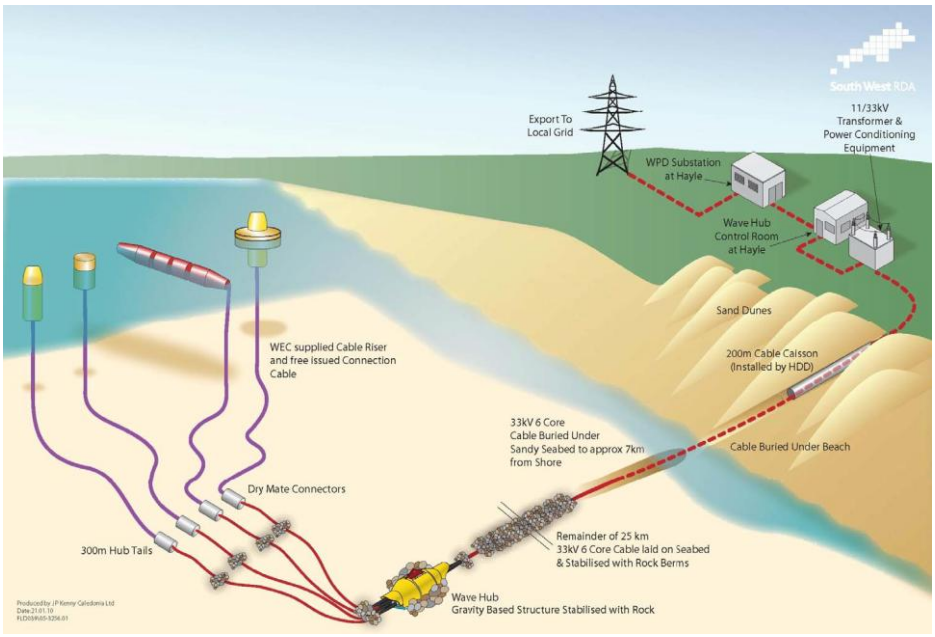

Figure 1.1 - Schematic of the proposed Wave Hub with wave energy converters (WECs) connected.

Wave Hub consists of an electrical hub sited on the seabed 16 km off the north coast of Cornwall (Figure 1.2), providing a connection point for different arrays of WECs. The Hub is then connected to the UK national grid via a 25km, 1300 tonne subsea cable. By providing suitable offshore infrastructure for the deployment and testing of arrays of wave energy generation devices Wave Hub enables developers to benefit from the energetic wave climate present in this region.

In 2007 The University of Plymouth with the University of Exeter formed the Peninsula Research Institute for Marine Renewable Energy (PRIMaRE), which *"…brings together a unique team of world-class researchers to provide unparalleled expertise and research capacity to address the wider considerations of all aspects of Marine Renewable Energy"*. PRIMaRE is in a unique position to address the impacts caused by this development with specific links to Wave Hub, through funding from the South West Regional Development Agency, In line with the priority research areas identified by PRIMaRE, the Coastal Process Research Group (CPRG) at the University of

Plymouth has established the Wave Hub Impacts on Seabed and Shoreline Processes (WHISSP) project. This project addresses the physical impacts on seabed and shoreline processes caused through the establishment of an array of WEC's, to be deployed at the Wave Hub site (Figure 1.2). The WHISSP project has been split into 6 work packages:

1 Natural morphological variability

Using historic data to define natural variability in response to hydrodynamic change.

2 Baseline morphology and bathymetry

Assessing present morphological variability at selected sites, and determine the nature and extent of change.

3 Wave, tides and currents

Assessing offshore wave and tidal climate through WERA coastal radar system, ADCP deployment and nearshore directional wave buoys.

4 Sedimentation and mixing

Deploying an Instrumented Benthic Frame to measure turbulence, suspended sediments, bed forms and bed loads (this aspect of WHISSP has not yet been executed).

5 Changing coastal morphology

Sustained monitoring and historic Argus imagery to identify specific response to morphology, including low tide bars and rip channels.

6 Impact of Wave Hub

Synthesis of all pre- and post-Wave Hub study results and produce an objective assessment of impacts observed. Future scenarios will be evaluated using data and models from other Wave Hub projects. This work will go towards developing generic environmental monitoring protocols and numerical modelling methodologies for the assessment of future wave energy systems worldwide.

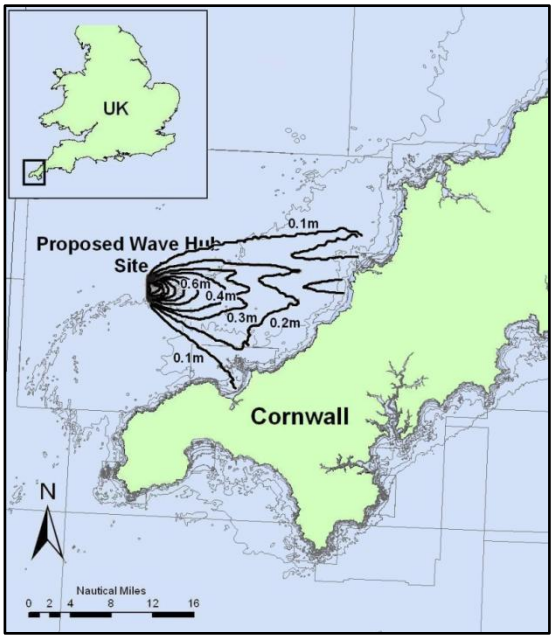

Figure 1.2 – Location map showing the Cornish coastline and the proposed Wave Hub location. Modelled changes in significant wave height due to wave energy converter (WEC) deployments are overlaid for 0% energy transmission for a wave climate of significant wave height H_s= 3.3 m, mean wave period T_m= 11 s and peak wave direction *Dir* = 1°. Adapted from a similar plot in Millar *et al.* (2007).

The current research project "*Morphological response of high-energy macrotidal beaches*" was devised to incorporate aspects from each of these work packages, especially 2, 3 and 6, and forms a central component of the WHISSP project. As will be discussed throughout, the stability of beaches is a function of wave conditions, sediment characteristics, present morphology and the underlying geology. It is argued that beaches are in constant transition to reach equilibrium with these environmental conditions and, as such, their stability is a reflection on the natural shifts found in these controlling environments.

Building on the high standard of beaches in the region, tourism represents a priority sector for the South West Regional Development Agency's Economic plan for 2006-2012 (www.southwestrda.org.uk). Within this it is estimated the region benefits from £21 million worth of direct spend from surfers drawn to the area to exploit the wave-rich coastline (Arup, 2001). With such a high value placed on these natural resources

the importance of ensuring that offshore developments do not have a negative impact on the coastal processes is clear.

With concerns over the impact of device deployment at the proposed site, Millar *et al.*(2007) undertook numerical modelling, using SWAN, of the change in the shoreline wave climate. This work identified a clear shadow zone in the lee of the site, with reductions in the mean significant wave heights of up to 0.2 m for a 3.3 m wave near the shoreline (Figure 1.2). A review by ASR (2007) of the work by Millar *et al.* (2007) and a separate study by Halcrow (2006) summarised: '*Wave height attenuation should be less than 3-6% at beaches in the direct shadow of the wave hub in "clean" (narrow-banded) swell*'. For a 'worst' case scenario with 100% attenuation of wave energy through a fully populated wave farm it was concluded that: **'***The wave height absorption is dependent on the number of devices connected, but the maximum absorption is highly unlikely to exceed 20% of wave height, assuming a 100% absorption, which is considered to be impractical*'. These modelling studies highlight the need for further monitoring of the offshore wave climate and nearshore wave conditions within the shadow zone, as well as the possibility of longer term morphological modelling (2007).

In addition to potential negative effects of the Wave Hub on the quality of surf conditions owing to a reduction in wave height, there may also be implications for beach safety. Recent research by Scott *et al.*(2007) identified rip currents were responsible for 71% of all rescue incidents in the southwest (UK) where the most hazardous beaches were intermediate sites dominated by low tide bar and rip systems. These sites fall within the predicted shadow-zone where the local wave climate is likely to be affected. Consequently there is a need to develop our understanding of these systems and the dominant inherent natural variability. Through a programme of

- Note: Due to delays with the Wave Hub infrastructure, installation at the site was completed in August 2010,

sustained monitoring at selected sites a comprehensive assessment of the likely responses under the proposed development can be obtained. Using beach classification models the relative state of a beach can be defined for the dominant conditions present, and therefore the long-term response to an alteration in the seasonal wave climate can also be assessed.

1.1.1 Thesis Structure

The central core of this project is the beach survey monitoring programme which began in February 2008 and continued for three years. In addition two separate field experiments (PX1 and PX2) were undertaken alongside complimentary desk studies and modelling work. A broad outline of the structure of this research project, and the subsequent chapters which make up the thesis is summarised in Figure 1.3.

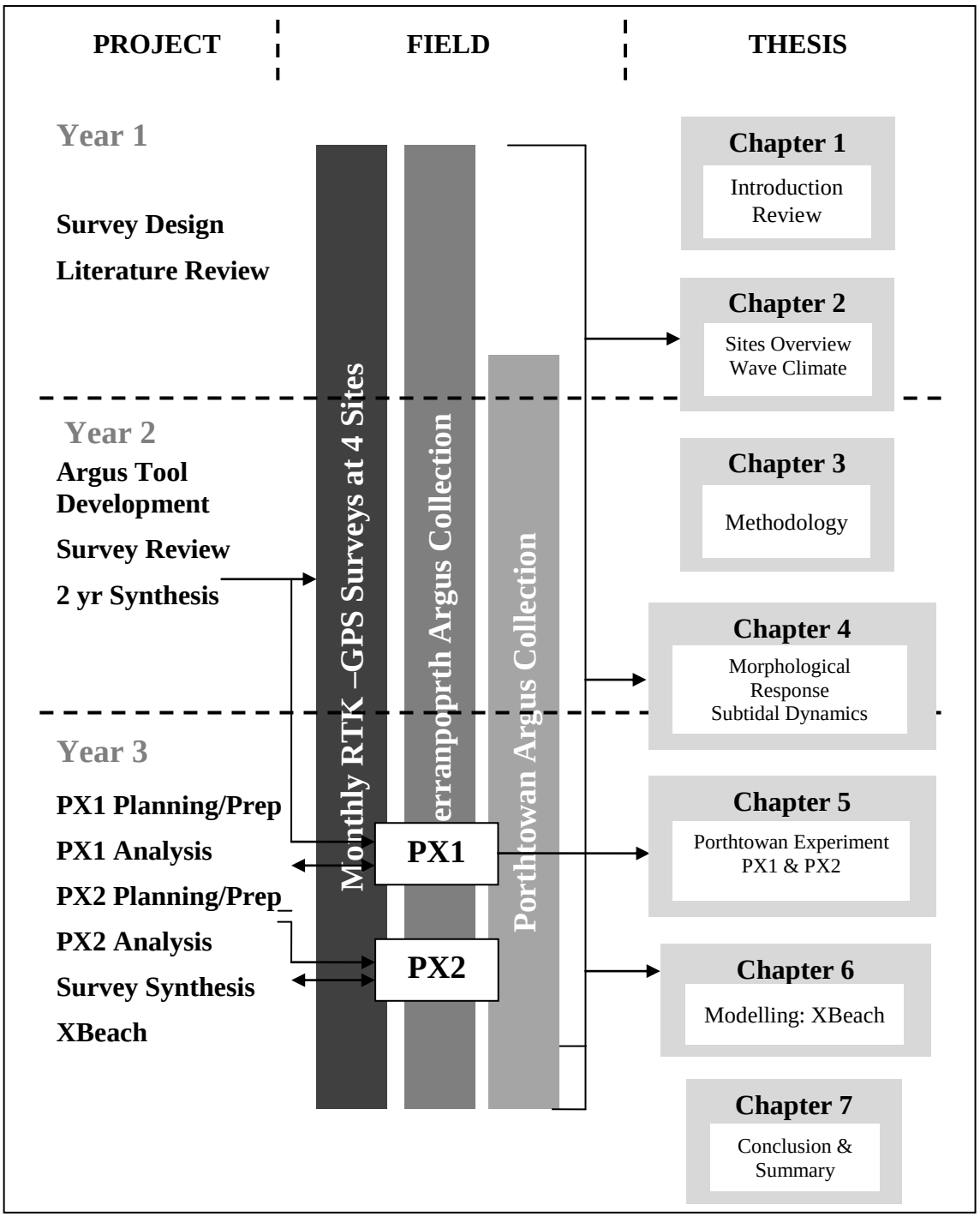

Figure 1.3– Summary structure of work flow and input for the thesis chapters.

1.2 Aims and Objectives

In addition to the broad WHISSP work packages, and incorporating the current scientific understanding, the central aim of this project is to *assess the morphological response of four high-energy macrotidal beaches to changes in the seasonal and storm induced wave climate*. To achieve this, the following more specific objectives are defined;

- Identify the morphological response to a naturally variable (seasonal) wave climate at four macrotidal beaches exposed to energetic wave conditions.
    - By defining the various beach states exhibited throughout the seasonal shift in wave conditions, the baseline variability at the four sites will be established
- Assess variability in storm characteristics and subsequent impacts with reference to shifts in morphology and beach state.
    - Detailed analysis of individual storm events will be used to provide further understanding of the recovery rates with reference to the temporal and spatial variability of individual events.
- Investigate the temporal and spatial distribution of nearshore bars and relate these to the intertidal morphological response.
    - The importance of the subtidal region in the balance of cross-shore transport will be addressed through the growth development of subtidal morphology.
- Assess future beach stability under projected shifts in boundary conditions.
    - Incorporating baseline beach states observed through seasonal change in wave conditions, address projected beach response through existing conceptual and numerical models (XBeach).

1.3 Review

1.3.1 Coastal Systems

The coastal zone incorporates a region of great diversity both in its physical composition and the forces acting upon it. Principally, the coastline acts as a zone of transformation as energy held within waves and currents is transferred through interaction with the seabed and surrounding sediments. The manner in which this energy flux takes place is a function of the geomorphology and hydrodynamics which are specific to each region.

Coastal research has been driven in part by the rising pressures on the coastal zone including: tourism, recreation, commerce, and development linked to increasing populations. These pressures have led to increased management from single beaches to whole coastlines and from the subtidal to the geological and riverine inputs. The system as a whole can change in its natural behaviour, further increasing the need for sustainable management which is achieved through a clear understanding of the dominant processes.

The nature and shape of the coastline is a reflection of the underlying geology and the available sediment supply, combined with the dominant forces acting upon them. Where such conditions exist and the combination of waves, currents and sediment processes allow, beaches are found representing a balance between these physical processes (Komar, 1998).

The concept of a balance between the driving forces shaping the beach and the sediment composition of the shoreface first led Cornaglia (1989) in Woodroffe (2003), to propose an equilibrium profile shape. He developed a concave-up profile which represents a balance in the grain size and wave asymmetry responsible for onshore transport. This concept has been extended over the years using both field and laboratory studies. One of

the first developments was the Bruun rule which still has applications in engineering work today. Essentially this is a simple model which predicts how shorelines would re-equilibrate to changes in sea level based on conservation of mass - forcing landward movement of the beach profile (Bruun, 1962). Dean (1977) developed the equilibrium profile equation further using 504 beach profile surveys and relating these to the destructive forces acting in the surf zone based on wave energy dissipation rates. This approach has received widespread attention with mixed success in lab and field studies (for a comprehensive review, see Komar, 1998).

Whilst the application of an equilibrium profile equation such as proposed by Dean (1977) poses many questions and its relevance has been questioned (Pilkey et al., 1993) it is generally accepted such states do exist within nature. The concept of an equilibrium beach state in balance with the forcing conditions and the environmental setting is therefore of significant interest in being able to understand and predict how the beach will respond to future changes. However the complexities inherent within the semi-deterministic nature of the coastal zone further add to the challenge of interpreting system wide response which in turn controls individual beach response.

1.3.2 Morphological Change

Although the concept of an equilibrium profile has enabled us to develop our understanding of cross-shore dynamics it has limitations where secondary morphological features are present such as longshore bars. In addition complexities introduced through intertidal geological controls and limited sediment inputs to a system further restrict the application of an equilibrium concept. The development of any beach-face lies in a combination of cross-shore and alongshore sediment movement which can lead to a range of 3D features which represent the dominant hydrodynamic

forcing through waves and tides as well as the local sediment characteristics and the underlying geology.

It is widely accepted that beaches can exhibit notable seasonality in profile shape in response to the changing wave conditions caused by periodic weather patterns. Most obvious examples of this seasonality lie in the winter (erosional storm waves) and summer (accretionary calm waves) profiles which have been observed at numerous sites (Komar, 1998). This response in the profile shape can be attributed to the manner in which wave energy is dissipated across the intertidal zone. As waves shoal towards the shore wave asymmetry results in net onshore sediment transport, before a decrease in water depth forces waves to break (Russell & Huntley, 1999). Inside the break point bed return flow produces a net offshore sediment flow, such conditions can lead to the formation of intertidal and subtidal bars developing owing to the sediment convergence(Masselink, Kroon & Davidson-Arnott, 2006). The development and stability of such features is dependent on the dominant wave conditions which determine the relative position of the break point. Under increased winter conditions waves break further offshore extending the inner surf zone and subsequent offshore sediment transport creating erosional phases. The transformation of incident waves at the shoreface is therefore largely controlled by the underlying morphology which will subsequently control the energy dissipation and relative sediment transport processes.

Long term monitoring projects are often developed to help understand the relative "stability" of a beach or coastal region. The extent of seasonal variability observed on beaches in profile shape and volume, usually lies within an envelope of dynamic equilibrium. Therefore the relative stability of a beach is a reference to its behaviour within this range of dynamic equilibrium. An unstable coastline is one which has moved

beyond this range e.g. through sustained sediment starvation. The longer the monitoring record the clearer understanding of a beaches stability at any given time.

1.3.3 Intertidal Dynamics

A common feature of sandy beaches is the presence of intertidal bars. As previously addressed nearshore bathymetry controls the wave shoaling and breaking processes which leads to energy dissipation across the beach-face. Therefore, the spatial extent and behaviour of intertidal bars plays a crucial role in controlling the generation of nearshore currents which ultimately drive profile response through sediment transport.

Intertidal bars systems can vary in number and spatial extent, and can exist between mean low water spring (MLWS) and mean high water spring (MHWS); however, they are predominantly located between mean sea level (MSL) and MLWS. They are generally orientated shore-parallel and are usually intersected by shoreward directed rip channels at regular/irregular intervals (Masselink, Kroon & Davidson-Arnott, 2006). The number of bars and their spatial scales can vary considerably with cross-shore and longshore scales of 20– 100 m and vertical elevations from < 0.5 m to > 1 m.

Within the literature the definition and description of intertidal bars has varied with different terminology used to describe similar types. Masselink *et al.* (2006) summarised the different groups into 3 main types: slip-face bars, low amplitude bars and sand waves. Similarly, the conditions under which these groups are observed range from energetic/microtidal to low energetic/macrotidal conditions; however, there are no set thresholds of occurrence/type and these grouping merely represent a range of bar morphologies.

Slip-face bars generally exhibit a more symmetric profile with a shallow gradient on the seaward side and a steep slope towards the upper beach. These bars are generally

thought to form under storm conditions as a breakpoint bar in response to offshore sediment transport generated from bed return flows (Aagaard et al., 2008). Low amplitude bars exhibit more gradual profile slopes with almost symmetrical profile shapes. These bar types are often found in settings with macrotidal medium energy wave conditions, and they can often exhibit long term residency (Masselink & Anthony, 2001). The formation of low amplitude bars is less clear, although the role of surfzone processes has been linked with bar growth (Kroon & Masselink, 2002; Masselink, 2004; Masselink et al., 2007). Sand waves make up the smallest intertidal features and are usually associated with multiple bars in macrotidal low energy regions.

The behaviour and dynamics of intertidal bars concerns the complex interaction of nearshore wave breaking, the subsequent development of cross-shore flows and the influence of any longshore flow components. Addressed further in Chapter 5, these complex hydrodynamics are further modified by the non-stationarity of the water level. The temporal variability of wave action across intertidal bars driven by the tidal range, controls the variation in sediment transport across the beach-face, affecting bar dynamics (Figure 1.4). Further details regarding cross-shore flows are discussed at the start of Chapter 5.

The response of intertidal bars is well linked to shifts in the dominant forcing conditions: onshore migration and development under calm conditions has been observed at a number of sites while flattening and offshore movement results under more energetic periods (Almar et al., 2010; Castelle et al., 2007a; Masselink *et al.*, 2007). While onshore migration of subtidal bars through wave shoaling is widely accepted, the onshore migration of intertidal bars is still relatively unclear. Under storm conditions bar flattening and offshore movement is best explained through wave breaking and the generation of offshore-directed undertow (Komar, 1998).

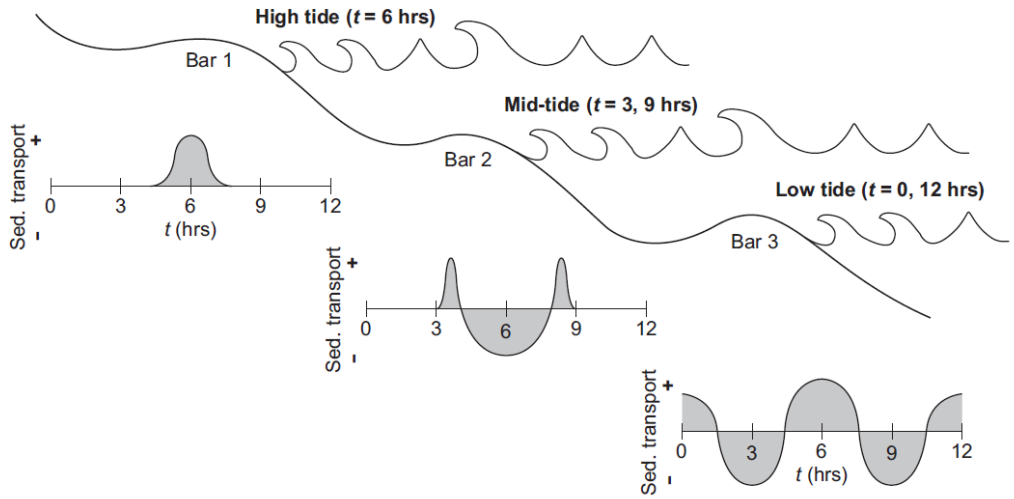

Figure 1.4–Variation in the cross-shore sediment transport rate and direction over a single tidal cycle (assumed to last for 12 h) for three different intertidal bar systems. The wave patterns represent the variation in wave type at the different stages in the tidal cycle with breaking waves on the bar crest, wave transformation in the trough and bores on the beachface, for a complete description see Masselink *et al*. (2006).

The temporal rates of bar behaviour vary extensively between sites and bar types, slip-face bars can exceed 1m per day and can migrate across the full intertidal profile. However, other studies have observed greater alongshore migration in response to wave forcing than cross-shore movement e.g. Lafon *et al.*(2005) found migration rates of 1.7-31 m per day under medium to calm wave conditions (<H_s = 2.5m); however, the dominant bar morphology remained stable. Under more energetic conditions the morphology experienced widespread adjustment as greater troughs developed through rip channel movement or rotation of existing troughs. In all instances the importance of wave orientation was identified as a controlling factor on the intertidal morphology (Levoy et al., 1998). Low amplitude bars exhibit a more gradual migration rate of 1-10m a month (Levoy *et al.*, 1998), while sand waves rarely exhibit significant migration in any direction. A consensus among previous field studies identifies greater response and variability in the characteristics of subtidal bars than their intertidal counterparts. Much of this can be explained as a result of primary breaking taking place on the outer bar systems before possible reforming and secondary breaking on the inner bars (Figure 1.4). These trends are more dominant in micro-mesotidal settings where breaking

regions vary little in a spatial sense; however, for macrotidal beaches the cross-shore position of breaking waves exhibits greater non-stationarity.

1.3.4 Subtidal Dynamics

Whilst the study of subtidal bars presents a more complex task for a field researcher owing to less convenient access, their importance in coastal dynamics has led to widespread focus within the literature. The relationship between intertidal morphology and nearshore bar dynamics has been widely addressed in both laboratory (summarised in Komar 1998), numerically and field studies (Aagaard, Nielsen & Greenwood, 1998; Almar *et al.*, 2010; Lippmann & Holman, 1990; Smit et al., 2008a). Nearshore bars are ubiquitous features of many sandy beaches and can vary from single alongshore uniform (2D), alongshore rhythmic (3D), double bar systems and multibar systems.

Bar behaviour is highly varied with changes in the shape, migration patterns (onshore and offshore), bar amplitudes and alongshore migration. Early studies utilised 2D profile measurements to assess bar dynamics; however, remotely sensed images are increasingly used to monitor long term change and the large spatial extents of bar characteristics (Holman & Stanley, 2007). Examples of such systems include Argus video cameras (Section 1.6) and satellite images which provide a greater spatial analysis of coast wide bar systems, but at a cost of less resolution (Lafon et al., 2004).

Two recent studies of bar systems similar to those relevant to this thesis are by Castelle *et al.* (2007a) and Aagaard *et al.*(2008). Both investigations highlight the behaviour of double barred systems, Castelle *et al.*,(2007a), on the Aquitaine coast, Aagaard *et al.*,(2008)on the Dutch coast.Castelle *et al.*,(2007a) observed a highly stable crescentic bar with wavelength of ~700m which became asymmetric in response to N.W swell and remained stable under conditions $<H_s$ = 3m. More intensive observations off the

Netherlands found greatest variability in bar behaviour in alongshore direction compared with onshore/offshore migration (Aagaard *et al.,* 2008). Although offshore bar systems in macrotidal settings will not encounter the surf zone variability experienced at intertidal bars (Figure 1.4) they are still subject to greater variability than their micro-tidal counterparts and experience a mixture of shoaling and surf zone wave conditions.

The presence of 3D bars further complicates wave breaking and subsequent transport pathways which can affect migration rates and direction, e.g. Aagaard *et al.*(1998) found onshore migration of 3D bars in response to storm conditions, while Lafon *et al.* (2005) found migration rates dependant on the bar orientation.

1.3.5 Morphological Classification

Early studies attempted to group and define the different beach types which were observed as a way to distinguish between the different moprhodynamics, sediments, and waves(King, 1972). This systematic approach provides a framework within which further analysis can be undertaken to address response and behaviour.

Following extensive field observation in Australia, Wright and Short (1984) categorized 3 separate beach profile shapes based on the beach slope (tan β) and the wave conditions: dissipative, reflective and intermediate (Figure 1.5). Dissipative beaches are characterized by shallow slopes where spilling waves tend to break further offshore before dissipating across a wide intertidal region. Reflective beaches have much steeper slopes with coarser sediments forcing waves to break in a surging manner at the beach-face, preventing the dissipation of energy over a wide area. Intermediate profiles consist of more complex beach profiles incorporating elements from either end of the spectrum and tend to be associated with plunging breakers. Intermediate beaches exhibit the

greatest 3D morphology, including rip channels, cusps and bar formations, such as crescentic, transverse and longshore bars. Figure 1.5 shows the classification model devised by Wright and Short (1984), which groups the various beach types into a continuum defined using three dimensionless surf zone parameters: the surf scaling parameter, dimensionless fall velocity and Iribarren Number (Table 1.1).

Table 1.1–Common wave parameters used to define beach states (adapted from Woodroffe, 2003); where tanβ = beach slope, H_b = breaker height (m), L_0 = offshore wavelength (m), g = acceleration due to gravity (9.81ms^{-2}), T = wave period (s) and W_s= sediment settling velocity (ms^{-1}).

Parameter	*Expression*	*Dissipative (Spilling Waves)*	*Intermediate (Plunging-collapsing waves)*	*Reflective (Surging waves)*	*Reference*
Surf Scaling Parameter	$\varepsilon = \frac{2\pi^2 H_b}{g\,T^2 tan^2\beta}$	> 20	20-2.5	<2.5	Guza and Inman (1975)
Surf Similarity Index (Iribarren Number)	$\varepsilon_b = \frac{\tan\beta}{\sqrt{H_b/\lambda_0}}$	<0.64	0.64-5.0	>5	(Battjes, 1974)
Dimensionless fall velocity	$\Omega = H_b/w_s T$	>6	5-2	<1	(Gourlay , 1968)

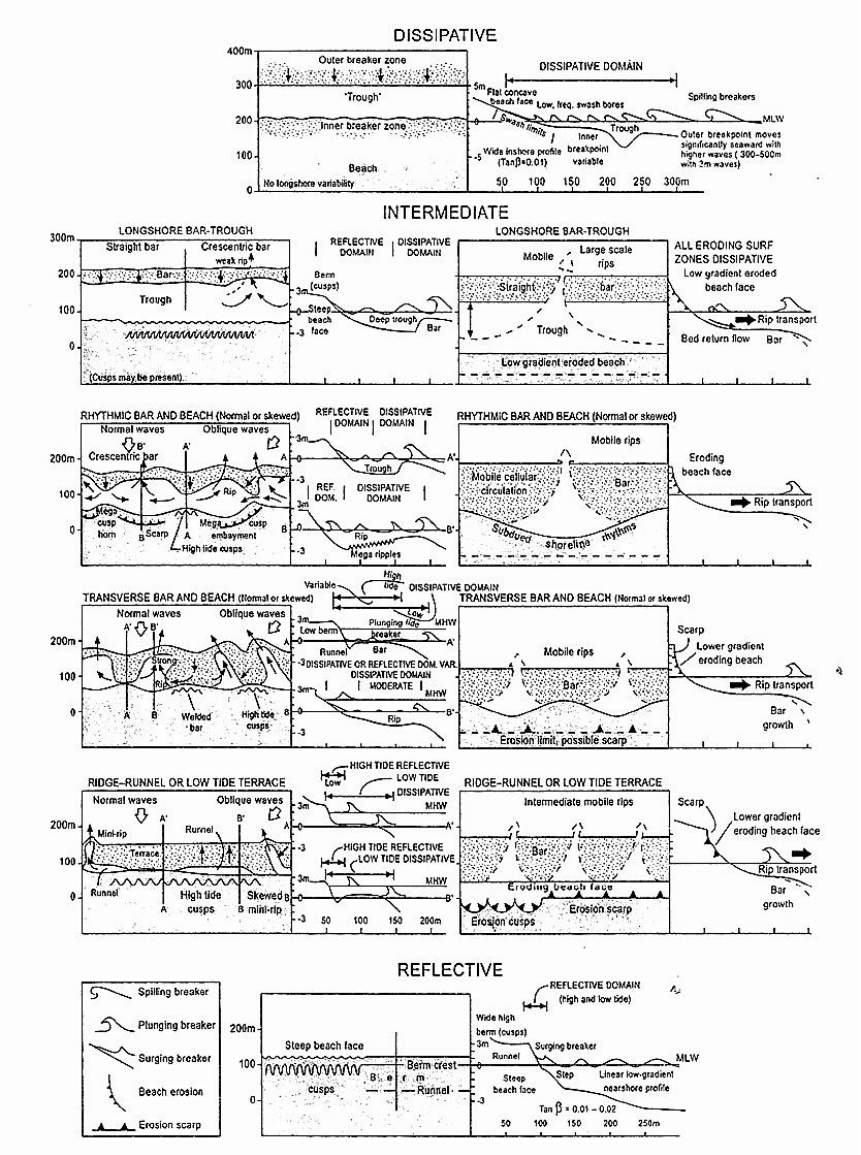

Figure 1.5– Beach state classification model based on wave dominated beaches, showing accretionary phases (left; decreasing wave conditions) and erosional conditions (right; increasing wave conditions) from Short (1999).

Much of the work undertaken by Wright and Short (1984) is based on the Australian coast which experiences a micro-meso tidal climate, and is therefore more subject to changing wave conditions. However Wright (1986, 1987) concluded that even on micro-tidal beaches, conditions during spring tides produced more subdued bar-trough topography compared with under neap tides. For macrotidal regions it is widely accepted that the increased tide range acts to smooth the morphological response.

However Masselink *et al.* (2007) also found that a shift in the tidal range (neap-spring) was the trigger for the development of an intertidal bar in the absence of a shift in wave conditions.

1.3.6 Tidal Modification

As previously identified, variation in sediment transport occurs across the surf zone as waves shoal towards the shore before breaking and continuing up the beach as swash. The position of these regions is understandably important in determining the dominant morphology. As such, any fluctuation in the mean water level will determine the position of these regions and subsequently the dominance each plays in sediment transport and the profile evolution (Masselink, 1993).

The influence of the tide is dependent on the range and the beach slope which control the relative tidal stationarity across the beachface. For a fixed tidal range a shallow beach will experience rapid tidal inundations compared with a steeper slope. The duration of relative stationarity will affect the dominance of the different surf zone processes (shoaling, breaking and swash) on the different regions of the beach, and subsequently the morphological response which takes place (Figure 1.6). As the water level rises the intertidal region is covered by the shifting surf zone, in particular shoaling waves dominate over swash processes which are confined to the narrow upper high tide zone (Short, 1996). The result of this high tide action often produces a beach with a shallow low tide profile which steepens further up the beach with coarse sediments found in the swash dominated region (Jago & Hardisty, 1984).

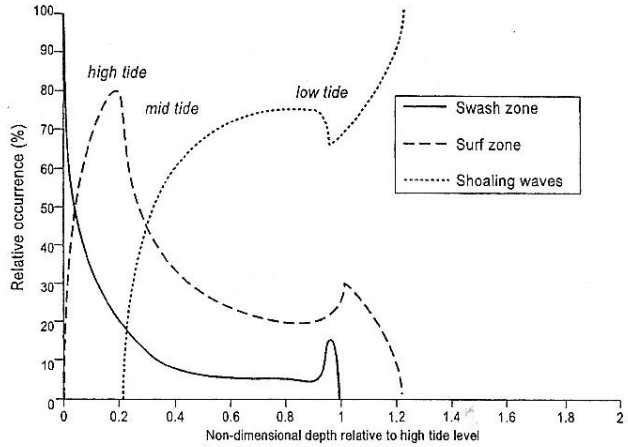

Figure 1.6– Relative occurrence of swash, surf and shoaling wave processes across the beach profile calculated over one tidal cycle where H_s = 1 m, T = 8 s, W_s = 0.03 m s^{-1}, γ = 0.8 and tide range TR = 6 m from a simulated tidal excursion model by Masselink (1993)

The primary result of large vertical transgression of the water level and the subsequent non-stationarity of the surf zone processes is to lead to more subdued morphological features with greater residence times, requiring more energetic/prolonged calm to generate significant shifts in the beach morphology.

The importance of tidal modulations in determining beach morphodynamics, and therefore the classification of beach states, lead Masselink and Short (1993) to incorporate a tidal component into Wright and Short's (1984) conceptual beach model through definition of the relative tidal range (RTR):

$$RTR = MSR/H_b \qquad 1.1$$

where MSR is the mean spring tidal range (m) and H_b is the breaker height. Combined with the dimensionless fall velocity (Ω) which has been shown to control beach slope, (Dalrymple & Thompson, 1977), we are able to classify sandy beaches into 8 beach types (Figure 1.7). Using this approach, changes in the wave heights are the driving force behind profile response (Short, 1987), with rising waves forcing much faster response in morphological change than decreasing conditions as experienced under storm environments (Wright & Short, 1984). The importance of waves remains as tidal

range increases; however, owing to the translation of the surf and swash zones, energy dissipation experiences reduced spatial stationarity and so we see less defined responses, depending on the antecedent conditions.

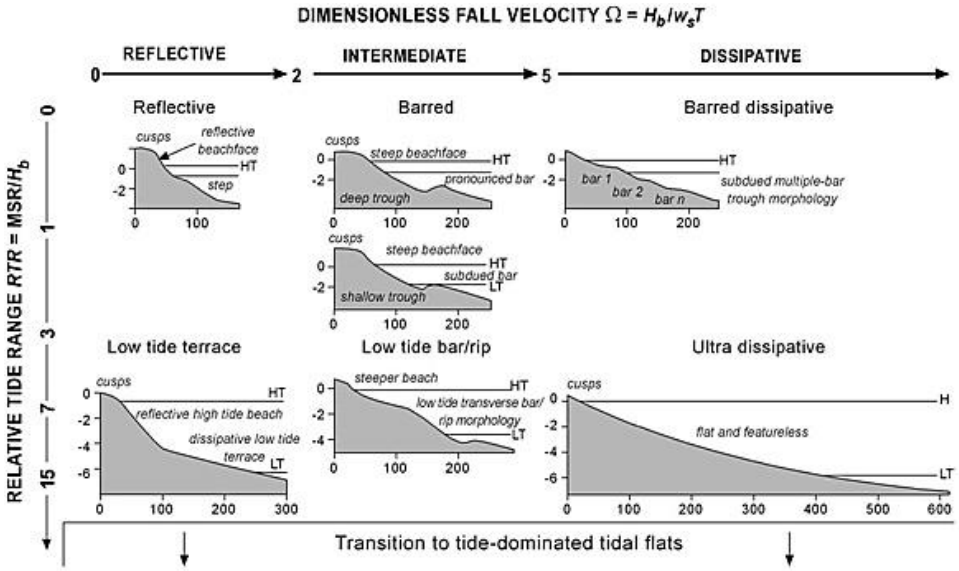

Figure 1.7– Modified conceptual beach state model incorporating the relative tidal range and dimensionless fall velocity (Masselink & Short, 1993).

Whilst the original work by Wright and Short (1984) and additions by Masselink and Short (1993) have done much to further the grouping and identification of different beach states, the models are not fully universal and care must be taken when comparing the effectiveness of such classifications to a new site. To this end, Scott *et al.* (2011) undertook extensive morphological and hydrodynamic surveys of 92 beaches across the UK to further develop the model for UK beaches (Figure 1.8). This approach identified 9 distinct beach types with absolute wave power proving a key parameter helping to differentiate between the classes.

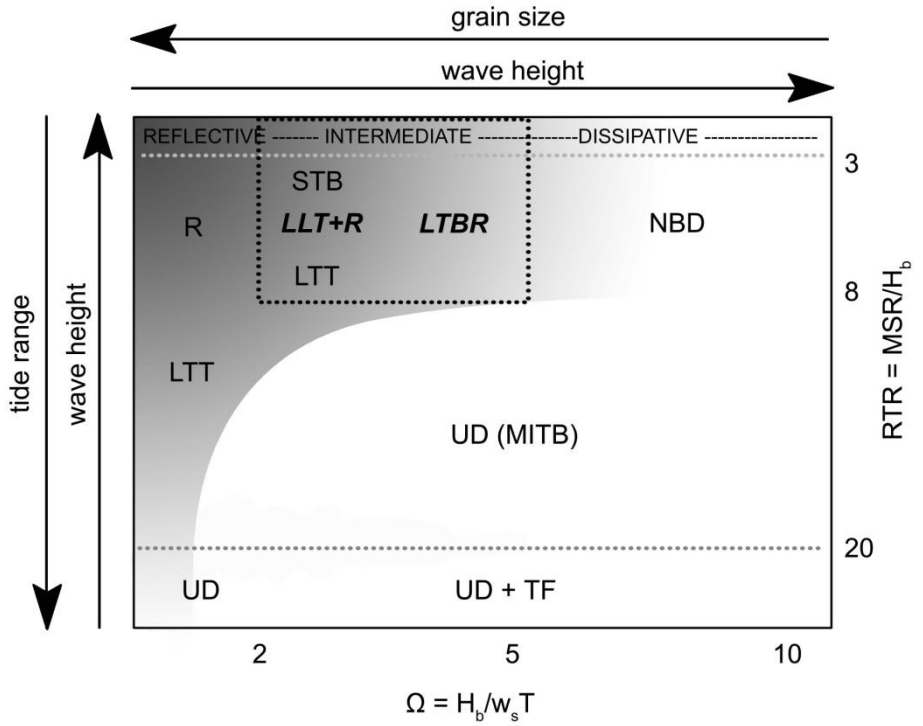

Figure 1.8– Conceptual morphodynamic framework for UK beaches from Scott et al. (2010). Dark and light shading represents a transition from reflective to dissipative surf zone conditions, respectively. Black dashed box indicates intermediate beach types. Bold italic states indicate high-energy wave conditions. R = Reflective, LTT-D = low tide terrace - dissipative, STB = subtidal barred, LLT+R=low tide terrace and rip, LTBR = tow tide bar/rip, NBD = non-barred dissipative, MITB = multiple intertidal barred, UD (+TF) = ultra dissipative and tidal flats. For further details see Scott *et al.* (2010).

1.3.7 Morphological Response

One of the primary applications of beach classification schemes is the ability to predict how beaches may respond under a change in the wave conditions. Such changes can occur over a range of timescales including, wave-by-wave, tidal cycle, storm, spring-neap cycle, seasonal, annual, decadal and longer term. From a baseline state we are able to assess a likely response under different temporal variations in the dominant wave conditions. Using Figure 1.8, an increase in wave height leads to a higher dimensionless fall velocity and a drop in the RTR, shifting the beach from reflective to increasingly dissipative. In a 2D profile we would see the removal of a berm feature and the development of bar type profiles. The response of the beach is then governed by the

duration of the event, sediment supply and geological constraints. The recovery of the beach towards its previous state is dependent on many factors; however, it is likely the beach will undergo several intermediate states before it returns to its original profile (Wright, Short & Green, 1985).

The most stable beach states exist at the extremes of the beach model. Those which are reflective or dissipative tend to exhibit a less variable seasonal profile (Wright & Short, 1984). For dissipative beaches this is clearly a reflection on the ability of the beach to dissipate wave energy across the profile which restricts significant morphological change, while reflective beaches experience change to the berm height and step depth the gradient remains constant (Wright & Short, 1984). Short and Hesp (1982) found the low temporal variability for reflective and dissipative states echoed the low longshore spatial variability for most sites. Intermediate beaches represent the more dynamic responsive states to the prevailing conditions. They are characterised by profiles which fall between the shallow dissipative and steep reflective states which results in increasingly 3D morphology as bars develop and rip channels become more defined. Such systems are more responsive to shifts in the wave climate such as seasonal variability and storm events (Figure 1.5). The different beach states which can be identified as a beach undergoes response to seasonal fluctuations in wave conditions will reflect the dominant wave conditions, sediment characteristics, geological controls and the antecedent conditions which play a significant controlling role (Haxel & Holman, 2004; Hill et al., 2004; Larson & Kraus, 1994; Lippmann & Holman, 1990). The terms up-state (increase in wave energy) and down-state (decrease in wave energy) have been used to describe these transitions between the morphodynamic states (Sénéchal et al., 2009; Smit et al., 2008b); however, it is also important to recognize response periods will vary between beaches for many of the reasons identified above.

Therefore, the beach state at any given time may not reflect the dominant conditions acting upon it at that same time (Wright, Short & Green, 1985). In general, however, studies have shown beaches which are exposed tend to respond more rapidly to increased wave conditions, forcing erosion, compared with reduced waves which result in accretionary periods (Short, 1996).

- **Storms**

Storm impacts can be split into 2 categories; the initial storm response which is a function of both the storm intensity and duration as well as the antecedent conditions which are discussed in more detail below; and the post-storm recovery. It is widely accepted storm events are characterised by erosive phases as offshore transport dominates however the impact of a single large event and the cumulative impact form repeated smaller events has also been explore within the literature (Lee et al 1998 and Birkemeier 1999). Lee *et al.* (1998) focused on the reoccurrence of storm events and the collective impact of such periods on the cross-shore profiles at Duck. They found repeated storms have a cumulative effect representing one larger low frequency storm event. Furthermore the ability of the beach to recover is dependent on the period between storm events, during which onshore sand transport takes place from the upper shore face (Birkemeier *et al*. 1999). While erosive conditions usually dominate beach response, under storm waves, longshore variability in morphology leads to varying levels of profile stability. Aagaard *et al.* (2005) measured greatest loss at megacusp embayments and relative stability at salients where profile slopes were more dissipative. 11 years of profile data was used to assess the profile response at Duck, North Carolina by Larson and Kraus (1994). In addition to the seasonality in profile shape which was observed they identified increased 3D morphology during post storm recovery phases in response to reduced wave heights and long period waves. This study also highlighted

the limitation of using absolute volume as a measure of response due to the 3D features present across the profile. Less consistency in storm response was observed over 2 years for a micro-tidal high energy beach in Northern Ireland (Backstrom, Jackson & Cooper, 2009). This was attributed to the antecedent morphology and the importance of wind patterns which were also identified by Hill *et al.* (2004).

- **Antecedent Conditions**

The importance of the preceding morphology was also identified by Lippman and Holman (1990). They recorded rhythmic bars developing between 5 and 16 days following storm peaks, which then remained stable once developed under moderate waves. Under accretionary conditions a sequential change in morphology was observed; however, as wave heights increased and erosion occurred the transitions became less direct between states supporting equilibrium models (Lippmann & Holman, 1990). Larson and Kraus (1994) also found it difficult to establish a clear link with wave conditions and the observed profile response, suggesting the antecedent morphology is of significant importance.

Observations of large scale coastal behaviour spanning 9 years were undertaken by Haxel and Holman (2004) off the north west coast of the USA. Their observations showed a clear phase lag between changes in H_s and sediment volume of ~45 days. Bar migration offshore also lagged behind an increase in wave conditions by ~30 days. Of particular interest, however, was the importance of short-term small scale changes in the beach morphology, such as bars and rip channels, which affected the cross-shore and alongshore sediment distribution. They argue these observations can mirror a similar response to longer term changes in the wave forcing (Haxel & Holman, 2004). As

extended data sets are rare the ability to discern long-term trends from shorter time-series is paramount for predicting beach response.

- **Geology**

The complexities of geology on the behaviour of beach morphodynamics has received less attention within the literature. McNinch (2004) identified the importance of the underlying geology in setting the boundaries within which the beach can exist while Jackson *et al.*(2005)discussed the importance of the nature of the surrounding geology as a source for the beach. While the antecedent conditions have been identified as important in determining the resulting beach states, Jackson *et al.*(2005)found beaches with dominant geological control did not fit current classification schemes. The importance of intertidal geology in determining rip location and behaviour was identified by Enjalbert *et al.*(2011) at a headland confined beach in SW France. More recent work by Scott*et al.*(2011), which assessed 92 beaches in the UK, further identified topographical control through intertidal geology which affected beach classification.

The availability of sediment or the presence of physical structures have also been shown to affect the subsequent profile shape (Hill *et al.*, 2004). Following 2 years of profile observations for micro-mesotidal beaches they found that where upper-shore sediment supply was available (un-developed beaches) post storm response was faster under increased wave conditions compared with more developed/constrained beaches.

1.3.8 Rip Currents

Rip currents can be described as shore-normal seaward-directed water flows which originate within the surf zone and broaden outside the breaker region (Figure 1.8; Shepard, Emery & La Fond, 1941). Such features are not only important for understanding nearshore hydrodynamics and sediment transport patterns, but also pose a significant threat to beach safety (Scott *et al.*, 2007).

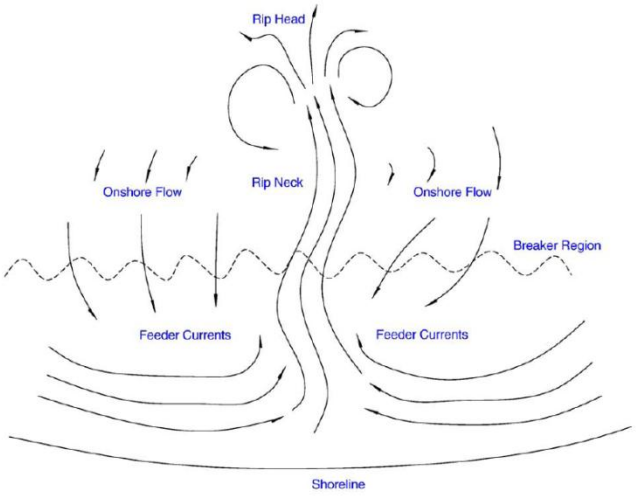

Figure 1.9– Schematic of a classic rip current (from MacMahan *et al.* (2006) after Shepard *et al.* (1941))

Rip generation is a response to variations in the alongshore wave induce momentum flux, termed radiation stress by (Longuet-Higgins & Stewart, 1964). Regions of larger waves result in larger set-up/set-down which creates alongshore pressure gradients both inside and outside the surf zone. Outside the surf zone this gradient is balanced by the alongshore gradient in radiation stress (MacMahan, Thornton & Reniers, 2006). However, inside the surf zone the gradient in the alongshore radiation stress produces a net flow towards regions of smaller waves (MacMahan, Thornton & Reniers, 2006). As morphology affects wave breaking and subsequent energy dissipation at the shoreface, many studies have attempted to relate the underlying morphology with the presence and

dynamics of rip currents. Bowen (1969) first demonstrated the importance of underlying bathymetry which acts to focus the wave energy driving rip currents. Variations in wave breaking create alongshore pressure gradients which help drive feeder currents. These currents usually form shore-parallel feeder currents which converge to form a shore-normal deeper channel. The channel then narrows seaward incising alongshore bars before the rip head expands and flow velocities drop in deeper water. Observations of rip flow velocities vary between 0 and 1 m s^{-1}(Shepard, Emery & La Fond, 1941), up to "mega" rips with offshore-directed flow up to 2 m s^{-1}(Short, 1999).

Building on early field campaigns using simple instrumentation, such as pressure sensors and visual observation (Mckenzie, 1958; Shepard, Emery & La Fond, 1941), more recent deployments have utilised electromagnetic current meters, acoustic doppler current profilers and GPS drifters (Austin et al., 2009b; MacMahan et al., 2005). Such approaches have done much to further our understanding of the dynamics of such systems, although ranging from 2-20 days the temporal period of observations has been limited. Long term Argus observations (Figure 1.10), have been used to correlate spacing with surf zone width, wave height and period (Holman, 2006; Ranasinghe et al., 2004; Turner et al., 2007); however, establishment of significant statistical relationships between the different variables has so far been limited.

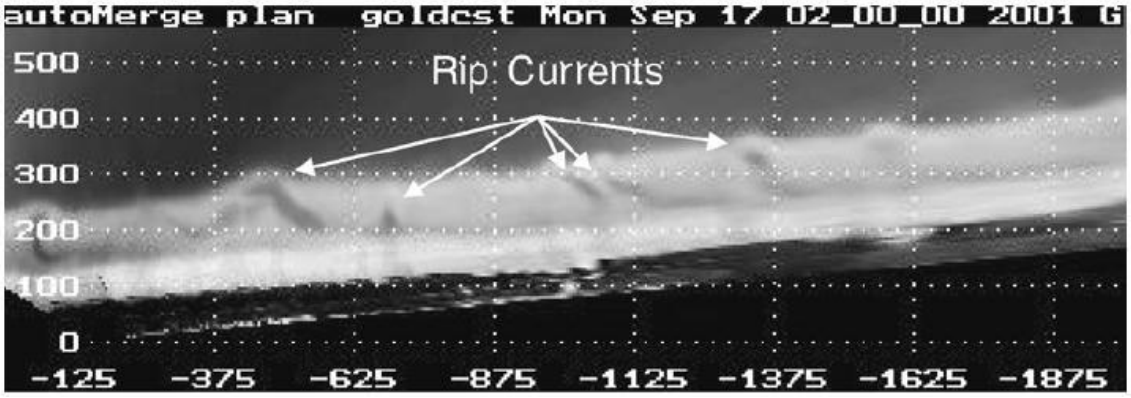

Figure 1.10 - Example of Argus plan view image used to locate and track rip spacing and migration (Turner et al., 2007).

Gallop *et al.*(2009) has also used Argus images to monitor long term trends in rip spacing and behaviour. This work identified the importance of reconfiguration events which act to reset the rip spacing evident at the beach. It is clear, however, that much work still remains to be done to further understand the relationships between bar behaviour, rip spacing and wave climate, which is only possible through extended comprehensive data sets.

1.3.9 Argus

The development and application of Argus systems over that past 25 years has been driven by the need for high frequency remote observations capable of assessing nearshore processes under conditions unsuitable for normal instrumentation (Holland et al., 1997). With over 20 Argus sites established worldwide and numerous Argus based systems in operation, advances and applications of video imagery have also grown (Holman & Stanley, 2007).

The Argus system allows for the non-intrusive observational approach to identify key aspects of nearshore processes which can be used to further our understanding of this complex region. The set-up and operational aspects of Argus sites have gone through several phases as improvements with computer and camera technology has allowed increased data capture and storage. The present system (Argus III) uses cameras with pixel resolution of 1024 x 768, with synchronous data collection achieved using a 2Hz external trigger. For a comprehensive review of previous Argus work see Holman and Stanley (2007).

Argus sites routinely provide 3 image "products". These include a snapshot image, a time exposure (timex) image collected at 2Hz over 10 minutes and a variance image which shows the standard deviation or "variance" in an image. All three image products

are taken every half an hour during daylight hours. Of principal interest for the present project are the snap and timex images.

The position and orientation of subtidal bars was one of the first applications of video data primarily achieved using the timex images (Lippmann & Holman, 1989). Bands of foam generated at the breaker point by waves collapsing can be related to the bar crest location. Identified as the intensity maxima within the images, long term records were used to map bar migration across the surf zone in response to varying wave conditions. The positional accuracy of bars has been shown to be affected by tide and wave components, requiring further correction to be necessary (Kingston et al., 2000; van Enckevort & Ruessink, 2001). The latest addition to detecting the bar position builds on the algorithm developed by van Enckevort and Ruessink (2001). Through a user-defined region of interest the BarLine Intensity Mapper (BLIM) algorithm searches vertically through the image for the maximum intensity value. Different levels of smoothing can be applied to reduce noise generated by pixel variability, and multiple lines can be generated to differentiate between visible bars (Pape et al., 2007).

Figure 1.11 – Example Argus timex image showing bands of foam caused by wave breaking over a nearshore bar and at the shoreline, from Holman and Stanley (2007).

Further efforts to derive subtidal bathymetry have used estimations of water depth from video observations of wave celerity (Stockdon & Holman, 2000) or wave breaking (Aarninkhof, Janssen & Plant, 1997). However, such methods encounter problems in the surf zone due to the non-linearity of the wave field in shallow water. Further work in this field has focused on both video-derived and model-predicted patterns of wave dissipation to map the bathymetry (Aarninkhof et al., 2003); however, this application of Argus is still under development and not widely used.

2 SITES

2.1 Introduction

To assess the possible impact of a shift in the dominant wave climate, arising from the Wave Hub, four sites were chosen which were within the extent of the predicted shadow zone (Millar, Smith & Reeve, 2007). In addition the sites were also selected to provide comparison of different beach shapes and their importance for beach users. The four sites chosen for the monitoring programme are located within a 23 km stretch along the North Cornish coast (Figure 2.1). This is a strongly macrotidal coastline (mean spring tidal range 6.1m) exposed to a highly energetic wave climate (mean offshore H_s= 1.6m) of both local wind-generated seas and North Atlantic swell (Davidson et al., 1997).

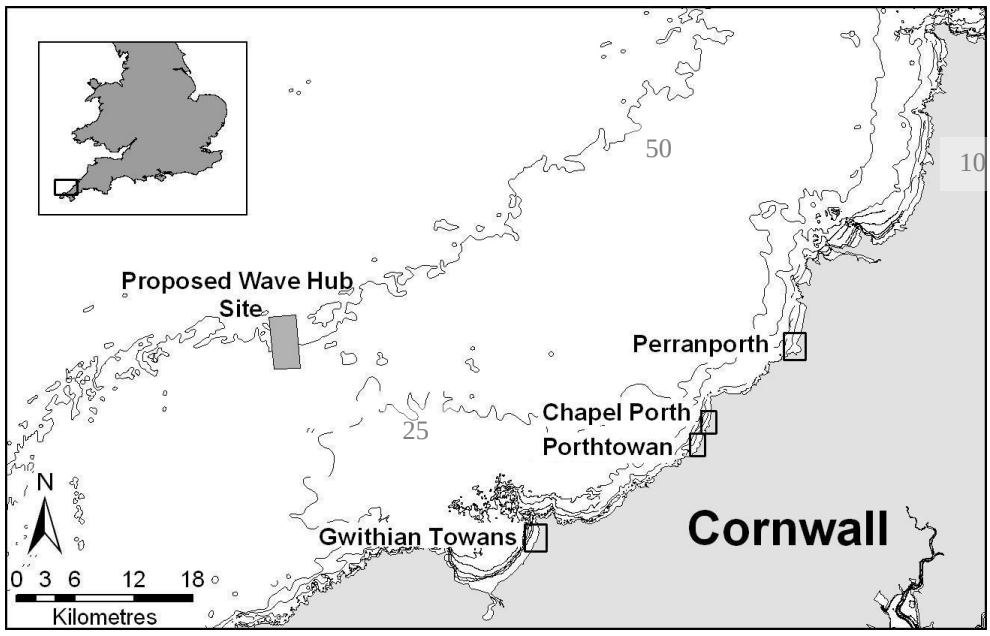

Figure 2.1– Location map of the four survey sites including offshore location of the proposed Wave Hub

Each of the beaches has a W-NW orientation ensuring they are exposed to the dominant wave approach discussed further in Section 2.2.The present chapter provides an overview of each site before a summary of the physical characteristics is included at the

end of the section (Table 2.1), representing a combination of *in-situ* observations and historical data (Buscombe & Scott, 2008).

2.1.1 Perranporth

Perranporth (subsequently referred to as PPT) forms the largest survey area with a cross-shore intertidal region of 500m and a longshore extent of 1.2 km (the beach extends 3.5 km alongshore, exposed when the tide drops below mean sea level of 0.24m Ordnance Datum Newlyn (ODN);Figure 2.2). The wide highly dissipative beach has a lowtide beach gradient of $\tan\beta \approx 0.012$ and is composed of medium sand (D_{50}=0.35mm). The relatively high carbonate content of the sand (~ 50%; Merefield, 1984) suggests that offshore sediment sources are of importance. Relatively featureless throughout the upper intertidal region, a well-developed bar system interspaced with rip channels is exposed at spring low water (Davidson *et al.*, 1997).

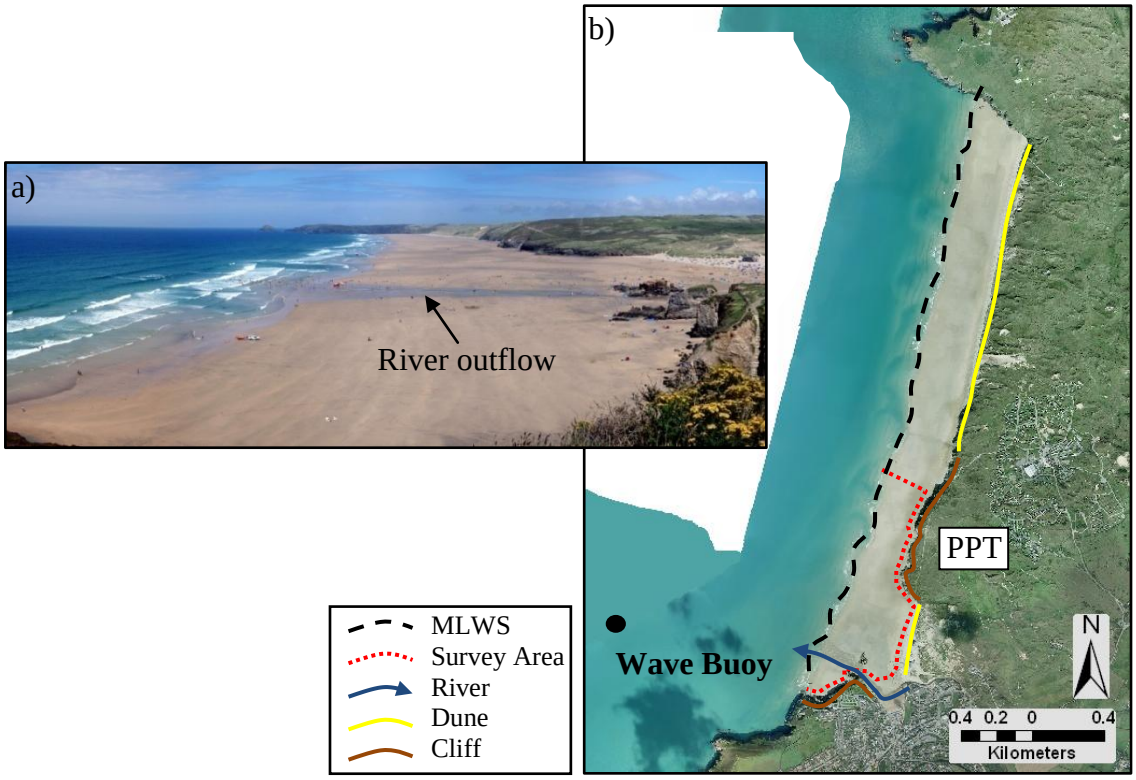

Figure 2.2 – Panoramic photograph of Perranporth (a) and aerial photograph of Perranporth (b) showing the location of the nearshore wave buoy. The black dashed line is the position of MLWS, the red dashed line indicates the survey area and the blue arrow highlights the river output across the beach face. The presence of rips is also evident as darker patches of water at the shoreline in both images.

Two small rivers, the Perran Stream and the Bolingey Stream, meet and discharge from channelised sections onto the beach to the south of the survey area and have a significant local effect on the beach morphology (Figure 2.2).The greatest threat to this site lies in coastal flooding of the beachfront development within Perranporth town (CISCAG, 2010), which was experienced during storm events in March 2008. The current plan for this site is for a period of "hold the line", before a process of managed realignment is adopted, with natural adaptation of the frontage to take place. The north end of the survey area is backed by resistant cliff faces before giving way to a well-developed dune system (Figure 2.2). Designated as a Site of Special Scientific Interest (SSSI) and a Special Area of Conservation (SAC), the Penhale dune system backing the study site is of great conservation importance. The most recent Shoreline Management

Plan for the region identifies the potential for undercutting of the dune system and cliffs to the north of the study area.

The proposed management strategy for this area suggests a non-intervention approach, allowing the dunes to roll back in response to rising sea level and increased storminess (CISCAG, 2010). Figure 2.3 gives an indication of the complex bathymetry found around MLWS compared with the relatively featureless subtidal and upper beach at PPT.

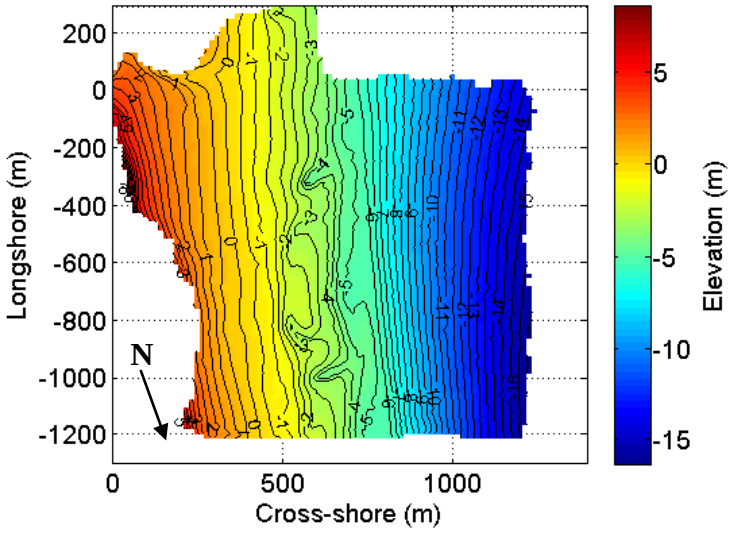

Figure 2.3 – Nearshore and intertidal bathymetry for the survey region at PPT. Subtidal data courtesy of the Channel Coastal Observatory (www.channelcoast.org).

2.1.2 Chapel Porth and Porthtowan

To the south of PPT the two central sites, Chapel Porth and Porthtowan (subsequently referred to as CHP and PTN), are in close proximity and connected at spring low tide, forming a 1.6 km headland-confined beach (Figure 2.4). Both sites are situated in neighbouring valleys flanked with high Devonian slate cliffs (70 m ODN) creating narrow pocket beaches from mid to high tide. Historical rates of erosion from these cliffs are low (maximum 3 m in the past 100 years; CISCAG, 2010) and the coves are relatively stable. At low tide the beaches extend up to 600 m cross-shore, depending on

bar/rip morphology present, with the alongshore survey area increasing to 500 m (Figure 2.4). CHP and PTN are the smallest sites; yet, they exhibit the largest dynamics in bar movement and profile shape. The beach faces north-west and is exposed to the dominant wave climate, and represents a swash-aligned beach.

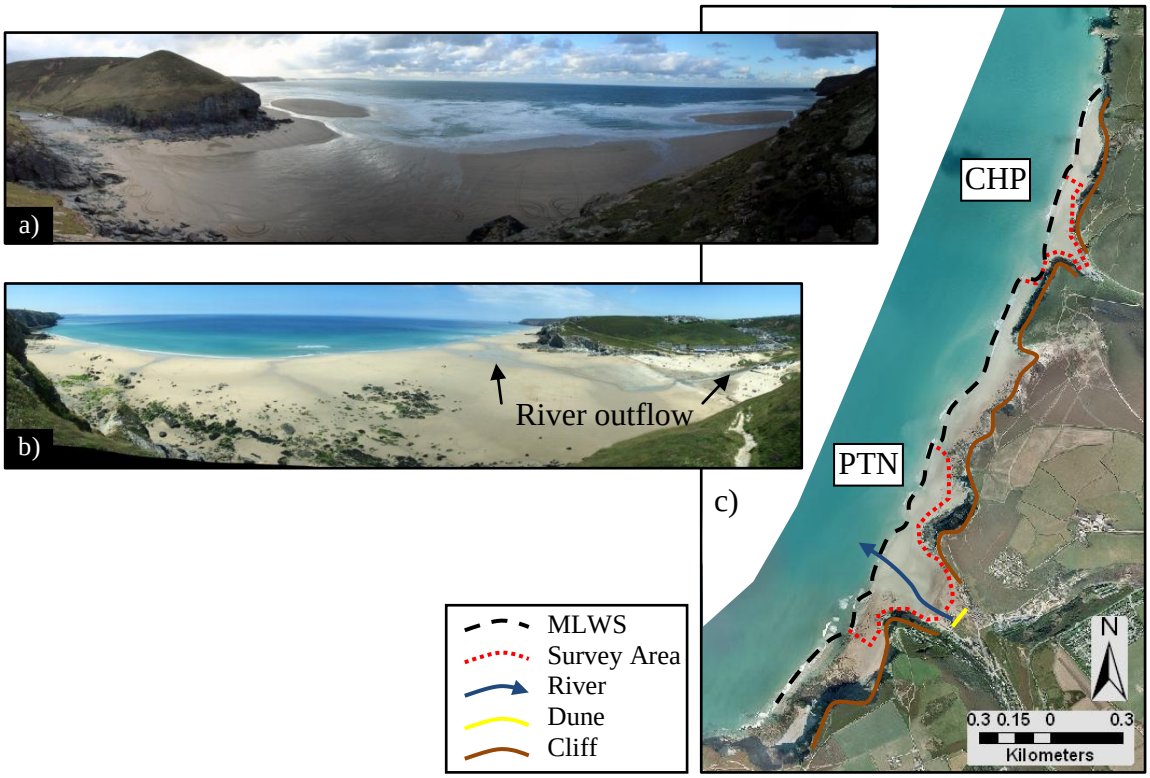

Figure 2.4 – Panoramic photographs of Chapel Porth looking south (a) and Porthtowan looking north (b). The aerial photograph (c) shows both Porthtowan and Chapel Porth. The black dashed line in the aerial photograph shows the position of MLWS, the red dashed line indicates the survey areas and the blue arrow highlights the river output across the beach face at Porthtowan.

On both beaches, the sediments across the lower slope ($\tan\beta \approx 0.015$) consist of medium sand (D_{50} = 0.38 mm), whereas the upper beach ($\tan\beta \approx 0.05$) represent a mixture of gravel and sand with exposed boulders during periods of sand removal resulting from beach erosion. Figure 2.5 displays the nearshore intertidal and subtidal bathymetry for PTN and CHP highlighting the complex morphology present at MLWS.

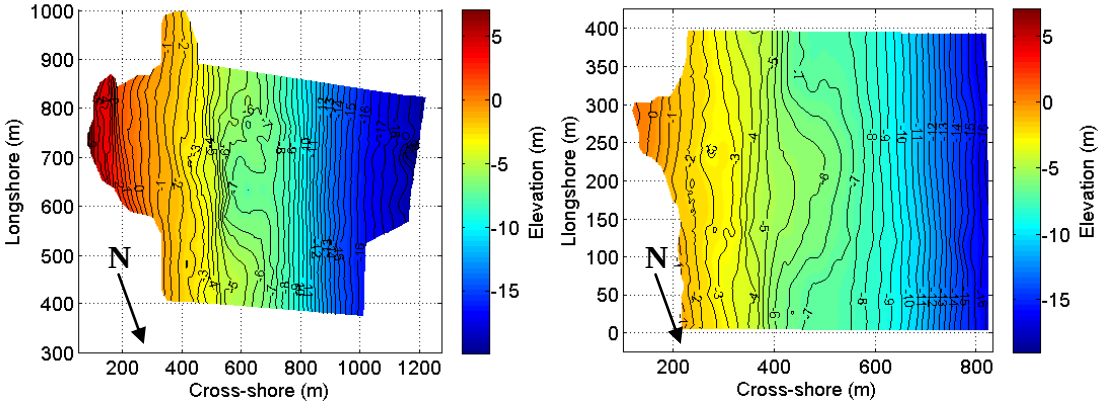

Figure 2.5 – Nearshore and intertidal bathymetry for the survey region at PTN (left) and CHP (right). Subtidal data courtesy of the Channel Coastal Observatory.

Also falling within an SSSI, the preferred management strategy at PTN is a policy of "No Active Intervention". Currently there are some small defences at the back of the beach including stone gabions protecting a car park and the lifeguard building, but these defences are unlikely to be sufficient for future stability (CISCAG, 2010). The gradual migration of the dune system up the valley from the back of the beach has been addressed through appropriate management and continued action is deemed sufficient. Further management is likely to be constrained by World Heritage Status, although this has the benefit of restricting inappropriate building development. Management at CHP is undertaken by the National Trust, who own the site, and a concrete wall is present protecting the car park and lifeguard hut.

Figure 2.6– Low tide panoramic photos of PTN and CHP looking NW in July 2009, highlighting the highly rhythmic longshore bay system connecting the two sites. The dashed line marks the MLWS water level.

2.1.3 Gwithian

The most southerly site is located within St Ives Bay, a large swash-aligned cresentic bay which is bound by Porthminster Point to the south and Godrevy Point to the north, creating a self-contained sediment cell fed by the Hayle estuary (Figure 2.7). Extending for 5 km at low tide, the deeply concave sand dominated shoreline is predominantly backed by extensive blown sands, known as "*towans*", with some sections of Devonian slate cliffs. Gwithian (subsequently referred to as GWT) lies at the northern extent of the bay, south of Godrevy Point. Active erosion of the less resistant low cliff section north of the survey area towards Godrevy Point has been observed with historical rates of 0.5 m yr^{-1}(CISCAG, 2010).

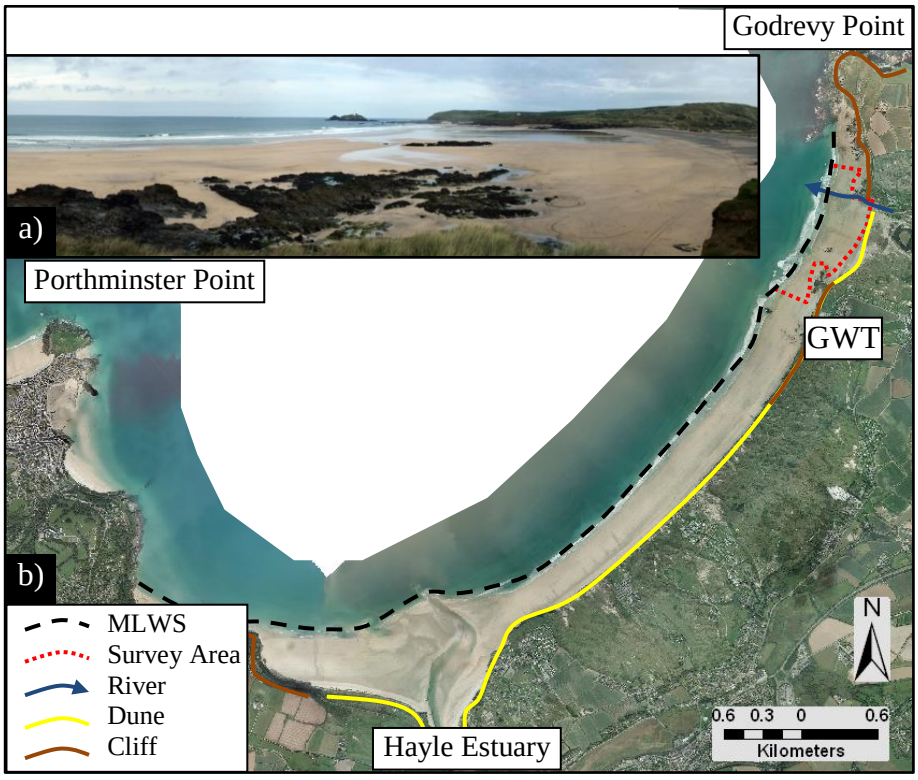

Figure 2.7– Panoramic photograph of Gwithian looking north (a). Aerial photograph of St Ives Bay with Gwithian marked to the north (b); the black dashed line is the position of MLWS, the red dashed line indicates the survey areas and the blue arrow highlights the river output across the beach face.

The high carbonate content at GWT (Merefield, 1984) also suggests offshore sediment sources, although the Hayle estuary and Red River (which exits through the survey area) provide notable additional sediment inputs. Historical sediment loads from the Red River were higher owing to mining activities and this lead to large amounts of material being deposited in the intertidal region and subsequent development of low tide morphology (CISCAG, 2010). While the sediment input has dropped following cessation of mining activities, the river remains sufficient to affect the nearshore bathymetry during periods of heavy discharge/deposition.

Prior to 2005, extensive sand extraction was in operation from the dune system behind the study area (Figure 2.8). To protect against these works an artificial bund was created which remains the only constructed defence within the bay (Figure 2.8). Mining activity ended in 2002 and the site has been re-established as a nature reserve with wetland habitats. With a current state of gradual erosion of the artificial bund (CISCAG, 2010), continued degradation of this feature is expected. Subsequently, a policy of managed realignment is recommended for the site to allow a natural response at the back of the beach to changing tide levels, although consideration of the nature reserve is identified.

Figure 2.8 – Aerial image of previous sand extraction activities at Gwithian with the Red river to the left of the image. The artificial bund is highlighted within the dashed box.

The survey area at GWT is ~700 m longshore by ~350 m cross-shore with a gently sloping (tan $\beta \approx 0.013$) profile composed of well-sorted medium sand ($D_{50} = 0.25$ mm). Similar to PPT, GWT reveals a relatively featureless intertidal region; however, subdued bar morphology is exposed at spring low water. The upper 75 m of beach has a steeper profile (tan $\beta \approx 0.06$) and consists of a mixture of sand and gravel. Beach cusps are often found around the high tide level. The upper beach extends into the artificial bund detailed above. Figure 2.9 provides an overview of the nearshore bathymetry which is found in the nearshore region of the survey area at GWT. The shallow offshore rock outcrops which form part of Godrevy Point are clearly seen.

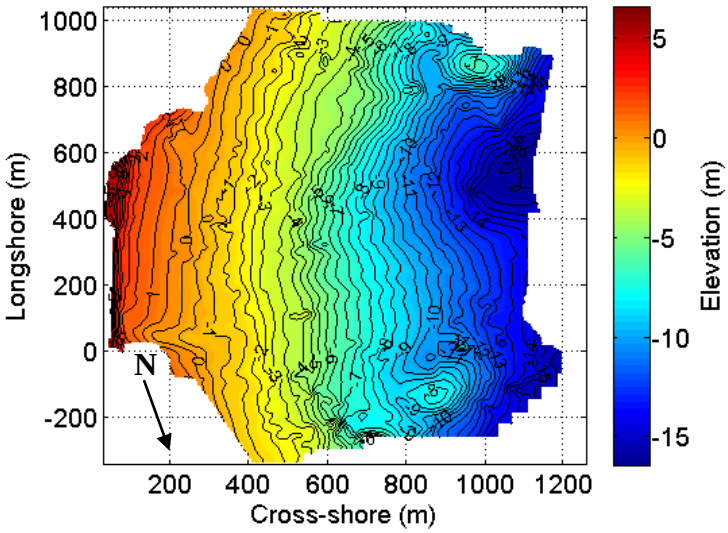

Figure 2.9 – Nearshore and intertidal bathymetry for the survey region at GWT. Subtidal data courtesy of the Channel Coastal Observatory (www.channelcoast.org).

Table 2.1 – Summary of the physical characteristic for each site, from in situ data and Buscombe and Scott (2008).

	Survey Sites											
Physical Characteristic	Perranporth			Porthtowan			Chapel Porth			Gwithian		
Latitude	50°21’23.95” N			50°17’12.92” N			50°18’1.92” N			50°13’17.84” N		
Longitude	5°9’20.92” W			5°14’35.16” W			5°14’6.95” W			5°23’53.03” W		
Local Authority	Carrick Council			Carrick Council			Carrick Council			Penwith Council		
Management Unit	Perran 7A3-09			Porthtowan 7A3-04			Porthtowan 7A3-05			Godrevy 7A2-07		
MSR (m)	6.15			6.0			6.03			5.87		
Alongshore length (m)	1100			600-800			450			900		
LW Length (m)	1100			600-800			450			900		
Cross shore (m)	550			350			150			350-400		
Average Area (m^2)	435000			70600			29500			280000		
Orientation (°)	285			300			290			295		
Sediment Characteristics	Lower	Mid	Upper	Lower	Mid	Upper	Lower	Mid	Upper	Lower	Mid	Upper
Beach tan β	0.012	N/A	0.038	0.015	N/A	0.045	0.013	N/A	0.05	0.013	N/A	0.06
Sediment classification	Sand	Sand	Sand	Sand	Sand	Gravel and Sand	Sand	Sand	Boulder, gravel and sand	Sand	Sand	Sand
Mean (Ψ)	-2.21 (0.22 mm)	-1.98 (0.25 mm)	-1.71 (0.31 mm)	-2.33 (0.20 mm)	-2.34	-2.46 (0.18 mm)	-2.64 (0.16 mm)	-2.48 (0.18 mm)	-2.48 (0.18 mm)	-1.70 (0.31 mm)	-1.70 (0.31 mm)	-1.80 (0.29 mm)
Sorting(Ψ)	0.37 (0.77 mm)	0.34 (0.79 mm)	0.34 (0.79 mm)	0.28 (0.82 mm)	0.28 (0.82 mm)	0.22 (0.86 mm)	0.26 (0.84 mm)	0.22 (0.86 mm)	0.26 (0.83 mm)	0.44 (0.74 mm)	0.44 (0.74 mm)	0.39 (0.76 mm)
Skewness	0.14	0.19	0.25	0.37	0.36	0.14	0.15	0.24	0.24	0.25	0.25	0.23
Mean fall velocity (cms^{-1})	0.0463	0.0395	0.0327	0.0503	0.0526	0.0552	0.0624	0.0557	0.0558	0.0369	0.0380	0.0390
D_{50} (Hallermeier equation, mm)	0.35	0.30	0.25	0.38	0.39	0.41	0.46	0.41	0.41	0.28	0.29	0.29
$CaCO_3$ %	43.80 ±8.80	N/A	N/A	55.70 ±6.48	N/A	N/A	53.14 ±0.77	N/A	N/A	38.25 ±15.20	N/A	N/A

2.2 Wave climate

The need for more sustainable sources of energy has driven the viability of marine renewable alternatives in both wave and tide driven devices. Currently the UK makes up ~25% of the global development into wave and tidal technology which reflects the large proportion of marine resources available (www.wavehub.co.uk; Figure 2.10). Exposed to the north east Atlantic, the south west experiences highly energetic conditions, which through the Wave Hub can be easily connected to the national grid, making it a suitable location for device deployment (Figure 2.10).

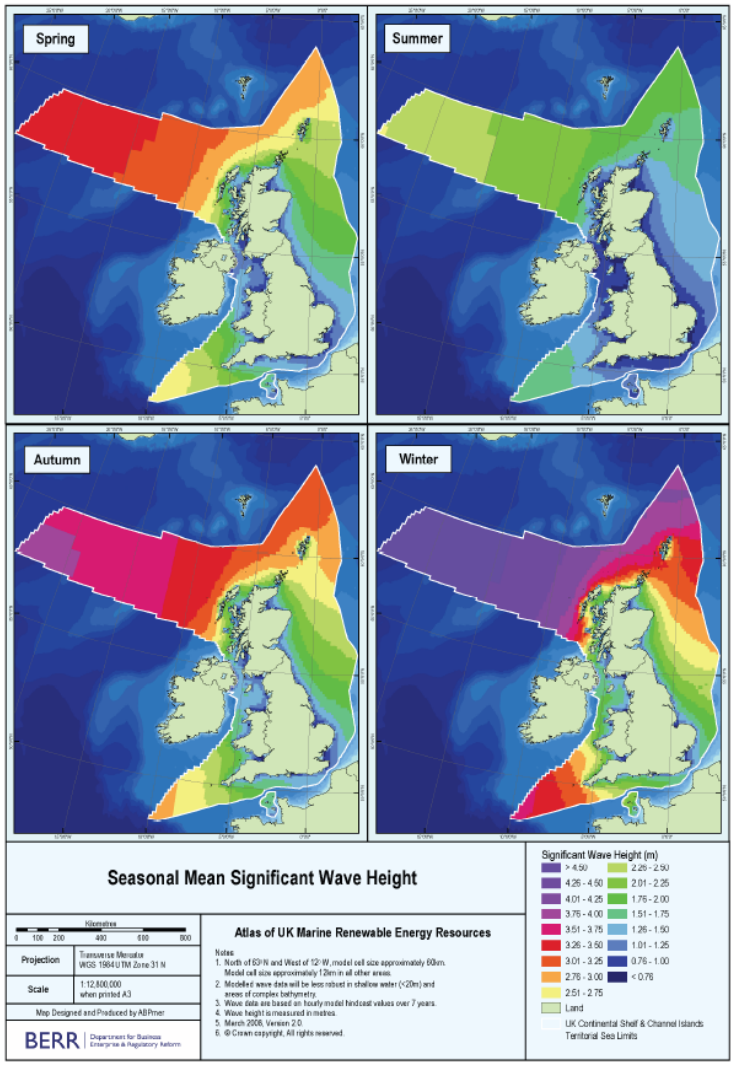

Figure 2.10 – Seasonal Mean Significant Wave Height for British territorial waters. The work was commissioned by the Department for Trade and Industry (DTI; 2004) to map the UK Marine Renewable Energy Resources and is available online from http://www.renewables-atlas.info/.

Accurate measurement of nearshore wave conditions throughout the present study is of paramount importance for interpretation of beach response. Understanding and interpreting the current wave climate is more applicable with a consideration of how the study period fits within longer term trends. To this end Section 2.2.1 introduces a 59 year hindcast wave model dataset recently presented by Dodet *et al*. (2010), and further extended to incorporate a local output. This allows a further appreciation of the longer term affects which may be felt at the sites in response to any trends in dominant wave conditions. Section 2.2.2 then introduces the wave conditions throughout the survey period derived from a nearshore wave buoy deployed in ~10 m (Chart Datum) located just offshore PPT (Figure 2.2).

2.2.1 Hindcast Wave Climate

The decadal trends of the north east Atlantic (NEA) wave climate have been summarised by Dodet *et al.* (2010) who looked at the change in $H_{s,}$ T_p and wave direction between 1953 and 2009. They used a hindcast model which was forced using NOAA Wavewatch III and 6 hr wind fields from the NCEP/NCAL Reanalysis project (Kalnay *et al.* (1996) in Dodet *et al.* (2010)). The model covered a spatial grid which extended from 80.0° W to 0.0°W longitude and 0.0° N to 70.0° N latitude with a 0.5° resolution. Data were extracted from 3 offshore output nodes spread vertically across the NEA section of the grid (Figure 2.11). Output data was validated using nearshore wave buoys located along the coast of Spain and Portugal. Subsequent analysis of the decadal variability of wave conditions showed a maximum linear increase in H_s of 0.02 m yr^{-1} and an increase of 0.01 s yr^{-1} for T_p, which was observed for the northern most region of the grid (P1; Figure 2.11).

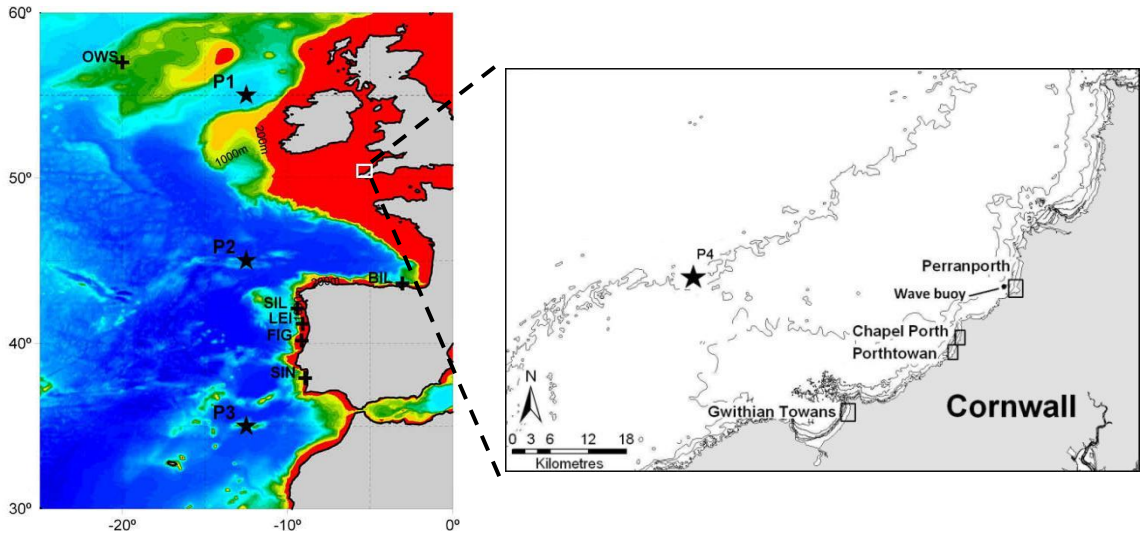

Figure 2.11– Bathymetric map from Dodet *et al.* (2010) showing the model area defined as the North-East Atlantic (left). The location of buoys used for model validation off the coast of Portugalare shown:Bilbao-Vizcaya (BIL), Cabo Silleiro (SIL), Leixões (LEI), Figueira da Foz (FIG), Sines (SIN) and Ocean Weather Station ‘‘Juliett” (OWS). Output locations are identified with a black star and labelled P1, P2 and P3. Figure to the right shows nearshore bathymetry for the North Cornish coastline, including the 4 beach sites and the nearshore DWR. P4 represents the location of an additional model output (1953-2010) provided by Dodet (pers comms) locatedat the site of proposed Wave Hub.

In addition to the model outputs P1, P2 and P3 used by Dodet *et al.* (2010), the model was run for a 59 yr period between 1953-2010 with output data provided at P4 which was located at 05.6° W, 50.4° N in St Ives Bay on the north coast of Cornwall, where the Wave Hub deployment was scheduled, (Figure 2.11). Validation of this data was undertaken using a Fugro Oceanor SeaWatch mini II directional wave buoy which was deployed at the same location (P4) during intermittent periods of 2009/2010, as well as the nearshore DWR located off PPT (Figure 2.12). Comparison of these datasets shows a good fit (0.86 Pearson correlation coefficient) with the model output for the comparable time periods.

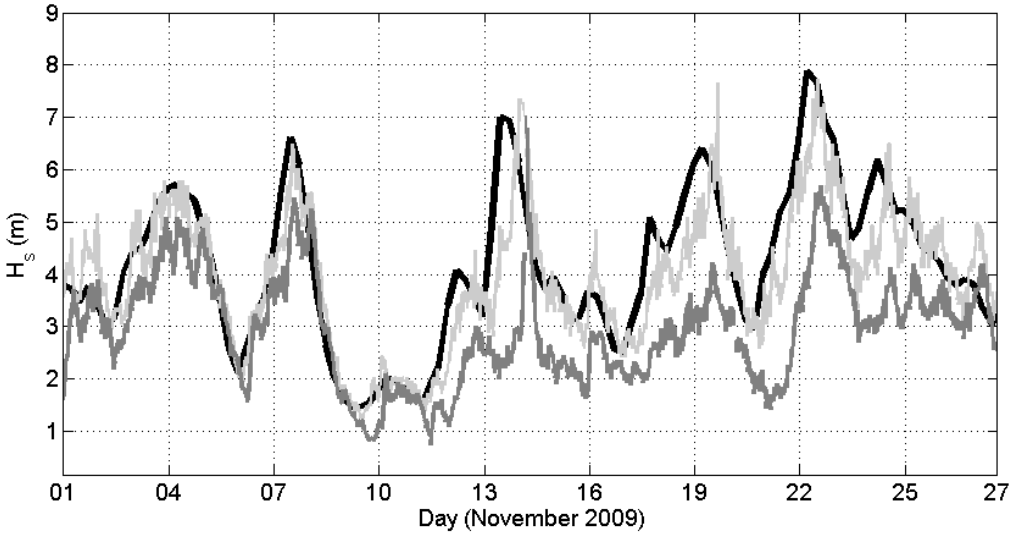

Figure 2.12 – Comparison of wave data sources for November 2009; Hindcast data (black line) from Dodet *et al*. (2010), the DWR at PPT (dark grey line, www.channelcoast.org) and the PRIMaRE wave buoy (light grey). The PRIMaRE buoy was located at P4 (Figure 2.11). The hindcast data and the PRIMaRE wave buoy have a Pearson correlation coefficient of 0.86 showing a good fit between the datasets.

The modelled data were then used to identify the relative wave conditions of the survey period with reference to previous years and the frequency and occurrence of storm events both during and prior to the survey period. For comparison, and to aid analysis, the model output was interpolated onto a 0.5 hr time series which corresponds with the wave buoy at PPT. For the purpose of storm assessment, a peaks-over-threshold approach was adopted whereby a storm was defined as having an H_s greater than 4 m and a duration greater than 1 hr, where the duration is defined as the time over which H_s exceeds 4 m. Using these criteria, monthly (annual) storm frequency, monthly (annual) storm duration and storm peak H_s were compiled.

The first observation of this dataset suggests a cyclic signal in storm activity over a 15-20 year period (Figure 2.13). This trend is most clear in the annual number of storms and subsequently the duration of storm events, suggesting the present conditions are in a falling stage of this cycle.

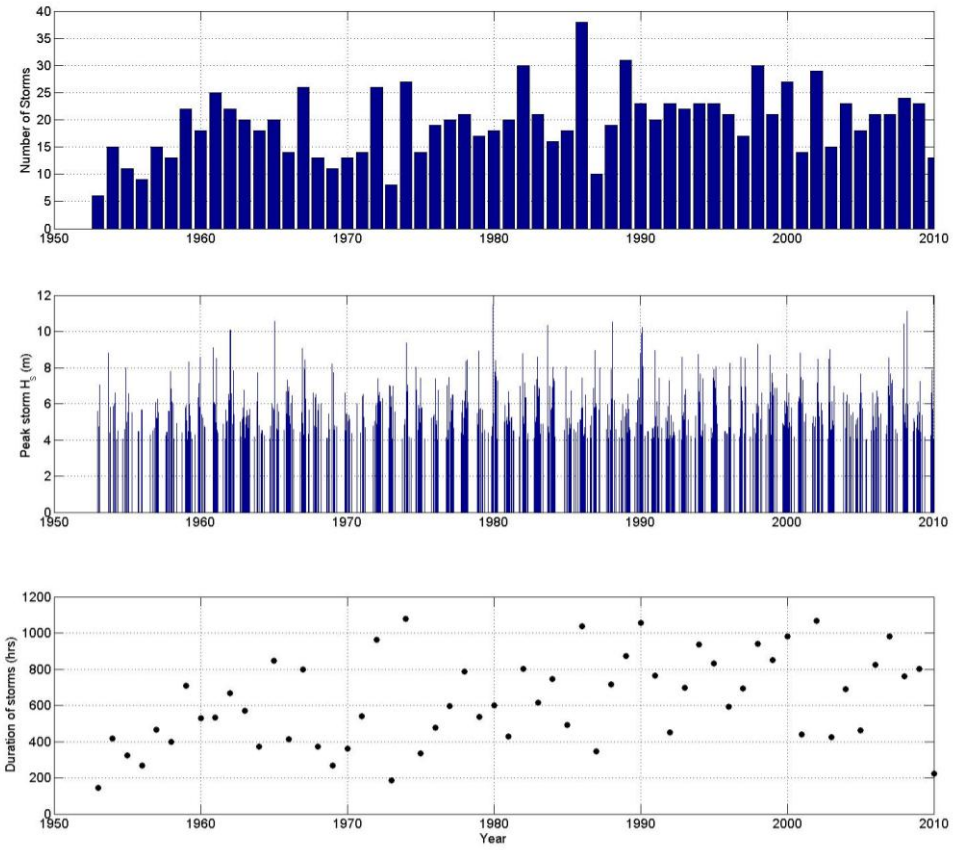

Figure 2.13– Hindcast storm occurrence using data wave data from Dodet *et al.*(2010). From top to bottom:number of storms per year, individual peak H_s for each storm and the total annual duration of storm events (H_s =>4m).

Linear trend analysis shows the frequency of storms from 1953 –2010 has an upward trend of 0.14 storms yr^{-1} (a total increase of 8.26 storms over the entire period), while the peak storm H_s is stable over the long-term. Storm duration also exhibits an upward trend with an increase of 6.2 hrs yr^{-1}(Figure 2.13). Of specific relevance for this study is the drop in total storm duration during 2010 (~200hrs) more than half the minimum total storm duration for the preceding 23 years.

Figure 2.14 shows the annual significant wave height exceedance statistics (H_s 90%, H_s 50%, H_s 10% and H_s 5%)for the full 59 yr hindcast period. This shows a small upward trend in the H_s 10% and H_s 5% record similar to that identified by Dodet *et al.* (2010). Table 2.2 summarises the trends observed during this period with greatest increase for the 5% and 10% exceedance values (R^2 0.19 and 0.16), although there is no upward trend evident in the H_s 50% and H_s 90% values.

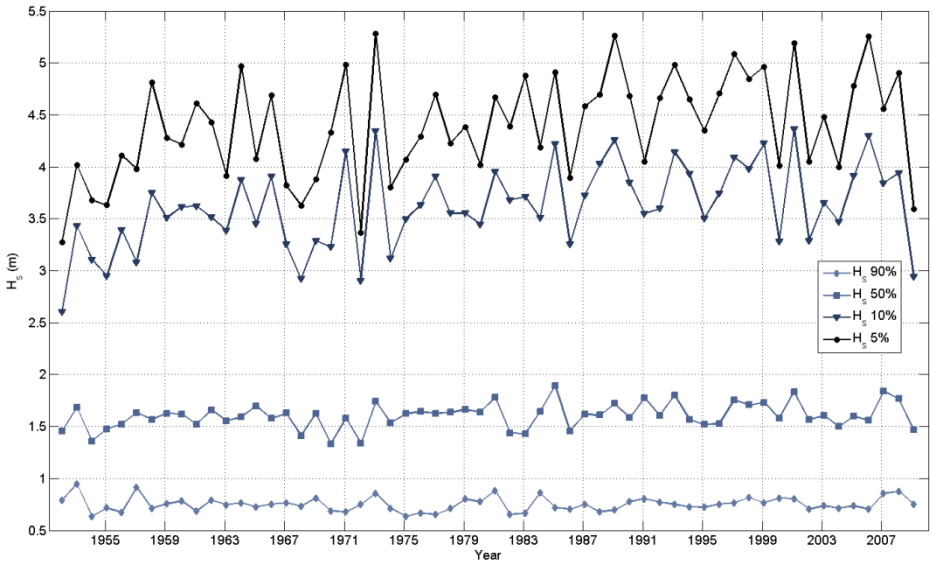

Figure 2.14– Annual significant wave height exceedance statistics for H_s 90%, H_s 50%, H_s 10%, H_s 5%. Linear trend analysis shows an overall increase in H_s10% andH_s 5% exceedance heights (Table 2.2).

Table 2.2 – Annual H_s exceedance statistics for output P4 (Figure 2.11).

***H_s* Exceedance**	**Mean (m)**	**Standard deviation**	**R^2**	**Linear trend (myr^{-1}) (net increase)**
H_s 5%	4.39	0.50	0.163	0.011 (0.65m)
H_s 10%	3.61	0.40	0.190	0.010 (0.59m)
H_s 50%	1.60	0.12	0.091	0.001 (0.118m)
H_s 90%	0.75	0.06	0.003	0.0002 (0.01m)

The observations made by Dodet *et al*. (2010), and supported by the additional data and storm analysis presented here, indicates an upward trend in the frequency and duration of storms. The importance of storms on any coastline is significant and the nature and extent of these events is fundamental to the overall state of a system. The impact of specific storms on the beach morphology during the current survey period is addressed in Chapter 4; however, it is important to also consider the longer term role of increased duration, frequency and maximum size of storms based on the trends outlined here. Whilst it is beyond the remit of this thesis to assess the projected increase in storm

events for this region, the most recent report from the Intergovernmental Panel on Climate Change (IPCC) states a further increase in storm intensity and a shift in storm maxima closer to European coasts (IPCC, 2007) combined with an increase in significant wave height by > 0.4 m by the 2080s for the NE Atlantic. In addition, the IPCC predicts sea level rise of 0.09 m to 0.88 m by 2100, with regional affects in Europe leading to rates 50% greater than the global estimates, resulting in fewer, but more extreme sea level surges (IPCC, 2007). Such scenario projections are of direct relevance to coastal managers and will affect the SMPs for the region.

2.2.2 Measured Waves

Wave data presented throughout this thesis are derived from the DWR located off PPT which provides real-time wave data as well as archive files for the duration of the survey schedule. Detailed summary wave conditions including Hs, Tp, Tz and wave direction are presented inFigure 2.15 and Figure 2.16. The seasonal variability in the wave climate is evident with wave height increasing during the winter months together with long period wave conditions, whereas the summer sees a reduction in wave height and period. Spikes of storm events are more prevalent through the winter periods, although the storm at the end of March 2010 stands out to extend this period compared with the sustained calm conditions experienced for the remainder of the year.

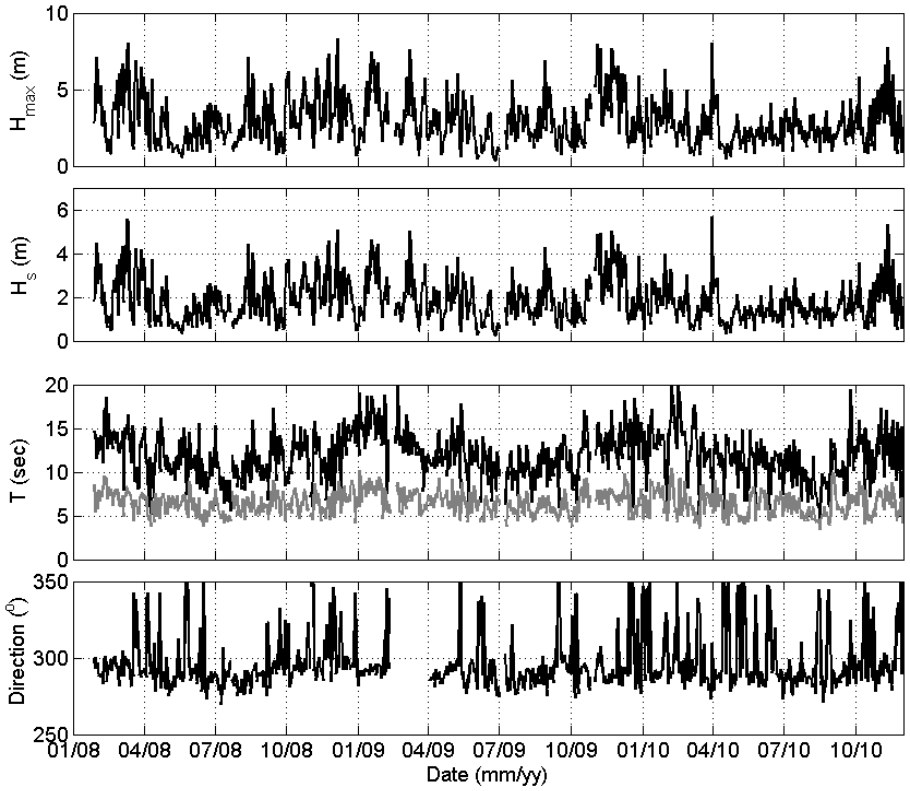

Figure 2.15– Summary wave statistics from the nearshore wave buoy at PPT (depth 10m CD) for 2008-1010. From top to bottom:H_{max}, H_s, T_p,T_z (grey), and wave direction.

The variability in wave direction evident in the bottom panel of Figure 2.15 is expressed more clearly in Figure 2.16 which shows the joint distribution of the main parameters. Dominant westerly waves form the majority of the wave directions, generated through the passage of north-east Atlantic low pressure systems; however, there is also a small but significant amount of energy from northerly waves which often occurs following sustained high pressures and northerly winds.

Table 2.3 - Summary wave statistics between 2008 and 2010.

	Min			Max			Mean			Std		
	2008	**2009**	**2010**	**2008**	**2009**	**2010**	**2008**	**2009**	**2010**	**2008**	**2009**	**2010**
H_s(m)	0.20	0.16	0.19	8.70	5.69	6.30	1.58	1.62	1.27	0.92	0.96	0.69
T_p(s)	2.10	1.90	2.60	18.4	19.2	17.3	10.31	10.81	9.99	2.77	2.88	3.19
T_z (s)	2.60	2.50	2.60	10.50	11.40	11.80	5.73	5.94	5.52	1.21	1.32	1.37
Dir (°)	-	-	-	-	-	-	284	282	286	17	17	25

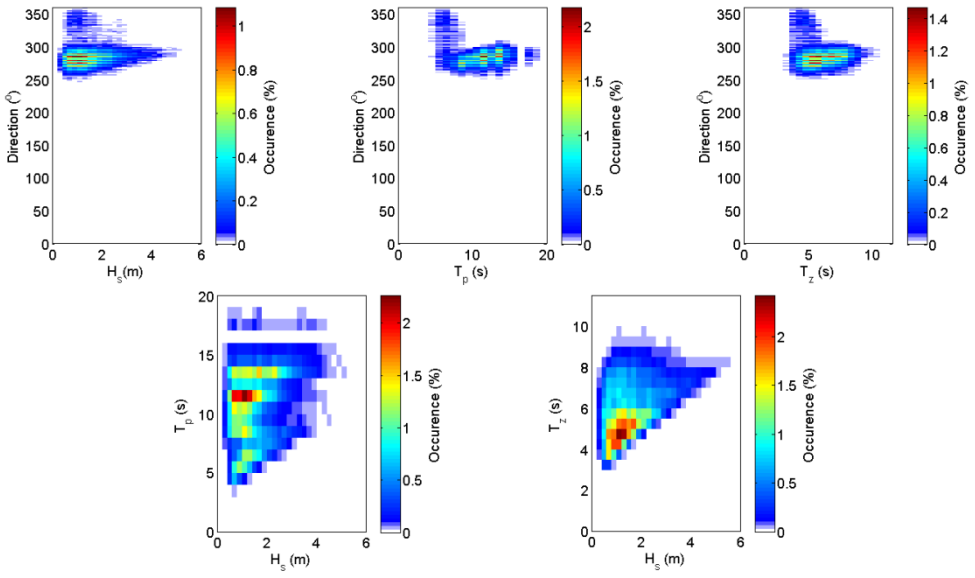

Figure 2.16– Joint distribution for H_s, T_p, T_z and direction for 2008 – 2010 from the nearshore wavebuoy at PPT.

Specific storm analysis for the survey period, with reference to morphological response, is undertaken in Chapter 4 using the measured wave data presented above. The exceedance values during the same period indicate a strong seasonal signal with increased wave conditions during the winter. The monthly distributions highlight peak

periods over the 3 years which occurred during March 2008, January 2009, November 2009 and November 2010 (Figure 2.17).

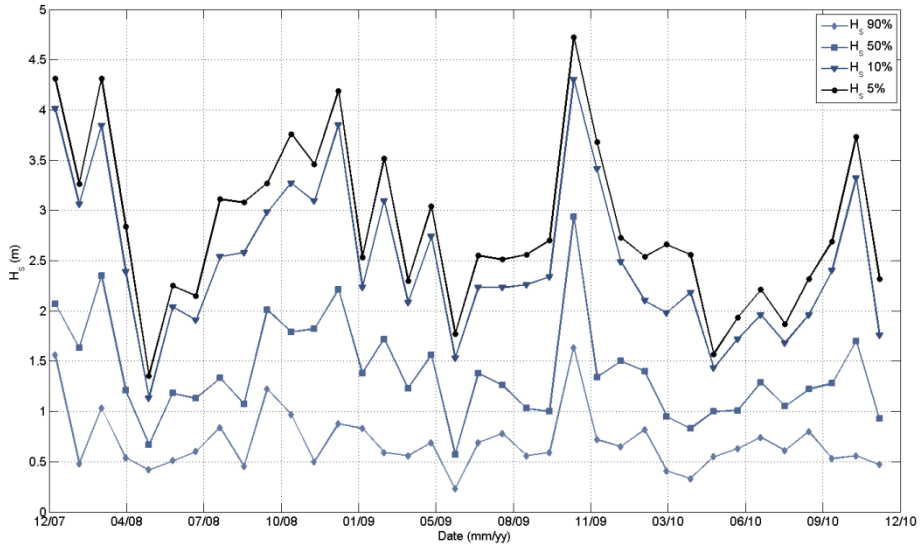

Figure 2.17– Monthly exceedance significant wave height for H_s90%, H_s 50%, H_s 10%, H_s 5%. Data taken from the wave buoy data (depth = 10m CD).

As well as the seasonal variability in the wave exceedance values, a gradual drop in heights is also present (Table 2.4). Supporting the trend shown with the hindcast wave data (Figure 13) the survey period experiences a drop in mean wave exceedance with 2010 the least energetic and subsequently least variable (Table 2.4).

Table 2.4 – Annual mean $H_s$exceedance statistics between 2008 and 2010 from the measured wave data.

H_sExceedance	Mean (m)			Standard deviation		
	2008	2009	2010	2008	2009	2010
H_s 5%	2.99	2.90	2.40	0.82	0.81	0.57
H_s 10%	2.62	2.59	2.04	0.75	0.76	0.50
H_s50%	1.47	1.40	1.15	0.49	0.59	0.25
H_s 90%	0.69	0.72	0.59	0.28	0.34	0.16

The majority of the wave data presented within this thesis is derived from the nearshore directional wave buoy (Figure 2.1), which is located to the north of GWT, CHP and PTN. Consideration of the alongshore variability in wave conditions between the sites due to the effects of refraction and shoaling needs to be addressed. Scott (2009) applied

a MIKE 21 third-generation spectral wind wave model to the north coast of Cornwall covering the area shown in Figure 2.1, which provided output nodes along the 15m (CD) contour for selected sites. More details of the model setup and boundary conditions can be found in Scott (2009); however, of principal interest for this work are the output values at the four sites (Table 2.5). Through wave shoaling and refraction, wave approach becomes increasingly shore normal in shallow waters: annual wave direction at P4 is 261°, compared with 284° recorded at the DWR off PPT (Table 2.3). Located at the northern end of St Ives bay, GWT is protected from large SW waves as waves refract around St Ives headland. In addition, Godrevy headland and the shallow water rock outcrops provide additional sheltering from any northerly wave approach (Figure 2.7). Subsequently, predicted modal wave heights at GWT according to Scott (2009) are ~25% smaller compared with the other sites, while storm conditions are ~35% smaller (Table 2.5). Variability between the relative energy levels at the northern sites is small: CHP and PPT have similar values while PTN is slightly less.

Table 2.5 – Variability in wave forcing between sites. Data derived from MIKE 21 spectral wave model as described by Scott (2009).

Site	H_s 10% (m)	H_s50% (m)	T_p(sec)	T_z (sec)
PPT	2.95	1.24	9.7	8.1
CHP	3.04	1.32	9.7	8.0
PTN	2.55	1.23	9.5	7.9
GWT	1.92	0.97	9.1	7.6

2.2.3 Wave Summary

The importance of accurate wave measurements for the assessment of morphological response is crucial. With limited nearshore records available reliance on one wave buoy requires an understanding of the temporal and spatial variability of such records for

further interpretation. Overall comparison with the available hindcast data indicates the survey period to be within a period of reduced storm occurrence which occurs every 15-20 years. The years 2008 and 2009 experienced very similar frequency of storms with 24 and 23, respectively, only 13 storms were experienced in 2010. Similarly storm durations were comparable for 2008 and 2009, with 760 and 800 hrs, respectively, compared with only 222 for 2010 (Figure 2.13). Although 2010 experienced a low number of storms relative to 2008/2009 the overall period is within the bounds of previous wave conditions.

2.3 Meteorology

Meteorological conditions are presented for the duration of the survey period in addition to river flow rates from the Red River located at GWT and the Perran River at PPT. River flows exhibit the strongest seasonal pattern with increased flows during the winter periods. Peak flows during the survey period in January 2008, February 2009, December 2009 and December 2010. Wind speed and direction show seasonal trends with calmer conditions experienced during the summer periods. Sustained strong winds are evident throughout most of November which correspond strongly with the increased wave conditions during this period (Figure 2.18). Similarly, wind direction is predominantly from the southwest (199°), although the northeasterly fluctuations reflect the wave direction shifts presented in Figure 2.15.

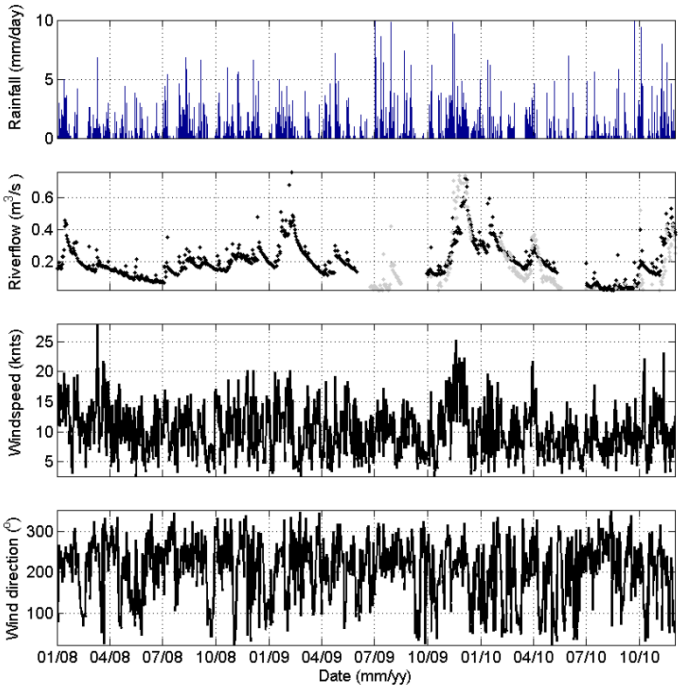

Figure 2.18– Summary meteorological conditions during the 2008–2010 survey period. From top to bottom: daily average rainfall, daily average river flow rate from the Red River at GWT (black line) and PPT (grey line), daily average wind speed and daily average wind direction from Perranporth. Rain and river data courtesy of The Environment Agency (2011), wind data courtesy of UKMO (2011). Gaps indicate missing or unavailable data.

Table 2.6 - Summary of the main meteorological parameters during the survey period 2008-2010.

	Min	**Max**	**Mean**	**Standard Deviation**
Rainfall (mm/day)	0	15.2	0.11	0.5
River flow, daily average (m^3/s), GWT	0.02	0.76	0.20	0.11
Wind speed (knts)	2.6	27.9	9.8	4.16
Wind direction (°)	22.6	351	199	77

From the long term hindcast wave data and the shorter term nearshore wave data together with the meteorological conditions we can identify periods of more energetic states and periods of relative dormancy in the forcing conditions. Specific periods of interest will be discussed further in Chapter 4 and such "events" will be identified from

morphologically-driven criteria (transitions between upstate and downstate morphology) and from storm-dominated wave conditions.

3 METHODOLOGY

3.1 Introduction

This project has utilised both *in-situ* and remote methods of data collection. In addition, data from third parties has been incorporated and novel analysis undertaken to better answer the research aims and objectives. This chapter details the principal methods and techniques used throughout the project including: (1) topographic surveys; (2) Argus images; and (3) wave data. Further techniques which are more specific to individual aspects of the project are introduced at the start of the relevant chapter.

3.2 Topographic surveys

The need for consistent, accurate and reliable beach topography forms a central part of this thesis, as well as most investigations into coastal processes. Such requirements have led to the development of field techniques to provide comprehensive data sets through space and time, and at the appropriate spatial and temporal resolution. Early approaches focused on 2D profile measurements through basic survey poles. Such methods are inexpensive, yet time consuming and rather restricted in spatial coverage. The need to map intertidal morphological features, such as berms and low tide bars, makes simple 2D profile measurements inadequate. Developments in GPS technology has resulted in increased accuracy, as well as more rapid data collection, allowing for greater spatial coverage with improved resolution.

Survey data presented here were collected using a real-time kinematic global positioning system (RTK GPS), which has become a standard tool to provide rapid data collection over a large spatial extent. By mounting the unit on an All-Terrain Vehicle

(ATV; Figure 3.1), the full intertidal region can be covered during spring low tide, providing coverage of morphological features at the relevant length scales.

Figure 3.1–ATV with RTK GPS handset mounted on the handle bar and receiver mounted on the front luggage rack

Monthly inter- and supratidal topographic surveys were conducted and analysed using:

- Trimble 5800 Receiver
    - 1 x base-station receiver (Figure 3.2)
    - 1 x ATV mounted rover receiver (Figure 3.1)
- Trimble TSC2 Handset (bluetooth connectivity)
- Survey measuring staff (for test points and areas beyond ATV access)
- Yamaha Grizzly 450 All Terrain Vehicle (Figure 3.1)
- Trimble Geomatics Office TGO© software
- Matlab©

Figure 3.2– RTK GPS base-station sited over a control point at PTN.

3.2.1 Survey Design

The use of RTK GPS requires a network of control points to be established close to the survey area. These were established prior to the survey schedule through post-processing of a stationary receiver that was installed over a fixed structure (e.g., survey pin or drain cover). This provides the *x*, *y* and *z* coordinates for this point in the local grid system (OSGB36). During a survey an initial receiver is set up as a base-station over the closest control point, ensuring line of sight with the rover receiver (located on the ATV; Figure 3.1). RTK GPS performs real time phase differential on the 3D vector between the rover and base antennas which is related via a radio link, providing increased accuracy in both horizontal and vertical precision of +/- 10mm and +/- 20mm respectively within 1 km of the base-station (Trimble, 2003). Figure 3.3 gives an example of the coverage attained using the ATV for rapid data collection obtained over a 3 – 4 hour survey period.

Figure 3.3– Aerial image of PTN, with survey points collected using the RTK GPS mounted on the ATV. Survey date and aerial image are not concurrent, and the two 'gaps' in the coverage at the seaward extent of the survey are caused by the presence of two large rip channels present during the survey.

3.2.2 RTK GPS

The use of GPS for surveying has become standard within industry and research. While RTK GPS helps to increase the survey precision, consideration of sources of error within the whole survey technique is important. The use of an ATV requires offsetting the vertical position of the antenna phase centre within the receiver head, and measurement of this offset is made on the beach and is subject to the ATV position. During normal use the ATV will adjust to ground features through its suspension system changing the relative position of the receiver. The presence of a steep slope will offset the vertical distance of the receiver head above the actual bed level. Because of the highly dissipative nature of the sites, particularly the dominant low tide morphology of interest, this possible error was not believed to be significant.

During consideration of the survey technique to be adopted, comparison of a single 2D profile line was undertaken to address the level of variability. The methods examined include: (1) on foot with a pole mounted receiver; (2) on an ATV (driven along the line); and a single cross-shore transect extracted from an interpolated surface generated from

an irregular grid of ATV mounted points. This identified a mean vertical error of ca.50 mm and a maximum variation of ca.80 mm. These error estimates are considered within tolerance for the large survey extents and the monthly survey intervals, and are offset by the ability for rapid data collection and for the interpretation of large scale morphological features.

3.2.3 Survey Area

The selection and designation of sites for long-term monitoring was based on consideration of: (1) locations most likely to be affected by the development of the offshore Wave Hub; (2) beach type; and (3) recreational use. The four sites extend either side of the main region likely to be affect by the Wave Hub, thereby ensuring full coverage of impacts (Millar, Smith & Reeve, 2007). To the north, PPT experiences the greatest recreational pressure through beach users, and has already undergone further studies into rip dynamics (Austin et al., 2010), and beach safety (Scott *et al.*, 2007), and benefits from having an Argus station in place (Davidson *et al.*, 1997).

The specific survey areas vary between sites from 400 to 500 m in the cross-shore and 800 to 1200 m in the longshore (Figure 3.4). With a GPS sampling rate of 1Hz a total of >3500 to >8000 individual elevation points are recorded for the smallest to the largest site, respectively.

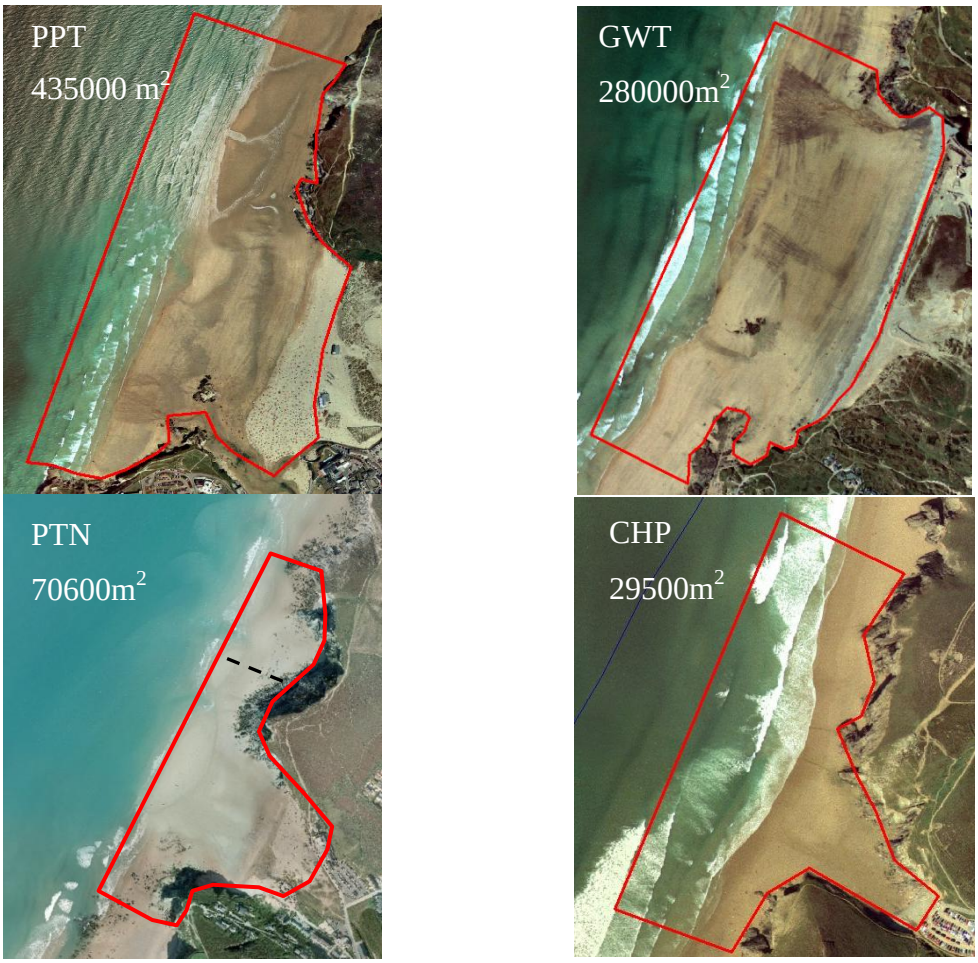

Figure 3.4– Aerial view of the four study sites: Perranporth (PPT); Gwithian (GWT); Porthtowan (PTN); and Chapel Porth (CHP). The approximate study area is detailed in red and north is at the top of the photographs for all sites. The dashed line for PTN shows initial survey extent for the first 8 months. The total area (m^2) is listed next to each site.

3.2.4 Survey Schedule

The survey schedule was designed to provide the most comprehensive data coverage from 4 sites within a cost and time-effective approach. With the project focused on the 3D morphology response, cross-shore profiles would not have been sufficient to capture the extent and dynamics of these features. Therefore an area covering the intertidal region for each site was mapped during each survey (Figure 3.4). With 4 sites to be covered it was decided this was best achieved through monthly surveys during the lowest spring tide. Tidal predictions were utilised to identify the lowest spring tide which varied between -2.4 m and -3.1 m (ODN).

Where possible post-storm surveys were undertaken to capture specific changes in response to energetic conditions. However, owing to the large tidal range in the region and the particular interest to the low tide morphology, these surveys were restricted to the closest spring tides.

3.2.5 Processing and Accuracy

Post-processing of GPS data is minimal where RTK coverage is attained owing to the computed real time phase differential (Trimble, 2003). Further quality control is undertaken during data processing, such as removal of data outside the survey area or points deemed unfit during the survey period. This includes comparative assessment of individual survey points recorded in close spatial proximity at different times. Accepted survey data is then extracted for further analysis. The eastings, northings and elevation points were logged using the OSGB36 Ordnance survey grid, and were subsequently then transformed with rotation and translation onto a local alongshore/cross-shore coordinate system which was identical to the grid used by the Argus video data (see below) to aid interpretation and comparison.

The generation of a 3D digital elevation map (DEM) is the final stage in the spatial data processing. As the basis for subsequent interpretation and analysis a reliable quadratic loess interpolation approach was adopted (Plant, Holland & Puleo, 2008; Schlax & Chelton, 1992).This technique is based on a form of linear interpolation which provides a scale-controlled interpolation method which minimises the effects of measurement error and aliasing. Within this the user can define the grid spacing on which to interpolate, the smoothing scales and the maximum permissible error. This approach allows control over the level of filtering and errors in the interpolated data which ensures preservation of features whose length scale are longer than 2 times the

smoothing scale (Plant, Holland & Puleo, 2008). The use of quadratic loess interpolation has been shown to be most suited to regularly spaced data, which best describes the grid structure used during beach surveys. For all the sites, raw data was interpolated onto a regular 2 m grid using smoothing scales of 5, 10, 20, 40 and 50 m, with a maximum permissible error of 0.05 m.

3.3 Topographic Analysis

Following interpolation of the intertidal survey data onto a regular grid with the loess interpolation routine, standard data products were generated, including intertidal volume and 2D cross-shore profile line extraction.

3.3.1 Volume

Calculation of the intertidal beach volume was undertaken for each site and each survey from the interpolated surface. Because of the highly dynamic nature of the low tide region, which restricted survey coverage and therefore subsequent comparison with previous surveys, a reduced region was defined (Figure 3.5). For each site, the intertidal volume was split into 3 regions to differentiate between the upper, mid and lower beach. The definition of these regions was based on the relative tidal position for each site(Figure 3.5); Upper beach = > MHWN; mid beach = MHWN to MLWN; and lower beach = <MLWN.

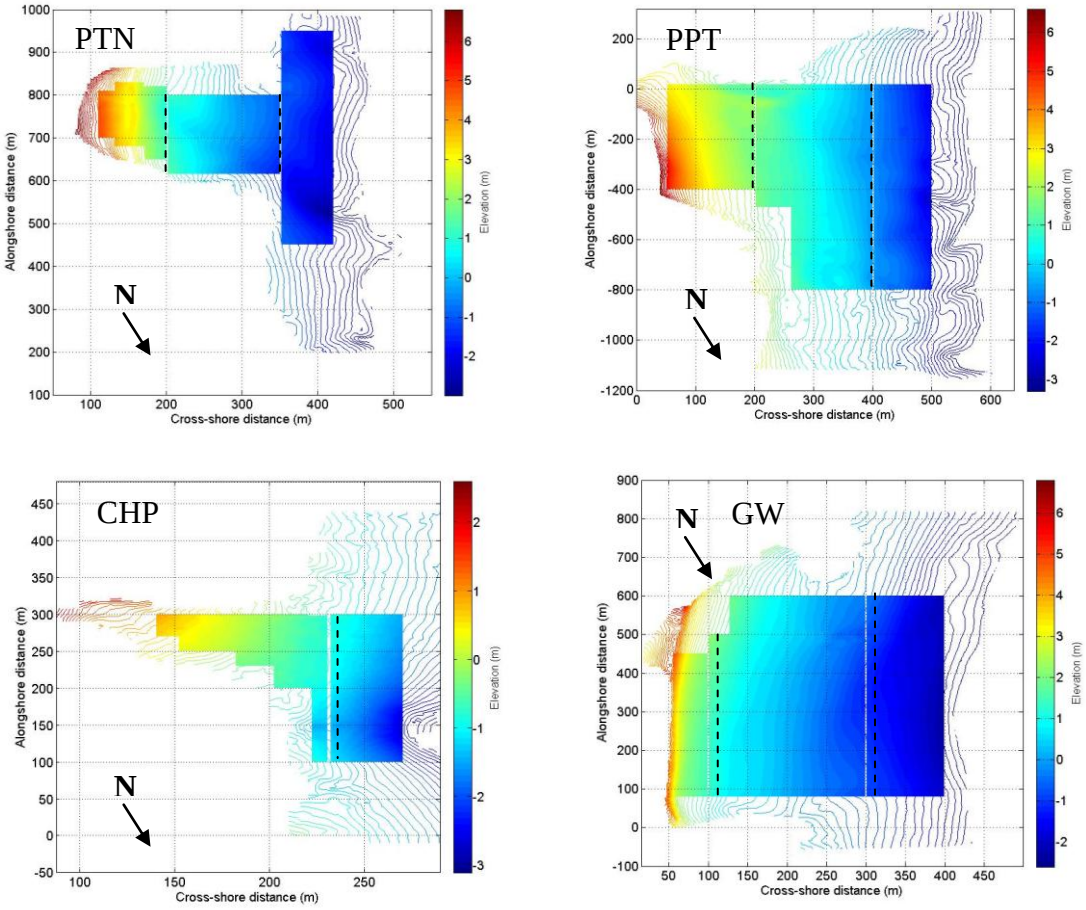

Figure 3.5– Contour plots for PTN, PPT, CHP and GWT showing a nominal survey area with the optimum region from which the volume can be calculated. Black dashed lines represent boundaries between upper, middle and lower beach based on approximate tidal elevations. Note CHP does not have a separate upper region owing to the exposed rocks in this area.

Volumes were then calculated by doubling the summed the area (because of the 2m interpolation) below the surface (down to -4m) for each region providing the total volume for each section in m^3. For surveys where the coverage of the original survey was more than 90% and less than 100% of the volume calculation area, a simple linear interpolation was used to extend the survey coverage. This was undertaken for calculation of the intertidal volume only to improve comparison with other surveys throughout the monitoring period and was not applicable to subsequent surface analysis. Where the survey coverage was <90% for an individual region, sediment volumes were not computed for that survey.

3.3.2 Profile extraction

In addition to 3D surface analysis, specific 2D cross-shore profiles were extracted from the interpolated surfaces for further investigation (Figure 3.6). Profile location was chosen to represent each site and the different morphology present. Where possible, locations affected by river outflow were avoided to focus the assessment of morphological response from wave action.

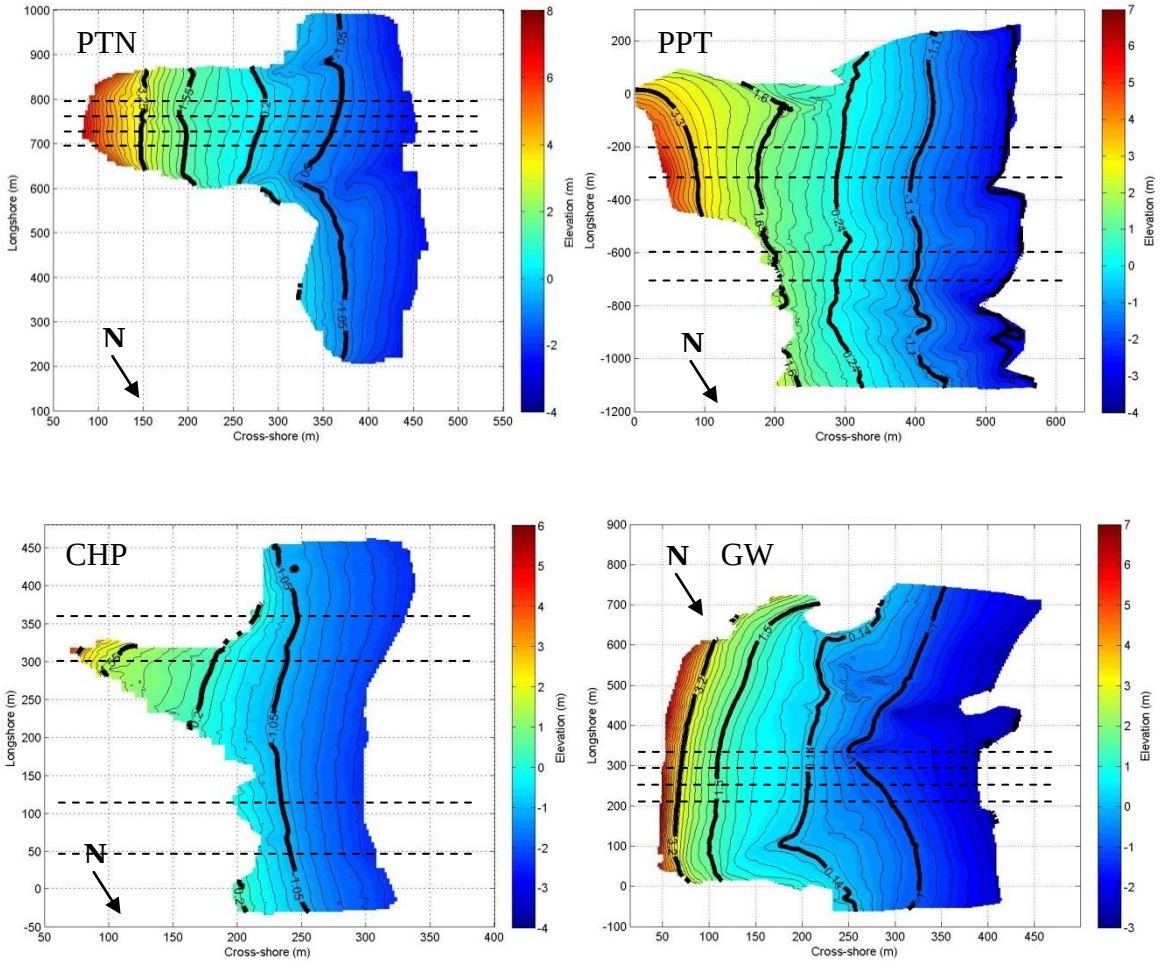

Figure 3.6– Surface plots for the 4 sites showing cross-shore positions of profile extraction. Lines were selected to provide greatest variability whilst minimising influence from river inputs or intertidal exposed rocks.

3.4 Bathymetry

The extension of the survey area into the subtidal zone is not possible using terrestrial devices; such data are only available through nearshore bathymetric surveys. Initial project objectives incorporated nearshore surveys to further extend the intertidal monitoring and incorporate subtidal sediment supplies. However the energetic nature of this region, the large tidal range, inhibitive costs and the distance to a safe port meant such surveys were unable to be undertaken with the optimum regularity.

Whilst regular subtidal data collection was not possible, bathymetric data for PTN, PPT and CHP were provided by the Channel Coastal Observatory (www.channelcoast.org), following a single survey in 2008. These data were collected using a single beam echosounder which mapped 1km shore-normal lines at 50m spacing (Figure 3.7). These datasets were then interpolated onto a regular grid using the loess interpolation technique described in Section 3.1.6. Where available, intertidal survey data was merged with the bathymetric datasets to create a full profile for the site (Figure 3.7). Full profiles from PTN were used for XBeach modelling, discussed in Chapter 6.

Owing to the lack of available bathymetric data for GWT, a nearshore survey was undertaken using a single beam Valeport MIDAS surveyor. Data was collected along 1km cross-shore transects with 50m spacing. Wave and tide correction was applied using RTK GPS which logged the sensor position continuously during the survey, which could then be used to reduce the depth soundings.

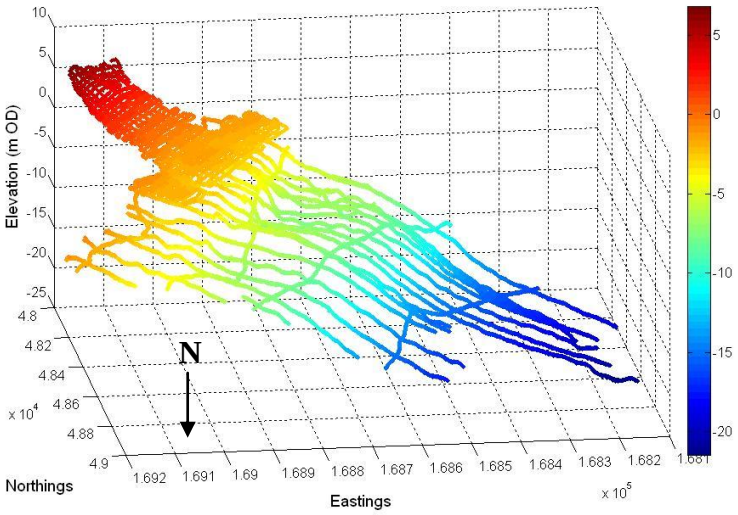

Figure 3.7 –Distribution plot of subtidal data from the Channel Coastal Observatory integrated with the intertidal topographic survey at PTN (July 2008).

3.4.1 Sediment samples

Surficial sediment samples were collected from each of the sites during the monthly topographic surveys. Owing to the size of the survey areas 3 samples were collected to represent the full intertidal range, at the spring low tide level, mean sea level and spring high tide level. Grain size analysis was undertaken using settling techniques which provides the grain settling velocity distribution. The measured settling velocity accounts for the particle density and shape, as well as its diameter, and better represents the hydraulic behaviour of the sediments while being transported by waves and currents. In addition, this approach is much quicker and requires smaller samples, although the samples are no longer available for further analysis. Settling analysis was undertaken using the settling tower shown in Figure 3.8 following the methodology described by Komar (1985).

Figure 3.8– Settling tower used for sediment analysis. Scales are located at the top of the tower connected to a flat disc which is suspended 2.17 m below at the base of the tower.

The settling tube shown in Figure 3.8 is 2.5 m tall with a diameter of 0.22 m. An electronic balance is located at the top of the tower which supports a tray suspended by thin nylon line at the base of the tower 2.17 m from the water surface. Samples from each location were washed to remove any organic material and any salt water. Each sample was then split using a mechanical splitter into 3 samples each approximately 5–8 g in weight. The samples were moistened and then placed on an inverted petri dish which held the sample until contact with the water at the top of the tower, causing the sample to settle through the water column onto the balance tray. The balance records the cumulative weight on the tray at a resolution of 1 mg and the weight is logged on a computer at 2 Hz.

The logged settling times are then converted to a settling velocity which was used to calculate standard statistical properties including the mean (eq.3.1), the sorting (eq.3.2) and the skewness (eq.3.3) of the settling distribution using the method detailed by Folk and Ward (1957). The psi measure (ψ -log2w) was used in place of the standard phi measure (ψ -log2d) for grain size.

$$Mean = \frac{\psi_{16} + \psi_{50} + \psi_{84}}{3} \quad 3.1$$

$$Sorting = \frac{\psi_{84} - \psi_{16}}{4} + \frac{\psi_{95} - \psi_{5}}{6.6} \quad 3.2$$

$$Skewness = \frac{\psi_{16} + \psi_{84} - 2\psi_{50}}{2(\psi_{84} - \psi_{16})} + \frac{\psi_{5} + \psi_{95} - 2\psi_{50}}{2(\psi_{84} - \psi_{5})} \quad 3.3$$

The percentiles were taken from the cumulative weight distribution. The mean settling velocity was then used to derive the mean grain size using Hallermeier (1981):

$$D_{50} = \frac{0.91\, w^2}{\gamma' \mathrm{g}} \quad 3.4$$

Where w is the settling velocity, γ' is the specific density (1.65), and g is the acceleration due to gravity (9.8).

3.5 Argus

In addition to *in-situ* measurements of beach morphology, remotely sensed images are collected at PTN and PPT. An existing site at Perranporth (2 cameras), which was first established in 1993 (Davidson *et al.*, 1997), was re-established following replacement cameras in 2006 (Figure 3.9).

Figure 3.9– Argus cameras at PPT with the field of view shown on the aerial insert.

At PTN a new Argus installation consisting of 4 cameras covering the full intertidal beach and offshore bar/rip system was installed in September 2008 (Figure 3.10). Both sites provide half hourly digital "image products" consisting of a single snapshot image, a time-exposure image and a variance image (Holman & Stanley, 2007). As detailed in Section 1.3.9 of principal interest for this study are the 10 min time exposure (timex) images which are used for the identification of the waterline at the beach face (Plant & Holman, 1997), the sub-tidal bar position (Lippmann & Holman, 1989) and the presence of rip channels (Ranasinghe *et al.*, 2004). For both sites, conversion from image coordinates (*u*, *v*), to real world co-ordinates (*x*, *y*) was undertaken using well established methods for Argus video systems (Holland *et al.*, 1997). The technique requires real world coordinates from fixed locations (ground control points) to be recorded and visible in the images from each camera and ideally where images overlap. These ground control points can then be used to geo-reference the images producing a geometry solution for each camera at the site. This will remain constant provided the cameras are stable and will allow oblique video images to be rectified onto real world coordinates (Holland *et al.*, 1997).

Figure 3.10 – Sample images from each camera at PTN. The top row shows the "snap" images, while the bottom row represents the "timex" version from the same time. The two central images provide more focus of the nearshore zone , while the outer images cover the full intertidal region

The spatial footprint of each pixel within a digital image will determine the spatial resolution of that region for a rectified image. This fact is also influenced by the slant angle of the cameras viewpoint which will vary within an image. Therefore areas close to the cameras will have a greater spatial accuracy than those further afield (Figure 3.11, Holman & Stanley, 2007).

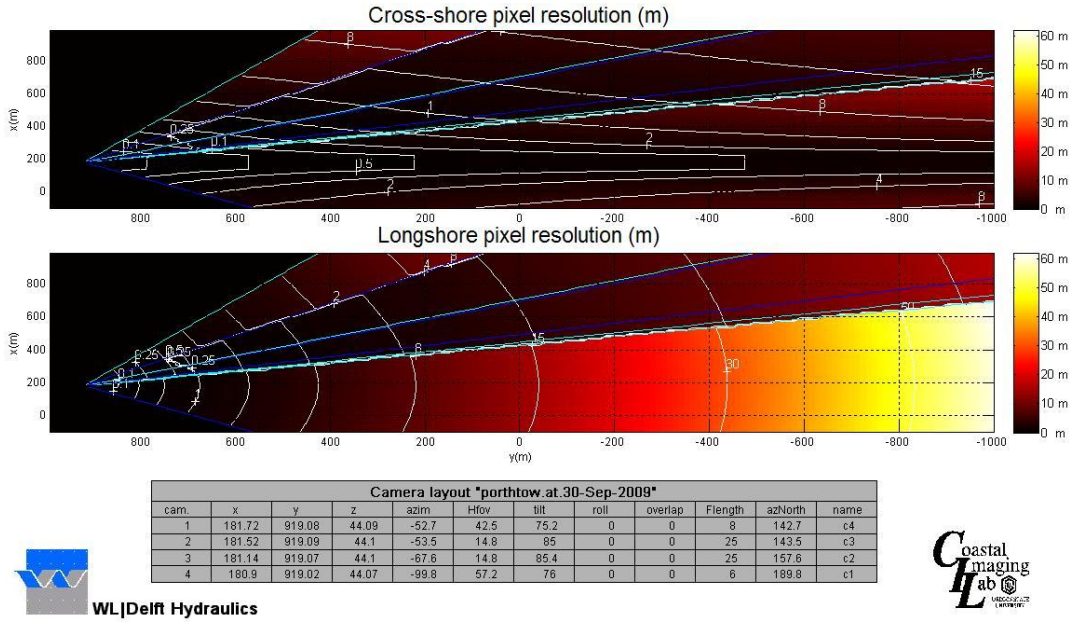

Figure 3.11 – Cross-shore (upper) and longshore (lower) pixel resolution maps for PTN. The different resolutions for each of the 4 cameras are the result of the different focal lengths of the camera lenses.

3.5.1 BLIM

As outlined in section 1.3.9 the detection of subtidal bar positions was one of the first tools identified from Argus images (Lippmann & Holman, 1989). Enckevort and Ruessink (2001) further developed this idea with a detection algorithm which finds the maximum intensity value for cross-shore pixels and which has specific relevance to regions of high intensity where wave breaking occurs. The BarLine Intensity Mapper (BLIM) provides a useful method to utilise this algorithm for the detection of bars from rectified Argus images (Figure 3.12). The ability to define a region of interest allows the

user to reduce error caused by shoreline breaking and other features. In addition, the bar line can be manipulated to compensate for any artefacts within the images, such as water droplets on the lenses which distorts rectified images.

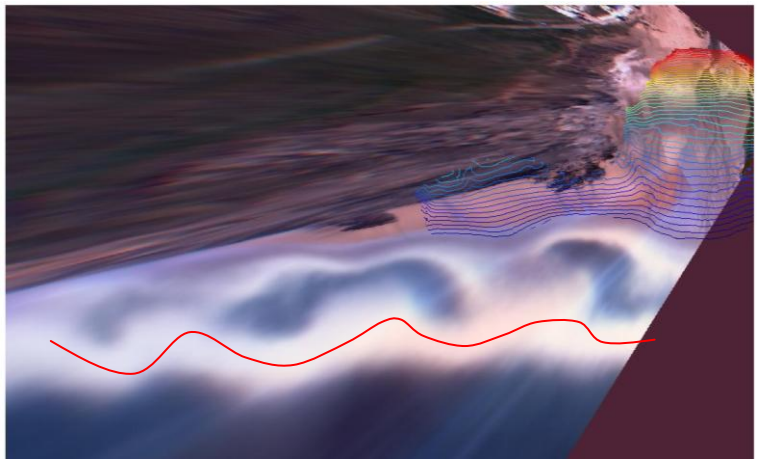

Figure 3.12 – Rectified plan-view Argus image from PTN showing the rip channels and the subtidal bar (red line) which has been identified using the BLIM tool. The intertidal beach morphology from a RTK GPS survey has also been overlaid as a contour plot for the upper beach.

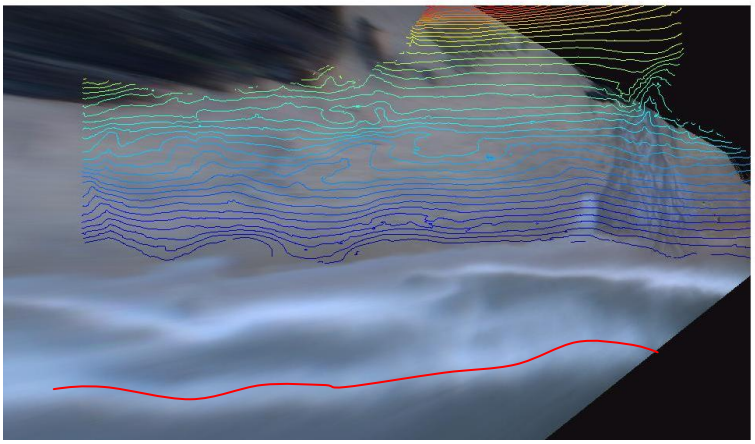

Figure 3.13– Rectified plan-view Argus image from PPT showing the rip channels and the subtidal bar (red line) which has been identified using the BLIM tool. The intertidal beach morphology from a RTK GPS survey has also been overlaid as a contour plot for the upper beach.

As commented, the positional accuracy of this approach is affected by breaker height and water level (Kingston *et al.*, 2000; van Enckevort & Ruessink, 2001). Owing to the energetic conditions and the macrotidal range, the number of suitable images for BLIM

analysis is constrained before image quality is considered. Therefore for the purpose of this work the following criteria were applied to select suitable images:

- Water level between -3.5 m and -2.5 m (ODN) for PPT, and -2.8 m and -1.5 m (ODN) for PTN
- Wave height H_s = >0.5 m and H_s = <1.5 m providing greatest chance of wave breaking on the bar, without causing excessive increased breaking zone which would reduce positional accuracy.

This approach combined with the need for good quality images severely limits the number of "useful" images available to be mapped. Although cross-shore position is not the primary export from these images, these thresholds allow interpretation of the long-term migratory patterns of bars to be linked with wave conditions. Of greater significance, however, are the bar shapes (e.g., *rhythmic crescentic, transverse, detached*) which can readily be identified from the rectified images.

Because of the restrictive criteria detailed above, there are often periods where no images are suitable. However, the principal application of the Argus images is to increase the temporal monitoring of the beach systems to reduce the need for *in-situ* measurements. To utilise this, images were merged for each low tide period providing a daily record of conditions. Once significant shifts in bar dynamics were identified through the BLIM images outlined above, further qualitative analysis was undertaken to extract periods of bar change. This approach allows identification of temporal bar behaviour which can then be incorporated into the intertidal beach surveys and the wave analysis.

3.6 Wave Data

Wave conditions are recorded using a Datawell Directional Wave-rider Mk III (DWR), which is deployed in ~10m water depth (Chart Datum) west of Perranporth (Figure 3.14). The buoy is owned and operated by the Channel Coastal Observatory (CCO; www.channelcoast.org,) and data can be obtained freely via a dedicated website.

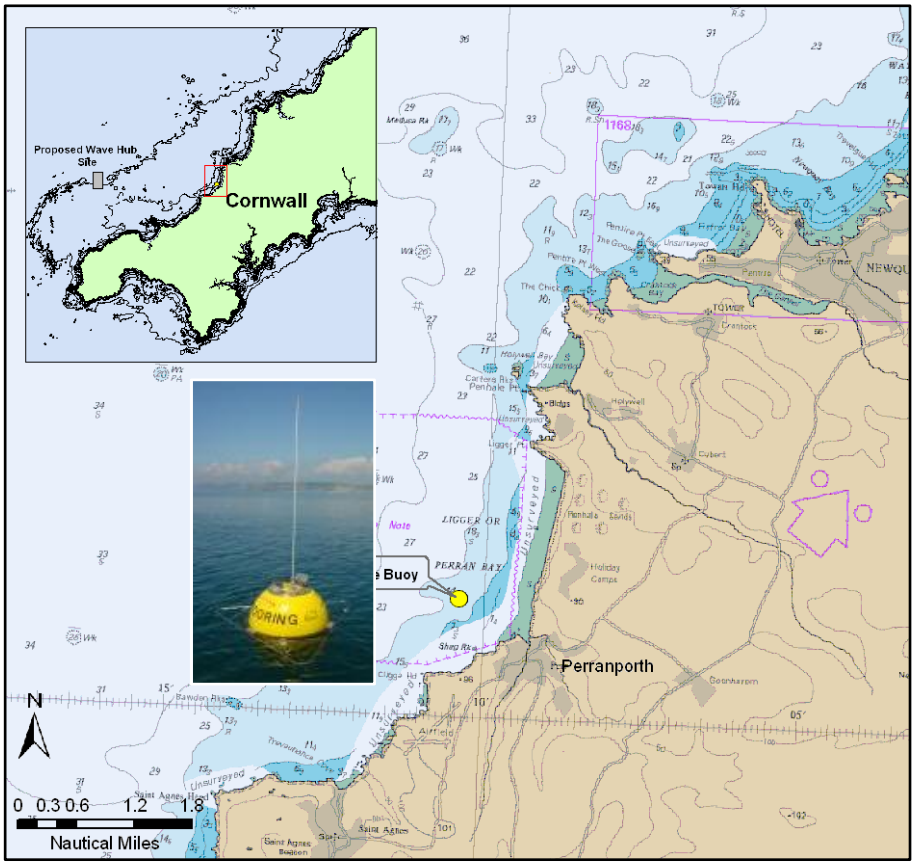

Figure 3.14–Location of the wave buoy deployed off PPT in approximately 10m CD. Chart courtesy of Marine Digimap;photo courtesy of www.channelcoast.org.

The buoy was deployed in December 2006 and has provided a near-continuous data series to date. During February 2009 following routine servicing the buoy developed a fault evident in the directional data which had a strong tidal signature. The buoy was

replaced and data collection resumed[2]. Wave conditions are measured by the buoy for 30 minutes at 3.84 Hz, and then transmitted at a reduced sampling frequency of 1.28 Hz to the shore station, where the wave parameters are calculated. Owing to the depth and proximity of the buoy to the beach no significant shoaling is expected before waves reach the shoreface and as such no transformation of wave parameters is undertaken. This assumption was supported by Austin *et al*. (2010), who used a pressure sensor deployed at LWS to compare wave heights with the nearshore buoy and found good correspondence between the offshore and inshore wave signals. There are 3 types of files which are provided by the DWR (.spt, .csv, and .raw) with the full details of each provided in Appendix 1.

Spectral partitioning was undertaken to quantify the relative importance of low-frequency (swell) and high-frequency (wind) components in the nearshore wave climate (Figure 3.15). Wave spectra were computed for each 17-min survey period from the wave buoy, allowing set criteria to be used to determine the energy contained within the various frequencies. The Datawell directional Waverider spectra provides 64 spectral frequencies with frequency spacing of 0.005 Hz up to 0.1 Hz, and at 0.01 Hz beyond.

[2] However a small tidal signal is still evident in the wave direction and the wave spreading data, despite further investigations by CCO no explanation is available, and this data was not used for further analysis.

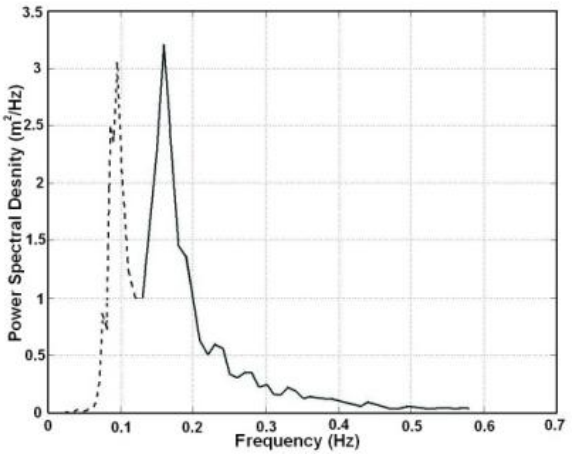

Figure 3.15–Example of spectral partitioning computed from the Perranporth Datawell Directional Waverider. The dashed line indicates a predominant low frequency (swell) component, while the black line identifies the high frequency (wind) waves.

The spectra are characteristically bi-modal and were split using the spectral trough between the longer period swell and shorter period wind waves (Figure 3.15). While set thresholds work in the majority of cases (e.g., partition at 0.1Hz), the growth and decay in swell events required peaks to be tracked as they move through the spectrum. The most consistent approach was found by first identifying the location of the spectral peaks and then using these to identify the biggest trough where the partition could be made.

A wave groupiness factor *GF* was calculated following Wright *et al.*(1987) based on the groupiness time series g_t generated by low pass filtering the modulus of the water surface elevation time series (reduced to zero mean and scaling the result with a factor of $\pi/4$);

$$GF = \frac{\sqrt{2\sigma_g}}{\bar{g}_t} \qquad 3.5$$

where σ_g is the standard deviation of g_t and $\bar{g}_t$ is the mean of g_t. This provides a *GF* with a range of 0 to 1, where 1 represents highly grouped waves and 0 represents a sea

state with no clear variability in wave amplitude. With raw heave data available from the wave buoys since December 2006, *GF* was calculated for each 17-min sampling period. This provided over 4000 values during the survey period. These were then averaged to produce a daily time series $\overline{GF}$.

3.7 Water level data

Reliable local water level data is crucial for Argus image analysis, as well as the interpretation of hydrodynamics with respect to morphological response. Whilst tidal predictions are available and provide a forecast from which the surveys could be planned, local wave and meteorological conditions can have a significant impact on the observed still water level at the shoreline. Therefore tidal elevation was recorded using two self-logging RBR Tide Wave Recorders (TWR) 2050. Deployed at PTN and PPT, the loggers are held within rock-mounted scaffold tubes and are exposed for ~1 hour either side of spring low water (Figure 3.16).

Figure 3.16–RBR TWR mounted to a low tide rock at PTN, insert shows the TWR extending from the scaffold tube during replacement.

Tidal elevation was burst-sampled every 15 min at a rate of 2 Hz, with a 2 min average time. Wave data was burst-sampled every hour with 1024 samples at a rate of 2Hz; however, the location of the sensors (in the lee of a low tide rock, in front of a cliff face) means wave records are unreliable. Data were downloaded every 2–3 months as conditions and access allowed.

Data quality control was undertaken to remove spikes, jumps, out of range values (based on the predicted range) and anomalous points. Within the RBR processing package water depth is calculated using a default value for atmospheric pressure. To adjust this for local atmospheric pressure, meteorological data from PPT was collected using a LaCrosse WS-3600 weather station with air pressure resolution of 0.1 hPa. The sensor was situated less than 1 km from the PPT site, and 10 km from the pressure gauge at PTN. Mounted at approximately 50 m (ODN) the record was adjusted to sea level and then used to correct the water level measured by the TWR. For periods of exposure during spring low water resulting in gaps in the tidal record, tidal harmonics were used to interpolate the low water record.

4 MORPHOLOGICAL RESPONSE ON HIGH-ENERGY MACROTIDAL BEACHES[3]

4.1 Introduction

Most studies of nearshore morphodynamics have focused on micro-mesotidal environments over a range of spatial and temporal scales while comparative macrotidal studies are less prevalent (Battiau-Queney et al., 2003; Masselink *et al.*, 2007; Reichmüth & Anthony, 2007). The importance of short-term beach response to hydrodynamic conditions is clear and such studies have done much to further our understanding of coastal processes and as such help advance model capabilities (Wright, Short & Green, 1985). Although there have been several medium to longer term (> 1 year) studies into the behaviour of high-wave energy/macrotidal environments (Jago & Hardisty, 1984; Reichmüth & Anthony, 2007), as well as more intensive short-term studies (Masselink *et al.*, 2007), these datasets have used multiple cross-shore profiles at varying alongshore spacing to assess beach response. Work by Ruggiero *et al.*,(2005) and Hansen and Barnard (2010) has utilised longer three dimensional (3D) datasets (~ 5 yrs) to assess seasonal variability for more energetic mesotidal siteswith a focus on larger scale shoreline response and beach management.There remains an obvious paucity of consistent, detailed 3D morphological data from energetic macrotidal sites.

[3] This Chapter contains work previously presented in the following papers included in Appendix 3;
Poate, T. G., Kingston, K. S., Masselink, G. & Russell, P. (2009) 'Response of high-energy, macrotidal beaches to seasonal changes in wave conditions: examples from North Cornwall, UK', Car (ed. *10th International Coastal Symposium*. Lisbon, Portugal Journal of Coastal Research, SI 56, pp. 747-751.
Poate, T. G., Austin, M.A., Masselink, G., Russell, P. and Kingston, K. S. (2011) 3D Beach Response to energetic wave climate, Cornwall, UK.*7th Coastal Sediments*. Maimi Florida World Scientific, pp 1893-1906.

Exposure to energetic wave conditions responsible for driving sediment transport which results in rapid profile response is seen most noticeably on micro-mesotidal beaches (Komar, 1998). The presence of a large tidal range forces the transitions of morphodynamic zones across the shore face resulting in morphological features being suppressed (Short, 1996). The complex dynamics exhibited through more subtle cross-shore and longshore morphological change requires 3D analysis over a wide spatial extent to promote understanding of such systems as a whole. Beaches at the intermediate/dissipative beach state boundary exhibit quasi-seasonal low tide bar/rip systems which are of significant interest to beach users in terms of surfing and as potential hazards (Scott *et al.,* 2007). The complex sensitivity of 3D morphology to shifts in forcing conditions requires a multifaceted approach to further understand the dominant processes and the subsequent beach response.

This chapter comprises the first long-term (3 year) data set of monthly 3D morphological survey data collected at four high energy macrotidal beaches. RTK – GPS survey data is supported by almost continuous Argus images at two sites and information on the hydrodynamic forcing is provided by a nearshore directional wave buoy. The principal aim of the data set is to assess the nature and variability of the morphological response at each site to the seasonal and storm-induced variations in the hydrodynamic forcing conditions. Within this central aim more detailed objectives can be addressed: 1) identify the variability in 3D morphology between the four sites; 2) identify site-specific up-state/down-state response behaviour; 3) characterise site specific response to storm conditions; and 4) quantify the temporal and spatial variability of response under normal and storm conditions.

The methodology used is described first (Section 4.2), followed by a summary of the response and observations of each site (Section 4.3) and then combined characteristics and comparisons of the different morphodynamics and volume responses for the different sites (Section 4.4). Classification of the 3D variability and beach states is then introduced in Section 4.5 followed by an assessment of the subtidal response identified using Argus images (Section 4.6). Specific storm/transitionary episodes are then explored in more detail before a discussion and summary of the central findings.

4.2 Methodology

The overall methodology is introduced in Chapter 3 but the following section describes some of the more specific tools which were used to aid the interpretation and analysis of the long term morphological response observed.

4.2.1 Momentary Coastline

As coastal monitoring has evolved, through the need for greater management of these resources, the definition of a beaches relative stability has been assessed through various coastal state indicators (CSI). Of these the momentary coastline position provides a quantitative approach which incorporates the volume of sand between two horizontal planes (van Koningsveld & Mulder, 2004). This can then be used to examine the long term behaviour of a site and allows coastal managers a reference from which to make decisions about defensive works. Figure 4.1 gives an outline of the method used to calculate the momentary coastline adopted by van Koningsveld and Mulder (2004) after Min V&W (1991). This approach was adopted as a measure of the system as a whole to quantify the longer term coastline stability for the four sites.

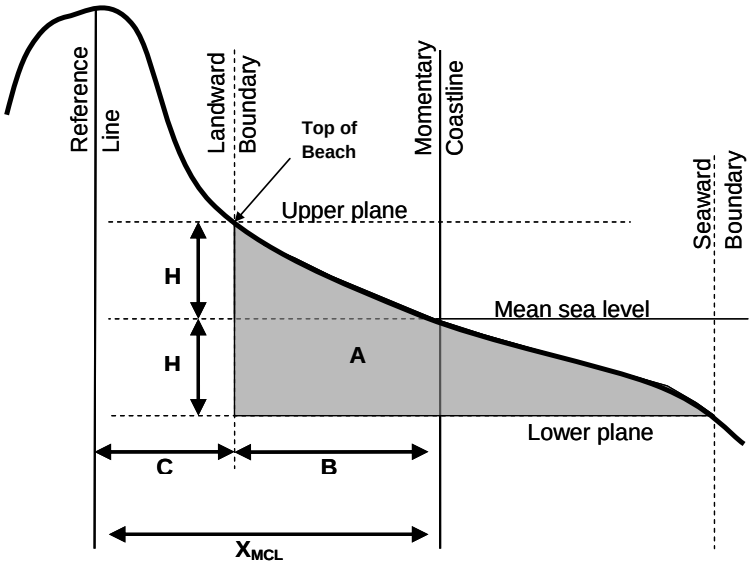

H = Height between top of beach and mean sea level
A = Momentary Coast line Zone m^3
B = A /2H =Momentary Coast line position (m)
C = Distance from top of beach to reference (m)
X_{MCL} = B+C

Figure 4.1– Calculation of Momentary Coastline (MCL), adapted from van Koningsveld and Mulder (2004) after Min V&W (1991).

Van Koningsveld and Mulder (2004) used the Dutch JARKUS dataset which provides yearly cross shore profiles extending 1 km from the top of the beach seaward. Due to the limited cross-shore extent available from the survey data, the intertidal momentary coastline(FBX_{MCL}) was calculated for the region between an upper plane of 2.6 m (MHWS) and extending down to a lower plane of -2.2 m for PPT, PTN and GWT (Figure 4.1). The limited upper beach at CHP made calculation of the FBX_{MCL} impossible. To express the cross-shore variability of the profile position, the momentary coastline was also calculated for a lower region (LBX_{MCL}) between 0.2 m (MSL) and -2.2 m. This approach also allows greater alongshore coverage for the sites which open up below MSL. For each site cross-shore lines were extracted with a 2 m longshore spacing within the regions shown in Figure 4.2, for each line the FBX_{MCL}& LBX_{MCL}

was computed and a monthly average was calculated, providing a time series of the momentary coastline position for each beach.

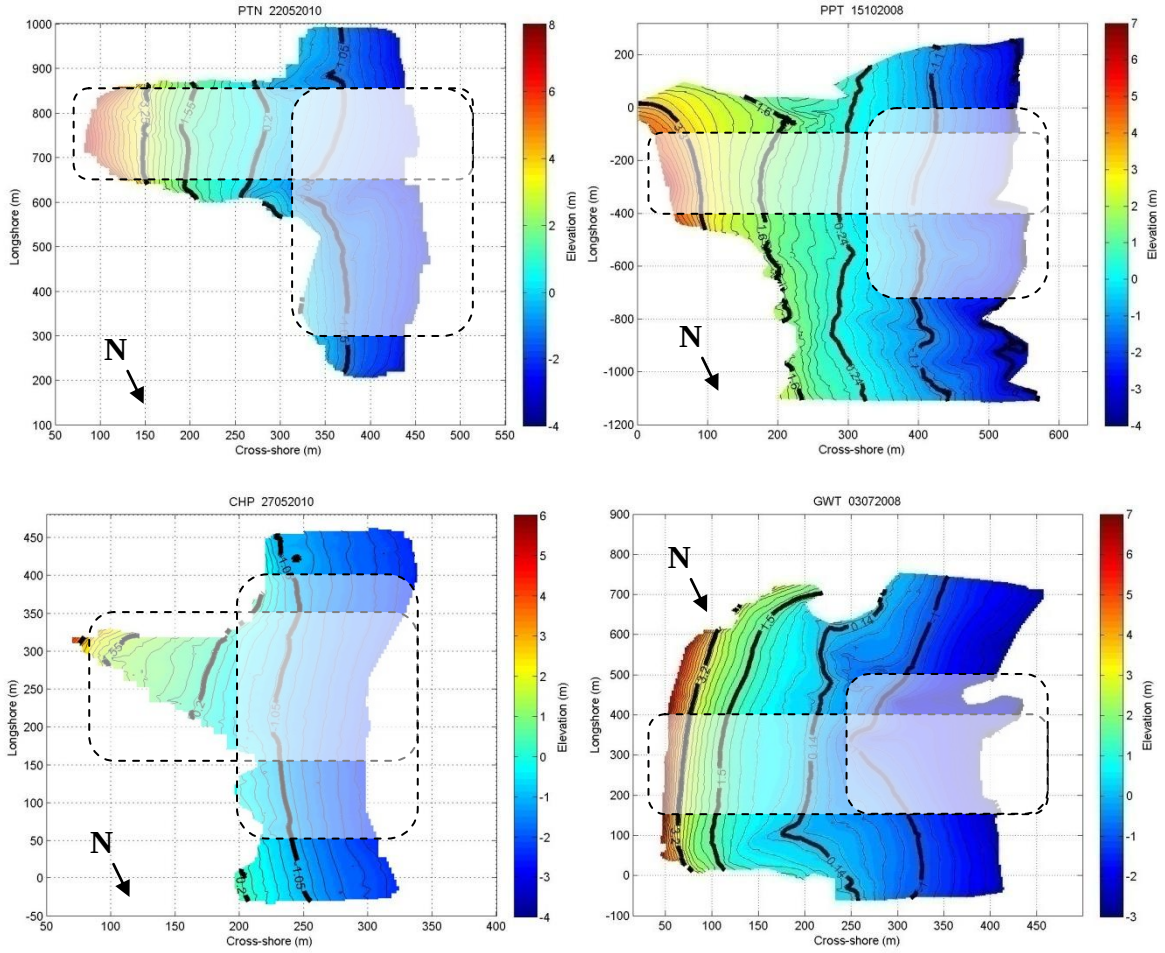

Figure 4.2– Surface elevation models for each of the sites with the 2 regions (full beach and lower beach) used for calculation of the FBX_{MCL} and LBX_{MCL}.These areas were designed to provide maximum comparison with subsequent surveys and correspond to other analytical approaches including volume calculations and assessment of low tide 3D.

4.2.2 Dimensionless fall velocity

The dimensionless fall velocity (Ω) has been widely adopted within beach classification schemes to help distinguish between different states (Masselink & Short, 1993; Scott, Masselink & Russell, 2011; Wright, Short & Green, 1985). The premise of which lies in the response of the beach slope to changes in the wave climate and the beach sediment:

$$\Omega = H_b/(w_s T_p) \quad 4.1$$

where H_b is the breaker height, T_p is the significant peak period and w_s is the mean sediment fall velocity of the beach sand. As previously addressed in Chapter 1, the beach state exhibited through the monthly surveys reflects the beach response to the antecedent processes as well the hydrodynamic conditions experienced during the inter-survey period. Following Wright *et al.*(1987; 1985), the conditions dominant in the period since the previous survey were computed. A weighted mean value ($\bar{\Omega}$) to reflect the wave forcing was calculated according to:

$$\bar{\bar{\Omega}} = \left[\sum_{j=1}^{D} 10^{-j/\phi}\right]^{-1} \sum_{j=1}^{D}\left(\Omega_j 10^{j/\phi}\right) \quad 4.2$$

where j = 1 on the day just preceding the intertidal survey and $j = D$ on D days prior to the survey. The parameter ϕdefines the rate of memory decay, where ϕdays prior to the survey the weighting factor will decrease to 10%. Wright *et al.* (1985) found the best fit using ϕ = 10 which was also adopted here as the most suitable.

4.2.3 3D Classification

Beaches which lie on the boundary between intermediate and dissipative classification experience a range of morphological features from highly planar to low tide bar/rip systems. Within these broad classification states, the range of morphology can be grouped further to identify dominant features/modal morphology. A key part of this chapter concerns being able to quantify the variability observed at a beach at any given time, which will allow greater interpretation of the wave conditions and the antecedent morphology which help control the resulting morphology.

Building on an approach adopted by Smit *et al.*(2008b), who looked at shoreline variability from Argus waterlines to identify beach re-setting following storms, a

measure is used by which a relative level of 3D is assigned to each survey. Although the term "3D" suggests a volumetric component is incorporated, in our approach the primary objective is to quantify the surface shape and intuitively the term 3D is adopted in keeping with current terminology. In order to quantify the level of 3D to each survey, contour lines were extracted between 0.2m ODN (mean sea level) and -2.4m ODN (0.2m above low water springs) at 0.2m intervals. A "curl value" (*CV*) was then computed using the ratio of total contour length and the straight line length of the contour, where *CV* = 1 represents a planar featureless intertidal region and *CV*> 2 indicates a highly variable coastline. For each survey, the *CV* was computed for every extracted contour and the mean value of the top 1/3rd ($\overline{CV}$)was recorded for each survey month (Figure 4.3).

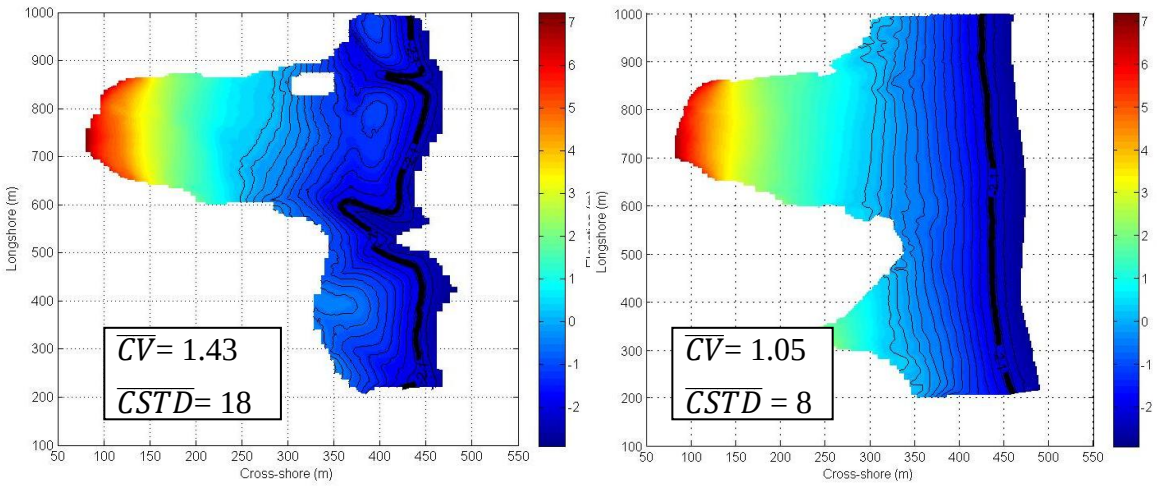

Figure 4.3– Surface models for PTN showing contours used for 3D analysis. On the left a highly 3D surface from May 2009, and on the right a featureless beach from October 2010 with respective $\overline{CV}$ and $\overline{CSTD}$ values.

In addition, the contour standard deviation (*CSTD*) was computed using the same contours extracted as above. To minimise any grid orientation bias contours were rotated so that the start and end points were rotated onto the same cross-shore position. For consistency the top third of the contours were used to compute the average *CSTD*

value ($\overline{CSTD}$). Figure 4.3 shows examples of two quite different beach morphologies and the representative values for both the $\overline{CV}$ and $\overline{CSTD}$ approaches

To ensure the automatic routines were a realistic representation of the conditions presented in a surface elevation map, the opinions of relevant researchers within this field was sought to verify the results. Following the same approach as Ranasinghe *et al.*(2004), 10 "experts" were asked to rank the same monthly surveys for levels of 3D on a scale of 0 – 100 providing a comparison of the accuracy of the automatic 3D classification methods. To facilitate assessment the results were first standardised before correlation analysis showed the relationship between the $\overline{CV}$ with the expert values had a p-value of <0.002, whereas the $\overline{CSTD}$ had a p-value of <0.009, indicating the $\overline{CV}$ was a closer fit to the expert assessment. The relative shifts in the 3D parameters each month are crucial for identifying trends in morphological response between the sites and to the forcing conditions. Importantly 80% of the changes in 3D level as indicated by changes in $\overline{CV}$and $\overline{CSTD}$ values were also recognised by the experts, supporting this method as a useful tool for identifying periods of importance. Following this assessment of the contour extraction techniques, the $\overline{CV}$is adopted within this chapter over the $\overline{CSTD}$ as its overall performance was considered more agreeable to the experts.

4.2.4 Up-state and Down-state Transition

When describing periods of transition, previous studies have adopted the terms "up-state" or "down-state" in reference to a shift in the beach state to increasingly dissipative or increasingly reflective, respectively, with reference to Wright and Shorts (1986) beach classification scheme (Smit *et al.*, 2008b). In general up-state transitions are associated with erosive conditions which result in more planar 2D dissipative

morphology which are usually evident following increased wave conditions. Conversely down-state transitions represent accretionary periods which can see the development of morphological features which are associated with intermediate beaches. However as will become increasingly apparent within this chapter, the automatic association of hydrodynamic conditions with each term does not hold for all instances.

For clarity the term “up-state” is used here as an indication of a reduction in the 3D nature of the low tide morphology, conversely “down-state” concerns an increase in the 3D features. The hydrodynamic conditions for these shifts are not implied and will be discussed separately where necessary to avoid confusion.

4.3 Site Summaries

This section introduces each site and provides an overall summary of the longer term morphological response observed throughout the survey period (2008–2010). Variability in volume, spatial surface change and cross-shore dynamics are introduced with key periods of interest identified

4.3.1 Porthtowan (PTN)

Of the four sites, PTN exhibited the greatest range of morphological response across the full cross-shore extent of the beach. The beach is dominated by an episodic low tide bar/rip system characterised by persistent seaward-directed channels located at the cliff base. Whilst significant shifts in the morphological features are generally concentrated below MLWN, there was also significant response observed at the top of the profile through the intermittent development of a high tide berm. Interaction of this berm with the riverine input onto the beach further added to the response within this section of the beach.

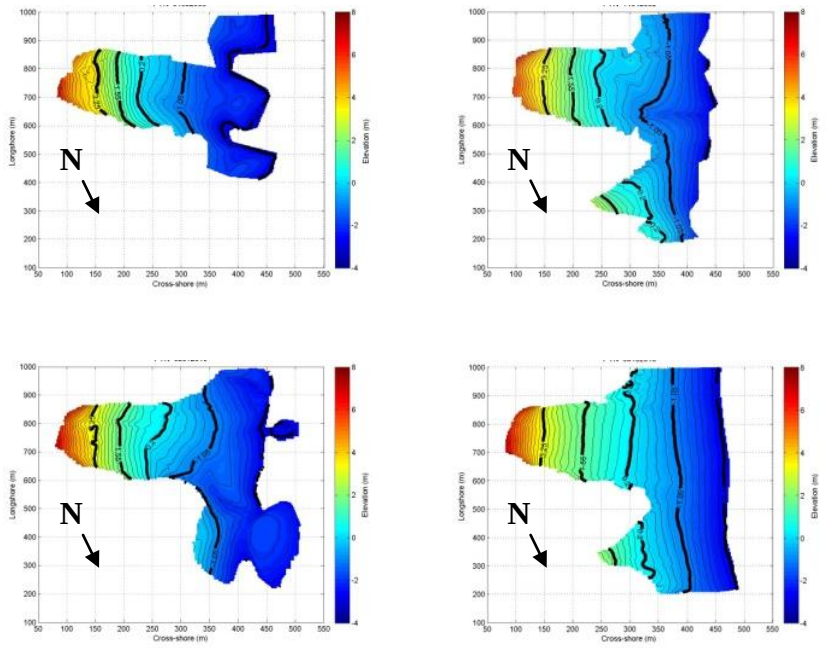

Figure 4.4– Surface elevation maps of PTN for selected periods; top panel, May 2008, January 2009, bottom panel, January 2010 and November 2010. Thick black contours identify MLWS, MLWN, MSL, MHWN and MHWS.

The intertidal volume increased throughout the survey period, with the net volume increasing by just under 1.1 times the initial volume (Figure 4.5). The low tide section of the beach experienced the greatest volume fluctuations with a peak of 1.4 times the starting volume. PTN experienced an initial widespread loss of material between February and May 2008 (Figure 4.5), but this was followed by a progressive increase in beach volume. Four periods of sediment removal were observed: (1) March 2008; (2) November-December 2008, mainly affecting the low tide region; (3) November – December 2009 resulting in more widespread loss; and (4) November and December 2009 during which the largest reduction in sediment volume took place (Figure 4.5).

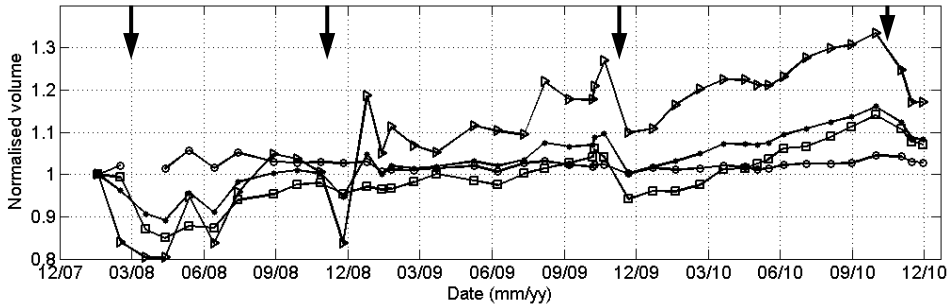

Figure 4.5 – Time series of beach volume at PTN (normalised by the first complete survey) for the upper (o), mid (square), lower(Δ), and total beach (•). Missing data points reflect restricted coverage. Vertical arrows indicate significant volume loss.

At the beginning of the survey period, PTN exhibited a highly 3D bar/rip system with well-defined channels at low tide, in addition to a high-tide berm (Figure 4.4). These features gradually evolved as the beach volume recovered from the initial loss, with the bars migrating onshore and the channels becoming in-filled, thereby smoothing the shoreface. This recovery continued through until September 2008 when a low tide bar developed just below MLWN and continued to grow until November. By December the low tide bar had been removed and the profile had become steeper. Following the loss of material in December the beach built up once again resulting in a relatively planar low tide region in January 2009, broken up by a single channel extending from the cliff edge. The lower intertidal then continued to develop becoming increasingly rhythmic with regularly spaced rip channels (Figure 4.6).

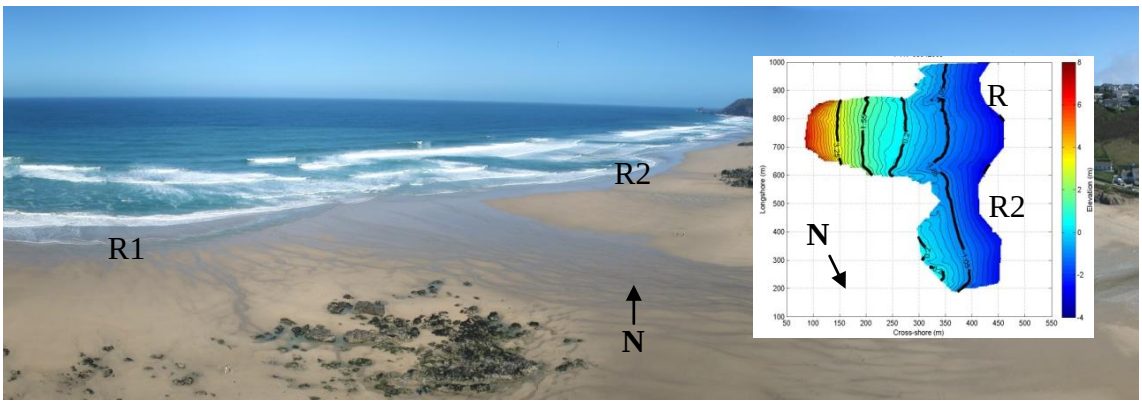

.

Figure 4.6 – Panoramic photograph from April 2009 showing the longshore rhythmic shoreline with regular subtidal rip channels. Inset shows the intertidal morphology for the same time.

Conditions then remained stable until May when the beach became increasingly 3D with the development of intertidal bar and rip morphology. By June, however, these features had become less defined and this smoothing trend continued until November with the beach gradually becoming increasingly linear. Between November and December the third significant loss of material at PTN occurred, resulting in the beach once again exhibiting a more 3D shoreline with strong channels extending from the headlands. As material was transported onshore through into January and February 2010, a subtidal bar welded to the shoreline, thereby extending the bar/channel dynamics and increasing the width of the low tide region (see Section4.6). By April these features had become increasingly alongshore smooth with small low amplitude features evident. In August, small-scale bar-rip morphology had started to develop along the MSLW line, however these are not stable or defined enough to persist and by November the beach had become highly 2D (Figure 4.4).

PTN main response timeline;

- Feb – Sep 08: established low tide bar/rip system gradually infill's
- Sep – Nov 08: development of more 3D low tide
- Dec – Jan 09: increasingly 2D
- Feb – May 09: stable rhythmic shoreline with regular subtidal rips
- Jun – Nov 09: smoothing results in increasingly 2D
- Dec – Jan 10: large loss followed by highly 3D period
- Mar – Dec 10: continued smoothing of bar/rip system, eventually highly planar

The long term spatial variability of surface change at PTN is presented in Figure 4.7. Due to the dynamic nature of the shoreline the survey coverage does not provide complete comparison for the furthermost seaward limit; however, clear regions of peak collective Δz are visible. The greatest cumulative Δz occurs off the northern headland with up to 12 m of surface variability (Figure 4.7). This observation is further expressed through the absolute change in surface elevation which highlights the region between MLWN and MLWS as the most dynamic. Importantly, the absolute surface change also highlights the variability at the top of the beach, which is a result of the episodic berm development along the MHWS line (Figure 4.7).

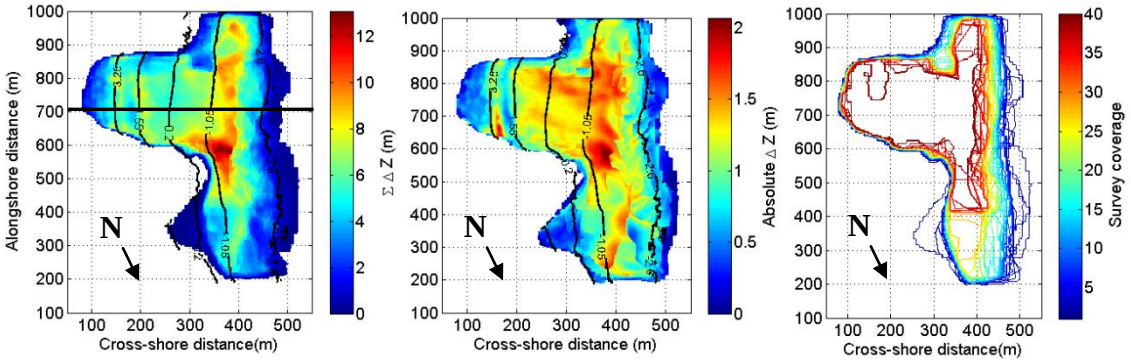

Figure 4.7 – Longterm variability of surface morphology at PTN expressed as the cumulative change (∑Δz, left panel), absolute change ($\Delta z_{max,zmin}$,central panel) and a contour map showing survey perimeter to aid interpretation (right panel). Black contours show the mean position of MHSW, MHWN, MSL, MLWN and MLWS. The horizontal black line shows the location of the 2D profile extracted in Figure 4.8

The 2D spatial variability of these features is further expressed through cross-shore profile analysis shown in Figure 4.8. At the top of the profile the MHWS berm is evident with a profile envelope of >1.5m, we then see a clear drop in variability identifying a key upper-mid beach nodal point where the absolute Δz =< 0.5m and the cumulative Δz =<3m. Below MHWN the profile envelope remains stable with the absolute Δz = >1.5m remaining constant across the profile; however, the cumulative Δz continues to rise further down the profile, peaking at >8m below MLWN.

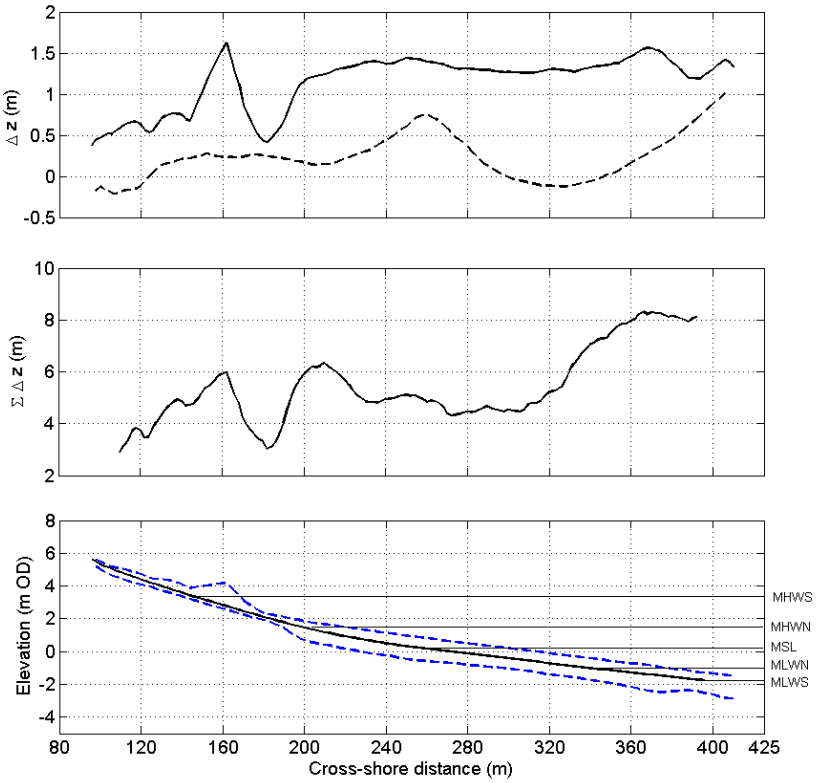

Figure 4.8– PTN profile variability: top panel shows net profile change ($\Delta z_{n,z1}$dashed line) and absolute profile change ($\Delta z_{max,zmin,}$solid line); mid panel shows cumulative Δz; and bottom panel shows mean profile shape (solid line) with minimum and maximum profile position (dashed lines).

In summary, observations at PTN show a highly dynamic beach with responsive morphological features across the entire intertidal beach. Figure 4.9 shows the recurrent up-state transition which was observed 3 times throughout the 3 years over 3 – 4 months. This process sees the in-filling of pronounced low tide bar/rip morphology. As sediment

is redistributed the rip channels are in filled, the system moves northward with a single channel remaining off either of the headlands. This process is illustrated and schematised in Figure 4.9 which shows this up-state development and highlights the straightening of the shoreline and reduction in the channel morphology.

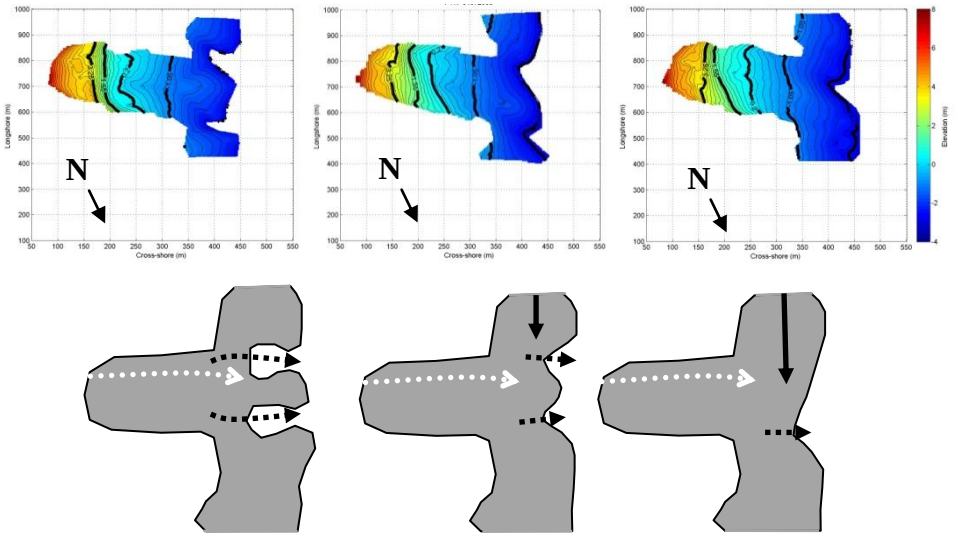

Figure 4.9 – Sequential up-state morphological evolution observed at PTN. The top panel shows monthly surface plots from June, July, and August 2008. Thick black contours identify MLWS, MLWN, MSL, MHWN and MHWS. The bottom panel shows an idealised schematic of the low tide bar/rip morphology at PTN throughout this up-state transition. Dashed arrows indicate rip channel locations (bigger size reflects more defined channels), solid arrows show direction of bar movement through the system (months) and white arrows indicate river location

The spatial persistence of bar/rip morphology at PTN (Figure 4.9) suggests a strong geological constraint in the hydrodynamics generated by the enclosed upper beach which opens up at MLWN. Such forcing leads to a sustained channel off the northern headland, accentuated during bar formation. Similar observations are present at CHP in Section4.3.3, which forms the northern end of the same bay.

4.3.2 Perranporth (PPT)

The morphological response observed at PPT was focused on the mid to low tide region of the beach. Unlike on PTN there was no significant development of a berm throughout the surveys, but, instead, the development of low tide bar/rip systems dominated throughout (Figure 4.10). The river input to the south of the beach was observed to limit

the alongshore variability in this area restricting channel formation and bar development. Moving north more regular and rhythmic channels became evident with associated bars.

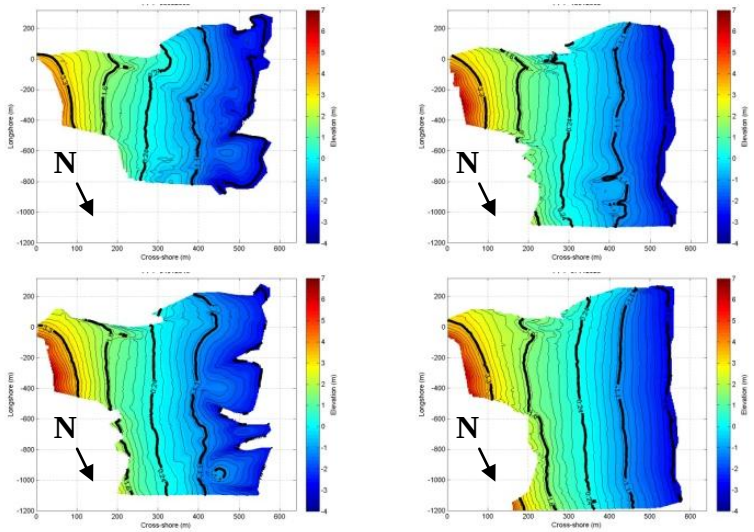

Figure 4.10– Morphodynamic variability at PPT, surface elevation maps showing the dynamic nature of PPT; top panel; May 2008, January 2009, bottom panel; January 2010 and November 2010. Thick black contours identify MLWS, MLWN, MSL, MHWN and MHWS.

Long term volume fluctuations at PPT followed a similar pattern to PTN, with a net increase of 1.15 times the initial intertidal volume over the three years. Two periods of sediment loss occurred at the start and end of 2009, with the low tide region experiencing the greatest shift in beach volume, while the upper beach remained stable throughout, experiencing only a marginal increase in volume (Figure 4.11).

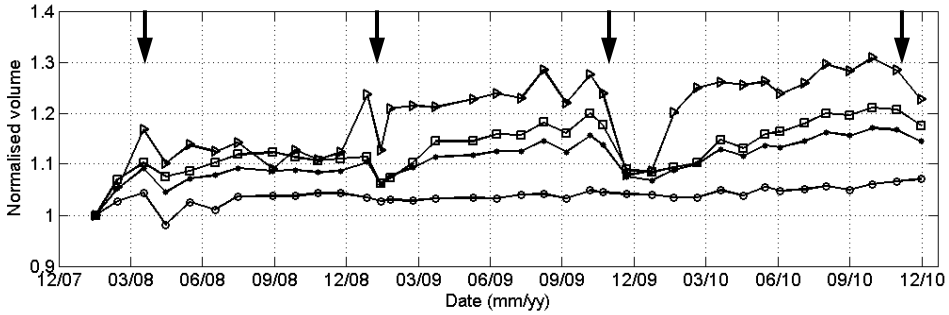

Figure 4.11– PPT volumes (normalised by the first complete survey) for the upper (o), mid (square), lower (Δ), and total beach (•).Vertical arrows indicate significant volume loss.

Unlike the other sites, PPT experienced an increase in overall beach volume following the first survey. Initial beach morphology in February 2008 exhibited low tide bar/rip morphology which underwent smoothing into March. During April and May the low tide bar systems developed further and became more defined by June. Through July and August the longshore variability moved landward with greater dynamics exhibited around MLWN, while the low tide region became highly rhythmic with regularly spaced rip channels (Figure 4.12).

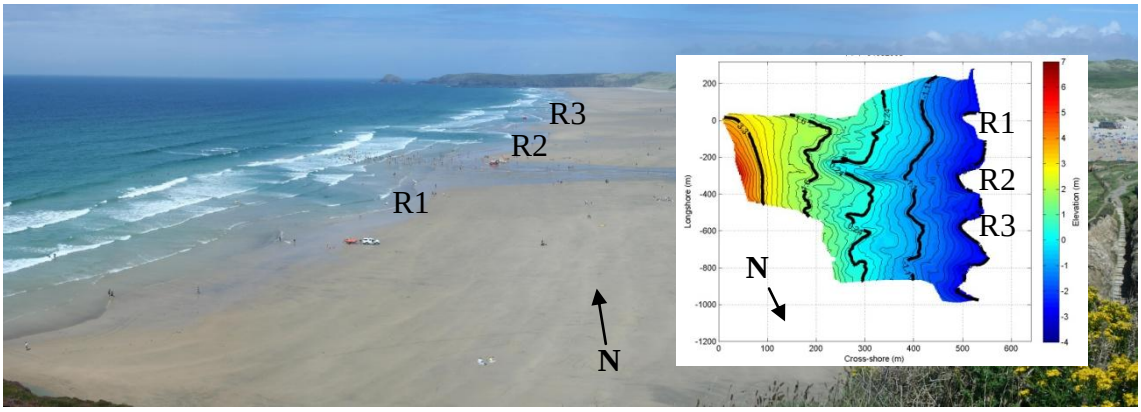

Figure 4.12 – Panoramic photo and surface elevation map of PPT for August 2008. Highly rhythmic alongshore rip spacing is evident.

By September the beach had become increasingly smooth, although a low tide intertidal bar remained in the centre of the survey area. This continued into October, but by November and December, despite increased wave conditions, the low tide morphology was dominated by low tide bar/rip channels, albeit less rhythmic than during the summer. The first major resetting of the system (an up-state transition) was observed in January when the beach became highly planar through in-filling of the low tide rip channels, resulting in a corresponding rise in the low tide net volume (Figure 4.11). However, over the following two weeks the beach experienced widespread loss in material and the low tide region returned to a more rhythmic state. This trend continued

into February when highly 3D morphology was present in combination with a significant increase in the volume across each region of the beach.

Morphological response throughout 2009 saw the highly 3D shoreline smooth out and become more alongshore rhythmic, with a dominance of two low tide bars and associated channels. These conditions remained dominant until August when the beach became smoothed out further, although smaller isolated bars remained. Energetic conditions in November and December resulted in widespread loss of material, yet low tide bar features remained. By January recovery of the low tide region resulted in quite pronounced bar/rip morphology with three well developed bars and deep channels (Figure 4.10). The start of 2010 was characterised by in-filling of channels and a corresponding increase in the net volume (Figure 4.11). This trend continued as the beach became increasingly 2D. A short period of small-scale rhythmic bars located at MLWS occurred in August and September; however, this morphology was short-lived and the beach continued to build and smooth out resulting in a highly 2D state by November 2010 (Figure 4.10).

PPT main response timeline;

- Feb – Oct 08: Well developed 3D morphology gradually in filled
- Nov – Jan 09: low tide bar/rip dominates before more planar conditions in Jan
- Feb – Nov 09: 3D conditions until August, in-filling leads to smoothing
- Nov – Jan 10: Widespread loss followed by highly 3D recovery
- Feb – Dec 10: Sustained smoothing and highly 2D dominate

The long-term spatial morphological response of PPT is shown in Figure 4.13. The upper beach was the least dynamic throughout the survey period with 2 – 3m cumulative Δz in the beach surface. With good low tide coverage the peak cumulative

change was concentrated between MLWN and MLWS, and in particular the greatest change occurred at *x* = 450 m, *y* = -800 m (Figure 4.13).

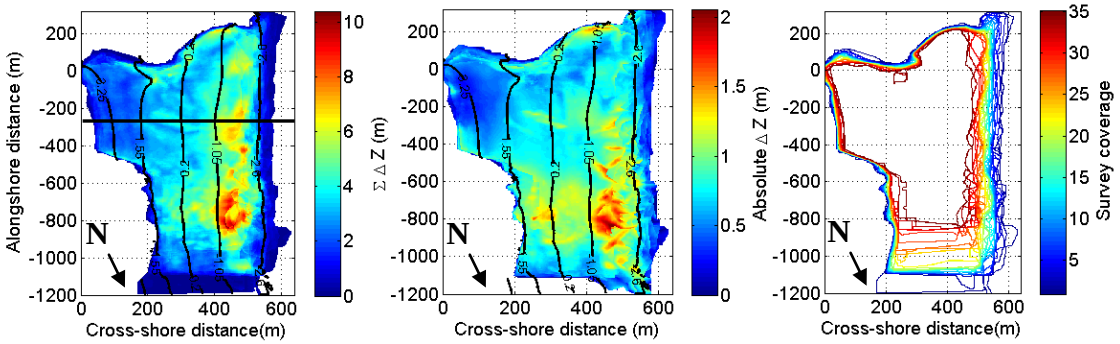

Figure 4.13– Long term variability of surface morphology at PPT expressed as the cumulative change (∑Δz, left panel), absolute change ($\Delta z_{max,zmin}$, central panel) and a contour map showing survey perimeter to aid interpretation (right panel). Black contours show the mean position of MHSW, MHWN, MSL, MLWN and MLWS. The horizontal black line shows the location of the 2D profile extracted in Figure 4.14.

The net change further highlights that the greatest variability occurred shoreward in front of the cliffs at x= 200m, which reflects the quasi-stationary bar feature which was prevalent throughout the survey period (Figure 4.13). Building on the spatial variability presented in Figure 4.13, 2D profile analysis further highlights the regions of more significant dynamics (Figure 4.14).

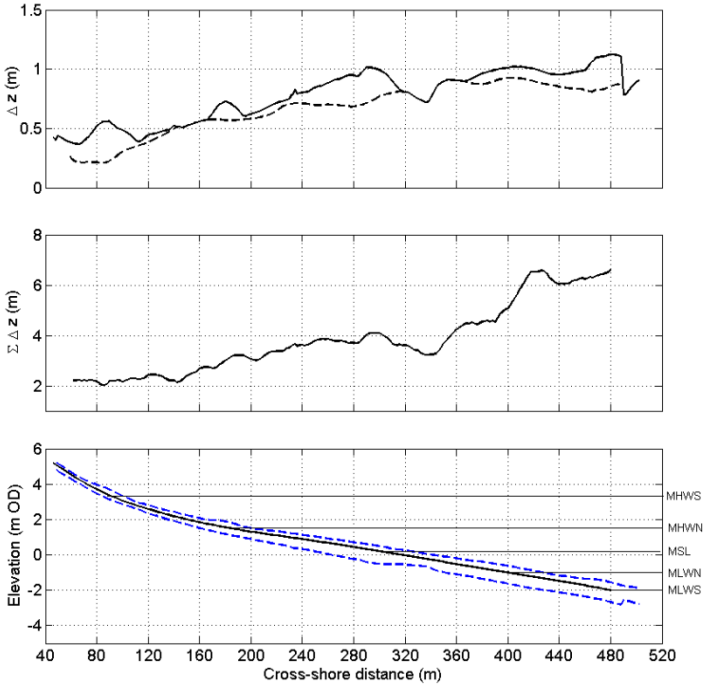

Figure 4.14– PPT profile variability; top panel, net profile change ($\Delta z_{n,z1}$dashed line) and absolute profile change ($\Delta z_{max,zmin,}$solid line); mid panel, cumulative Δz; bottom panel, mean profile shape (solid line) with minimum and maximum profile position (dashed lines).

The profile envelope peaks at just over 1m reflecting the absolute and net variability; however, the cumulative Δz peaks at 6.5m highlighting the dynamic nature of the low tide region. These observations further support the notion of a highly stable upper beach that becomes increasingly dynamic in the seaward direction.

The low tide bar/rip systems at PPT have been well defined and persistent throughout the 3 years. Whilst the onset of these features is complex and discussed further in subsequent analysis, gradual up-state transition to a more 2D beach state is well represented (Figure 4.15). This steady process evolves over 3 – 4 months and sees the gradual smoothing of the low tide bar-dominated features as sediment is moved onshore/redistributed, resulting in a more planar beach state (Figure 4.15).

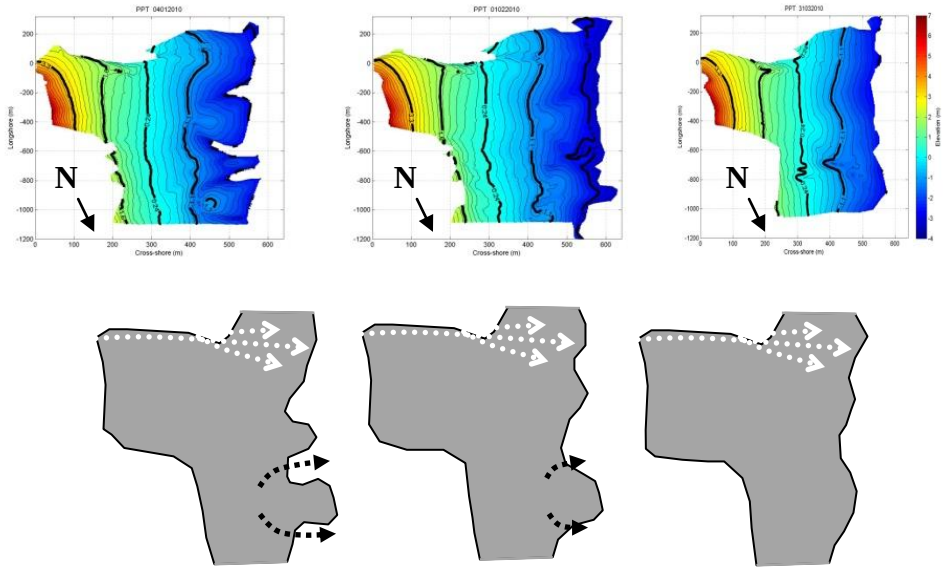

Figure 4.15 – Sequential up-state morphological evolution observed at PPT; The top panel shows monthly surface plots fromJanuary, February, and April 2010. Thick black contours identify MLWS, MLWN, MSL, MHWN and MHWS. The bottom panel shows an idealised schematic of the low tide bar/rip morphology at PPT throughout this up-state transition. Dashed arrows indicate rip channel locations (bigger size reflects more defined channels), solid arrows show direction of bar movement through the system (months) and white arrows indicate river location

4.3.3 Chapel Porth (CHP)

CHP forms the northern end of the PTN – CHP bay system (Figure 2.4) and turned out to be the most morphologically dynamic beach in the data set. Figure 4.16 highlights the variability at this site with a selection of the dominant states observed. As evident in Figure 4.16, the survey area at CHP varies considerably both in the lower and upper region of the beach. Because of the deep channels backed by steep cliffs in the low tide region and the exposed boulders in the upper section of the beach, maintaining consistency in survey coverage was a challenging task. For the duration of the survey period the sandy part of the beach was surveyed, however this only extended up to MHWN for 7 out of 36 surveys. The main impact of this limitation at CHP is a reduced area used for volume calculations and monthly comparisons, which has some bearing on subsequent analysis as will become evident.

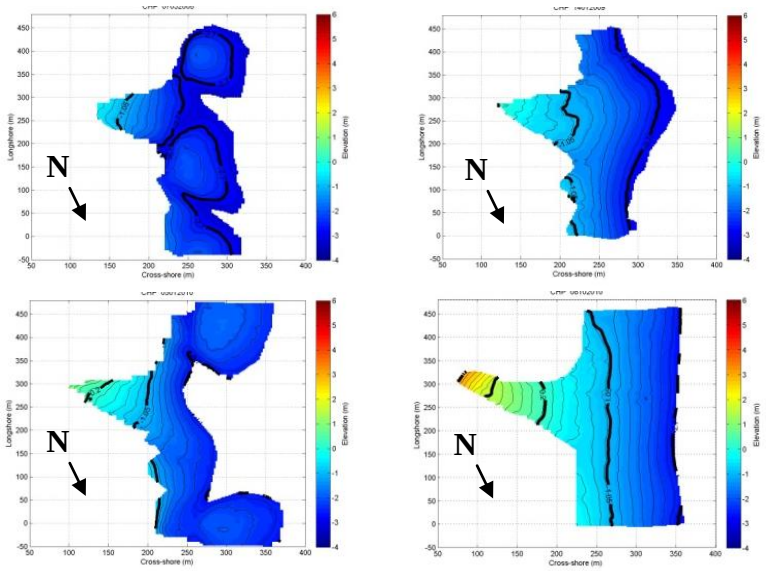

Figure 4.16 – Morphodynamic variability at CHP, surface elevation maps showing the dynamic nature of CHP; top panel, May 2008, January 2009; bottom panel, January 2010 and October 2010. Thick black contours identify MLWS, MLWN, MSL, MHWN and MHWS (all 5 are only visible in the surface plot for October 2010).

Overall, the beach, responded in a similar manner to PTN with a low tide bar/rip dominated system. Similar to the other beaches, the sediment volume on CHP increased steadily over time, but CHP experienced the greatest magnitude with the beach increasing by 1.5 times its initial volume (Figure 4.17). However, owing to the lack of coverage in the upper region of the beach, volume calculations relate to mid-low region of the beach only.

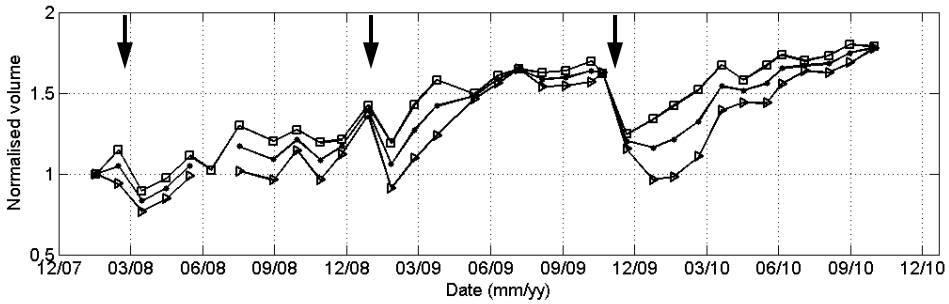

Figure 4.17– CHP volumes normalised by the first complete survey (February 2008) for the, mid (square), lower (Δ), and total beach (•). Data from the upper beach of CHP is omitted owing to restricted survey coverage. Vertical arrows indicate significant volume loss.

At the start of the survey period the beach possessed a full profile with sand up to MHWS and the low tide region extended into a large single bar. Between March and

April the beach experienced widespread loss across the beachface with a significant drop in beach volume (Figure 4.17). The result of this sediment loss was the growth of a low tide bar rip morphology below MLWN. By May, these features evolved into 3 well-developed low tide bars which underwent a process of smoothing during June/July as the channels became in-filled. A northward migration of the remaining channel was observed and this became a characteristic up-state transition which occurred 3 times over the 3 years. By September the low tide beach had developed with the cross-shore region expanding seaward as well as an increase in the beach volume. The return of the large scale low tide bar systems followed with access to the south restricted owing to a deep channel running from the cliff offshore. Over September, October and November again a northward migration of the low tide bar features took place in response to the in-filling of the channels. During November and December 2008, beach volumes remained stable, yet extensive redistribution of low tide material resulted in a narrow low tide bar at the centre of the survey area with deep channels at either side. By January 2009, beach width had increased substantially and the widespread in-filling of previous channels resulted in a relatively smooth rhythmic shore face with two well-defined subtidal rip channels at the survey boundaries (Figure 4.16).

During January-February 2009 the beach experienced the first significant loss of material from the intertidal region (Figure 4.17). Whilst the net volume decreased, the width of the beach extended offshore as the low tide region flattened. Through the first half of 2009 the beach became increasingly planar within the survey region, while a rhythmic shoreline dominated by two large rip channels remained at either side of the survey area (Figure 4.18).

Figure 4.18– Panoramic photo of CHP during March 2009 showing large well defined subtidal rip systems either side of the survey area. ATV track marks are visible on the upper beach.

By June a small low tide bar became exposed at the centre of the survey area, which gradually welded to the shoreface by August forming a much larger rhythmic system which was evident between CHP and PTN. Through to November the beach underwent limited change, but the upper sediment volumes increased, while the low tide region became increasingly longshore parallel. During November and December the second significant loss of material was observed (Figure 4.17). Upper beach material was removed, while the lower beach became highly 3D with clear bar/rip morphology. Calmer conditions in January exposed a 3D beach with 2 large and well-developed bars flanking the survey region and the low tide cliffs (Figure 4.16). This system then dominated while it gradually moved north through the survey region over the subsequent 6 months becoming increasingly planar as the channels in-filled.

CHP main response timeline;

- Feb – May 08: Highly 3D low tide bar/rip system
- Jun – Nov 08: 3D system gradually in-fills becoming more planar
- Dec – Jan 09: rhythmic shoreline with defined subtidal rip system
- Jan – May 09: Sediment loss and beach widening leads to planar morphology
- May – Nov 09: rhythmic shoreline dominant
- Nov – Jan 10: widespread loss before increase in 3D morphology
- Feb – Oct 10: Sustained in-filling and smoothing results in wide planar beach

As commented previously, the extent of the variability in the low tide morphology at CHP makes long-term trend analysis complex. Figure 4.19 presents the 3D variability in the beach face through the cumulative change in elevation (Δz) and the absolute change. These plots shows extensive change across the low tide region with significant change observed close to the survey edges, in particular the cliff backed regions (x = 225, y = 200). However, the distribution of survey coverage (Figure 4.19, right) also highlights the intermittent spatial extent for comparison which needs to be considered during further analysis.

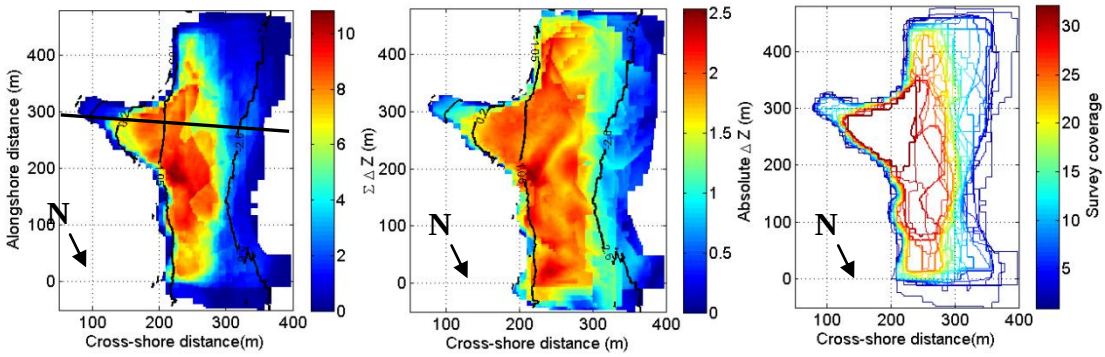

Figure 4.19– Long term variability of surface morphology expressed as the cumulative change (∑ Δz, left panel), absolute change ($\Delta z_{max,zmin}$,middle panel) and a contour map showing survey perimeter to aid interpretation (right panel). Black contours show the mean position of MHSW, MHWN, MSL, MLWN and MLWS. The horizontal black line shows the location of the 2D profile extracted in Figure 4.20.

The cross-shore distribution and behaviour of sediment also serves to restrict the profile analysis, with highly variable profile extents making month by month comparisons difficult. Figure 4.20 shows the mean profile line for CHP and the envelope of change which shows a peak of >2m variability at the centre of the profile.

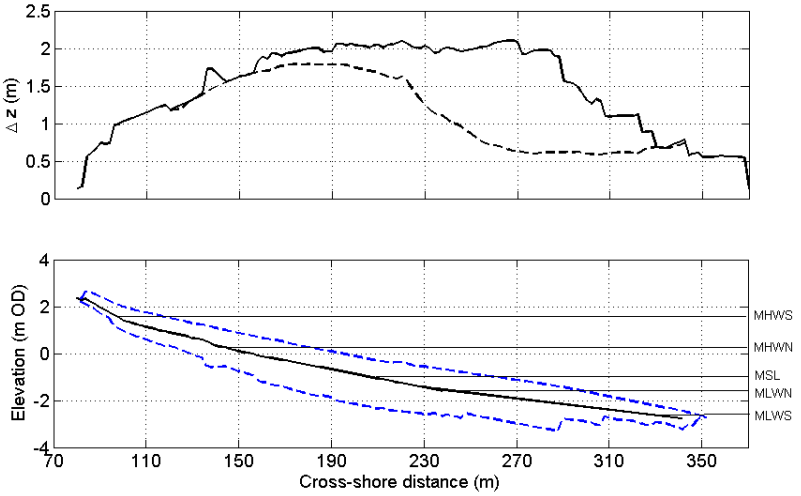

Figure 4.20– CHP profile variability; top panel, net profile change ($\Delta z_{n,z1}$, dashed line) and absolute profile change ($\Delta z_{max,zmin,}$ solid line); bottom panel, mean profile shape (solid line) with minimum and maximum profile position (dashed lines). Cummulative profile change is missing from CHP owing to the large variability in the cross shore coverage.

Overall the behaviour observed at CHP over the 3 years can be summarised as follows. During sediment removal the beach becomes increasingly 3D with well-defined low tide bar rip morphology. The location of these features generally exhibit spatial persistence with dominant channels evident where the upper beach opens up at low tide. The behaviour of the low tide bar/channel features shows consistent dynamics with clear growth and migratory patterns northward through the system associated with longshore straightening (Figure 4.21). This behaviour is idealised in Figure 4.21 which demonstrates the gradual migration of the low tide bar/rip system through the survey area and eventual recovery of the system, similar to that observed at PTN.

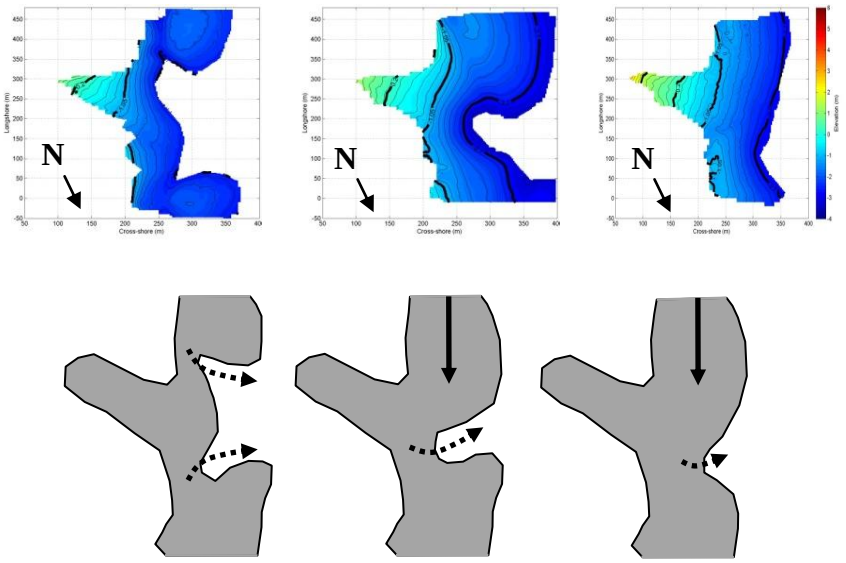

Figure 4.21– Sequential up-state morphological evolution observed at CHP; The top panel shows monthly surface plots from January, March, and April 2010. Thick black contours identify MLWS, MLWN, MSL, MHWN and MHWS. The bottom panel shows an idealised schematic of the low tide bar/rip morphology at CHP throughout this up-state transition. Dashed arrows indicate rip channel locations (bigger size reflects more defined channels), solid arrows show direction of bar movement through the system.

In keeping with the other study sites, CHP experienced two significant reductions in the total intertidal volume. The first occurred during January and February 2009 and resulted in a flattening and seaward extension of the beach as sediment was removed from the upper beach face. The width of the lower beach grew, while the upper beach volume decreased. Following this response a steady onshore migration was observed over the following months. The second widespread removal of material occurred during November and December 2009. Over this period the beach became narrower as well-defined low tide bars developed either side of the survey region in front of the cliff areas.

4.3.4 Gwithian (GWT)

GWT was morphologically the least dynamic of the sites. Forming one end of the three mile long beach which forms St Ives bay, the beach is backed by a man-made bund built to protect sand extraction operations (Section 2.7). The Red River forms the most dominant feature within the survey area, cutting a channel next to the headland before

spreading across the beach face to the sea. Overall the beach is gently crescentic as it extends north towards Godrevey Lighthouse and south towards Hayle (Figure 4.22). Throughout the three year survey period low amplitude shore parallel low tide bar/channels were evident for short durations. The majority of the survey period was characterised by a planar dissipative beach with occasional high tide cusps.

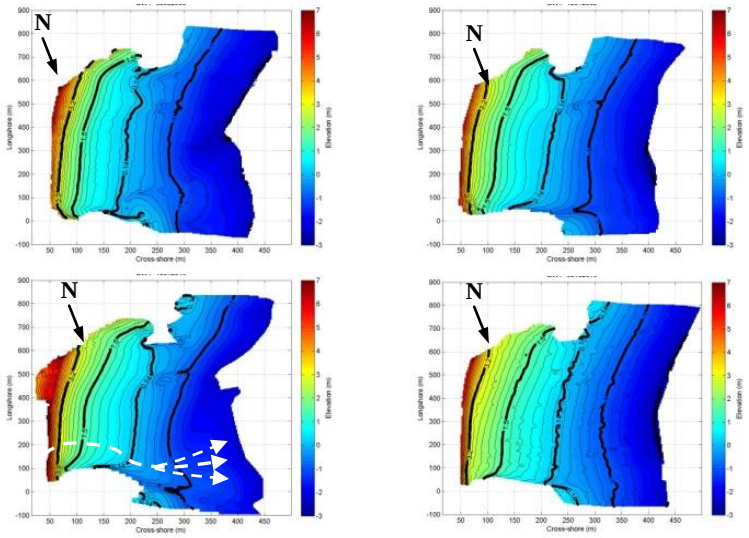

Figure 4.22– Morphodynamic variability at GWT, surface elevation maps showing the relatively stable nature of GWT; top panel, May 2008, January 2009; bottom panel, January 2010 and October 2010. Thick black contours identify MLWS, MLWN, MSL, MHWN and MHWS. The location of the river outflow is shown in white on one of the plots.

The outflow of the Red River to the north of the survey area had a significant effect on the overall crescentic shape of the beach shoreline. The widening of the shoreline in this region was the most dominant behaviour through the survey period, forming a central part of shoreline evolution, (Figure 4.22). Through the first part of 2008 the cross-shore width increased moving south through the survey area, this migration resulted in the formation of an alongshore low-amplitude bar and channel in the centre of the low tide region(Figure 4.22). By August the beach smoothed out and the longshore bar became less prevalent. The morphodynamics then remained stable until February 2009 (five months) with the reduction in volume occurring between January and February having

little impact on the beach shape. From February a repeat of the previous low tide migration and channel formation took place, with increased beach width to the north of the area in line with the river output gradually extending south. By April the beach volume began to increase with the mid-beach flattening out as the low tide channel deepened in the centre of the survey area. By May the longshore low amplitude channel had in-filled resulting in a smooth planar beach face. This weakly crescentic planar beach state continued as the beach gradually increased in volume until November (Figure 4.23). During November and December GWT experienced the second significant reduction in volume resulting in the largest shift in low tide morphology. At the northern end of the survey region the river input extended the beach face, while the southern end of the survey region saw the development of the low-amplitude longshore bar. Through 2010 again longshore redistribution of material took place as the beach face realigned itself over the first 5 months as the channel migrated south and the beach became increasingly planar. By July low tide morphology was absent, and this remained until the end of surveys in November 2010.

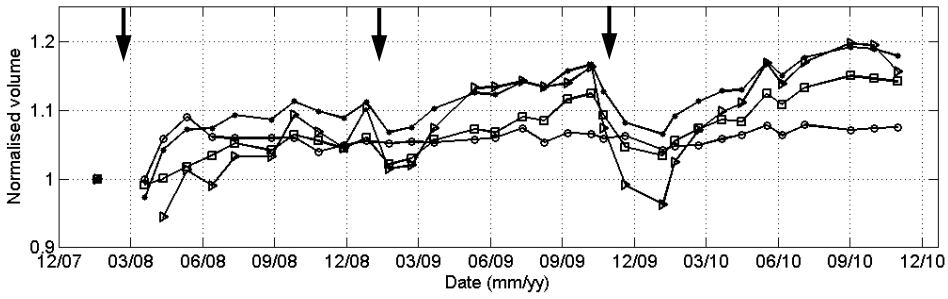

Figure 4.23– GWT volumes (normalised by the first complete survey) for the upper (o), mid (square), lower (Δ), and total beach (•). Missing data points reflect restricted coverage. Vertical arrows indicate significant volume loss.

GWT main response timeline;

- Feb – Aug 08: low amplitude channel infill's to the south
- Aug – Feb 09: stable planar state
- Feb – May 09: low amplitude channel infill's to the south

- May – Nov 09: stable planar state
- Nov – May 10: widespread loss followed by channel in-filling to the south
- May – Nov 10: Stable planar state

The long-term variability of the full survey region for GWT is assessed through Figure 4.24, which highlights regions of significant change. With good spatial consistency in survey coverage (Figure 4.24, right), two regions are notable in experiencing more intense morphological variability. To the north of the survey region there is an area with large cumulative (8 – 9m) and the net surface change (1.6m). This is the location of the Red River and as such we would expect significant fluctuations in bed level in this region. There is a second area to the south of the survey region with a well-defined peak in the cumulative (6 – 7m) and net (1.5m) morphological change, just seaward of the headland towards MLWN (Figure 4.24). This position highlights the episodic development of the longshore channel/low-amplitude bar which is observed in Figure 4.22. The upper and central part of the beach sees the least amount of change with cumulative variability of only 2 – 3m.

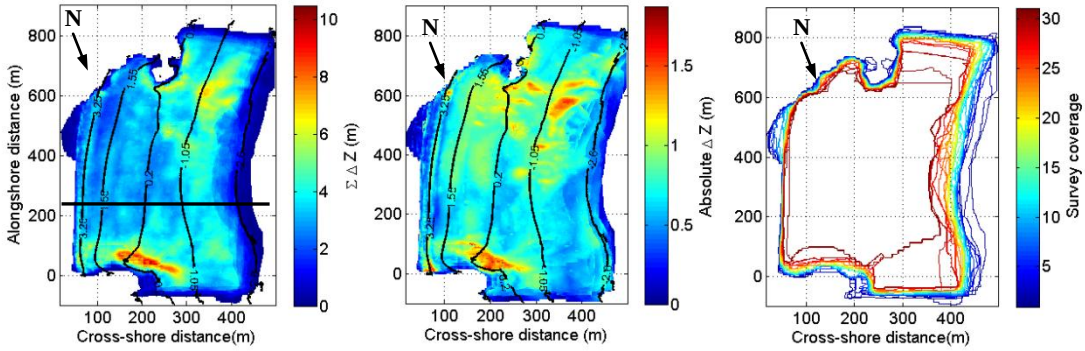

Figure 4.24– Long term variability of surface morphology expressed as the cumulative change (∑Δz, left panel), absolute change ($\Delta z_{max,zmin}$central panel) and a contour map showing survey perimeter to aid interpretation (right column). Black contours show the mean position of MHSW, MHWN, MSL, MLWN and MLWS.The horizontal black line indicates the location of profile extract presented in Figure 4.25.

The growth and decay in upper beach cuspate features is evident as a MHWS longshore peak in the absolute Δz (Figure 4.24, middle). This is identified more clearly in Figure 4.25 which shows a peak in the morphological variability between 50 and90m in line

with MHWS. Moving down across the profile two nodes of minimum variability are found at x = 90m and x = 230m, separating the regions of greatest cumulative response. As indicated from Figure 4.24 the peak cumulative change occurs below MSL and is centred around MLWN. Due to coverage limitations (Figure 4.24) it is not clear if the drop in cumulative Δz below MLWN is an artefact of limited coverage or representative of the true dynamics for this region.

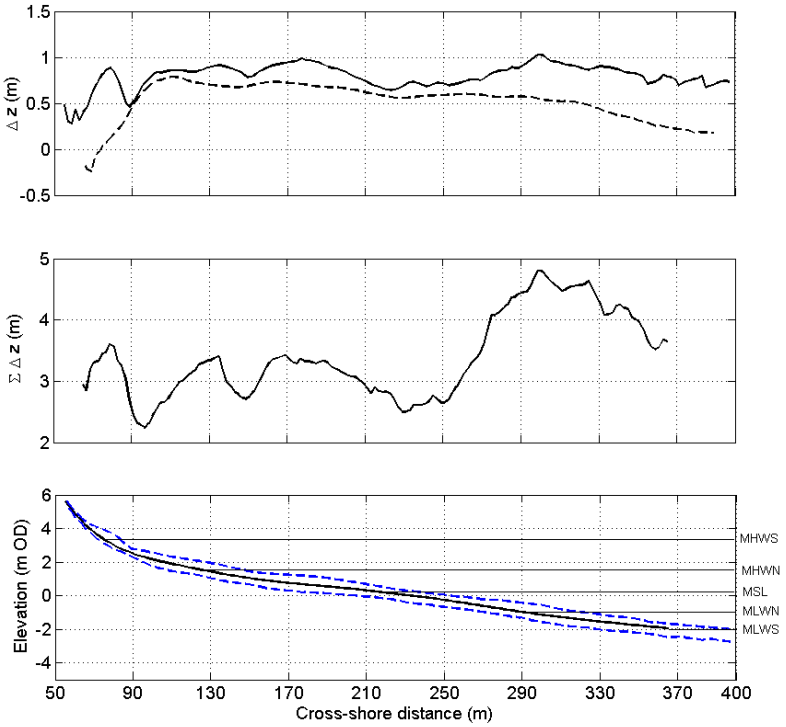

Figure 4.25. GWT Profile variability; top panel, net profile change ($\Delta z_{n,z1}$, dashed line) and absolute profile change ($\Delta z_{max,zmin,}$ solid line); mid panel, cumulative change ($\sum\Delta z$) ; bottom panel, mean profile shape (solid line) with minimum and maximum profile position (dashed lines).

In summary, GWT experiences two reductions in intertidal beach volume in response to energetic conditions, the first having little affect on the beach state, while the second resulted in the establishment of a low-amplitude bar/channel to the south end of the survey region. The main trend observed at GWT is the longshore redistribution of material which is characterised by a southward movement of material from the river out-flow at the north of the survey area. This serves to create a low-amplitude transverse bar and channel which gradually infill leaving a smooth cresentic shoreline. Figure 4.26

shows the surface morphology for one of these periods which is expressed through a simple idealised schematic in Figure 4.26, highlighting the salient features of this sediment redistribution.

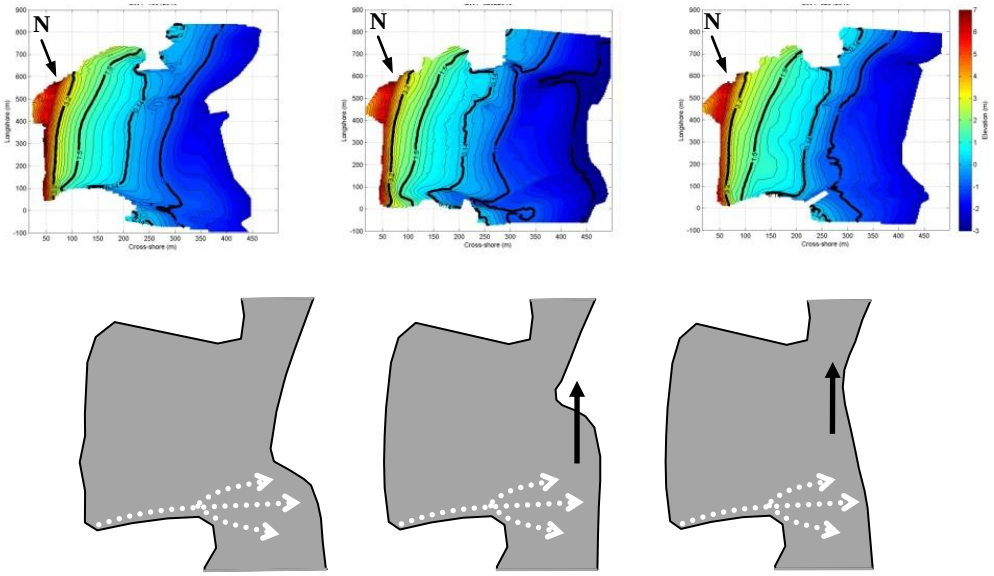

Figure 4.26 – Sequential semi up-state morphological evolution observed at GWT; The top panel shows monthly surface plots from January, February and April 2010. Thick black contours identify MLWS, MLWN, MSL, MHWN and MHWS. The bottom panel shows an idealised schematic of the low tide bar/rip morphology at GWT throughout this up-state transition. Solid arrows show direction of low tide morphology movement through the system, dashed white arrows indicate position of river outflow.

4.4 Combined response

4.4.1 Volume

Consistency between the four sites is expressed through the monthly variation in the intertidal volume as observed in Section 4.3. The importance of onshore-offshore movement of material in shaping the response and subsequent morphodynamic features is self-evident, in this section a comparison of the different responses at the four sites will be undertaken to further identify similarities in their behaviour.

The individual site summaries presented above highlight the cross-shore variability in volume fluctuations observed at each of the sites. Figure 4.27 provides a clear comparison of the overall change at each site which identifies a high level of similarity

throughout the 3 years. Although CHP stands out as undergoing greater growth, much of this reflects the lack of an upper section of beach incorporated in the intertidal total, which skews the result towards the more responsive lower beach.

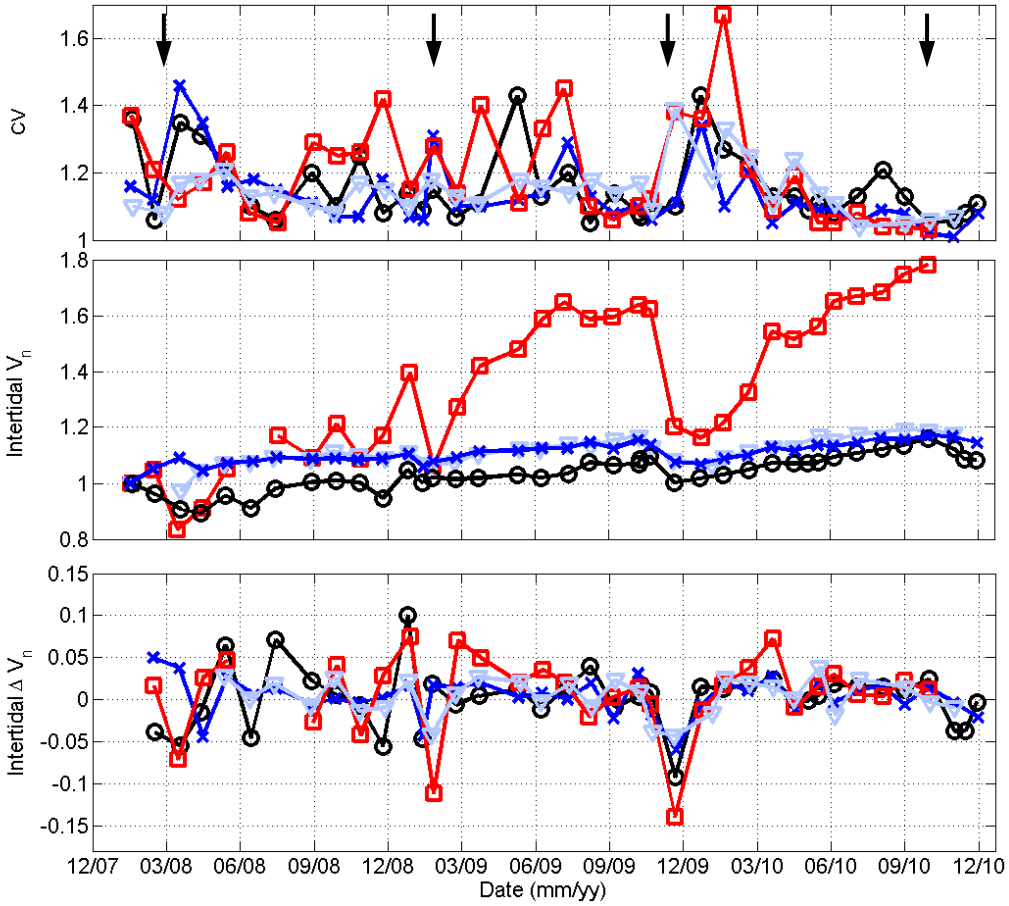

Figure 4.27– Volume change at all sites. The top panel shows the intertidal volume normalised by the first survey (V_n), the bottom panel shows the monthly change in the normalized intertidal volume (ΔV_n) for; Black circles = PTN, blue squares = PPT, light blue triangles = GWT and red squares = CHP. *Note* CHP does not have an upper beach volume which is reflected in the larger variation in total volume in the upper panel. Additionally in the lower panel CHP has been reduced by 2/3 to ease comparison with the other sites. The vertical black arrows identify periods of significant loss at most sites.

However it is fair to say from the survey data CHP is likely to represent the most varied site despite this bias. Overall 4 periods of loss are identified by the arrows in Figure 4.27, which are made clear in the lower panel which addresses the ΔV_n, in particular the significant loss in February 2009 and December 2009 which is discussed further in Section 4.8. Comparison with the 3D classification (CV) highlights distinct increased 3D morphology following sediment removal in March 2008 and November 2009, with the other periods less defined.

4.4.2 Momentary Coastline

Calculation of the momentary coastline provides a quantitative assessment of the state of a beach and as such can be used by beach managers as a Coastal State Indicator (CSI) (van Koningsveld & Mulder, 2004). Figure 4.28 shows the standardised FBX_{MCL} and LBX_{MCL} for each of the sites. Whilst the profile does not extend to the depth of closure for these sites the intertidal volume can still be used as a proxy for the system as a whole. As identified in Section 4.3, the low tide regions of each of the sites exhibited the largest amount of variability throughout the survey period. The addition of a lower beach LBX_{MCL} allows the cross shore variability at these sites to be examined. Each site exhibited progressive widening of the beach, briefly interrupted by two short phases of narrowing (Figure 4.28). The FBX_{MCL} for each site (except CHP owing to survey coverage) increased by the smallest amount (20 – 32m), with rates of 0.02, 0.02 and 0.014m day^{-1} for PTN, PPT and GWT respectively. LBX_{MCL} changed over a greater amount; GWT extended by a maximum of 47 m, PTN and CHP by 76m each and PPT by 56 m, with rates of 0.05, 0.05, 0.03 and 0.03 m day^{-1} for CHP, PTN, PPT and GWT respectively.

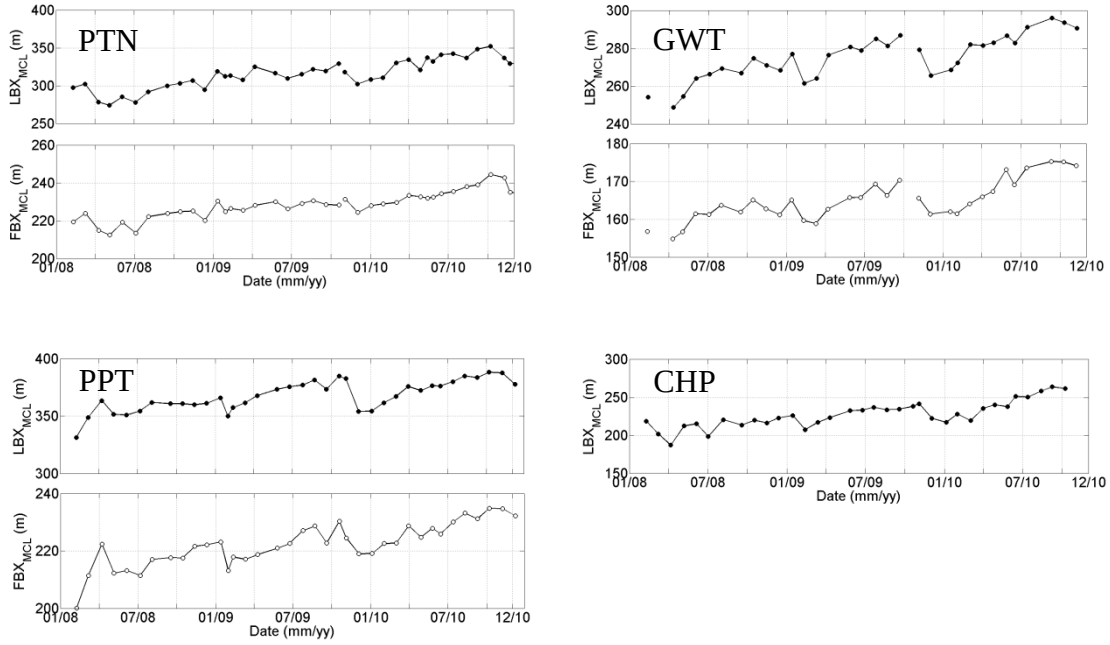

Figure 4.28 – Momentary coastline position for each month and for each site; LBX_{MCL} (black lines) and FBX_{MCL} (grey lines) for each site. FBX_{MCL} is missing for CHP owing to restricted coverage at the top of the beach, see text for further details.

PTN experienced greatest movement in the momentary coastline between November-December 2008 and November-December 2009, while the other sites experienced significant shifts between January and February 2009 and November and December 2009 (Figure 4.28). PPT undertook the largest shift in LBX_{MCL} in November 2009 with a movement of 40m over 30days, compared with 20 – 30m at the other sites (Figure 4.28). The greatest correlation between sites was observed between PTN and CHP (0.83, p-value), between PPT and PTN/GWT the relationship was 0.79, while the lowest correlation was between GWT and PTN (0.57).

Figure 4.29 provides a summary of the beach as a whole using the alongshore averaged FBX_{MCL} to highlight the overall state of the beach. This can be further applied to assess the longshore variability in the long-term response of the beach by calculating the individual FBX_{MCL} for numerous cross-shore profiles. For PTN the alongshore variability is minimal with offshore migration evident punctuated by landward shifts in the FBX_{MCL} in response to storm conditions. Similar trends are evident at CHP with the

central beach having a dominant effect on the cross-shore position. PPT and GWT, however, both exhibit a clear longshore variability in the FBX_{MCL} position. Importantly, the two periods of loss across the shoreface acts to re-set the entire beach before a period of seaward migration resumes. The pattern observed at GWT highlights the shift from an alongshore linear beach profile to the crescentic dominated shape which sees the FBX_{MCL} extend further offshore to the south of the area more rapidly than the response seen at the north of the area.

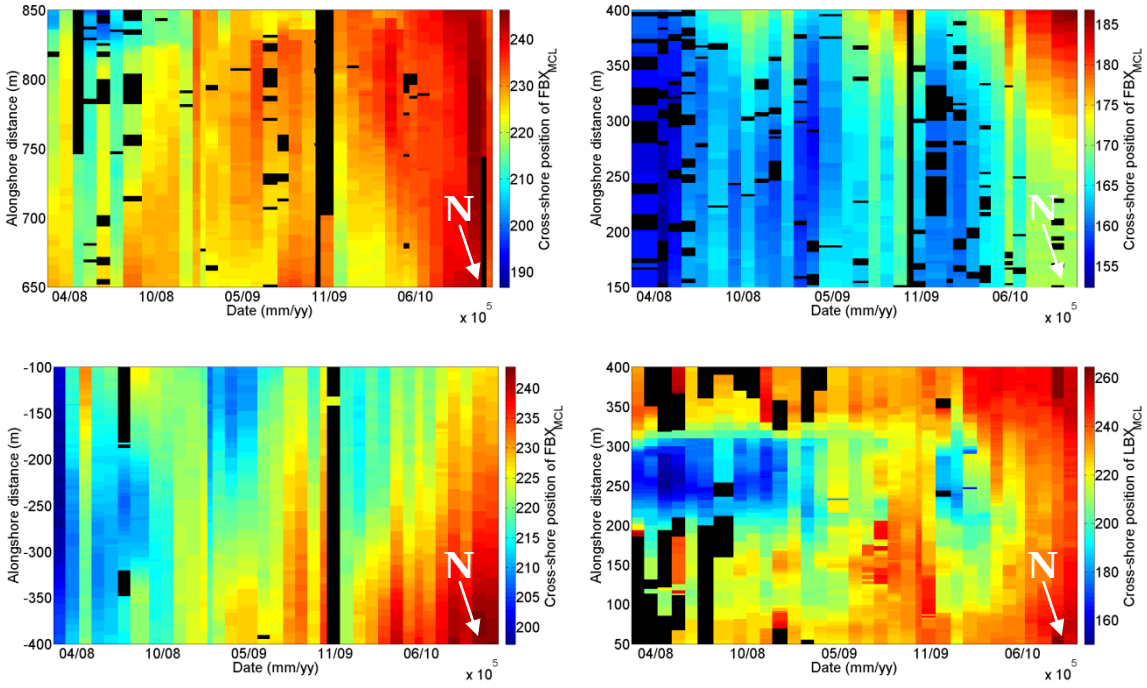

Figure 4.29– Surface plots showing alongshore variability of FBX_{MCL} for the survey period; Top row (l-r), PTN and GWT, bottom row (l-r) PPT and CHP. Black regions indicate where the surveyed profile width was insufficient to calculate the FBX_{MCL} and so have been omitted. For all plots north is at the bottom and south is at the top.

4.4.3 Comparison with beach model

The beaches can be classified using the conceptual beach classification for UK beaches (Scott *et al.*, 2010) which builds on the initial scheme devised by Masselink and Short (1993). All four sites are predominantly distributed within the intermediate grouping (Figure 4.30) and, as expected, display a move towards more dissipative classification

as a result of increased wave conditions. Whilst this model does not resolve the more detailed shifts within the intermediate state, it provides clear context for the grouping of these beaches.

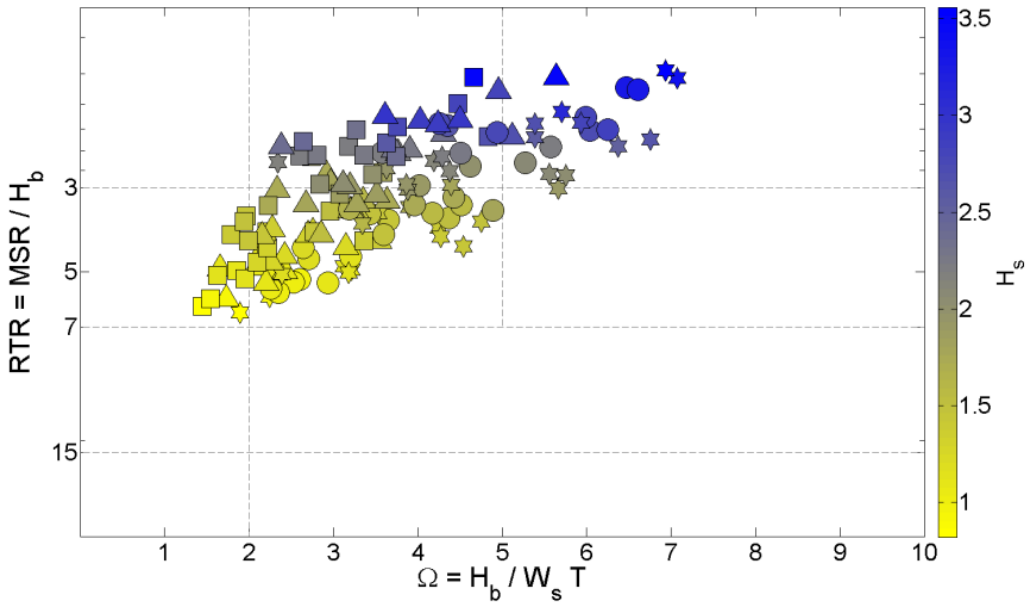

Figure 4.30– Conceptual classification of monthly beach states for each site incorporating the relative tide range (RTR= MSR/H_b) and the weighted mean dimensionless fall velocity (Ω= H_b/W_sT). Shading indicates the wave conditions with blue indicating more energetic larger waves and yellow for smaller waves. The central dashed box represents intermediate beaches, based on (Masselink & Short, 1993), see text for detail

4.5 Beach Classification

Tools such as the momentary coastline provide a means to compare different beaches and assess the coastal response as a whole. More detailed assessment of beach response requires a reference point from which it is possible to identify state transitions. Whilst some transitions are subtle, others are more distinct and can be easily observed; both are important in understanding the characteristics of a beach and how it adapts to the changing forcing conditions. To identify the occurrence of transitions it is necessary to classify the four sites from the observations made over 3 years into dominant beach "states".

Using the idealised morphological responses outlined in Section 4.3, qualitative descriptors of the dominant low tide variability have been summarised with comparative surface elevation models in Figure 4.31.

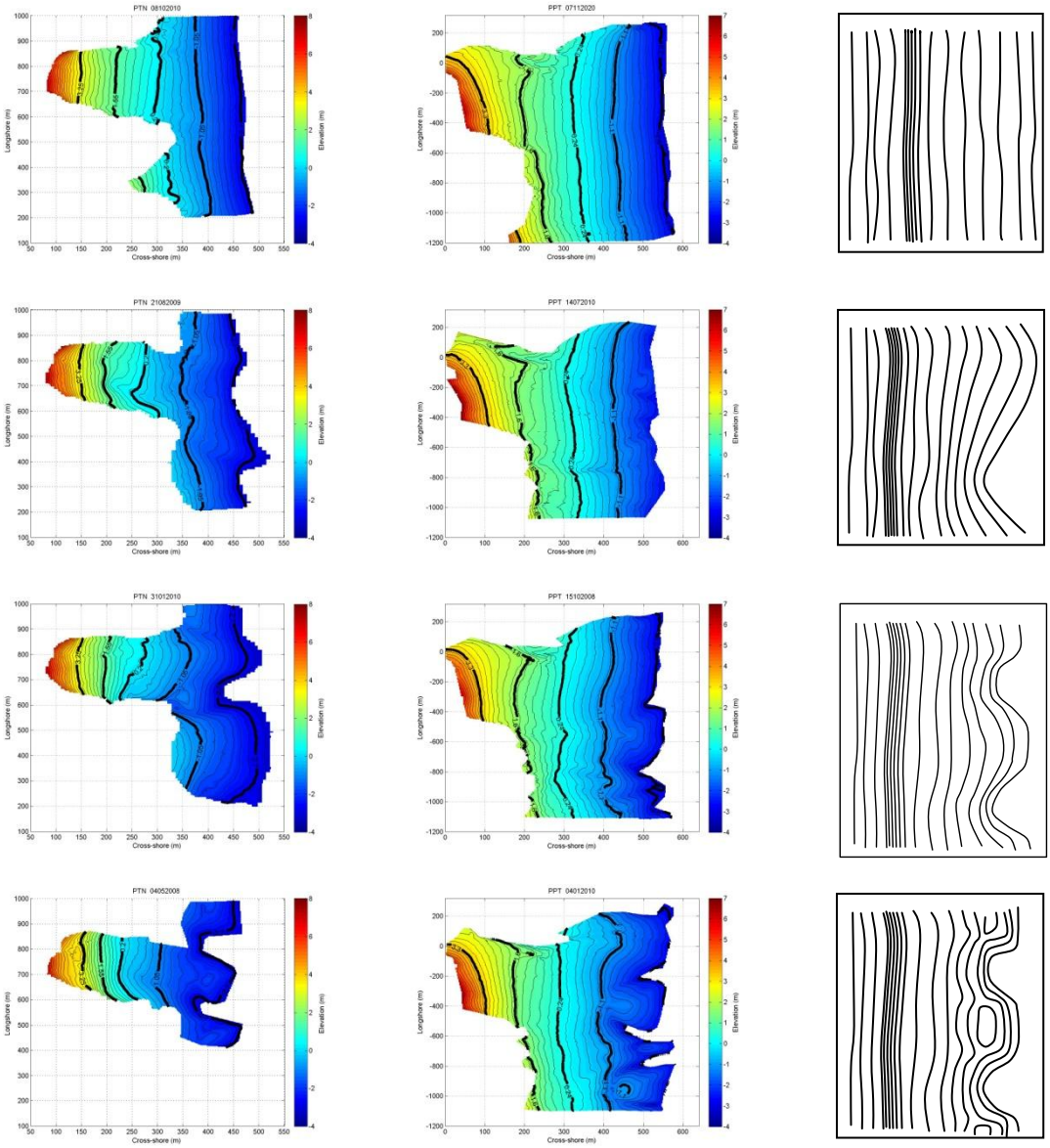

Figure 4.31– Schematic contours of idealised intertidal beach states based on the four sites (right column) with example morphology from PTN and PPT (left and middle column); from the top, low tide **planar**, low tide **rhythmic**, low tide **rhythmic/channel** and low tide **bar/rip.** For PTN each state can also incorporate an upper beach berm as identified by grouping of contours in the upper beach.

Four different beach states were identified: “planar”, “low tide rhythmic”, “low tide rhythmic / channel” and “low tide bar / rip” (Figure 4.31). These states build on the present literature and will be further incorporated into the subtidal variability discussed in Section 4.6. Transition from planar (top) to low tide bar/rip (bottom) is referred to as a down-state shift.

Time series of beach state for the different sites are shown in Figure 4.32 and demonstrate that PTN is the most dynamic and GWT varies the least. There is reasonable correspondence between PTN, CHP and PPT, with the overall up-state/down-state transitions well represented, despite disparity between exact states. For example PTN CHP and PPT exhibit a down-state transition from January 2009 to March 2009, (Figure 4.32), followed by an up-state return.

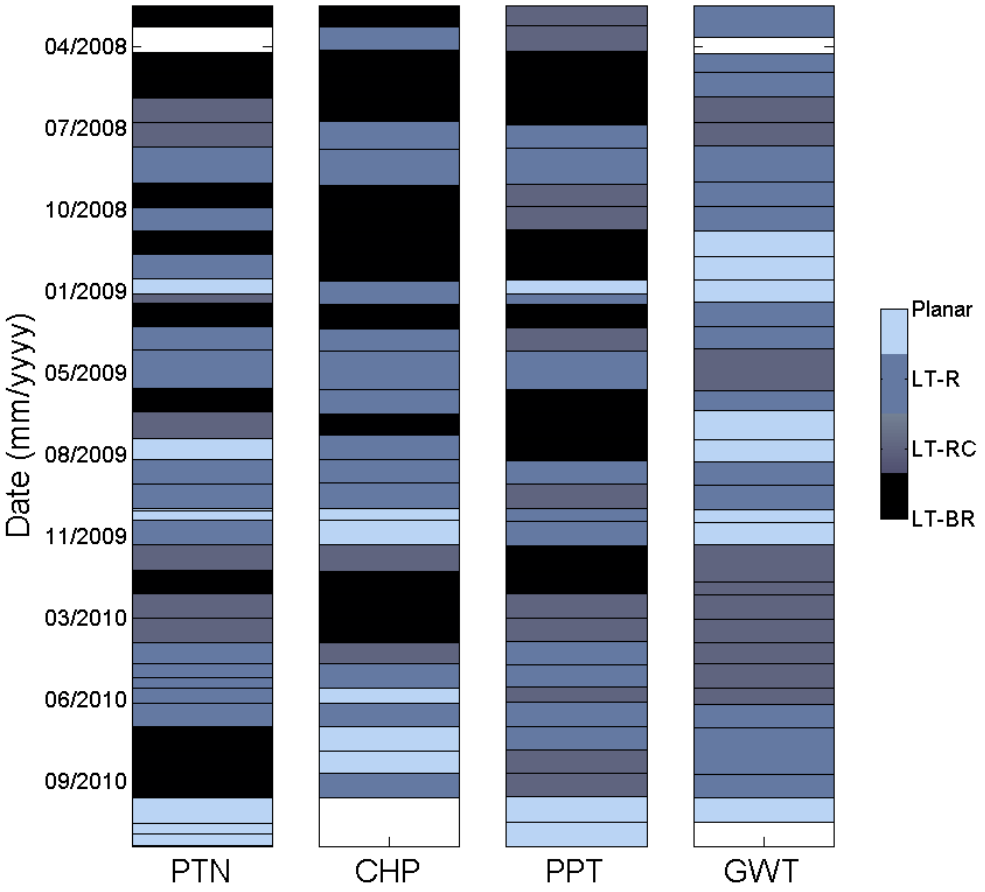

Figure 4.32– Intertidal morphodynamic classification for each site. Dark shading represents highly 3D bar/rip system, lighter shading indicates planar conditions. White strips represent missing data/classification unavailable.

None of the sites exhibit a significant dominance towards any of the four beach states (Table 4.1),although the planar condition is predominantly the least common.

Table 4.1– Percentage occurrence of beach states for individual sites

Site	Low Tide Bar/ Rip	Low Tide Rhythmic/ Channel	Low Tide Rhythmic	Planar
PTN	30	19	32	19
PPT	30	30	30	11
CHP	39	6	39	15
GWT	–	31	44	25

Comparison of these "states" with the automated $\overline{CV}$ value shows good correlation (Figure 4.33) with overall up-state/down-state phases well identified. Sites with more defined low tide features (PTN, CHP) fit the data more closely, but PPT also shows good overall agreement. The shifts between planar and rhythmic for GWT are subtle with only occasional development of channels to distinguish these phases. These plots also act to identify the relative response between the sites. In a similar trend to that identified with the fluctuation in volume we see greater variability in the beach state within the first year of observations, particularly at PTN and CHP (Figure 4.33). From January 2009 a clearer response is observed which sees a peak in increased 3D states at that start of the year before beaches becoming increasingly 2D towards the mid-end of year. The largest response occurs over the 2009 – 2010 winter, with all sites experiencing a pronounced and sustained increase in 3D beach morphology.

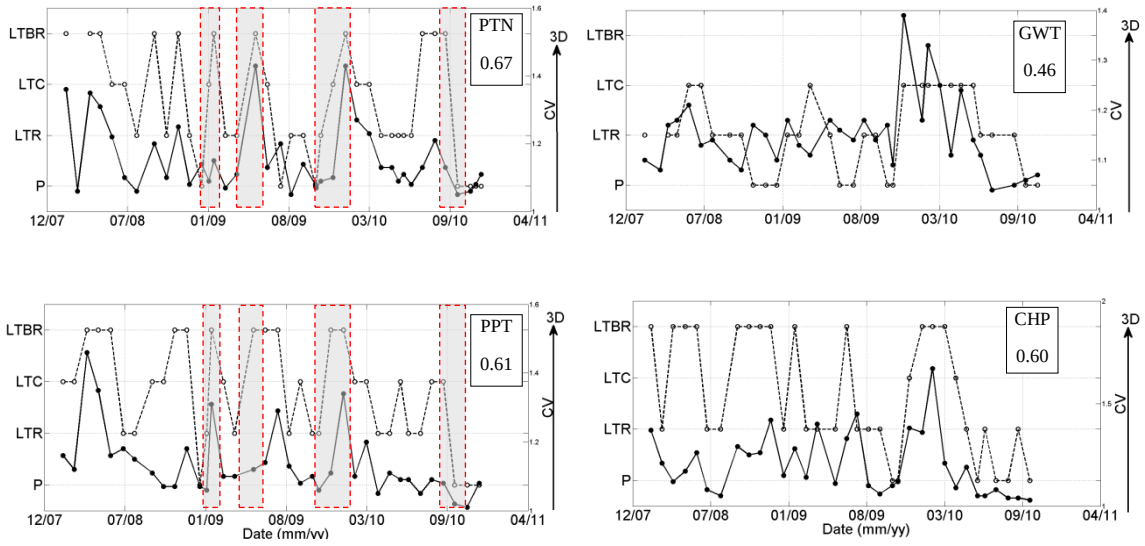

Figure 4.33 – Comparison of qualitative beach states (dashed lines) with contour derived CV values (solid lines); Top row (l-r), PTN and GWT, bottom row (l-r) PPT and CHP. The correlation coefficient of the two approaches for each site is displayed. Red shaded boxes highlight periods of response further discussed in Section 4.8.

Whilst there is coherence between sites with up-state/down-state transitions observed on the same temporal scales, a seasonal signal in response to varying wave conditions is

not clear (Figure 4.34). Monthly wave height frequency distributions highlight the seasonal nature in wave conditions; however, the response observed through the relative $\overline{CV}$ and $\bar{\bar{\Omega}}$ does not follow this seasonal pattern (Figure 4.34).The classic winter/summer beach morphological response does not occur with any consistency; instead, 3D/2D conditions are experienced throughout most months at some interval during the 3 year dataset, and a clear correlation between wave forcing and beach state cannot be discerned (Figure 4.34).

While the comparison between the beach states and the automated CV value is well correlated, neither approach indicates a seasonal signal in the beach response. while a longer record may reveal a more long-term pattern the present data suggests a more event driven system. the important aspect of this response is the speed of recovery following specific state changing storms. where the morphological response is slow any seasonal beach state development will be masked by recovery phases.

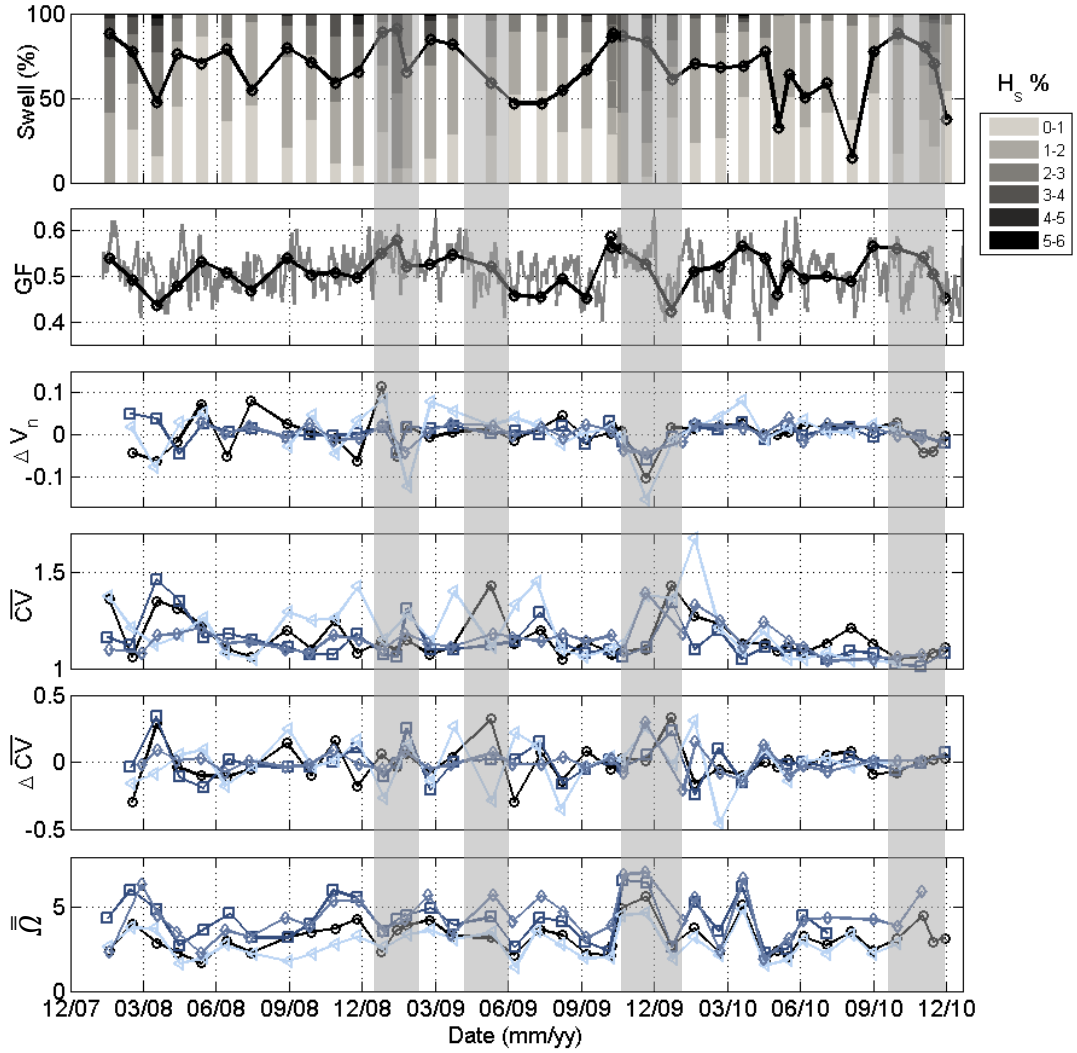

Figure 4.34– Morphological summary showing from top to bottom: percentage occurrence of significant wave height during survey intervals (bars) and percentage swell component of spectral energy (solid line); daily mean Groupiness Factor (grey line) and weighted survey interval GF; monthly change in the beach sediment volume; degree of 3D parameterised by $\overline{CV}$; monthly change in $\overline{CV}$; and dimensionless fall velocity $\bar{\bar{\Omega}}$. Vertical boxes highlight periods identified in Figure 4.33. Symbols reflect the four sites; CHP (triangle); PTN (circles); PPT (square); GWT (diamonds).

4.6 Subtidal Response

4.6.1 Introduction

This section introduces the nearshore response observed using the Argus images from PPT and PTN. Breaker patterns were identified using the BLIM Argus tool (Pape *et al.*, 2007), which provides a good representation of the nearshore bathymetry, albeit qualitative. The objective of this technique was to identify and classify the nature and

extent of morphological variability within the subtidal region. It was intended to link the intertidal morphological response with corresponding shifts in the subtidal bathymetry, helping to further address the timescales of response between the spatially distinct systems.

The accurate identification of nearshore bars requires limits to the image selection to prevent false identification of bar morphology and the following criteria were employed for bar identification:

- H_s= 0.8m to 1.8m
- Tide level between -2.5m and -3.5m ODN
- Good image quality (no rain, fog etc)

This approach maximised image quantity, whilst restricting the cross-shore artificial "movement" of the bar through varying breaker/water level conditions and resulted in 692/1083 images for PTN/PPT collected over 2.3/3 years.

4.6.2 Bar Classification

Similar to the intertidal responses observed at PTN and PPT, the Argus images indicate a range of variability within the subtidal region, and the main beach states were manually categorised (Figure 4.35). To maintain consistency and aid comparison, the key "states" have been grouped under headings dominant in recent literature and include the generally accepted sequence of stages associated with transition from up-state dissipative planar beaches with a longshore bar-trough system down-state through crescentic bars, attached crescentic bars, transverse bars intersected by dominant rip channels. A multi bar state has also been recognised.

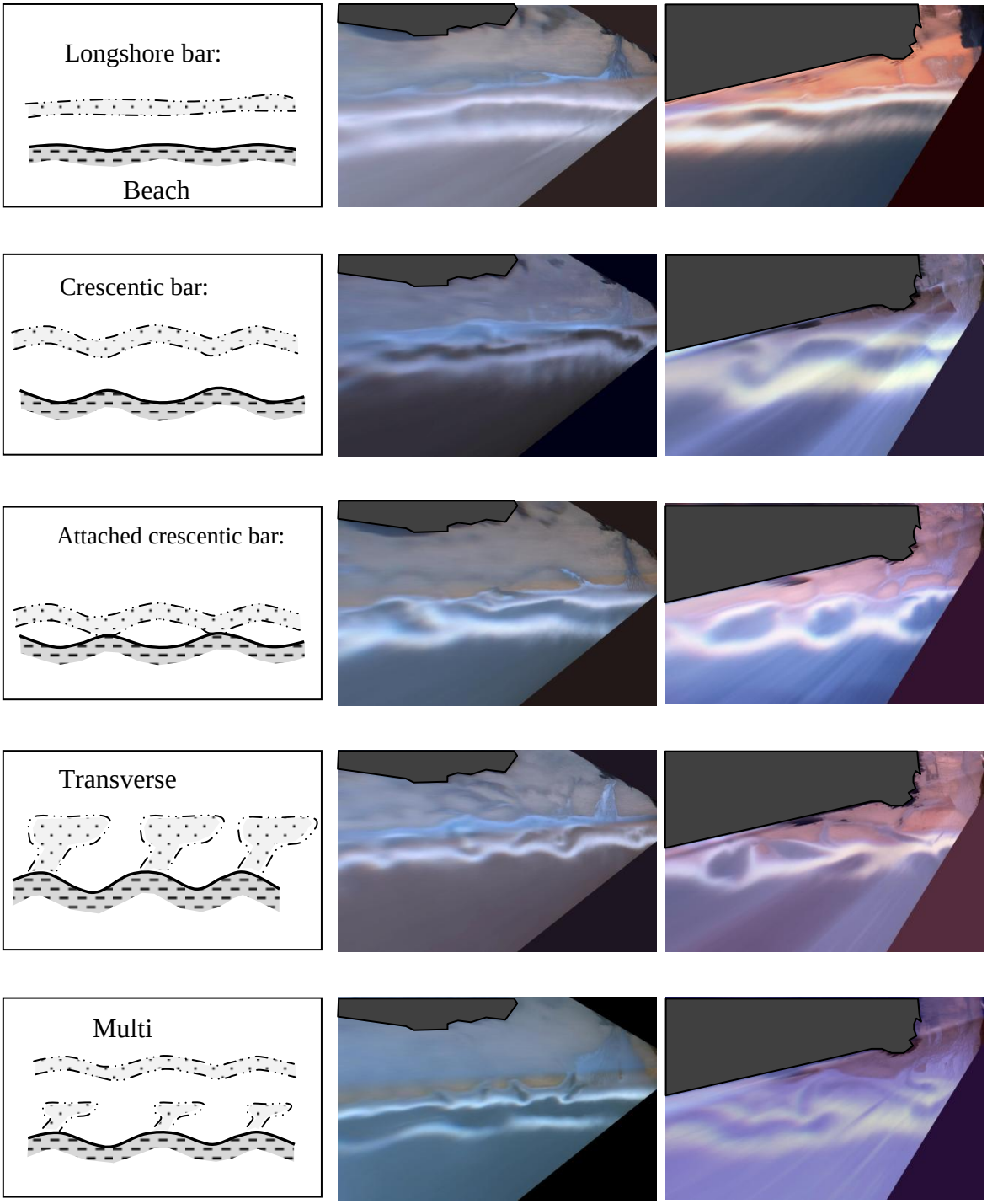

Figure 4.35 –Subtidal bar classification (left column) based on observations of the dominant bar dynamics at PPT (central column) and PTN (right colmun) rectified Argus images. The above images identify the dominant states observed but not a sequence of states for either site, these are presented in Figure 4.36.

4.6.3 PTN Bar Dynamics

There is little evidence of a seasonal cycle in bar behaviour or dynamics at PTN. At the start of the image collection (September 2008) the system was dominated by low tide bar/rip morphology, affecting the breaker pattern at the shoreline, with little evidence of a nearshore bar. Throughout the 2008/2009 winter the subtidal region developed with complex transverse bars defining the breaking zone. Intensive storm events during Nov – Dec 2008 (discussed further in Section 4.8) resulted in the formation of an alongshore rhythmic bar. Following further storms in January, further material was moved offshore from the intertidal region and in-filled sections of the subtidal trough between the shoreline and the existing bar (Figure 4.36). The resulting highly crescentic attached system remained dominant at PTN throughout most of 2009, whilst the intertidal beach volume gradually increased.

Energetic storm conditions during Nov-Dec 2009 (discussed further in Section 4.7) caused widespread redistribution of intertidal sediment to the subtidal region, resulting in detachment of the bar to the north and a build-up of material in the centre of the survey area, forming a complex multi bar system. Over the subsequent 3 months this material gradually moved onshore, resulting in the creation of an extensive low tide bar system. Under continued onshore movement this bar gradually merged fully with the shoreline resulting in a small single bar that was still present in the nearshore region by April 2010 (Figure 4.36).

During the remainder of 2010, the bar continued to move onshore and weld with the shoreline, which became increasingly 3D as low tide channels developed. However, these were small-scale features and not sufficiently developed to withstand destruction during energetic wave conditions in September/October 2010 which left the intertidal

beach relatively featureless. Following intensive storm events in November, resulting in a loss of material from the intertidal region, a longshore bar/trough developed.

4.6.4 PPT Bar Dynamics

At the start of 2008, PPT exhibited a complex system with a nearshore longshore rhythmic bar and well developed low tide bar/rip morphology. This developed into a more pronounced transverse bar system as these channels extended offshore through the breaker line during the calmer summer wave conditions. As conditions became increasingly energetic (Nov/Dec) the low tide rips intersecting the longshore bar were removed and the system was defined by a crescentic longshore bar which remained attached at the centre of the survey area. Throughout 2009 and much of 2010 this state dominated with the greatest change observed in the position of the alongshore attachment of the bar (Figure 4.36). Storm conditions in November 2009 resulted in the bar detaching and a longshore crescentic state developed; however, by February 2010 a transverse connection with the shoreline became re-established (Figure 4.36). Calm conditions throughout most of 2010 lead to the bar reducing in size and moving closer to the shoreline. More energetic conditions from September onwards resulted in a similar response to that observed at PTN with a longshore shore parallel bar developing, although again full detachment from the shoreline did not occur.

Although there is evidence of both in-phase and out of phase coupling of the nearshore bar and the shoreline at PTN and PPT (Figure 4.36) the relatively short length of the dataset and the variability in the subtidal bar shape restricts more detailed analysis. Price *et al*, (2011) utilised 9.3 years of Argus images to identify coupling of a double barred system of the Gold Coast, Australia. They found coupling during 40% of the observations with the angle of wave incidence a controlling factor on coupling

behaviour. While PTN and PPT are characterised by a single bar, the low tide bar development has been shown to be well correlated with the bar behaviour following storm events, continued image collection at both sites will enable further work on this trend to be undertaken.

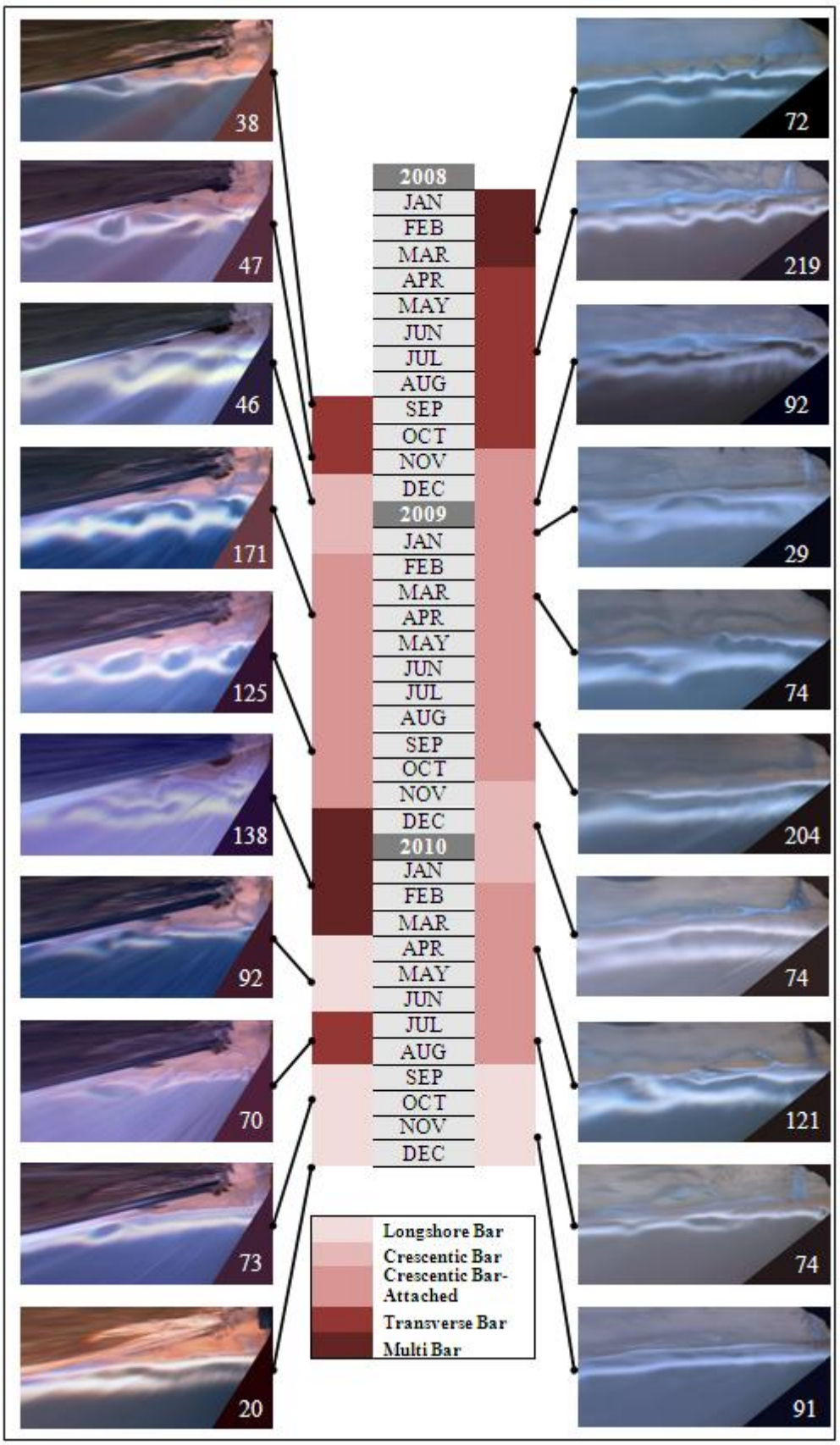

Figure 4.36 –Subtidal classification (red shading) for PTN (left column) and PPT (right column) throughout the 3-year survey period. Images depict breaker patterns present during relevant phases while the numbers correspond to the approximate number of days the depicted bar shape lasted.

4.6.5 Bar Migration

The subtidal bar dynamics at the two sites showed a distinct similarity. Both sites exhibited low tide dominated morphology which then developed into alongshore rhythmic bar following storm events. Whilst PTN was characterised by a highly rhythmic crescentic bar (λ = 350m), PPT is defined by a longer wavelength rhythmic system (λ = 550m).

By the end of the survey period both sites exhibit similar longshore parallel bars, reflecting consistencies observed in the intertidal morphology. The cross-shore position of the nearshore bars at both sites also exhibit similar trends (Figure 4.37). Both PTN and PPT experienced offshore migration of their bar systems between mid-2008 and the start of 2010 (Figure 4.37). The offshore bar migration rates for PTN and PPT were 0.13 and 0.21 m day^{-1}, respectively, and these rates correspond closely with the offshore migration rate of 0.06 m day^{-1} for the cross-shore position of the LBX_{MCL} (Figure 4.37). Following the extensive volume reduction experienced at both sites in November 2009, the LBX_{MCL} position again continued to move offshore as the beaches recovered; however, the bars migrated onshore with migration rates of 0.74 and 0.31m day^{-1} for PTN and PPT, respectively.

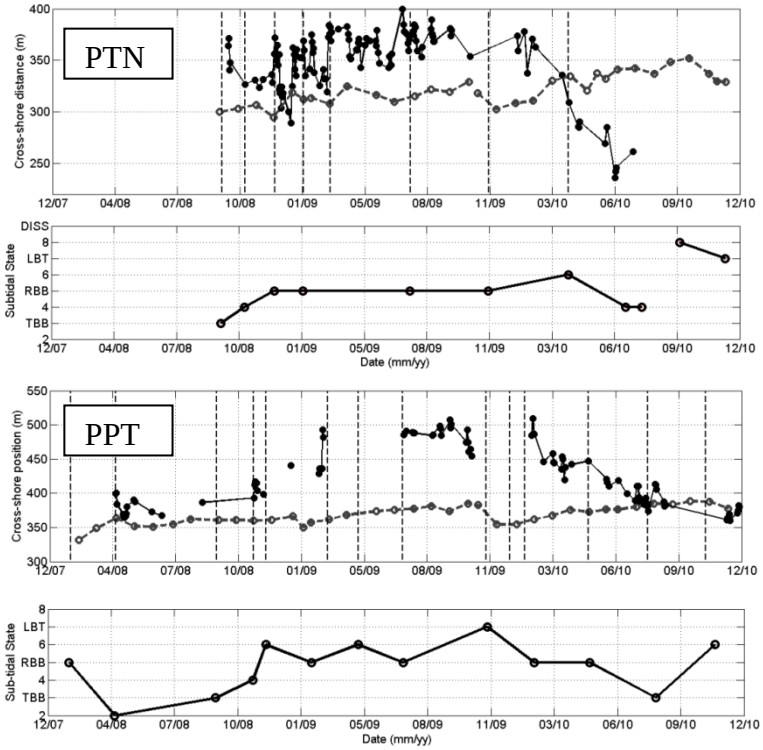

Figure 4.37– Bar dynamics throughout the survey period for PTN (top 2 panels) and PPT (lower 2 panels); for each site the top panel shows the cross-shore bar position (solid line) and X_{MCL} position (dashed line), and the subtidal bar state in the bottom panel. Bar positions have been adjusted onshore to aid comparison with the X_{MCL} position. The vertical dashed lines indicate periods of change in the bar shape, identified from the Argus images, although not always sufficient to change the classification.

4.6.6 Bar and Beach Response

The long term relationship between the subaerial state and the subtidal response is explored in Figure 4.39. Grouping the weekly/monthly images/morphology into different states helps identify patterns in the behaviour of each system and in turn any joint response which may be present. While the limitations in the image analysis prevents more detailed quantification of the changing subtidal patterns it is clear from Section 4.6.3 that the subtidal system has a longer residence than the more dynamic intertidal morphology (Figure 4.38).It is possible to identify a more combined response in both the subaerial and subtidal behaviour for PTN than PPT, especially during 2010, while the long residence of bar behaviour at PPT does not reflect the more responsive

low tide region of the beach face. However without a longer record such assessments are hard to define conclusively.

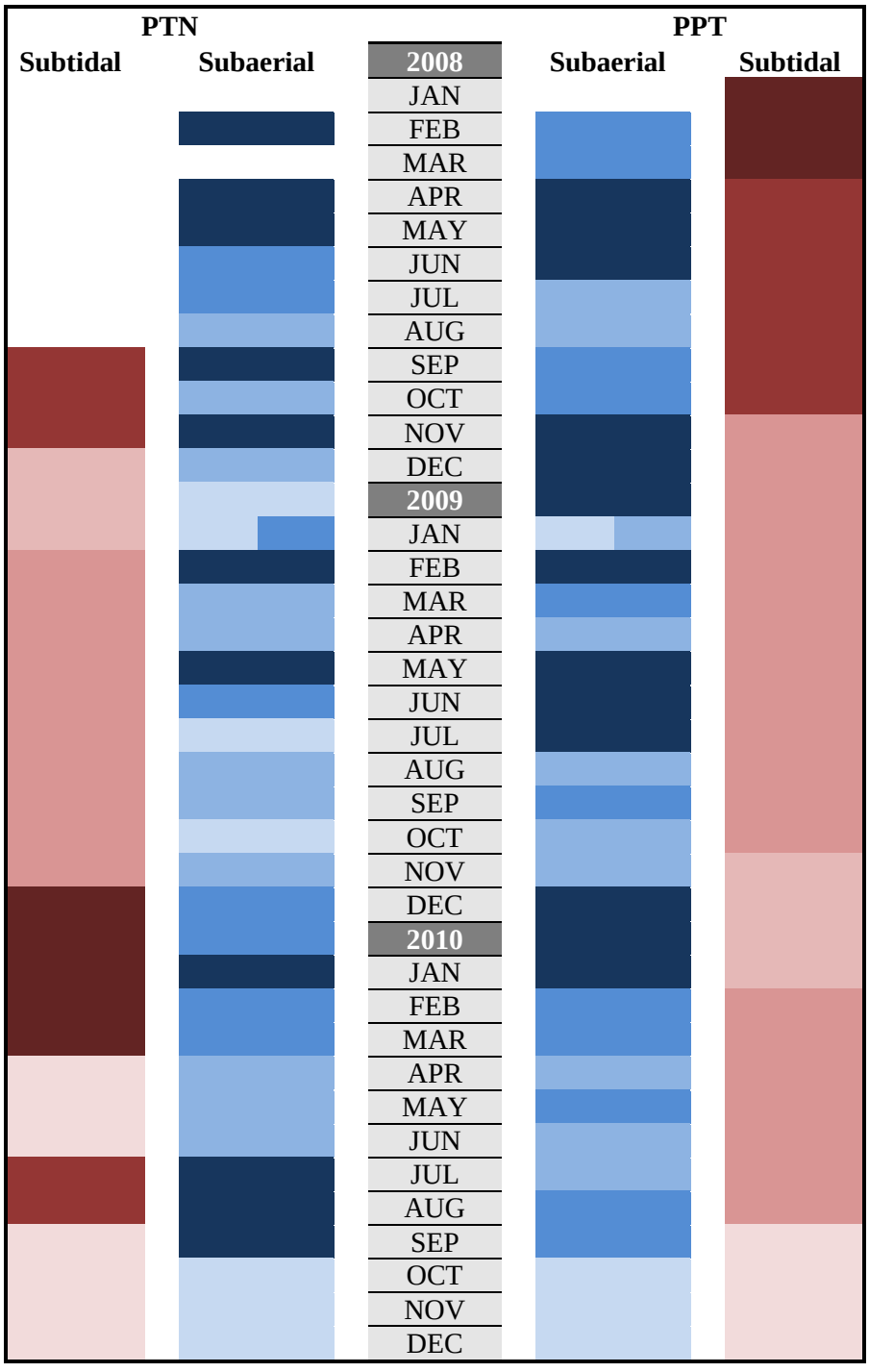

Figure 4.38 –Previous page: Temporal variability of intertidal beach state (blue shading) and subtidal bar states (red shading) throughout the survey period.

4.7 Storm Response

Nearshore wave data from Perranporth was used to identify periods of energetic conditions throughout the survey period. Individual storm events were classified using the peaks-over-threshold approach described in Section 2.2.2, with storms classified as having an H_s=> 4m and a duration > 1.5hrs (Table 4.2). Storm distribution follows a strong seasonal behaviour with peak events occurring during winter months (Figure 4.39). Whilst individual storms exhibited similar values of significant wave height and wave period, the cumulative duration of events between surveys identifies specific periods during which sustained storm-dominated wave conditions were experienced (Figure 4.39).

Table 4.2– Summary wave conditions and duration of storm events experienced between 2008 – 2010. Dashed boxes highlight events occurring prior to substantial intertidal volume loss at most sites.

Date	H_{max} (m)	H_s(m)	T_p(s)	T_z (s)	Dir (°)	Duration (hrs)
31-Jan-08	9.15	5.12	12.5	7.7	287	9
04-Mar-08	8.48	5.01	15.4	8	296	8
10-Mar-08	9.37	8.7	18.2	10.3	272	24
12-Mar-08	9.18	6.53	15.4	8.5	293	15
21-Mar-08	7.15	4.56	11.1	7	295	14
28-Mar-08	7.43	4.58	13.3	7.5	282	7
31-Mar-08	9.22	4.28	14.3	7	290	3.5
13-Aug-08	6.88	4.83	12.5	7.4	287	7.5
18-Aug-08	5.36	4.28	16.7	8.9	280	8
24-Nov-08	9.63	4.9	10.5	7.4	298	19
05-Dec-08	8.44	5.98	16.7	8.5	290	20
18-Jan-09	7.17	4.81	20	10	289	72
25-Jan-09	8.89	5.18	18.2	10.3	287	22.5
08-Mar-09	7.05	5.64	15.4	8.3	-	19
28-Aug-09	8.74	4.67	11.8	7.3	288	7
04-Nov-09	9.13	5.29	16.7	8.5	289	37.5
07-Nov-09	8.18	5.46	18.2	8.2	296	23
14-Nov-09	5.57	5.18	15.4	7.4	275	6.5
22-Nov-09	7.71	5.69	18.2	8.7	287	29
30-Nov-09	6.65	4.68	10.5	7.4	322	7.5
03-Dec-09	6.24	4.36	15.4	7.8	284	5.5
09-Dec-09	6.01	4.13	18.2	10	288	2
29-Jan-10	7.98	4.6	10	7.3	306	2.5
31-Mar-10	8.68	6.25	11.8	8	297	19
03-Nov-10	6.47	4.11	18.2	8	291	4
11-Nov-10	9.29	6.3	14.3	8.7	290	16.5

Using duration of storm events as a measure of erosive conditions we see strong correlation with periods of widespread sediment loss between February 2009 and December 2009 in response to >90hrs of energetic wave conditions; conversely, there is poor correlation with the sediment removal observed at PPT and PTN in November

2010 with <20hrs of storm conditions. In addition there is disparity in the response to >60hrs of storms in March 2008 with PTN and CHP experiencing loss while PPT experienced a net increase in beach volume (Figure 4.27).

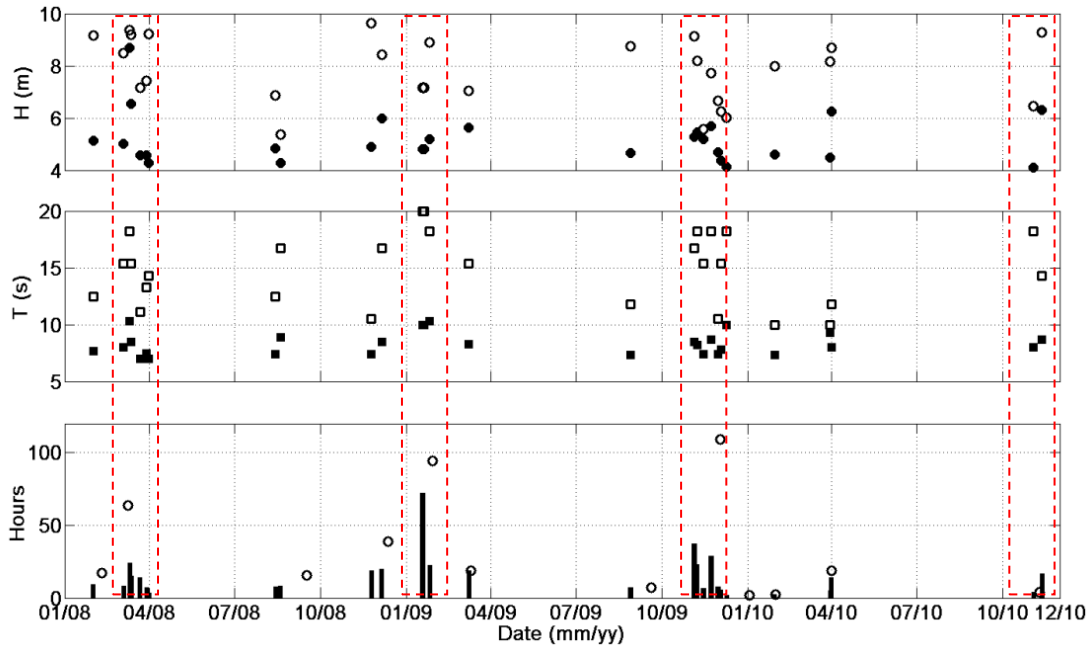

Figure 4.39 – Summary storm statistics derived from data presented in Table 4.2. From the top; Peak wave height (H_s black circles, H_{max} hollow circles), peak wave period (T_z black squares, T_p hollow squares) and duration of individual storm events (bars) with the total storm durations between individual surveys (hollow circles, hrs). Dashed red boxes indicate periods of intertidal loss observed at most sites.

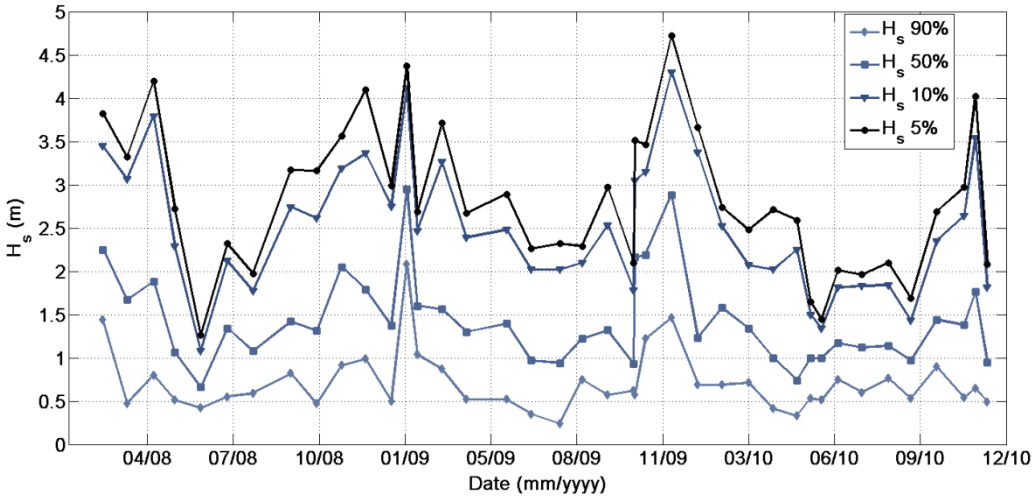

Figure 4.40– Significant wave height exceedance values for H_s90%, H_s 50%, H_s 10% and H_s 5%. Data points are derived from the nearshore wave buoy (10m CD) and indicate the conditions since the previous survey.

From the 27 individual storm events detailed in Figure 4.39, storm analysis has been undertaken for 13 storm periods using pre and post-survey data as close to the storm events as available (Table 4.3). As identified in Section 4.3, the maximum morphological response at all sites generally occurs between MLWN and MLWS, but for macrotidal regions the ability to obtain comparative data severely restricts the ability to survey immediately prior to or immediately following a storm. In addition, the nature of highly dissipative beaches means cross-shore run-up distances can be in the order of 200m, again restricting access to the region of interest. Because of this, the pre/post-storm intervals are often larger than ideal, and as such the Argus images are used when possible to aid in interpretation. Summary intertidal response, incorporating beach state and volume, from PTN and PPT is presented in Table 4.3. This highlights the similar response observed between both sites from 2009 – 2010, where we see down-state shifts in intertidal morphology in conjunction with drops in beach volume following sustained periods of energetic conditions. However, where storm events are more short lived the transitions are predominantly mixed, reflecting no coherence between sites.

Table 4.3– Summary of storm activity between surveys and the beach response observed for PTN and PPT. Periods in bold/dashed boxes highlight matching response at each site. NC = no change.

Storm Period	Duration of storms (hrs)	Storm Impact (No/hrs)	RTR	Beach Response (up-state/down-state)		Volume (increase = +, decrease = -)	
				PTN	PPT	PTN	PPT
Mar –Apr 2008	**63.5**	**13**	**0.84**	**Down**	**Down**	**-**	**+**
Aug – Sept 2008	15.5	8	1.09	Down	Up	+	-
Nov –Dec 2008	39	19	0.81	Up	Down	-	+
Jan 11th – Jan 29th 2009	**94.5**	**47**	**1.07**	**Down**	**Down**	**-**	**-**
Feb – Mar 2009	19	19	1.09	Down	Up	-	+
Aug – Sept 2009	7	7	0.79	Up	*NC*	-	-
Nov– Dec 2009	**109**	**18**	**1.19**	**Down**	**Down**	**-**	**-**
Dec 2009 –Jan 2010	**2**	**2**	**1.56**	**Down**	**Down**	+	-
Jan – Feb 2010	**2.5**	**2.5**	**0.88**	**Up**	**Up**	**+**	**+**
Mar– Apr 2010	**19**	**19**	**1.48**	**Up**	**Up**	**+**	**+**
Oct –Nov 2010	4	4	0.38	*NC*	*NC*	-	-
Nov – Dec 2010	46.5	47	0.74	*NC*	*NC*	-	-

4.8 Transitionary Events

Monthly topographic surveys have provided a comprehensive overview of the dynamic nature of the four sites in response to seasonal shifts in the wave climate. However the dataset does not provide a clear interpretation of the behaviour of the beaches, therefore more constructive discussion is produced through in-depth analysis of specific events incorporating all aspects of the forcing conditions and the antecedent beach state. Due to the availability of video imagery, only PTN and PPT are used here for detailed response characterisation analysis. These sites exhibited strong low tide bar rip morphology, as well as highly 2D planar beach states, and incorporate the full range exhibited by intermediate beaches. These sites also show strong coherence in volumetric response as well as more generalised beach states.

The following section identifies four key periods of morphological change (Section 5.5) as a result of distinctive wave forcing. For each period detailed analysis incorporates wave climate characterisation, morphodynamic behaviour, tidal states and nearshore breaker patterns. The periods of interest are;

- **January 11th– January 29th 2009**
  - Persistent storm conditions for >3days.
- **April 8th – May 25th 2009**
  - Development of low tide bar/rip system under "normal" conditions.
- **November 4th 2009 – January 4th 2010**
  - Recurrent storms and the development of a low tide bar/rip system
- **July 14th – September 9th**
  - Small scale low tide channel system response to increased waves.

4.8.1 January 11th– January 29th 2009

The first period of response follows a sustained period of storm conditions which occurred over two weeks in mid-January 2009 (Figure 4.41). With 50% H_s exceedance

= 2.95m and 10% H_s exceedance of 4.37 m the event was the second-largest over the 3 years. The period was characterised by swell dominated waves with the peak waves coinciding with neap tides (Figure 4.41).

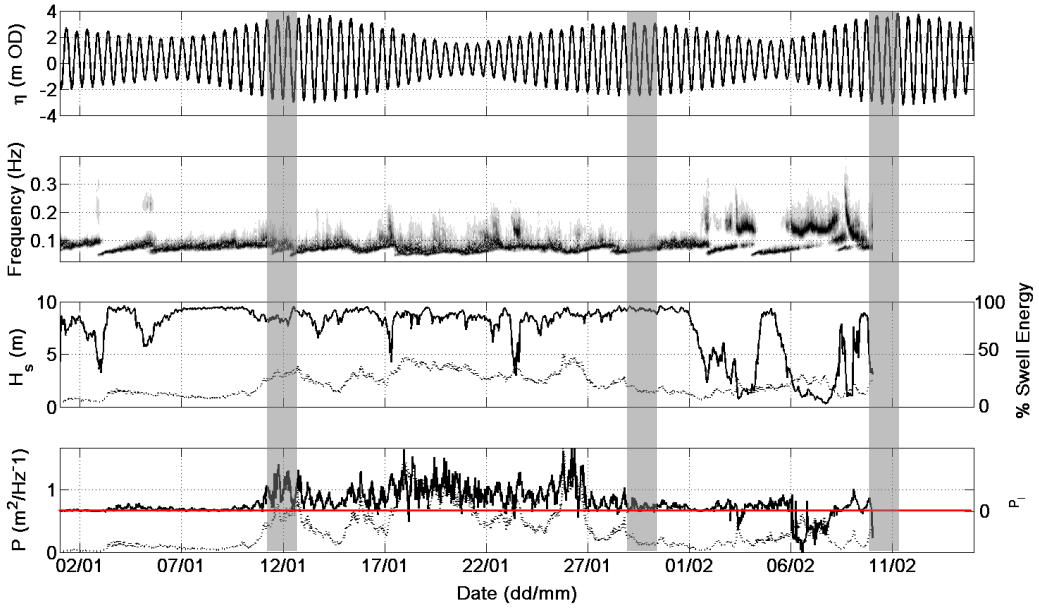

Figure 4.41– Summary of the wave conditions for January 2009. From top to bottom: still water level η; wave spectrum; significant wave height H_s(dashed line) and % swell energy (solid line); wave energy flux P (dashed line) and longshore component of the offshore wave energy flux P_l (dashed line), where positive indicates northerly directed. The grey shaded boxes indicate beach surveys. Missing data at the start of February owing to buoy fault.

.

The beach response observed at PTN showed removal of material from the upper and lower beach, and accretion at the centre of the beach as the profile became increasingly planar. PPT experienced the largest loss of material across the lower and mid-section of the beach with some accretion between MLWN and MLWS (Figure 4.42). This removal of material at both sites is also reflected by a shift in the subtidal morphology inferred from the Argus derived breaking patterns (Figure 4.43). These show that the removed material from the northern headland at PTN was deposited offshore connecting the detached rhythmic subtidal bar to the beach. The channel separating the bar also narrowed as the bar widened. A similar pattern is observed at PPT; before the storm the shore-parallel subtidal bar was attached at the north end of the survey area; after the

storm this attachment had migrated south fed by widespread removal of material above MLWS (red arrows; Figure 4.42).

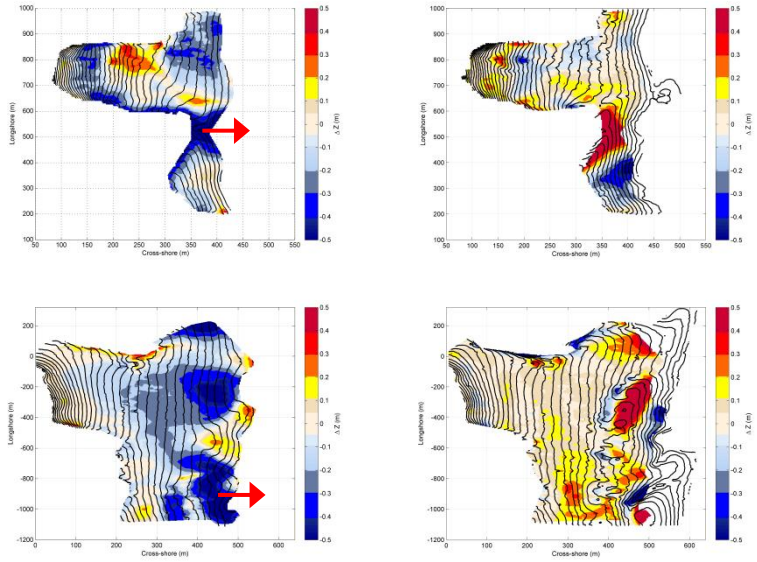

Figure 4.42– Surface plots showing Δz surface plot between January 11th– January 30th and January 30th– February 10th 2009, for PTN (top row) and PPT (bottom row), colours indicate regions of accretion (yellow/red) and erosion (blue). Contour lines show the subsequent morphology. Red arrows indicate movement of material based on subtidal Argus patterns.

Following the storm period, wave heights decreased as the swell dominance was replaced by more localized northerly wind seas. This resulted in the longshore component of the wave energy flux becoming more southerly directed (Figure 4.41). The resulting morphology at the start of February at PTN showed onshore material gain across much of the beach face, in particular the upper high water mark. In addition two low tide bars are present at low tide, as material moved offshore during the storm moves back onshore(Figure 4.43). More extensive response was evident at PPT which underwent widespread accretion across the mid-low tide region with highly 3D morphology developing (Figure 4.42). Within the subtidal region a similar response to the one at PTN was observed with material in-filling the northern end of the channel between the shoreline and nearshore bar (Figure 4.43). This further developed under the post storm conditions.

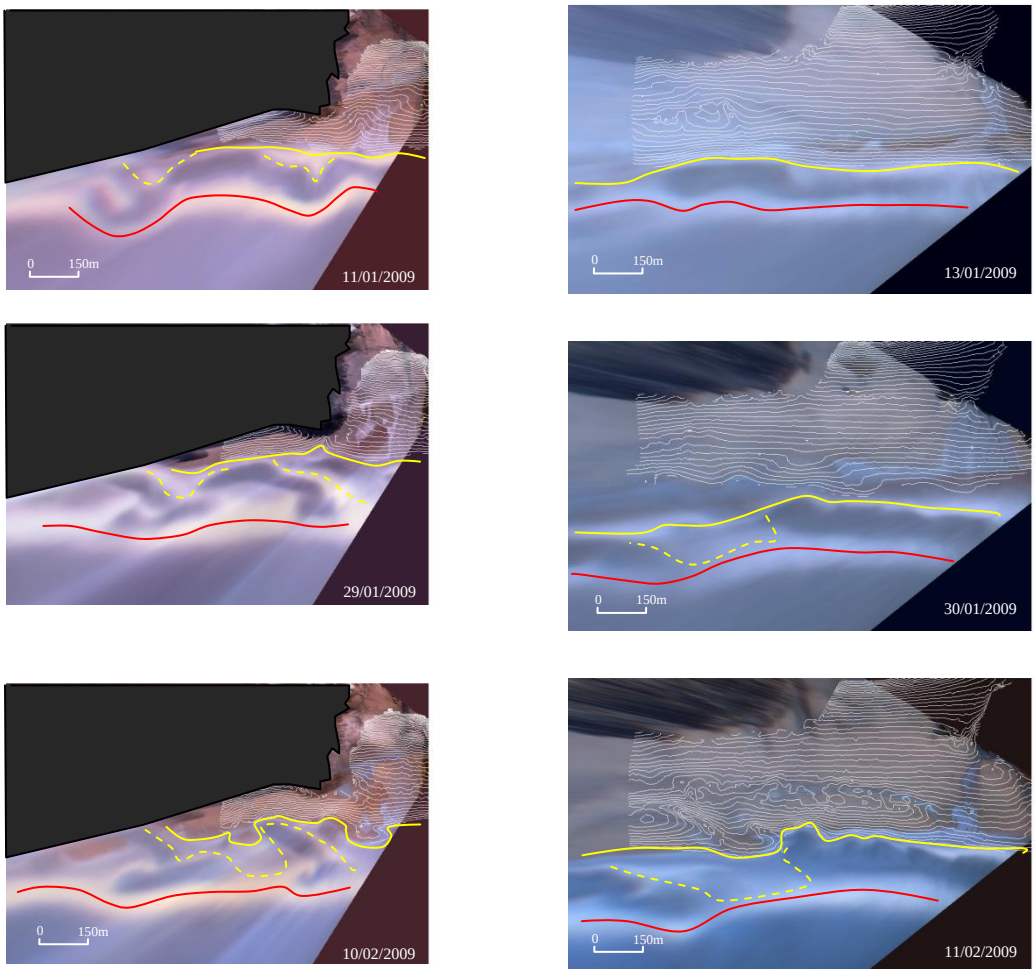

Figure 4.43– Rectified timex images from PTN (left) and PPT (right) with contours of intertidal morphology overlaid. The offshore bar position (red line), shoreline breaker position (solid yellow) and nearshore breaker zone (dashed yellow) are also indicated.

Following a period of sustained energetic conditions widespread removal of material was recorded at both sites. PTN experienced “flattening” of its profile while PPT saw greater erosion at the lower beach. For both sites material was deposited in the nearshore region affecting the subtidal morphology between the main rhythmic shore parallel bar. Overall the widespread removal of material acted to reshape the shoreline (particularly evident at PTN) and resulted in the mobilisation of large volumes of material to the region just below MLWS. Under calm waves this material was then shifted back onshore building on the already 3D shoreface.

4.8.2 April 8th – May 25th 2009

From April to May 2009, wave conditions remained relatively calm (H_s= < 2 m) with mixed wind/swell wave conditions present throughout and little change in the northerly directed offshore wave energy flux (Figure 4.44).

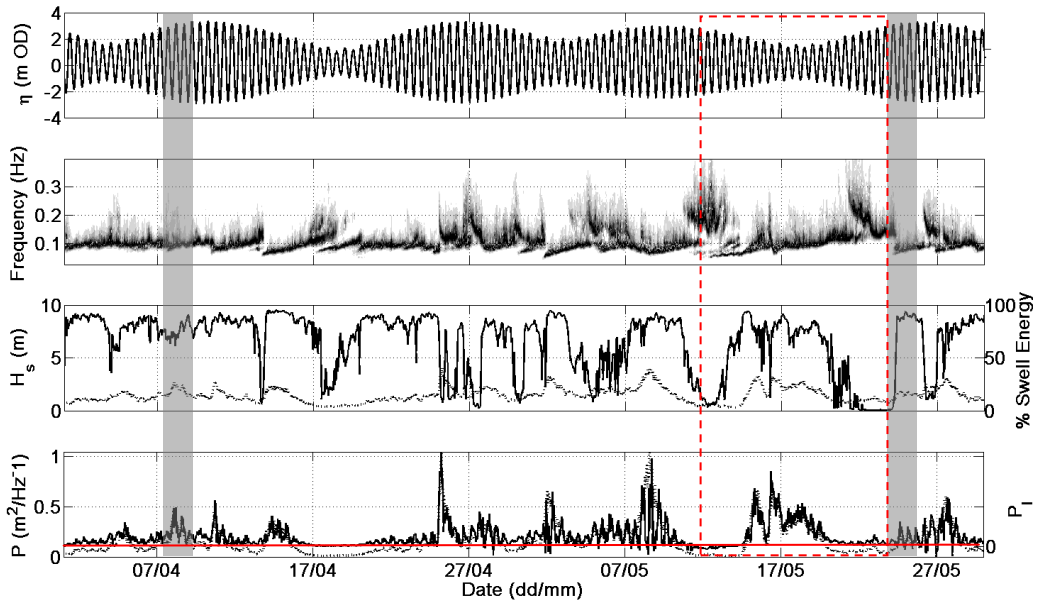

Figure 4.44 – Summary of the wave conditions present between April and May 2009; From top to bottom: still water level η; wave spectrum; significant wave height H_s(dashed line) and % swell energy (solid line); wave energy flux P (dashed line) and longshore component of the offshore wave energy flux P_l (dashed line), where positive indicates northerly directed. The grey shaded boxes indicate beach surveys, the red dashed box indicates the period of morphological response derived from Argus images, see text for details.

Over the 6 week interval between surveys the intertidal morphology changed from a rhythmic embayed shoreline to a low tide bar/rip system (Figure 4.45). Both sites experienced redistribution of sand below the MSL with material being lost around MLWN and accumulating above MLWS, resulting in the development of a more 3D low tide with well-defined bar features and channels, with little change in the upper beach.

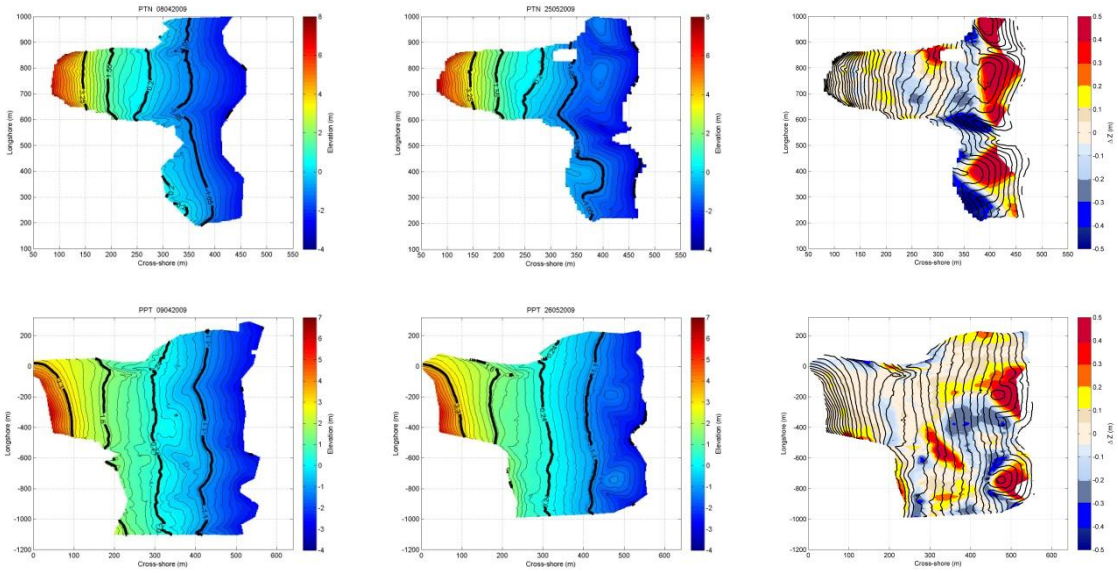

Figure 4.45– Surface plots showing Intertidal morphology between April – May 2009 for PTN (top row) and PPT (bottom row). Δz surface plot (right column), colours indicate regions of accretion (yellow/red) and erosion (blue). Contour lines show the subsequent morphology.

The subtidal bar response varied between the two sites: PTN exhibited little change in the nearshore breaker pattern with a rhythmic bar dominant throughout, whereas the shore-parallel bar at PPT became fully detached from the beachface as accretion resulted in the formation of two intertidal bars (Figure 4.46).

Inspection of the Argus images between the topographic surveys reveals that the main morphological change occurred between 10thand 25thMay (Figure 4.46). This period coincides with a brief energetic wave event with an H_s=3.3m which occurred under neap tide conditions (Figure 4.44). Despite fairly similar wave conditions present through much of May the combined increase in waves and a reduced tide range has resulted in extensive redistribution of low tide material at both sites. There was no evidence of a change in the wave direction or any storm influence. Although it is not clear how much onshore movement of sediment occurred from the subtidal region, the pattern of sediment change in Figure 4.45 suggest greater removal of material from the MLWN region feeding the lower beach face resulting in the bar morphology.

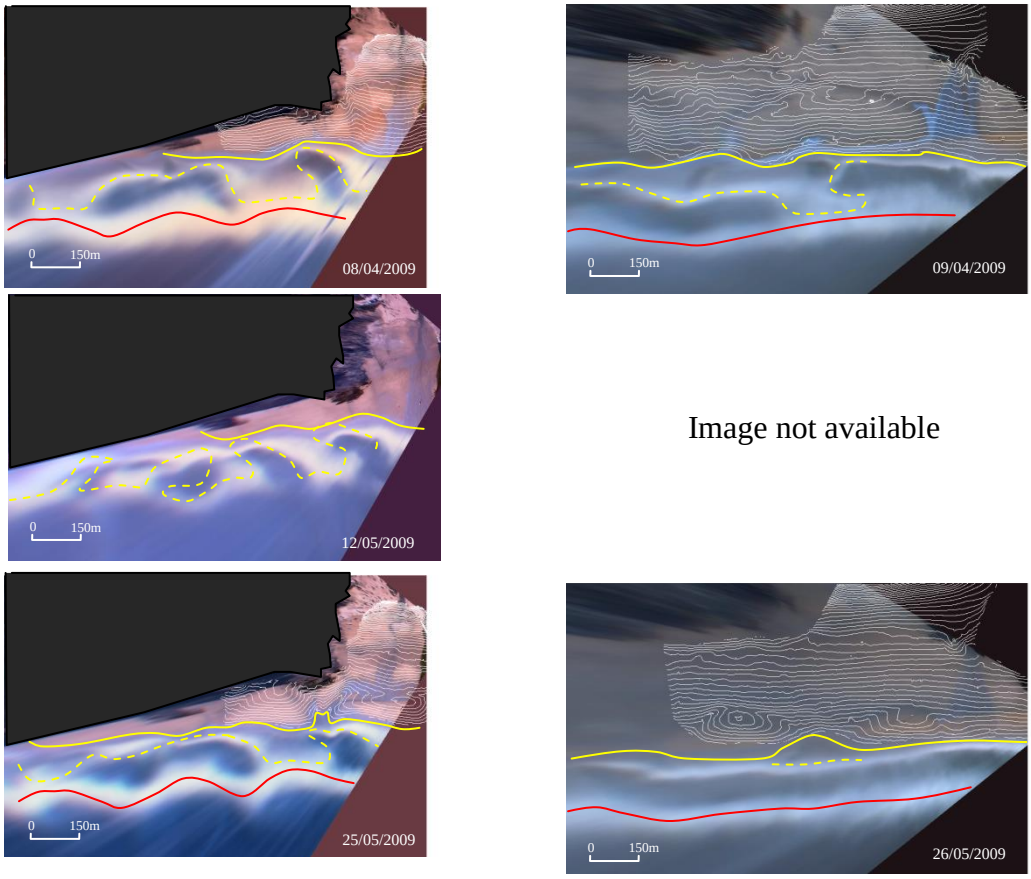

Figure 4.46– Plan-view rectified timex images from PTN (left) and PPT (right) with contours of intertidal morphology overlaid. The additional Argus image highlights the limited morphological change prior to the 12th May. The offshore bar position (red line), shoreline breaker position (solid yellow) and nearshore breaker zone (dashed yellow) are also indicated

4.8.3 November 4th 2009 – January 31st 2010

November 2009 to January 2010 was a period characterised first by significant storm activity and which led to the widespread removal of material at both PPT and PTN (refer to Figure 4.27), followed by a period of calm. Between the surveys in November and December there were 6 separate storm events resulting in the 5% exceedance H_s reaching 4.7m, 50% exceedance H_s = 2.88m and the 90% exceedance H_s = 1.46m, representing the largest exceedance waves throughout the 3-year survey period (Figure 4.40). Following the November storms December experienced a very calm wave climate with 50% and 90% exceedance H_s= 1.2m and 0.69m respectively.

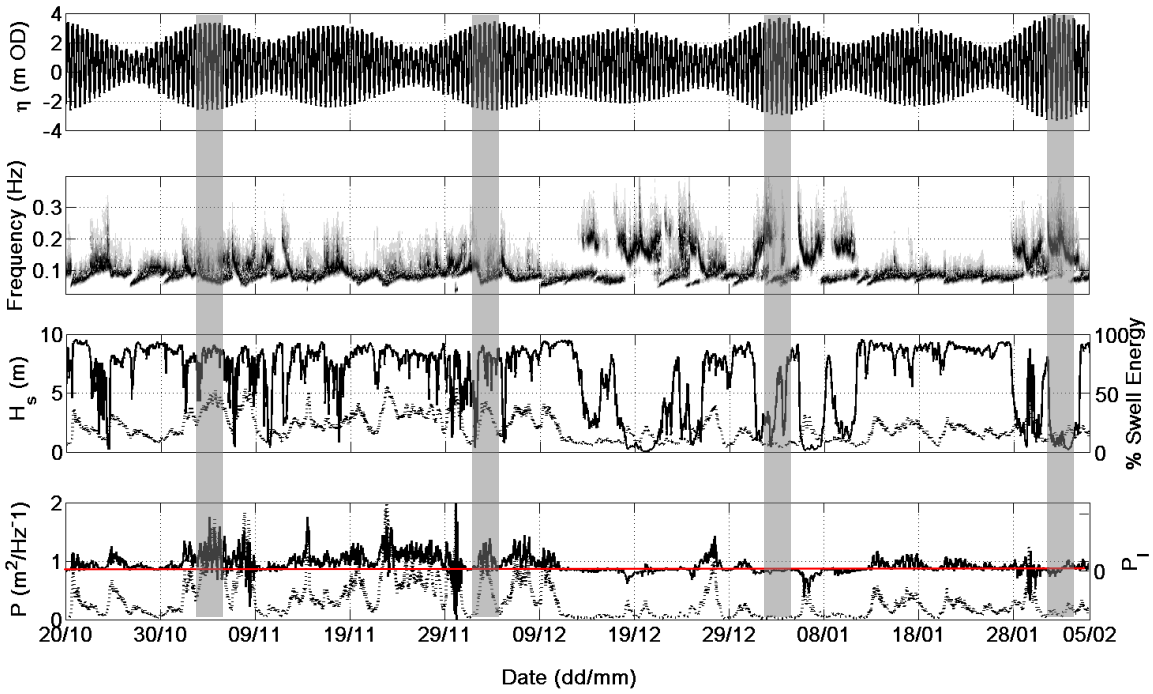

Figure 4.47– Summary of the wave conditions present between November 2009 and February 2010; From top to bottom: still water level η; wave spectrum; significant wave height H_s(dashed line) and % swell energy (solid line); wave energy flux P (dashed line) and longshore component of the offshore wave energy flux P_l (dashed line), where positive indicates northerly directed. The grey shaded boxes indicate beach surveys.

Widespread removal of material occurred at both sites across the majority of the beach face from MHWN down (Figure 4.48), with greatest loss in the lower to mid (Figure 4.49). Although both sites experienced extensive removal under the sustained storm conditions, the surface morphology remained fairly rhythmic at the shoreline, with a bar feature evident at PPT. By January the calm conditions lead to onshore accumulation at both beaches, at PTN the upper and mid beach face increased in volume and two large low tide bars formed at the shoreline, while PPT also developed highly 3D bar/rip morphology (Figure 4.48). Wave conditions remained relatively calm throughout January with 50% exceedance H_s= 1.58m. By February the beaches remained 3D, however in-filling of the channels resulted in a smoother low tide region as reflected in the $\overline{CV}$ values (Figure 4.33).

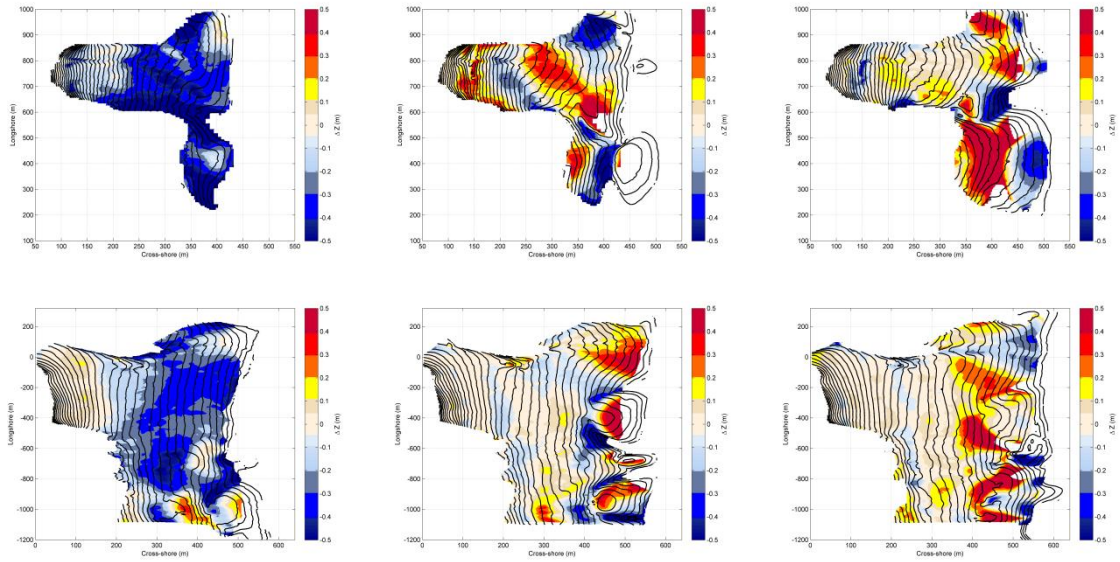

Figure 4.48 – Surface plots showing Δz for November – December 2009, December – January 2010 and January – February 2010 for PTN (top row) and PPT (bottom row). Colours indicate regions of accretion (yellow/red) and erosion (blue). Contour lines show the subsequent morphology.

At both sites the Argus images highlight the shift in nearshore bathymetry in response to the storm conditions; at PPT the shoreline moves landward while a secondary breaker line develops between the shoreline and the nearshore bar indicating a build-up of material causing secondary breaking in this region. At PTN the rhythmic shoreline and near-shore breaker pattern which was stable for the preceding 125 days (Figure 4.50/Figure 4.36) is redistributed with more complex longshore/cross-shore channels present.

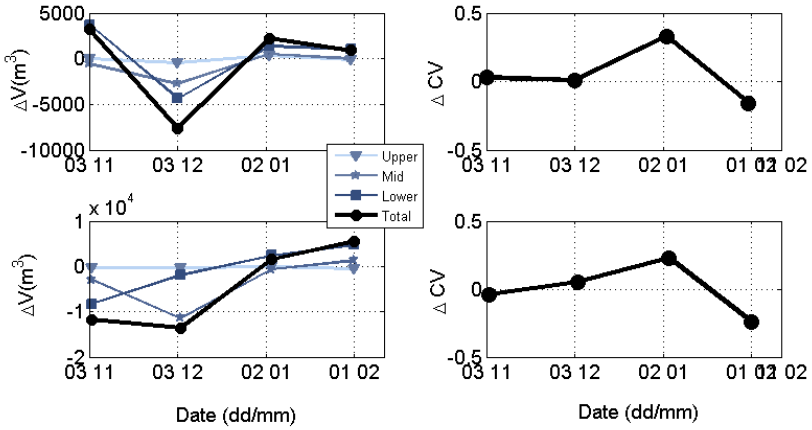

Figure 4.49– Summary of volumetric change (Δv^3, left column) and change in lower beach 3D (ΔCV, right column), between November 2009 and January 2010 for PTN (top row) and PPT (bottom row).

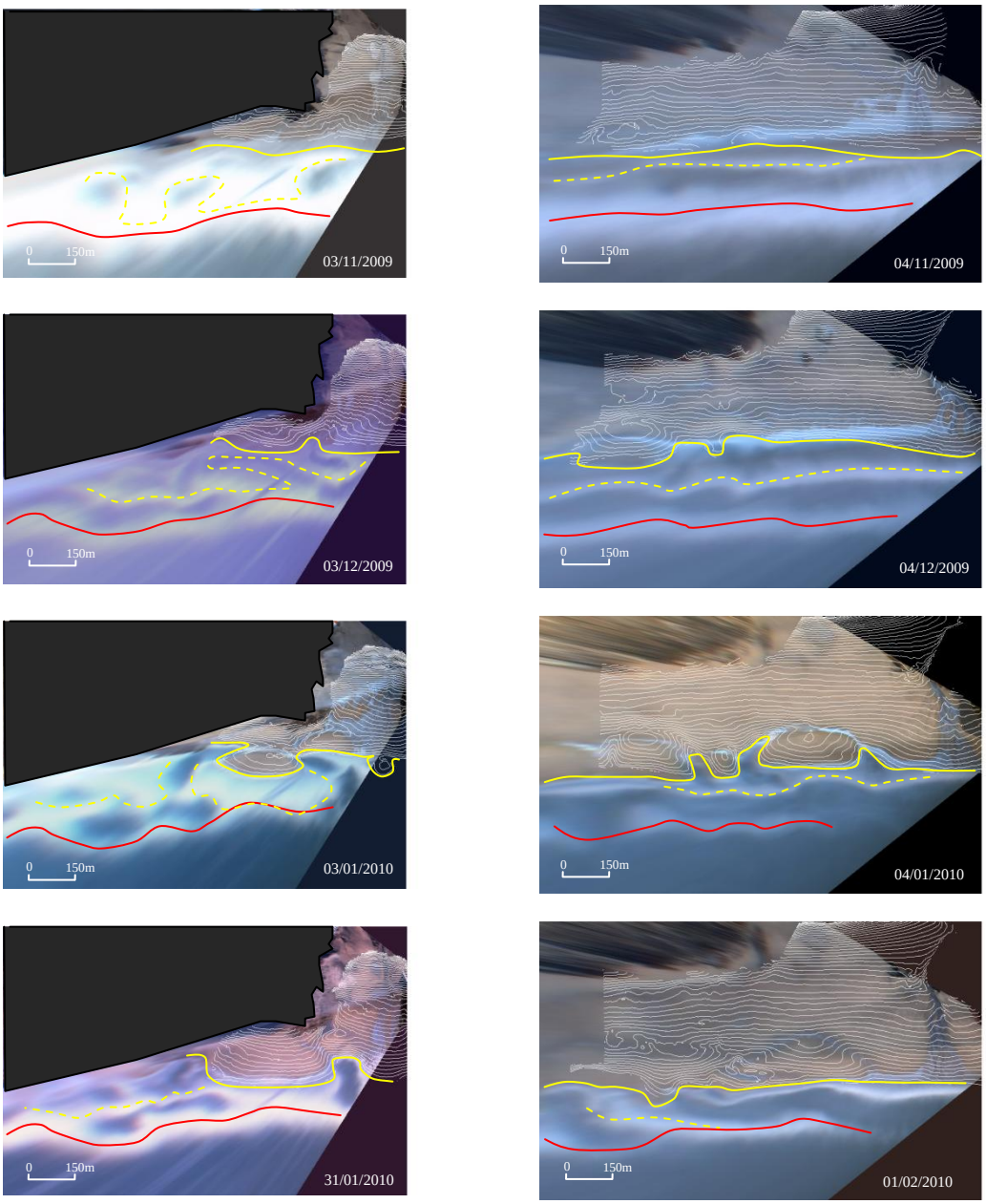

Figure 4.50– Plan-view rectified timex images from PTN (left) and PPT (right) with contours of intertidal morphology overlaid. Images show transition between November 2009 (top row) to January 2010 (bottom row). Offshore bar position (red line), shoreline breaker position and nearshore breaker zone (solid and dashed yellow line). *Note* the November Argus images are taken during large conditions and so positions are approximate.

Overall following sustained storm events throughout November (H_s= > 4m for 109hrs) widespread removal of material was observed at both sites. Over the following two months reduced conditions with no storm events resulted in onshore transport from the subtidal area to the low tide beachface, resulting in the formation of large well

developed 3D shorelines. Under more mixed conditions these channels became in-filled and the 3D features were gradually smoothed.

4.8.4 July 14th – October 9th 2010

Between July and October 2010 four surveys were undertaken during a period during which wave conditions were dominated by highly mixed seas with no significant storm periods or sustained calm conditions (Figure 4.51).

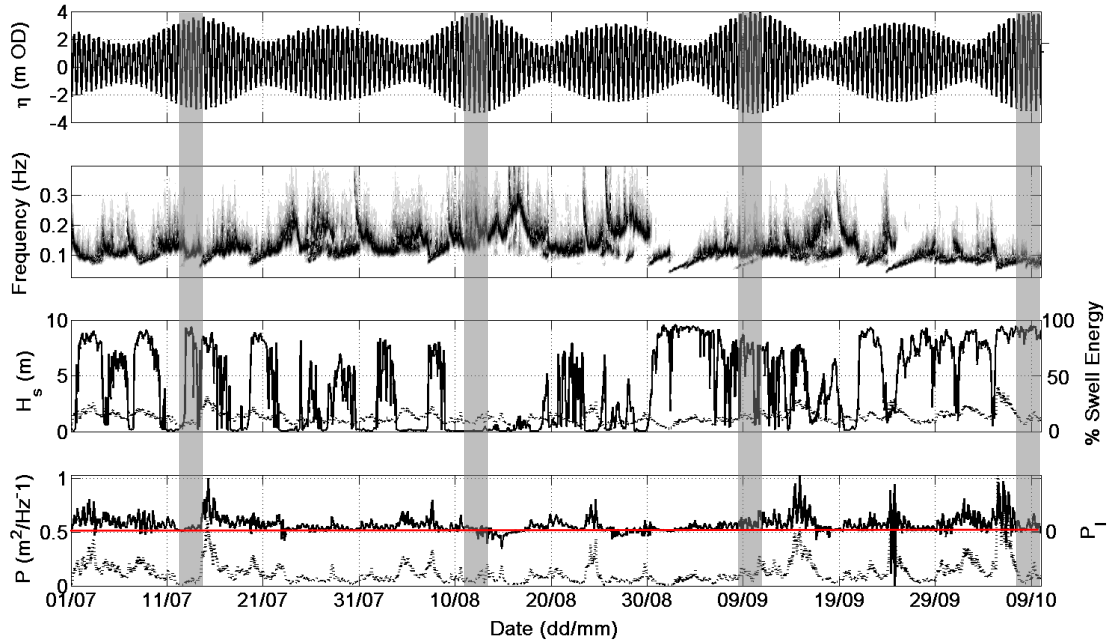

Figure 4.51– Summary of the wave climate between July 2010 and October 2010; From top to bottom: still water level η; wave spectrum; significant wave height H_s(dashed line) and % swell energy (solid line); wave energy flux P (dashed line) and longshore component of the offshore wave energy flux P_l (dashed line), where positive indicates northerly directed. The grey shaded boxes indicate beach surveys.

The morphological response over this period was characterised by an up-state shift from a low tide rhythmic shoreline to a highly planar beach face (Figure 4.52). Under the calm low energy conditions during July and August (<0.25m^2/Hz), the morphological response consisted of localised in-filling of channels and merging of features, gradually smoothing out the shoreline and steadily increasing the overall volume (Figure 4.53).

During October wave conditions increase marginally, yet no significant swell events or storm periods occur, however these conditions result in more pronounced smoothing and flattening of the profile, with greater accretion evident in the upper beach (Figure 4.52).

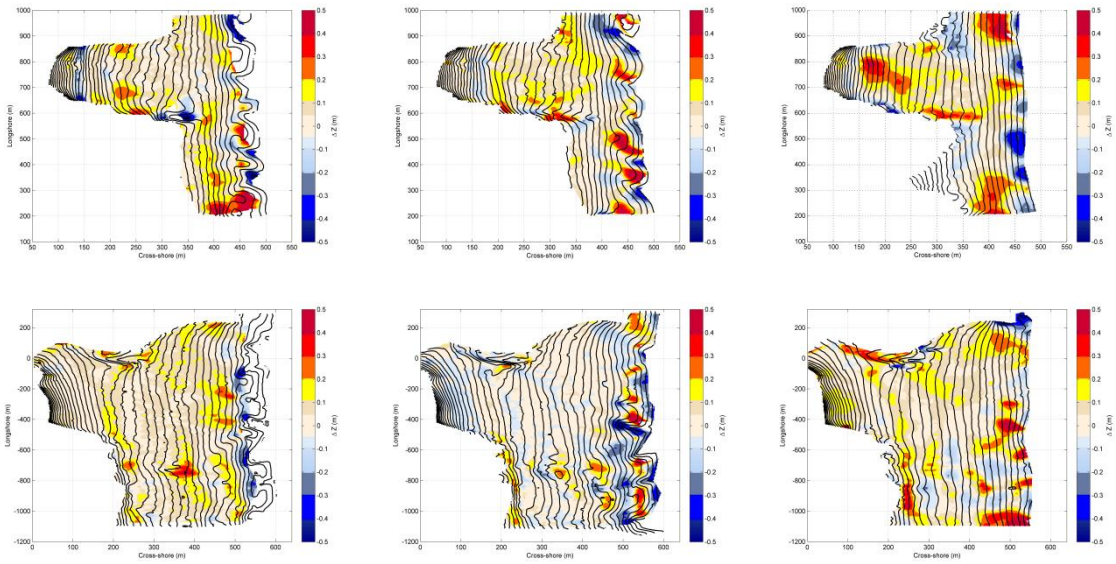

Figure 4.52 – Surface plots showing Δz for July – October 2010 for PTN (top row) and PPT (bottom row). Colours indicate regions of accretion (yellow/red) and erosion (blue). Contour lines show the subsequent morphology.

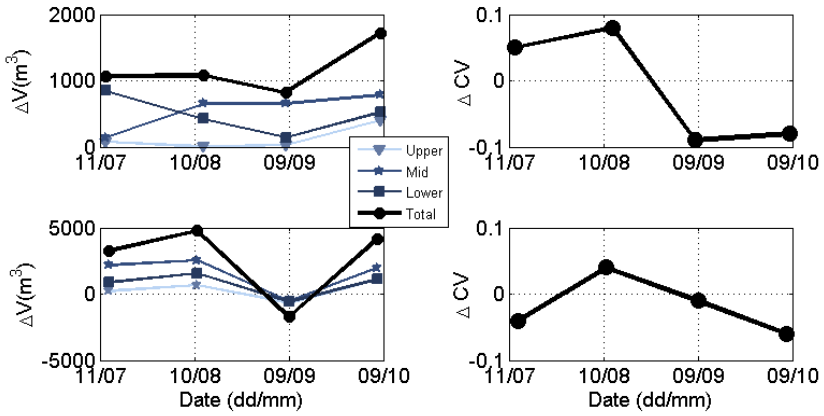

Figure 4.53– Summary of volumetric change (Δ*v*, left column) and change in lower beach 3D (Δ*CV*, right column), between November 2009 and January 2010 for PTN (top row) and PPT (bottom row).

Subtidal analysis using Argus images for the corresponding period shows little or no change in the spatial pattern of the nearshore breaking. The morphological response is evident from the rectified images, however the breaking pattern remains constant with both sites exhibiting shoreline breaking with no evidence of nearshore bars. In addition

to the low tide channels evident in Figure 4.52, a single subtidal channel is evident to the north of the survey area at PTN. This feature remains steady over the four months, while PPT sees a similar feature at the centre of the survey region, which becomes more defined by October (Figure 4.54).

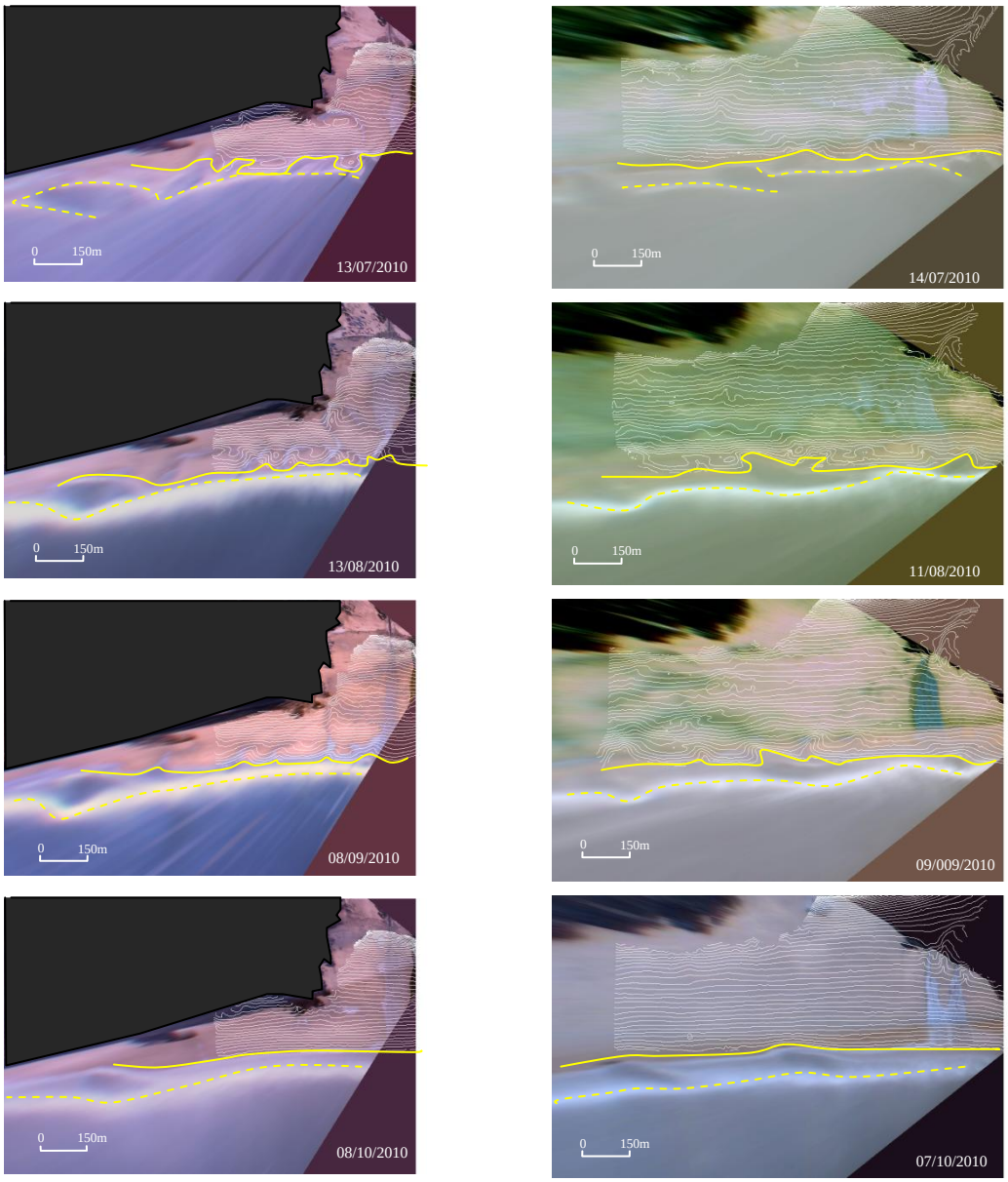

Figure 4.54– Plan-view rectified timex images from PTN (left) and PPT (right) with contours of intertidal morphology overlaid. Images show transition between July 2010 (top row) to October 2010 (bottom row). Shoreline breaker position and nearshore breaker zone (solid and dashed yellow line).

Overall this period identifies the removal of small scale low tide bar/rip morphology which is present at the MLWS line only. Mixed moderate seas result in gradual in-

filling of any channels; this is increased as conditions build in October, resulting in a highly planar 2D beachface.

4.9 Discussion

In this chapter the morphological and subtidal behaviour of four macrotidal sandy beaches has been assessed through a variety of approaches and techniques. This chapter has identified the key morphological behaviour in response to varying wave conditions at four sites. Whilst oversimplification of the complex processes which govern these large scale changes can restrict detailed assessment, the longer-term trends become apparent as short term "noise" is removed.

Of the four sites monitored over 3 years GWT stands alone in terms of morphology and setting. Located the furthest south of the sites GWT is protected from N– NW waves by a pronounced headland and offshore rocky reefs which is reflected in the reduced wave height predicted by Scott (2010). GWT is also distinct from the other sites as it forms a small section of a much larger bay system which is likely to have larger sources of sediment input longshore into the system from the Hayle estuary to the south. As a result the morphological trends at GWT are dominated by a very low amplitude channel and bar feature at the low tide region, which appears to be linked closely with the outflow of the river across the beach. PTN and CHP are located within the same headland confined system and as such we see strong similarities in their low tide behaviour throughout the surveys, however the confined upper beach at CHP restricts complete comparison between these sites. Similar in setting PPT is located within a headland confined system with the survey area covering approximately half of the beach extent.

On a coast-wide scale, the long term behaviour has been very similar between the sites. The larger more dissipative sites (GWT and PPT) have exhibited the slowest offshore movement in the momentary coastline position (0.03 m / day) compared with 0.05 m / day for PTN and CHP. As they are within the same system we would expect PTN and CHP to show a strong correlation (0.83), however there is also strong correlation between GWT and PPT (0.79). Although there are periods of retreat overall there is an upward or beach growing trend observed at all sites, which reflects the decrease in storm events and storm durations throughout the survey period. With only 3 years of relevant data, and conflicting accounts from long term local residents with regard to previous sand levels, clear interpretation is limited. The momentary coastline position provides an effective tool for looking at the relative shoreline position which can be used to identify longer-term trends in shoreline response (Davidson, Lewis & Turner, 2010). While this approach is useful as a coastal state indicator (van Koningsveld & Mulder, 2004), and suggests current growth in the system, it does not explore the variability in beach morphology. Building on previous efforts to characterise shoreline variability by Smit *et al.*(2008b) the $\overline{CV}$ allows long term data sets to be quickly analysed and periods of transition to be identified for further interpretation.

The results presented here show significant variability in beach morphology at PPT, CHP and PTN, with bar/rip systems dominating the low tide region. While there is fairly good agreement in the development and removal of such features between the 3 sites, of interest is the lack of any clear trend in the seasonal/annual morphological feedback in response to the distinctive seasonal signal in the wave conditions. Instead the results suggest large scale beach change is dominated by a series of storm events which serve to redistribute material to the lower beach.

The dominant response behaviour at CHP, PTN and PPT was characterised by rapid transitions towards increased 3D states following more energetic wave conditions. These events resulted in the removal of material from the upper beach and accumulation around the low water line. While this response supports previous studies which have shown a flattening of the upper profile (Komar, 1998), the low tide bar/rip features remained present despite the storm waves. As post storm conditions lead to onshore directed transport, during the recovery phase, the weakly 3D shoreline promotes spatially variable deposition which acts to accelerate the development of highly 3D morphology. However through continued onshore accretion, as we have seen from the momentary coastline data, the initial bar/rip features gradually become smoothed through in-filling. These periods of up-state transition were observed 2/3 times over the survey duration, idealised for PTN, CHP and PPT (Section 4.3), occurring over a 3 – 4 month period. With large storm events often evident in March, the presence of such highly 3D beach states during the summer months is increased, supporting the argument their formation is primarily a response to calmer accretionary conditions. The results presented support the accretionary development of increased 3D morphology, however it is argued this process is only possible following storm conditions. The removal of material from the mid/upper beach feeds the subtidal which supply material during the accretionary recovery phases. The results move away from a "seasonal" concept of beach state, and move towards storm event-driven response, where the "seasonal" climate controls the subsequent morphology. This conclusion is supported by the distinctive bar/rip morphology which was observed during December and January in response to energetic November conditions, preceding a gradual straightening of the shoreline.

By incorporating the $\overline{CV}$ into the classification scheme presented in Figure 4.30, the distribution of 3D beach states can be expressed with reference to the RTR and the Ω (Figure 4.55). The distribution of increased 3D states is centred on the medium energy boundary (H_s = 1.5– 2 m), with more planar states present at the more energetic/calmer regions. This supports the field observations where: 1) post storm (energetic) conditions result in increased 3D morphology; and 2) calm conditions lead to in-filling and smoothing out of features resulting in reduced 3D. The "optimum" 3D states exist within a central threshold which requires "input" into the system through energetic events to re-distribute the sediment to the lower beach.

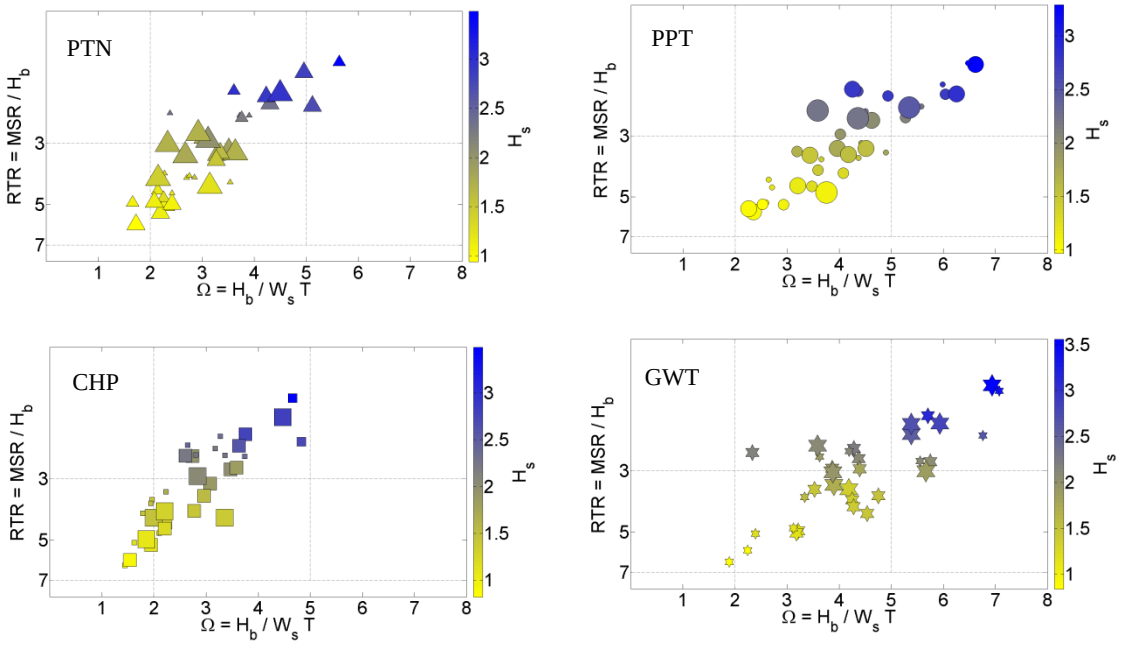

Figure 4.55 – Conceptual classification of monthly beach states as presented in Figure 4.30. In addition to the trends in wave forcing (yellow shading = calm wave conditions, blue shading = larger waves) the marker size reflects the relative 3D level derived using the $\overline{CV}$(larger markers indicating more 3D intertidal morphology and smaller markers indicating more planar 2D conditions).

The concept of a modal state for GWT is fairly straightforward, the beach exhibits only small changes from a relatively planar crescentic shoreline to a low amplitude bar. For the remaining sites a modal state is less obvious. The sustained in-filling of channels and smoothing of the beach which was observed during the 3/4 month accretionary

cycle suggests a shift towards a more planar state. However despite continued net accretion over the 3 years of surveys, intermittent storms have led to increased 3D morphology. The balance between storm driven removal and onshore accretion is maintained through periodic events. This would suggest for a longer record a correlation with storm events and 3D morphology would develop and ultimately reflect the cyclicity in storms every 15– 20 years (Figure 2.13).

The difference in the beach settings is also pronounced and reflects the variability in the morphology observed. Both PTN and CHP have a narrow low tide beach which is backed by steep cliffs and exhibited strong periodicity in bar development and migration with defined channels extending from the cliffs. The central region of the survey area is more likely to be affected by the flows constrained by the narrow upper beach at both sites, however the longshore areas display strong rhythmicity which suggest the proximity of the intertidal geology may be important in controlling the nearshore dynamics.

The long-term (years) variability in bar behavior and orientation has been presented using bar line detection of rectified images at PTN and PPT. Overall both systems exhibited medium term stability (weeks-months) of attached nearshore bars. PTN underwent greater variability of bar structure and orientation with highly rhythmic crescentic features dominating the system, whereas PPT was characterized by alongshore rhythmic attached bar behavior.

Principal response at both sites to removal of material following storm conditions during the first two years was clear, with sediment deposition occurring between MLWS and the attached bar. Such processes resulted in more complex bar definition through the increased deposition in this region. These deposits then acted as sources for

the post storm onshore transport which has been discussed above. This behavior is comparable to observations in Almar *et al,* (2010) where crescentic horns developed under storm conditions as material (SPAWs) moved onshore while the bar moved offshore, however the present study suggests maximum 3D growth occurs during the recovery phase. Longer term trends in the cross-shore position of the outer break point of the nearshore bars shows a strong relationship to the intertidal volume expressed using the LBX_{MCL} position.

Comparison of bar behaviour with the intertidal beach state highlights the longer residence times exhibited in the subtidal states compared with the variability of the beach morphology. This is evident in the subtidal response to specific storm events explored in Section 4.8. Instead of distinctive "re-setting" of the bar, or offshore movement, the bar shape and position undergoes more gradual change.

4.10 Conclusions

The foregoing presents a comprehensive assessment of the morphological response of four high energy macrotidal beaches on the north coast of Cornwall. This represents the longest record of survey data which has been collected within the UK for these environments. The morphological responses observed at PTN, CHP and PPT exhibit strong correlations in sediment deposition and erosion as well as the low tide morphological evolution. Through long term observations of beach state, and shorter term storm response, morphological cycles have become evident with common trendsidentified between sites. From these cases we can summarise the following points to address the central aim of evaluating the nature and extent of variability in the morphological response at the four sites:

- The four sites remain stable with beach widening and net accretion observed. Inter site response to seasonal wave conditions is temporally and spatially consistent.
- Morphodynamic variability is high at PPT, CHP and PTN, with dissipative-intermediate states observed. While no states dominated highly planar morphology was intermittent.

Sustained storm conditions (> 50 hrs) are required to generate significant shifts in sediment and nearshore morphology.

- Post storm response is characterised by;
    - onshore movement of recent sand deposits under medium wave conditions, resulting in pronounced low tide bar/rip morphology
    - continued onshore transport forces in-filling of shoreline features and gradual smoothing of the beach face

Subtidal morphology was characterised by rhythmic attached bars which showed gradual transition not synchronous with the intertidal response.

With all time series data the longer the dataset the more reliable the trends identified. It is clear the three northern sites of PTN, CHP and PPT exhibit large variability in their low tide morphology. Exposed to energetic conditions the sites require sustained periods of storm waves (H_s =>4m) for significant shifts to occur. However the post storm recovery phases are the builders of the extensive bar/channel systems present.

5 PORTHTOWAN EXPERIMENT; PX1 & PX2

5.1 Introduction

Analysis of two years of monthly surveys presented in Chapter 5 found distinctive periods of morphological transition at PTN, CHP and PPT. These periods were characterised by significant downstate and upstate shifts in the dominant intertidal morphology in response to persistent long and short-term changes in wave conditions. With daily ARGUS images some interpretation of the shifts in morphology has been possible; however, quantitative analysis has been limited. The need for greater temporal resolution of the morphological response to varying wave conditions was identified to help further understand the driving forces behind change evident on these beaches. Subsequently 2 x 14 day field experiments were planned which would incorporate daily topographic surveys with nearshore flow measurements under contrasting conditions. PTN was chosen as a suitable site based on the following criteria;

- Dynamic responsive morphology
- Medium survey area for sufficient coverage in a short-time period
- Argus image collection

To provide contrasting datasets the first deployment (PX1) was planned for calm conditions in the spring, and the second (PX2) was planned for more energetic conditions in the autumn. PX1 took place in the period 14^{th}– 27^{th} May under very calm low-energy conditions (max H_s= 1.5m), PX2 took place between 9^{th}– 22^{nd} of November under a period of highly energetic storm conditions (max H_s= 6m) followed by a period of low energy waves. The first field campaign (PX1) was scheduled to coincide with persistent calm conditions associated with an accretionary phase.

November was chosen for PX2 and, fortuitously, the survey period turned out to be the most energetic period of the year.

Both of these field deployments were designed to contribute to the wider understanding of long-term morphological response which has been identified in Chapter 4, and involved daily intertidal RTK GPS surveys and eulerian flow measurements. The central aim of the two experiments was *to link the morphological response with measured flow dynamics over a tidal frequency*; to support this more specific objectives were identified:

- Quantify variability in nearshore flow dynamics arising from to tidal cycle
- Quantify variability in nearshore flow dynamics caused by wave forcing
- Identify key morphodynamic response regions
- Establish morphodynamic response to wave forcing through tidal cycle

This chapter presents a synthesis of these two field deployments following a brief review of the cross-shore processes that dominate. Additional methodology and instrumentation used during the field experiments are covered in Section 6.3, followed by separate results from PX1 and PX2, prior to analysis of both datasets. This is followed by a discussion and summary of the results relating these intensive field experiments to the wider project.

5.1.1 Nearshore Processes

The generation of nearshore currents is a function of the complex process by which wave energy is dissipated across the shoreface at incident and infragravity frequencies, (Greenwood & Osborne, 1990; Greenwood & Osborne, 1991; Russell & Huntley, 1999). Shifts in the wave conditions drives changes in the breaking patterns and subsequent transport processes which feedback into the profile morphology. This complex balance

between forcing conditions and resulting beach shape remains an area of significant interest.

Figure 5.1 identifies the idealised regions which are present as waves undergo transformation into shallow water before breaking and collapsing across the beachface. For dissipative/intermediate beaches with a gentle slope these regions are usually wide and the boundaries broad. As waves shoal from deeper water they become increasingly *skewed* as the wave shape loses its sinusoidal symmetry as more peakey crests develop separated by relatively flatter troughs (Figure 5.1). A second component of the wave transformation is the vertical asymmetry which is apparent in the wave crests. The result is a shift in the crest shape as the shoreward side becomes increasingly steep (Elgar, Gallagher & Guza, 2001). Both the wave *skewness* and the *crest asymmetry* increase towards a maximum at the breakpoint before reducing through the surfzone to a minimum at the shoreline (Russell & Huntley, 1999). For more dissipative beaches under natural waves the breakpoint can occupy a wide region forming the outer part of the surfzone. The inner surfzone consists of broken waves and bores undergoing transformation towards the shoreline. The final region (swash zone) is characterised by periods of inundation and exposure between individual swash events.

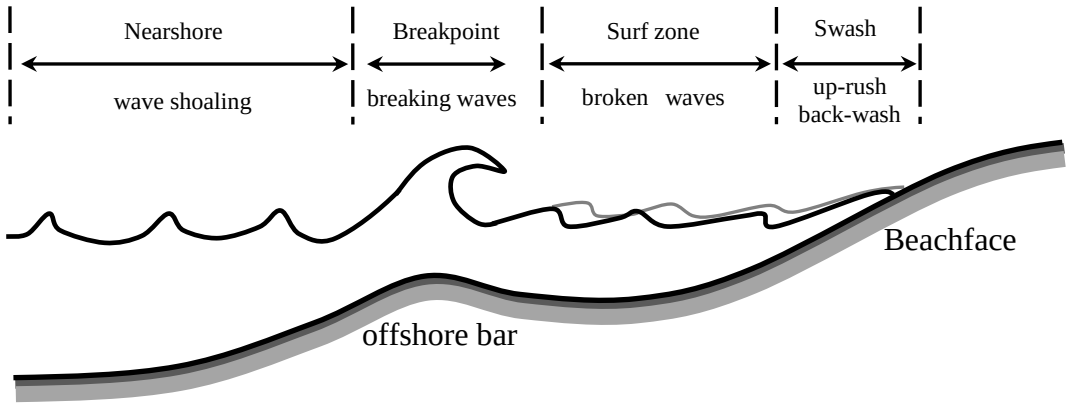

Figure 5.1– Idealised schematic diagram of nearshore breaking patterns and wave dynamics.

Within the shoaling zone the wave asymmetry has been shown to generate a net sediment transport onshore through weak mean onshore flows and onshore directed short wave skewness (Guza & Thornton, 1985; Roelvink & Stive, 1989; Russell &Huntley, 1999; Thornton, Humiston & Birkemeier, 1996). During wave breaking strong velocity accelerations occur under steep asymmetric wave faces. These onshore-directed flow accelerations can cause significant sediment entrainment from the seabed, which is then transported within the weak onshore flow (Russell & Huntley, 1999). Austin *et al.*(2009a)explored the relative importance of wave asymmetry (flow velocity skewness) and flow accelerations owing to the crest asymmetry in driving onshore sediment transport under moderate waves. They found strong correlations between the onshore-directed flow accelerations under the steep front faces of the asymmetric waves with the entrainment of sediment and therefore onshore transport. Inside the surfzone, transport is dominated by offshore directed nearbed currents referred to as the *undertow*. The flow rate is driven by vertical differences between the depth dependant radiations stresses and the uniform pressure gradient in place owing to set-up at the shoreline (Komar, 1998). As a result the rate of return flow will vary in response to the wave conditions, but also the profile slope. Undertow is most clearly represented under 2D laboratory conditions, whereas on a natural 3D beach the balance in onshore directed radiation stresses and offshore directed pressure gradients will vary across the beach face (Russell & Huntley, 1999). Further variability in offshore flow rates can occur through the interaction with nearshore rip currents. Whilst mean flows remain offshore, Elgar *et al*. (2001) found maximum flow accelerations strongly correlated with bar crest location during onshore bar migration, which supports flow acceleration driven onshore sediment transport.

For macro-tidal sites tidal transgression across the beachface is increasingly important, with periods of maximum quasi-stationarity, and therefore increased sediment transport rates, occurring at low water and high water (Aagaard et al., 2006). For dissipative sites a small difference between the spring/neap tidal range can affect the spatial region of the low/high water lines, and as such the concentration of increased sediment movement. For intermediate beaches this pattern results in the low tide bar/rip morphology and upper beach berm growth.

Whilst storm conditions are generally associated with strong offshore flows generated from breaking waves and energetic bores, onshore migration of 3D bars has also been observed through cell circulation induced onshore transport (Aagaard *et al.*, 2006). Storm conditions also lead to a widening of the surfzone and subsequent adjustment to the location of onshore/offshore transport dominance across the beach face

The importance of swash dynamics for sediment transport has received increasing attention to improve present profile models. Importantly recent field experiments have used high frequency acoustic sensors to further understand the importance of swash by swash dynamics on overall sediment fluxes, with observations of large net onshore and offshore fluxes comparable with beach response over a full tidal cycle Austin *et al.*(2009a). It is beyond the scope of this work to contribute further to current research into the importance of swash dynamics, for a complete review see Butt and Russell (2000); Masselink and Puleo (2006); Brocchini and Baldock (2008), however the role of swash in generating morphological response is acknowledged.

5.2 Methodology

5.2.1 Topographic surveys

Intertidal morphology was surveyed following the method outlined in Chapter3. Morphology was measured every low water where light conditions permitted. During

PX1 spring low tide coverage was maintained by mounting the RTK GPS receiver on a backpack (Figure 5.2) which allowed the user to wade through the water to attain greater coverage. During PX2 the ATV was unavailable which meant surveys were conducted on foot for the duration of the survey period. This was undertaken in the same manner at PX1 with a backpack being used to house the receiver. However, owing to the energetic conditions, extension of the survey area below the neap low tide region was not safe and daily coverage was restricted by the low tide line.

Figure 5.2– Photograph of the RTK GPS mounted on a surveyor for access to low tide regions during neap tide cycle during PX1, and for complete coverage during PX2.

5.2.2 Eulerian measurements

Surf-zone hydrodynamics were measured during PX1 and PX2 using mobile and freestanding rigs deployed at the first spring low tide of the survey periods (Figure 5.3). The primary rigs (R1 and R3) were located just above spring low tide and so access was maintained for the majority of the survey period, allowing instruments to be checked and re-adjusted to maintain constant height above the bed. Calm conditions during PX1 allowed the deployment of an additional rig within the spring low tide breaker zone

(Figure 5.3, R2); however, owing to the rig settling too low into the bed the data are of limited use and are presented here in the summary section only.

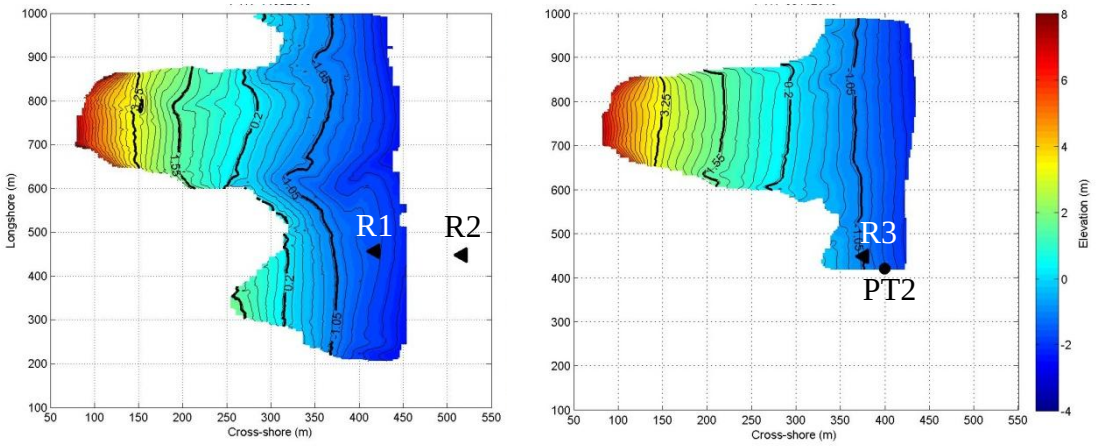

Figure 5.3– Surface morphology for the start of PX1 (left) and PX2 (right). Each plot shows the position of the rig deployments and the location of the pressure sensor during PX2 (PT2). Note the reduced survey extent during PX2 owing to surveys undertaken on foot.

During PX2, rig deployment was delayed owing to a forecast of storm wave conditions. Deployment was, therefore, undertaken midway through neap tides when the H_s had dropped sufficiently. For stability the rig was secured to 3 x 8ft scaffold tubes which were buried into the bed. To capture the nearshore wave conditions an additional pressure sensor (PT2) was deployed prior to the rig during the storm conditions.

Directional wave conditions were recorded using a Datawell MkIII DWR located in 10m (CD) water depth just north of the field site (see Chapter 3 for a full description). Water depth and nearshore wave conditions were recorded using a self-logging RBR TWR2050 (tide wave recorder) which was mounted on the frame leg. Flow dynamics were measured using a Nortek Vector 3D-ADV (Acoustic Doppler Velocimeter) which was initially located with the sensor head 30 cm from the bed with the sample region located 16 cm above the bed. The ADV also housed an internal PT (Figure 6.4). Atmospheric pressure was provided from a weather station at Perranporth and was used to convert the absolute pressure recorded by the PTs to water depth.

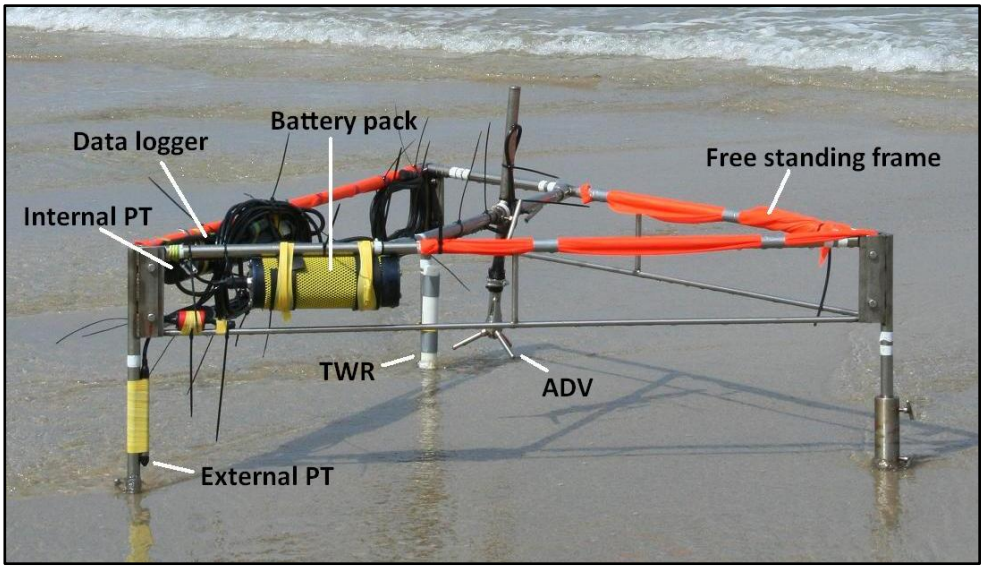

Figure 5.4– Photograph of the instrument rig used during PX1 and PX2, with ADV, TWR, internal and external PT labelled.

All instruments were programmed using the same laptop to provide synchronous data collection at 4 Hz for 8.5 min bursts (2048 samples) every 20min. Post-processing of data was undertaken to remove erroneous data (during rig exposure at low tide) and out of range/data spikes. All data were initially corrected for vertical position with reference to the bed height. This was done using instrument positions recorded using RTK GPS. Data were then processed to remove data spikes and out of range data. Standard processing of the ADV data was undertaken using minimum velocity amplitude and correlation thresholds set at 55 and 70, respectively. The ADV also records the distance from the bed at the start and end of each burst and this information was used to remove data when R1 settled too close to the bed. A final data quality check removed all points that were greater than three times standard deviation of the burst, clearing any remaining outliers.

A range of hydrodynamic summary statistics were computed for each 8.5 min burst every 20min throughout the instrument deployment. In addition to the time-averaged

cross-shore (<*u*>) and longshore (<*v*>) flow velocities, the following parameters were calculated from the data after Austin *et al.* (2009): the cross-shore orbital velocity (U_m),

$$U_m = \sqrt{8}\sigma u \quad 5.1$$

the time averaged related normalised flow velocity skewness (u^3),

$$< u^3 >_n = < u^3 > / < u^2 >^{1.5} \quad 5.2$$

and the normalised flow acceleration skewness (a^3),

$$< a^3 >_n = < a^3 > / < a^2 >^{1.5} \quad 5.3$$

Where *u* is the cross-shore velocity, and *a* is the cross-shore flow velocity acceleration.

Power spectra of the cross-shore and longshore currents were also computed for each sample burst. The spectra were partitioned into incident sea (>0.09 Hz) and infragravity (<0.05Hz) wave energy, based on the flow spectra presented in Section 5.4.

In addition to the flow statistics outlined above, the adapted Bailard (1981) suspended load formulation for predicted sediment transport after Puleo *et al.*(2003) is used to assess the morphological response with respect to fluid velocities. Puleo *et al.*(2003) incorporate Bailards (1981) original formulation without the downslope term which has previously been omitted (Masselink & Hughes, 1998);

$$q_{B} = \frac{\varepsilon_s \rho f}{2w} u|u|^3 = ku|u|^3 \quad 5.4$$

Where u is the cross-shore velocity, ε_s is the suspended load efficiency (0.01), *w* is the sediment fall velocity (0.035), ρ is the fluid density (1025 kg m^{-3}), and f is an empirical friction factor (0.01). By incorporating acceleration effects this becomes;

$$q_{pred} = k_b u|u|^3 + k_a|u|^2 a \quad 5.5$$

where a is the fluid acceleration and subscripts b and a represent coefficients for the Bailard model and the acceleration effect, respectively.

5.2.3 Argus

Argus imagery was available throughout PX1 with the standard image products generated (see Section 4). Unfortunately, midway through PX2 a power failure caused the Argus system to go down and it was not possible to reinstate the system before the end of the experiment. Images are presented here as a qualitative assessment of the nearshore breaking conditions and beach morphology, and are used to identify the rig location with reference to the breaker zone.

5.3 Results

The following section will provide separate summaries of the wave conditions, morphological response and the flow dynamics during the two experiments.

5.3.1 PX1: Waves

Wave conditions experienced during PX1 can be split into three phases; 1) short period small wind waves for 4 days, 2) small swell dominated waves for seven days and 3) two days of short period waves from the north (Figure 5.5). A sustained high pressure system tracked NW from the Bay of Biscay to the SW of the study area, moving gradually over the UK bringing with it settled weather. Winds remained light below 10knts throughout. Wind direction was W-SW for the first half of the experiment before veering to NE after 7 days (Figure 5.6).

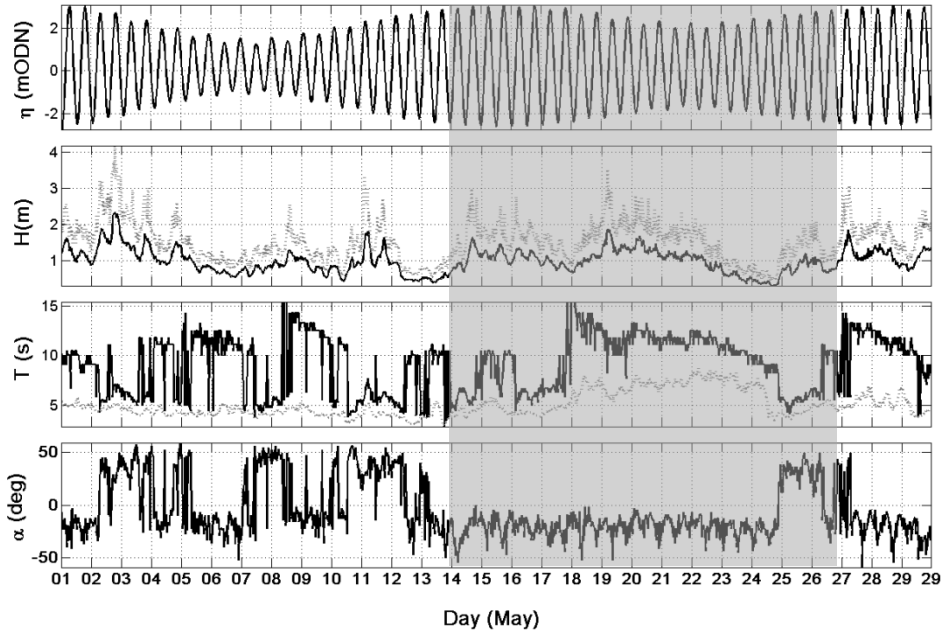

Figure 5.5– Summary wave conditions during May. From top to bottom; tidal elevation (m ODN), wave height (dashed line = H_{max}; solid line = H_s), wave period (dashed line = T_z; solid line = T_p) and wave direction relative to shore normal. Grey box indicates the PX1 time period.

A more detailed summary of the wave climate is presented in Figure 5.7, in general, wave conditions were calm throughout the study period with a significant wave height range between 0.5 and 1.5m and a peak H_s= 2.07m. The wave period followed a similar pattern peaking at T_p = 15.4 sec on day 5 as the main swell arrived. Wave direction also remained steady for the first 11 days with a W-SW approach (the dominant direction for this site); however, on day 12 a shift in wave approach occurred as the northerly winds become dominant.

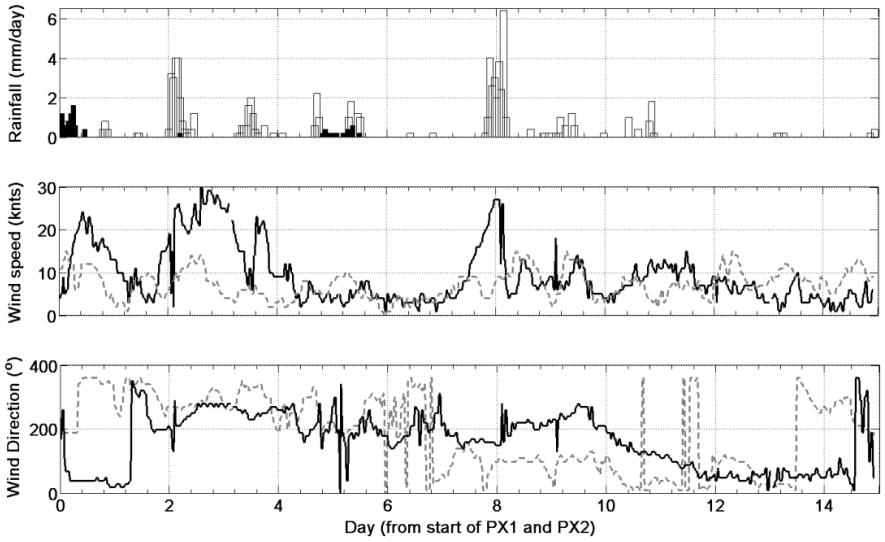

Figure 5.6– Summary meteorological conditions during PX1 and PX2; From the top; Rainfall (mm/day), wind speed (knts); wind direction (°). Solid black bars and dashed lines are for PX1, hollow bars and solid lines are for PX2.

The more detailed view in Figure 5.7 allows us to break the period into three distinct "phases": (1) a short phase with low-energy, short period wind waves with very little underlying swell component; (2) arrival of a narrow-banded swell on day five leading to an initial increase in the H_s and swell dominance for the following six days; and (3) arrival of a low energy northerly wind sea reversing the alongshore component of the wave energy flux (Figure 5.7).

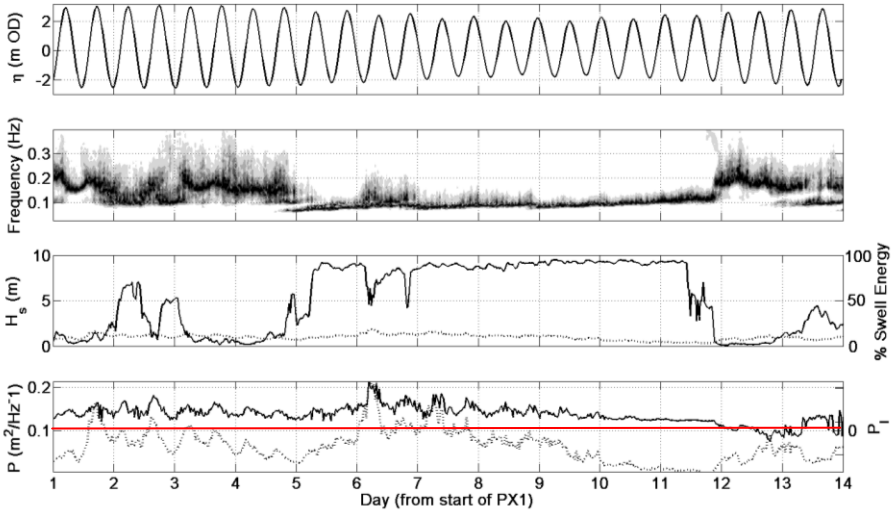

Figure 5.7– Summary spectral analysis of wave conditions during PX1. From top to bottom: tidal elevation (m ODN), wave spectrum, wave conditions (H_s = solid line; percentage swell energy = dashed line), wave energy flux (cross-shore flux P = dashed line; longshore wave energy flux P_l= solid line). Positive values for P_l indicates northward fluxes.

5.3.2 PX1: Morphology

Morphological response during PX1 was characterised by onshore accretion across the beachface. Sediment volumes (calculated as described in Chapter 3) increased across the beach face with a net rise of 1300m^3 for the computed area (Figure 5.8). The mid tide region increased by 1200m^3 while the upper increased by 250m^3 and the lower region saw a net loss. With the exception of an unexplained fluctuation on day eight, a steady increase in volume is observed up to day ten. Following this the volume shows a small drop by the end of the surveys. Grain size trends are also presented in Figure 5.8, which shows relatively stable sediment size during the experiment, with small variation in the upper and lower beach.

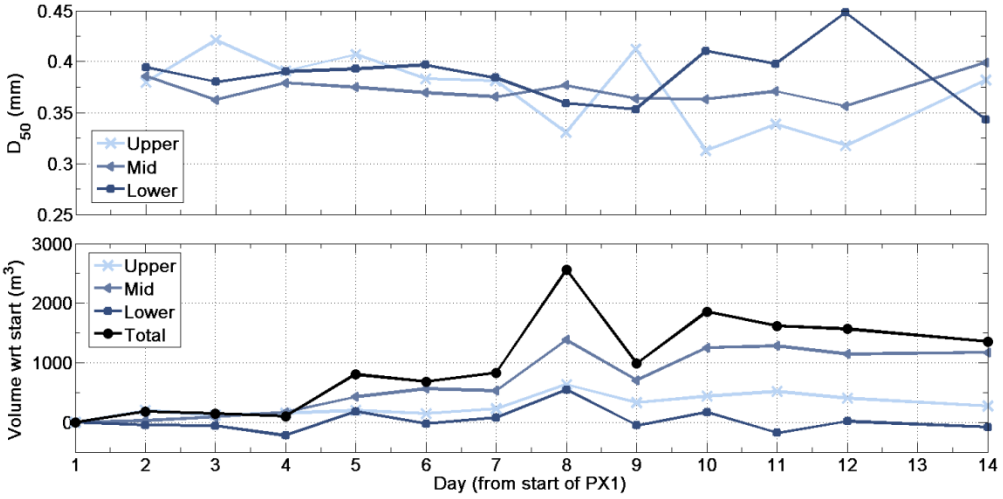

Figure 5.8 –Summary of the cross-shore sediment D_{50} during PX1 (top panel) and the intertidal volume(m^3) normalised with reference to the initial surface (bottom panel).

Profile extraction from the interpolated surfaces provides a quantitative tool to assess the cross-shore redistribution and onshore transport evident during PX1. Lines L1 and L2 are shown in Figure 5.9 which shows the mean profile line as well as the net, absolute and cumulative surface change. For both L1 and L2 we see the upper and lower beach experiencing the majority of vertical change consistent with quasi-stationarity in

tidal transgression across the shoreface (Masselink, 1993). L1 shows the development of the high tide berm as well as some growth of the low tide bar. L2 shows some berm development but the main surface change is evident at the low tide bar growth. The net response for both these profiles identifies the position of nodal points separating the erosion/deposition regions. The upper is found at 160 – 170m seaward of the berm between MHWN and MHWS. The second nodal point occurs at 390m, just above MLWN and separates the deposition evident across the mid-beach with the erosion just below it. The third nodal point is located at MLWS (430m), and separates the region of accretion which forms the low tide bar with the rest of the profile.

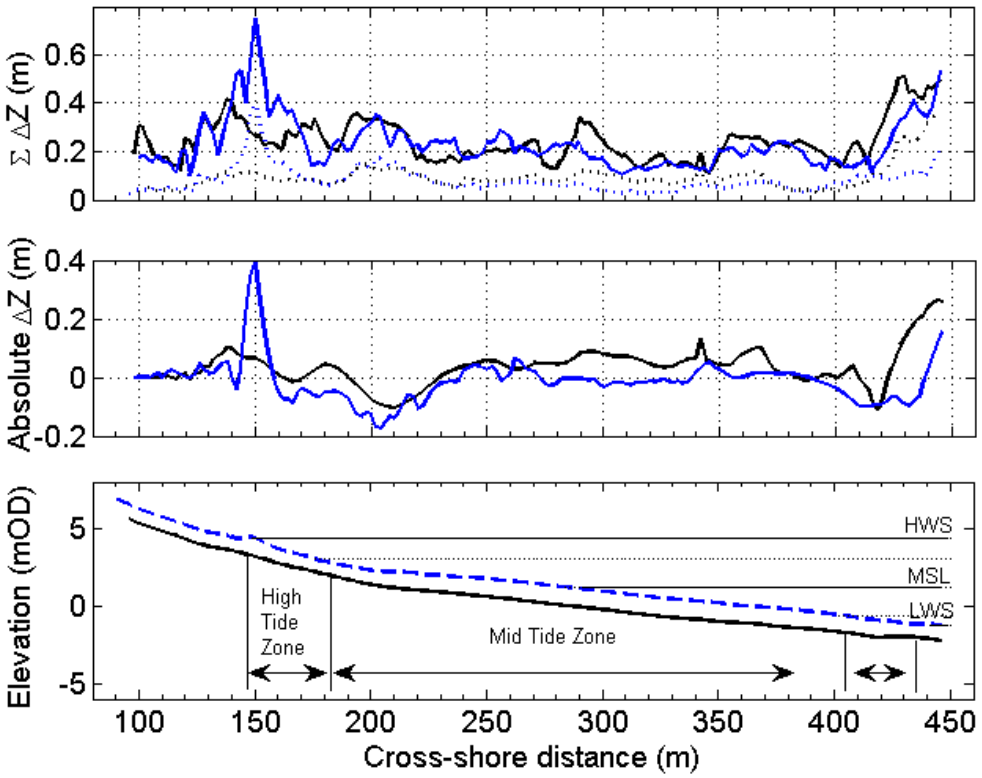

Figure 5.9– 2D beach response for the intertidal region during PX1. From the top; the cumulative change in surface elevation both erosive and accretionary (solid line), the absolute change in surface elevation which shows the maximum range of change observed over the study period (dotted line); the net change in surface elevation reflecting the erosion and accretion over the study period, blue lines are from L1, black lines are L2; profile line (L1 solid, L2 dashed with 1m vertical offset) and tidal zones during PX1.

At the start of the survey period the beach exhibited a weakly three dimensional surface with a small berm present near the high water mark Figure 5.10. At spring low water a

well-defined channel running southwest from the northern cliff cut through the beach with a low-amplitude alongshore bar seaward of this. By the end of the 14 days the berm had developed into a well-defined feature, the intertidal bar had migrated onshore and a new low tide bar had started to develop at the centre of the survey area. The development of these features is expressed clearly in Figure 5.10 which shows the net and absolute surface change throughout the survey period.

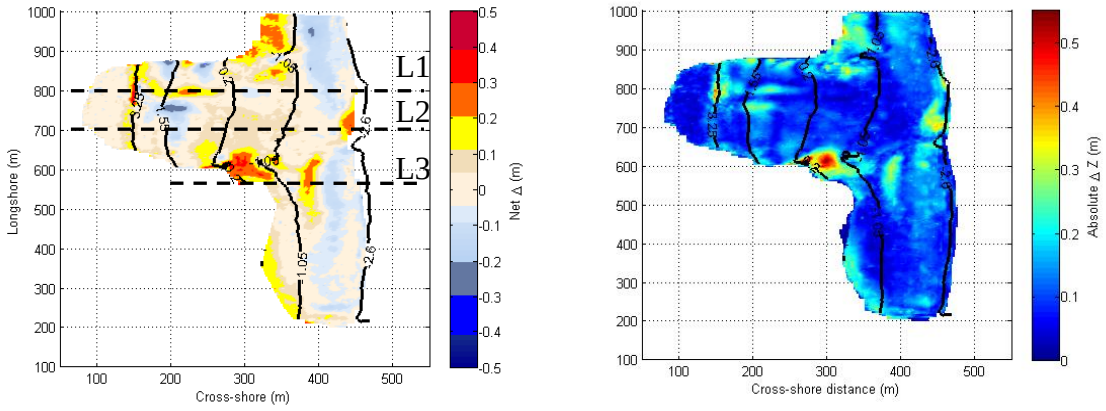

Figure 5.10 – 3D morphological response during PX1; the left panel shows the net Δz (m),and the right panel shows the absolute (maximum- minimum) Δz (m) for the duration of PX1. Thick contour lines indicate the position of MHWS, MHWN, MSL, MLWN and MLWS. The horizontal black lines show the location of extracted profiles presented in Figure 5.9.

Overall the beach experienced onshore migration of sediment across the intertidal region. The upper beach face was fed by the upper-mid beach, resulting in the development of the berm at 150m cross-shore, (Figure 5.10), whereas the upper-low beach acted as the source for growth in the mid beach above the MLWN line. However, much of the more significant accretion occurred through infilling of existing channels and rocky areas located at the survey boundaries where the beach opens up at low tide (cross-shore = 325m; Figure 5.10).

At the start of PX1 the small berm forced the river to pool and then split into two channels down the beach. As the berm developed over the following days, the river was forced northward down a single channel and the previous channel was subsequently in-filled (cross-shore = 200 m; Figure 5.10). The onshore migration of the longshore bar

crest (cross-shore 400m; Figure 5.10) is further expressed through profile L3 in Figure 5.11 which displays a sustained onshore migration rate of ca. 20m over 14 days.

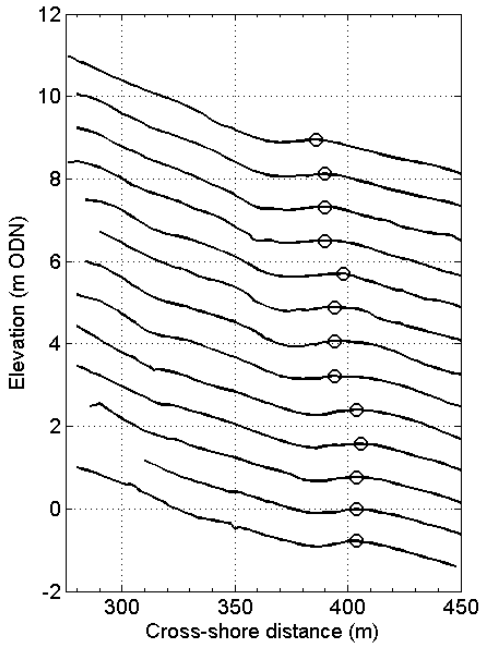

Figure 5.11– Profile stack of L3 showing onshore migration during PX1. The first profile is at the bottom with subsequent profiles offset by 0.5m for clarity. The hollow circles track the peak of the bar which exhibits a maximum horizontal onshore migration of ca.20m

5.3.3 PX1: Flow dynamics

Summary flow dynamics from R1 and R2 are presented in Figure 5.12 and Figure 5.13. R1 was located further inshore and was exposed at low tide; therefore, the data records are punctuated by periods of exposure at low water. As stated, R2 suffered from the rig settling into the sand making data between day 6 and 10 unavailable. R2 was located at the breaker zone during spring low tide with the instruments submerged throughout the 14 days.

Both time averaged cross-shore (<*u*>) and longshore (<*v*>) flows speeds varied between 0.05 and -0.25 m s^{-1} throughout PX1. Speeds for both flow directions remained fairly steady for the first 6 days, before a small increase which resulted in peak cross-shore flows of 0.3 m s^{-1} and peak longshore flows of 0.25 m s^{-1} occurred on day seven

(Figure 5.12). This response to the arrival of a small swell event was short-lived with flow speeds dropping off over the remaining six days as the swell decayed. Peak $<u>$flows are consistently associated with shallow conditions decaying gradually as the water depth increased. This depth dependant structure in flow speeds is clearest under moderate to calm conditions either side of the small swell event on day six (Figure 5.12). Similar structure in the flow speeds of $<v>$ are also observed with greatest flows observed under shallow depths, however the increasingly calm wave conditions towards the end of PX1 allow the tidal affect to become more evident. The shift in wave approach in response to the more northerly winds results in the normal northerly directed flows being weakened.

Cross shore orbital velocities (u_m) remained fairly constant throughout PX1 with maximum velocities of 1.3 m s^{-1} coinciding with maximum wave conditions on day 6. Some tidal modulation is evident with flows increasing by 0.4 m s^{-1} during low tide, although this is less evident during the peak wave heights. Variability in the peak offshore flow rates is small despite changes in wave conditions between daysone-eight; as the wave height decays further and the tidal range increases, flow rates also drop, however they remain steady with peak flows between 0.1 - 0.15 m s^{-1}. Flow velocity skewness ($<u^3>$) remains offshore throughout, with little variation as wave conditions increase. Offshore skewness is most negative at low tide, with weakly onshore skewness evident at high tide during day 3 and 4 and at the end of the survey period once the swell conditions have been replaced by wind waves. Acceleration skewness ($<a^3>$) shows the least variability remaining stable throughout with onshore peaks at low tide (Figure 5.12).

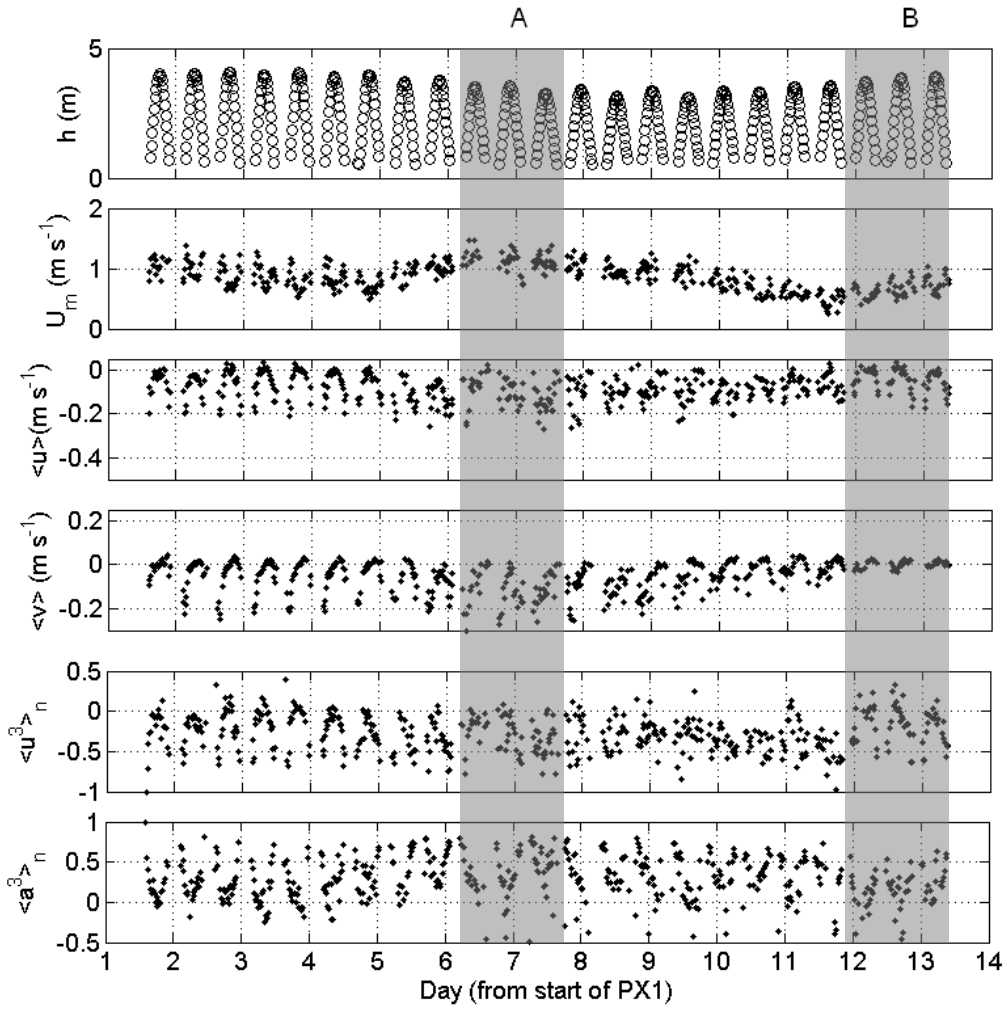

Figure 5.12– Summary of the flow statistics measured at R1 during PX1. From top, water depth *h(m)*; cross-shore orbital velocity U_m,; mean cross-shore flow velocity <*u*>, positive onshore; mean longshore flow velocity <*v*>, positive south; $\langle u^3 \rangle_n$ normalised flow velocity skewness; $\langle a^3 \rangle_n$ normalised flow acceleration skewness. Individual points represent burst sample means (ca.8.5min of data collection at 4Hz). The gaps in data occur when the rig was exposed above low water. The shaded boxes identify periods used forfurther analysis (see text). Axis scales have been set to ease comparison with subsequent plots from Rigs R2 and R3.

Located in deeper water R2 recorded much weaker nearshore flows throughout PX1 with mean <*u*> speeds of 0.05 m s^{-1} and mean <*v*> of 0.03 m s^{-1}. Both <*u*> and <*v*> start to increase on day 5 as the new swell arrives with peaks of at ca.0.1 m s^{-1}. Cross-shore flows were characterised by offshore flows (strongest during shallow water depths), while onshore-directed flows remained weak and present during deeper water depths only. Weak northward-directed longshore currents prevailed during the experiment, but a clear tidal modulation is apparent with a reversal in the longshore current occurring around mid-tide. Towards the end of the experiment period, as the

northerly wind waves become dominant, the tidal signature becomes more pronounced with both the flood and ebb tides interacting with the nearshore wave-induced currents to produce peaks in the northerly and southerly longshore currents respectively (Figure 5.13). The wave orbital velocity *(U_m)* shows a less clear trend during the survey period, in general we see increases under shallow depths with U_m reaching a peak of 1.2 m s^{-1}. Negative velocity skewness ($<u^3>$) prevails under shallow water depth, but positive skewness occurs during high tide. During the first 5 days the acceleration skewness ($<a^3>$) shows both positive and negative variability throughout the tidal cycle. As wave conditions increase on day 5, positive skewness becomes dominant particularly at low tide which is most evident on day 11 when wave conditions have dropped to H_s = 0.5m.

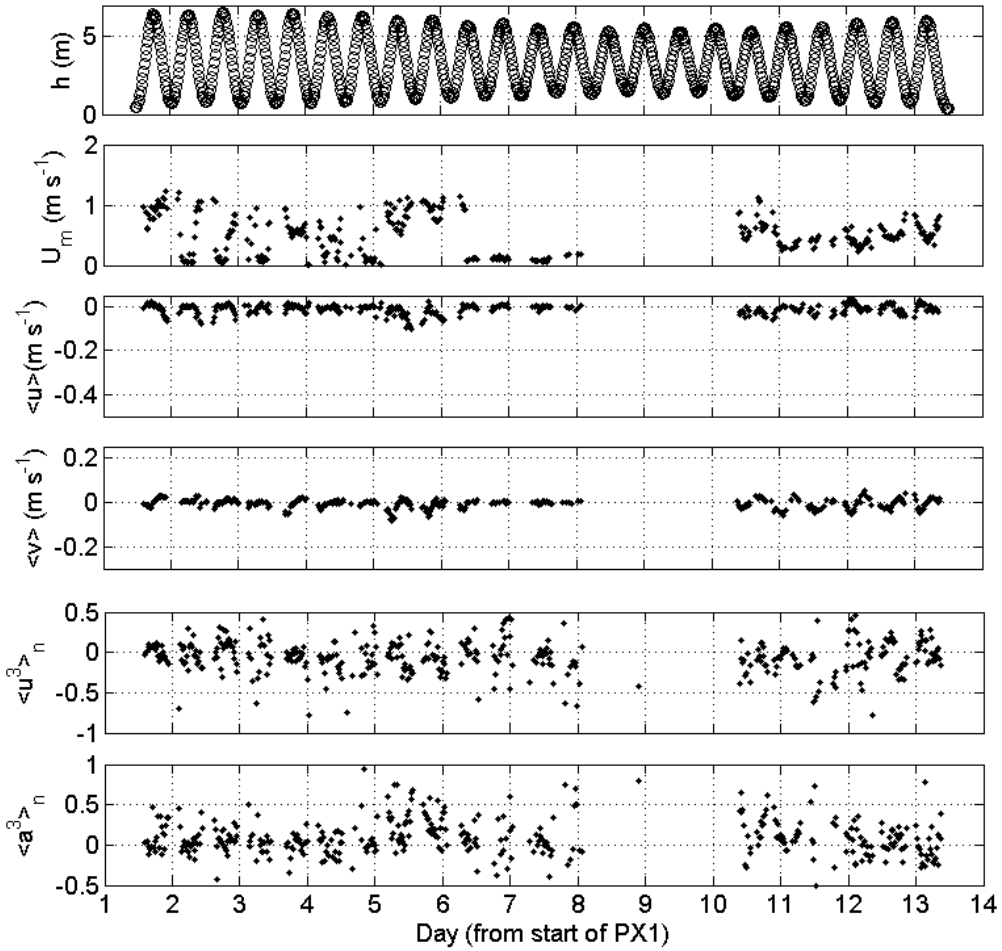

Figure 5.13 – Summary of the flow statistics measured at R2 during PX1. From top, water depth *h(m)*; cross-shore orbital velocity U_m,; mean cross-shore flow velocity <*u*>, positive onshore; mean longshore flow velocity <*v*>, positive south; $\langle u^3 \rangle_n$ normalised flow velocity skewness; $\langle a^3 \rangle_n$ normalised flow acceleration skewness. Individual points represent burst sample means (ca.8.5min of data collection at 4Hz). Gaps in the data occur when the rig was exposed above low water.

5.3.4 PX2: Waves

Wave conditions during the 2 weeks of PX2 were dominated by 2 storms. The first occurred on the 12th November with a peak H_s = 6.3m, recording the largest wave event since November 2009, and the second peaked on the 18thNovember with a peak of H_s= 3.9m (Figure 5.14). Following the second storm, wave conditions dropped significantly to H_s = 0.6m. The storms were generated by two deep (957mb and 967mb) north Atlantic lows which tracked SE across the SW of England during the survey period.

These brought with them strong (25knt) SW winds and heavy rain fall increasing river flows onto the beach (Figure 5.6).

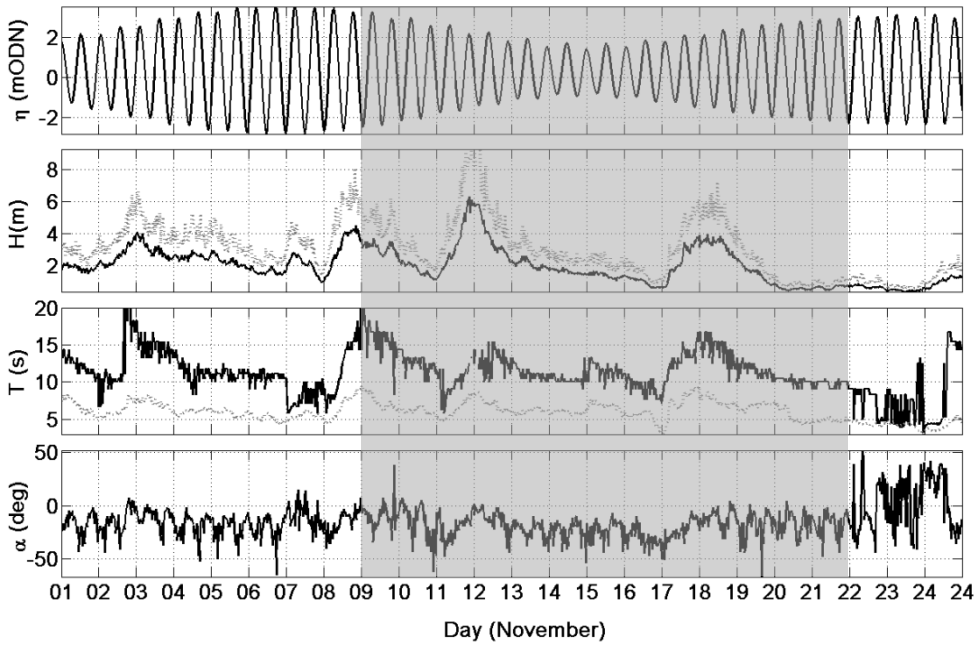

Figure 5.14– Summary wave conditions during November. From top to bottom: tidal elevation (m ODN), wave height (dashed line = H_{max}; solid line = H_s), wave period (dashed line = T_z; solid line = T_p) and wave direction relative to shore normal. Grey box indicates the PX2 time period.

Spectral analysis of the wave climate over the 2 weeks is presented in Figure 5.15 and shows the arrival of the two storm systems producing long period swell conditions throughout PX2. The classic storm profile saw a rapid rise and gradual fall in wave height, with the wave energy tail off as the storm passed. The alongshore component of the offshore wave flux remained positive (northward) throughout. Both storms occurred during mid-tide conditions in the middle of the spring-neap cycle.

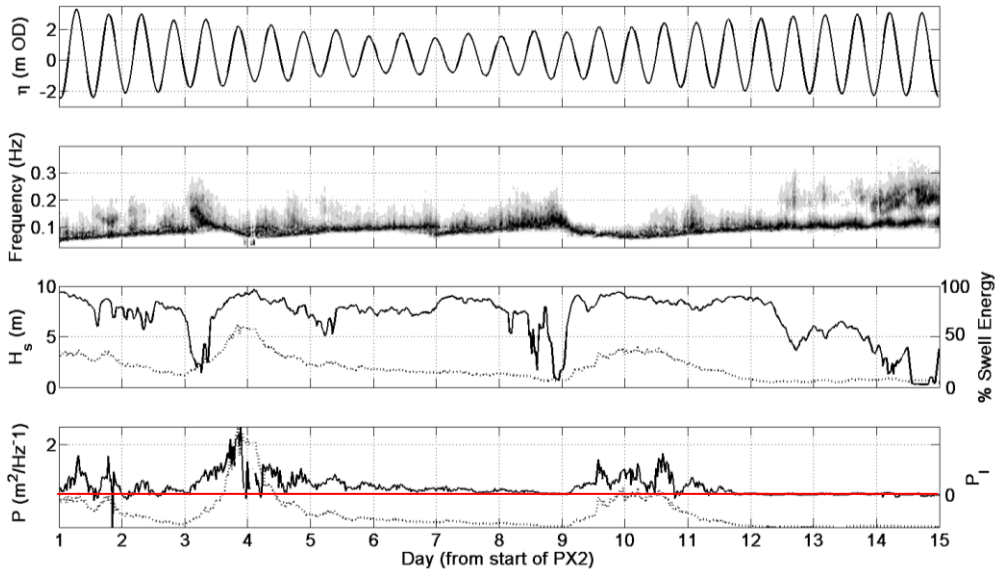

Figure 5.15– Summary spectral analysis of wave conditions during PX2. From top to bottom: tidal elevation (m ODN), wave spectrum, wave conditions (H_s = solid line; percentage swell energy = dashed line), wave energy flux (cross-shore flux P = dashed line; longshore wave energy flux P_l= solid line). Positive values for P_l indicates northward fluxes.

5.3.5 PX2: Morphology

Detailed analysis of the daily morphological response across the entire spring intertidal region during PX2 is limited due to the increased set-up and subsequent (infragravity wave-driven) run-up that restricted the spatial extent of the surveys. Overall, the beach experienced a net loss of 10000m^3 of sand (4% of initial volume) across the intertidal region. This was felt most in the lower beach where 5700m^3 was removed compared with 3400m^3 and 1000m^3 for the mid and upper beach respectively (Figure 5.16). Overall sediment grain size trends remain stable throughout with slight fining observed for the upper beach (Figure 5.16).

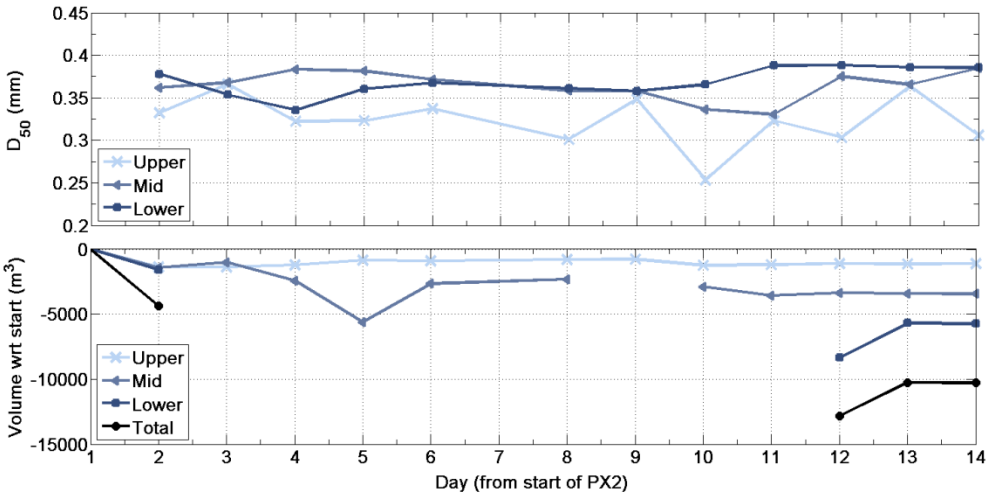

Figure 5.16 – Summary of the cross-shore sediment D_{50} during PX2 (bottom panel, and the intertidal(m^3) normalised with reference to the initial surface (bottom panel). Gaps in the data indicate restricted coverage owing to neap tides limiting the survey coverage.

Owing to the high levels of rain fall (Figure 5.6) which resulted in high river discharge rates which subsequently affected the morphology in this region, L1 is omitted from 2D profile analysis during PX2. The cross-shore variability of L2 indicates a net loss across the profile with greatest removal evident at the lower upper beach (200-270m) and the upper lower beach (320-400 m; Figure 5.17).

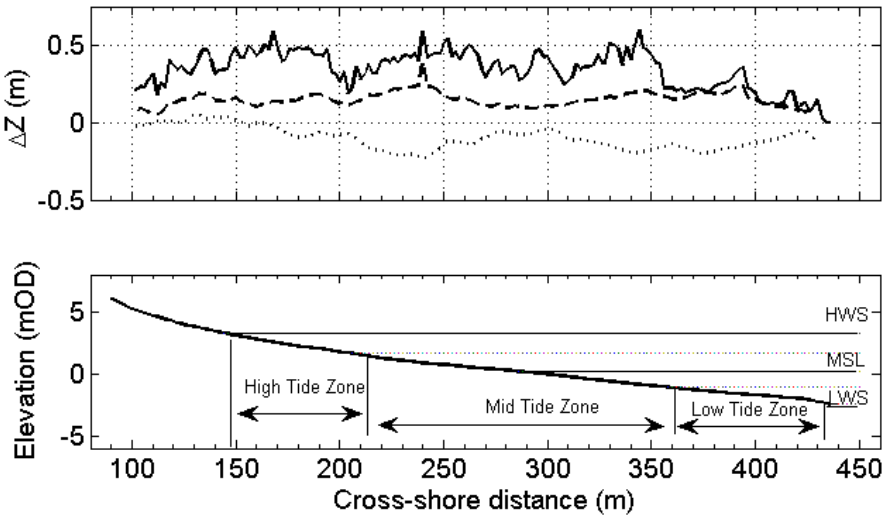

Figure 5.17– 2D beach response for the intertidal region during PX2 (L2). From the top; the cumulative change in surface elevation both erosive and accretionary (solid line), the absolute change in surface elevation which shows the maximum range of change observed over the study period (dashed line) and the net change in surface elevation reflecting the erosion and accretion over the study period (dotted line).

Following energetic conditions at the start of November, the morphology at the start of PX2 represented a very planar upper and lower beach with no significant three-dimensional features (Figure 5.3). The 3D response to the widespread loss of material is presented in Figure 6.18 which highlights the net and absolute change in surface elevation. Over 14 days the greatest loss of sediment and surface change was observed in the upper – lower beach and the lower–upper region (Figure 5.18). Sediment accretion can be seen at the survey edges in the upper beach and at the low tide region. By the end of the survey period, the greatest change was evident in the low tide with the development of a small low tide bar at the northern edge of the survey area. Changes in the upper beach, particularly evident in Figure 5.18 b) (longshore position ca.800m), represent the increased river flow in this region which scoured a channel through the beach causing significant redistribution of sand.

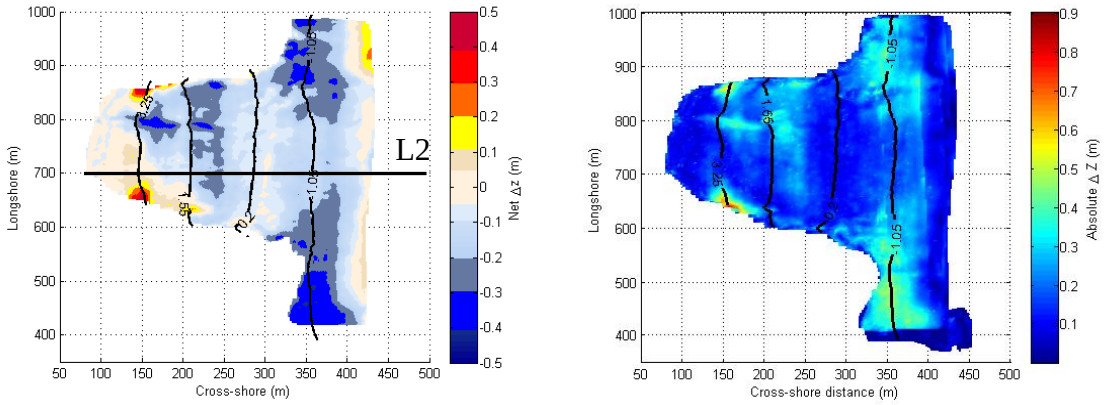

Figure 5.18– 3D morphological response during PX2; the left panel shows the net Δz (m),and the right panel shows the absolute (maximum- minimum) Δz (m) for the duration of PX2. Thick contour lines indicate the position of MHWS, MHWN, MSL, MLWN and MLWS. The horizontal black lines show the location of extracted profiles presented in Figure 5.17.

5.3.6 PX2: Hydrodynamics

Results from R3, which was located at low water neaps (Figure 5.3), and was deployed for the duration of the second storm, are presented in Figure 5.19. Cross-shore flows

were generally dominated by offshore-directed currents throughout the tidal cycle, with maximum flow velocities of -0.2 m s^{-1} occurring in the shallowest water depths either side of the peak H_s which occurred between days 9-11 (Figure 5.20). Longshore currents were predominantly northerly directed, with peak flows between -0.2 m s^{-1} and -0.3 m s^{-1} (Figure 5.19).

On day nine as the H_s increased, a reversal in the depth dependence structure of the cross-shore flows was observed with peak $<u>$ rates of -0.5 m s^{-1} occurring under high tide. During the same period longshore flows also increased with peaks of -0.2 m s^{-1}(northerly) and 0.3 m s^{-1} (southerly), however there is little evidence of clear depth dependence of the flow rates during this period (Figure 5.19). By day 11 the H_s has decreased from 3.8 m to <1 m, this results in peak cross-shore flows of < -0.2 m $s^{-1,}$ which are present under shallow conditions. Longshore flow rates also respond to the drop in wave conditions with peaks flows of <0.05 m s^{-1} evident for the remainder of the experiment. Under calmer conditions the tidal modulation of the longshore flows is more apparent, with mid-tide northerly and southerly directed peaks occurring during the flood and ebb currents.

The normalised flow velocity skewness ($<u^3>$) remained negatively skewed throughout the experiment with greatest skewness under shallow conditions. During the increased wave conditions between days 9-11, the skewness ($<u^3>$) remained strongly negatively skewed throughout the tidal cycle. The opposite is evident for the acceleration skewness ($<a^3>$) which remains positively skewed throughout PX2 (Figure 5.20). Similar to $<u^3>$ greatest $<a^3>$ occurs during shallow water depths, except under large wave conditions where a sustained positive skewness of 0.5 remains throughout the tidal cycle (Figure 5.19).

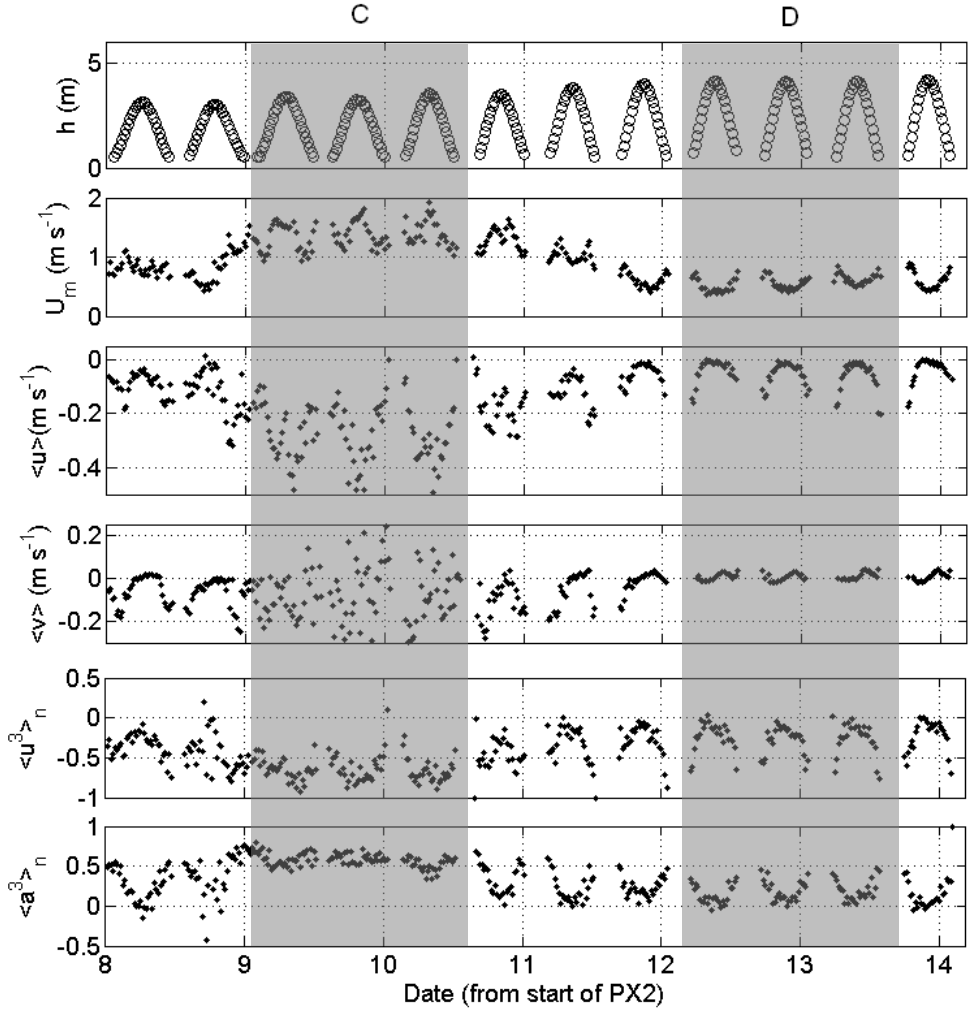

Figure 5.19 – Summary of the flow statistics measured at R3 During PX2. From top, water depth *h(m)*; cross-shore orbital velocity U_m,; mean cross-shore flow velocity <*u*>, positive onshore; mean longshore flow velocity <*v*>, positive south; $\langle u^3 \rangle_n$ normalised flow velocity skewness; $\langle a^3 \rangle_n$ normalised flow acceleration skewness. Individual points represent burst sample means (~8.5min of data collection at 4Hz). Gaps in data occur where the rig was exposed above low water. Shaded boxes identify periods of further analysis (see text).

5.4 Analysis

Specific periods have been identified to provide maximum comparison of the forcing conditions and the dynamic responsesin order to discuss the two contrasting datasets provided during PX1 and PX2. The chosen periods are identified in Figure 5.14 and Figure 5.19, and a summary of the forcing conditions are collated in Table 5.1. The phases during PX1 include (A) medium energetic waves during neap tides and (B) low-energy conditions under spring tides but with a northerly wave approach. PX2 provides a more contrasting dataset with highly energetic storm waves during neap tides (C) and

very low energy spring tide conditions (D). The variation in the tidal range is small between each period (~0.7/0.5m).

Table 5.1– Summary of the hydrodynamic conditions during selected phases (A – D) which occurred during both PX1 and PX2 and used for comparison of nearshore flows.

Period		H_s (m)	T_p (s)	Dir (°)	Energy (m^2Hz^{-1})	Tide Range (m), above rig
PX1	**A**	1.50	11.6	280	0.12	3.16
	B	0.84	6.0	327	0.04	3.4
PX2	**C**	3.20	14.2	285	0.65	3.06
	D	0.60	9.8	287	0.02	3.75

The distribution of the different wave heights with water depth for each period identified in Table 5.1 is presented in Figure 5.20. Because of the dissipative relatively flat ($tan\beta$ = 0.012) profile at the location of the rigs during PX1 and PX2, the breakpoint is likely to be fairly wide and occupy much of the outer surfzone, reflected in the scatter of values in Figure 5.20. From this however we can identify the breaking region occurs at a relative wave height of H/h = ca. 0.5.

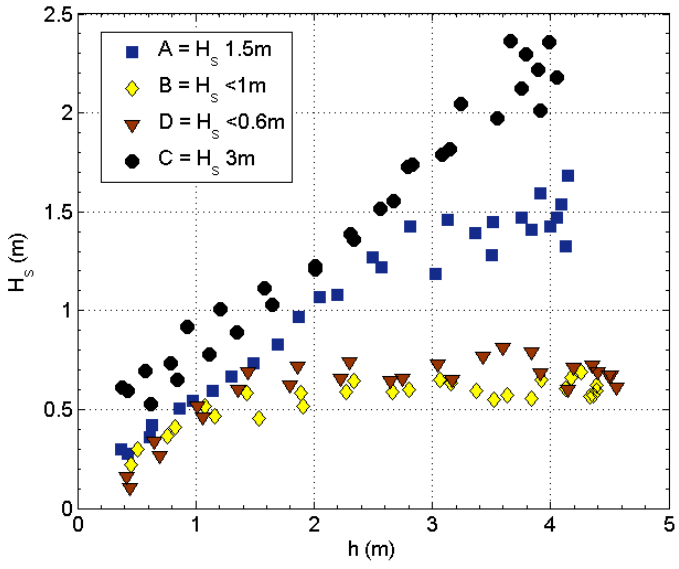

Figure 5.20– Measurements of local wave height (H_s) against local water depth (h) over individual tides during different wave conditions during PX1 and PX2. The position wave breaking levels off (H/h =0.5) identifies the breaker zone.

Summary variability in cross-shore and longshore currents with regard to water depth for periods A and B (Figure 5.21) and periods C and D (Figure 5.22) highlight the main

changes under increasing wave conditions. Under moderately energetic conditions (A) we see less depth dependence as both <*u*> and <*v*> exhibit variability in flow rates at all depths. Figure 5.21 shows <*u*> speeds experience an overall reduction under increasing depth, although there is a wide distribution of values and they remain offshore directed throughout. Longshore flows exhibit a similar distribution with northerly (negative) flows dropping under increased depth. Throughout the small wave conditions (B), we see a clear trend of increased offshore flows under shallow water depths, as the depth increases the near bed flow rates decrease steadily yet remain predominantly offshore directed. As wave conditions drop below H_s= 1m (B) and the wave direction becomes more northerly, the longshore flow speeds drop with no change in flow rates relative to water depth (Figure 5.21). Under these conditions the longshore currents are dominated by tidal flows across the beach face, producing the asymmetric profiles shown in Figure 5.12.

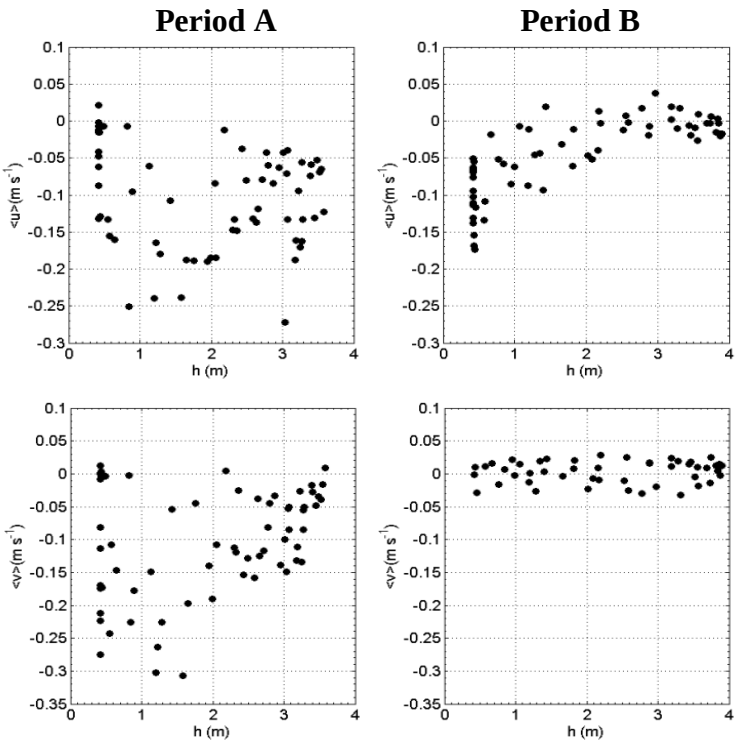

Figure 5.21– From the top; Scatter plots of cross-shore current velocity (<*u*>) vs water depth (*h*); longshore current velocity (<*v*>) vs water depth (*h*) from Rig 1, for periods A and B shown in Figure 5.12 and discussed in the text.

Under the highly energetic conditions present during phase C (H_s = 3.2m), a reversal of cross-shore flow structure is evident with offshore current speeds increasing with increased water depth (Figure 5.22), however at peak water depths (h = >3m) flow speeds drop. Longshore flow dynamics during the energetic conditions of period C show widespread distribution, with strong flows present under shallow and deep conditions (Figure 5.22). Whilst northerly flows dominate this period, with speeds up to -0.3 m s^{-1} under shallow depths, strong southerly flows (0.2 m s^{-1}) occur under deep conditions. The calmest period of interest (D) occurred during PX2 following the storm conditions (Figure 5.22), which result in a return to the flow dynamics observed in period A and B. Cross-shore flows decay steadily under increasing water depths, while longshore flows remain weak (<+/- 0.04 m s^{-1}) with both northerly and southerly directed flows reflecting the tidal signal on the currents.

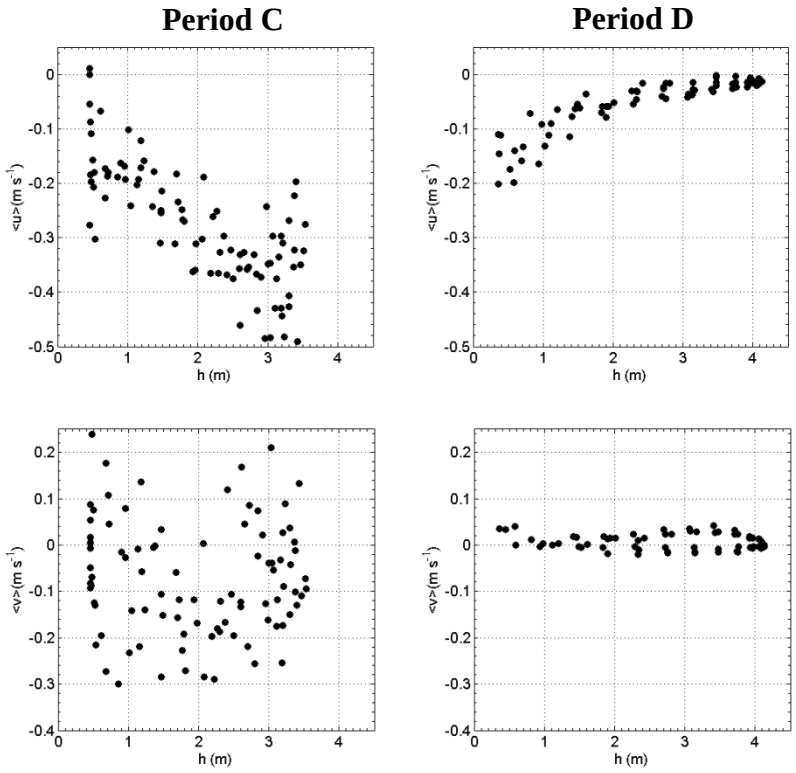

Figure 5.22– From the top; Scatter plots of cross-shore current velocity (<*u*>) *vs* water depth (*h*); longshore current velocity (<*v*>) *vs* water depth (*h*) from R3, for periods C and D shown in Figure 5.19 and discussed in the text.

Comparison of the combined flow dynamics for the four periods with the relative wave height (*H/h*) highlights the response of the nearshore currents under different stages of

wave transformation across the shoreface (Figure 5.23). Using a breaker zone of *H/h* = 0.5 identified in Figure 5.20, a dominance of weak flow velocities under shoaling conditions (*H/h* =<0.3-0.4) is evident under the small wave conditions of periods B and D (Figure 5.23). Under more energetic conditions during period A, the rig is located within the surfzone for longer as the increased conditions extends the outer surfzone resulting in the rig located under occasional breaking waves at high tide.

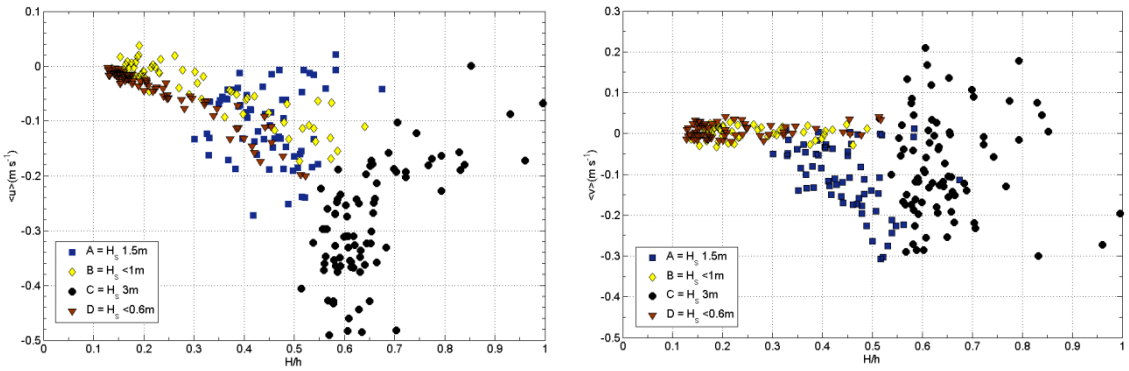

Figure 5.23 – Distribution plots showing cross-shore (left) and longshore (right) flow velocities with reference to the relative water depth (*H/h*). Shaded symbols indicate the 4 different periods of wave energy introduced in Table 1. *H/h*>0.8 indicates swash zone, *H/h* 0.5-0.6 identify the surfzone and *H/h*<0.4 indicate shoaling waves.

This is confirmed by qualitative assessment using the Argus images during this period, which allows us to establish the surfzone position relative to the instruments (Figure 5.24). The most notable change flow dynamics is evident during period C, with the large wave conditions the rig is within the surfzone throughout the tidal cycle (Figure 5.24), and we see no evidence of shoaling related flow velocities throughout the tidal stage.

Figure 5.24– Argus images from PTN showing the location of the rig mounted ADV (red dot), all images are at approx same high tide but show different wave conditions; from the left, period B, period A (during PX1), and period C (during PX2).

Further consideration of the relative surfzone position can be undertaken using the flow velocity skewness ($<u^3>$), and the flow acceleration skewness ($<u^a>$) (Figure 5.25). Through shoaling conditions towards the outer surf zone we see a steady increase in the negative skewness of the flow velocity, following a peak at H/h = 0.6 following wave breaking negative skewness is reduced under broken waves as they move through the inner surfzone (Figure 5.25). Conversely the acceleration skewness becomes increasingly positive as the relative wave height increases, with peak skewness (0.8) occurring following wave breaking, before levelling out within the swash zone (Figure 5.25).

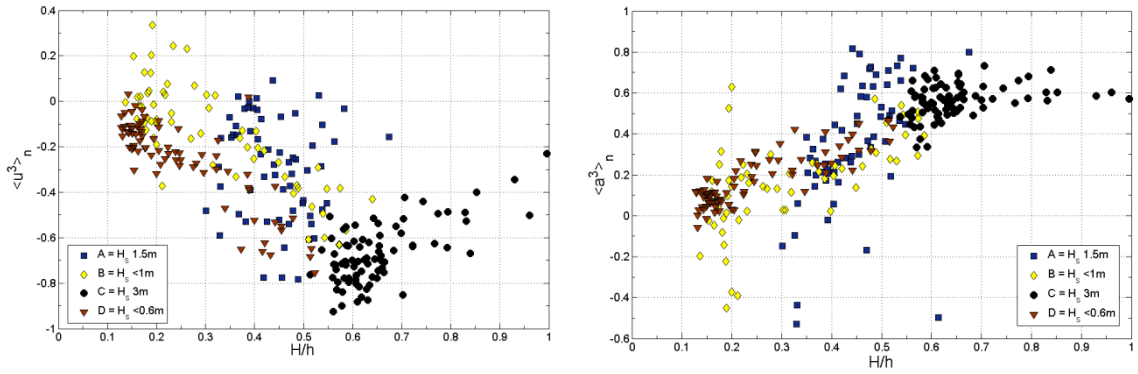

Figure 5.25 – Distribution of flow velocity skewness ($<u^3>$), left, and the flow acceleration skewness ($<u^a>$), right, vs relative wave height under contrasting wave conditions.

Spectral partitioning of the cross-shore spectra under the contrasting conditions highlights the dominance of shoaling conditions during periods A, B and D, with peak PSD within incident wave frequency (Figure 5.26). The presence of distinct infragravity

peaks in the normalised spectra during period C support the previous observation that the instrument rig remained in the mid-inner surfzone throughout the tidal cycle, (Figure 5.26).

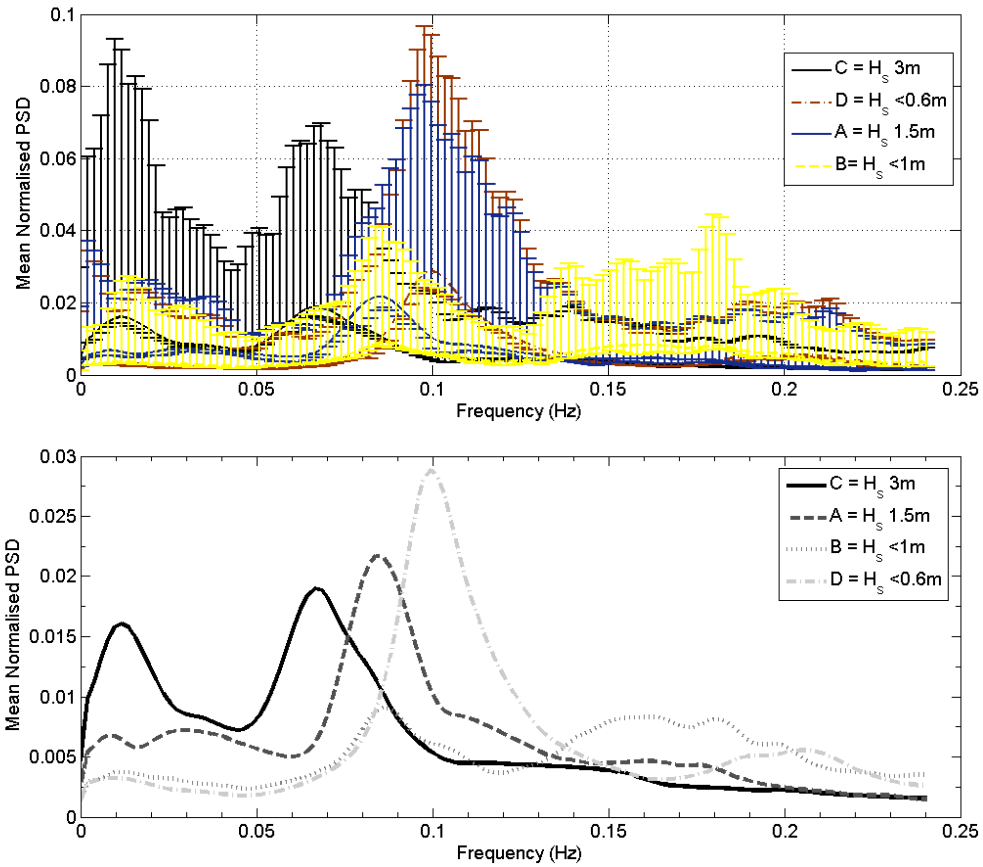

Figure 5.26 – Summary of the cross-shore flow spectra under the different wave conditions. Normalised spectra are presented for each of the four periods identified in Table 5.1. The top panel shows the data variability during the selected periods, the bottom panel shows the mean normalised spectra.

The normalised spectra presented in Figure 5.26, is further supported by Figure 5.27 which summarises the percentage infragravity partition of the cross-shore spectra. This again highlights the dominance of infragravity frequencies under large conditions within the surfzone.

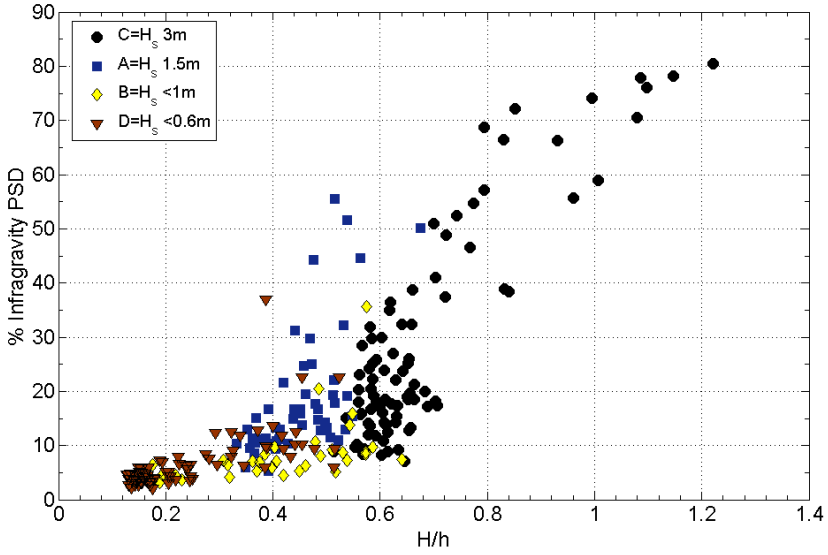

Figure 5.27 – Summary plot showing the percentage infragravity component of the cross-shore flow spectra against the relative water depth (*H/h*). Point symbols relate to the 4 periods of contrasting wave conditions discussed in the text.

5.5 Discussion

Using the two data sets of contrasting morphological response and associated nearshore flow dynamics we can begin to understand more about the dynamics of this site. PX1 was characterised by steady rates of accretion, while PX2 experienced sustained loss of material throughout the surveys. Time series analysis of the profile evolution with respect to the survey at the start of the fieldwork is presented in Figure 5.28. For both PX1 and PX2 the morphological response is steady and gradual. Under calm conditions we see regular onshore transport with two regions of growth; 1) the development of a berm in response to sediment moved onshore from the neap high water line (Figure 5.28 a); 2) the onshore movement of a bar at two locations below mean low water neaps (Figure 5.28, b and c).

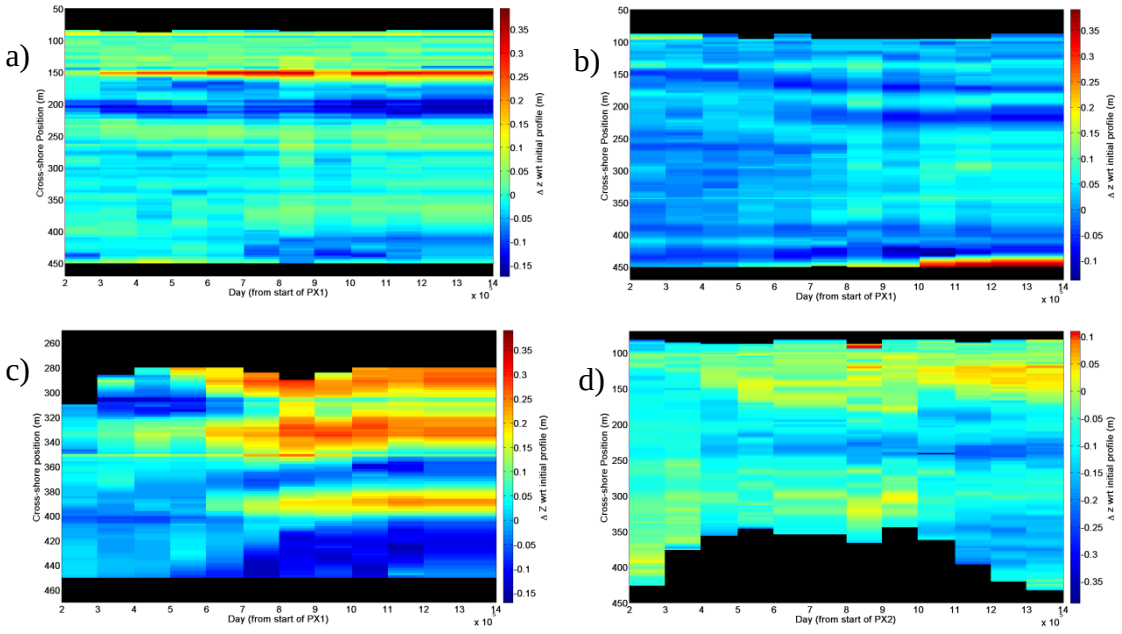

Figure 5.28– Surface plot showing temporal variation in 2D profiles with reference to the initial profile during PX1 and PX2. From PX1; profile L1 which shows berm development (**a**), profile L2 capturing bar growth at low water (**b**) and profile L3 highlighting onshore bar migration at x = 380m (**c**). From PX2; profile L2 which displays the widespread loss in the mid to lower beach, and small accretion in the upper beach towards the end of the experiment (**d**).

Whilst mean flows were offshore throughout PX1, under calmer (H_s= <1m) conditions onshore flows and onshore velocity skewness were also recorded (Figure 5.25). Combined with the positive flow acceleration skewness, the onshore sediment transport supports similar observations made by Austin *et al*. (2009), which were highly correlated with onshore sediment flux. Without corresponding suspended sediment concentrations it is not possible to quantify the sediment flux through the tidal cycle, however, using Bailards (1981) energetic based suspended sediment transport prediction adapted to incorporate flow acceleration (Puleo *et al.*, 2003), we are able to further assess this conclusion. Figure 5.29 collates the predicted suspended sediment transport using eq.5.5 for each of the contrasting conditions during PX1 and PX2. While the presence of large storm conditions (PX2) dominates the plot, periods of positive transport are evident under calm-moderate waves experienced during PX1. The adapted model by Puleo *et al*., (2003) is specifically designed to account for the additional

transport present during swash conditions. It is suggested the under representation of onshore transport, predicted in Figure 5.29 during PX1 conditions, is likely to result from limited data points within the complex swash events. It is plausible with more detailed measurements in this region we would be able to support observations by Austin *et al.* (2009) that the onshore transport was a result of flux coupling between the oscillatory component of the incident waves and the instantaneous suspended sediment concentrations.

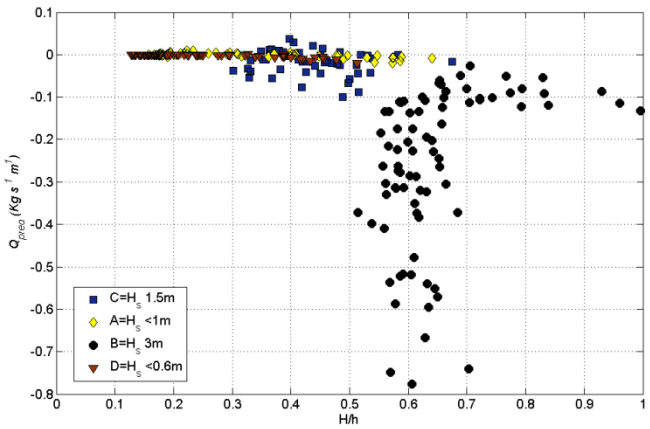

Figure 5.29 – Predicted suspended transport (Q_{pred}) incorporating flow acceleration (Puleo *et al.*, 2003) under relative wave heights (H/h) during contrasting wave conditions.

Building on the predicted sediment transport rates presented in Figure 5.29 we can compare these with the change in volume between the daily surveys (Figure 5.30). Although the net change during PX1 was positive there is daily fluctuation throughout the survey period, not reflected in the Q_{pred}, which remains mostly offshore directed (negative). PX2 presents a clearer picture with a drop in volume present almost throughout and the two storm events clearly identified. Equally the Q_{pred} supports this with offshore directed transport throughout.

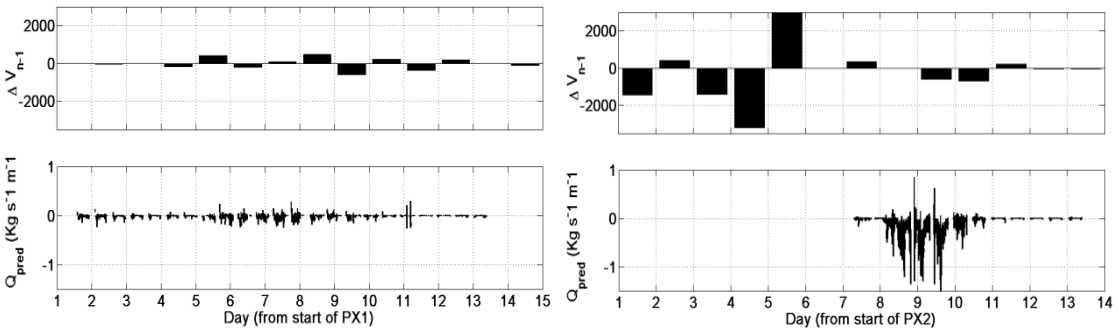

Figure 5.30 – Comparison of the measured change in volume (with reference to the preceding day) and the predicted sediment transport rate (Q_{pred}) incorporating flow acceleration (Puleo *et al.*, 2003); PX1 on the left; and PX2, on the right. The gap at the start of PX2 reflects the lack of nearshore flow data during this period owing to the storm conditions.

In the four weeks preceding PX2 wave conditions increased from a 10% H_s= 3.2 m to 5.2 m, this resulted in a net loss of 3.24% of the intertidal volume, with a drop of 6.1% for the low beach. This response was the first significant reduction in beach volume since December 2009. Despite two storm events with H_s=>4m prior to PX2 the large conditions during PX2, including a peak H_s= 6.2m, further resulted in the loss of material across the intertidal region, with a net reduction of 3.28% and 6.% loss in the low tide region. The sustained loss of material over 6 weeks of increased wave conditions suggests a continued movement towards a more "equilibrium" beach face under the storm waves. Between the end of PX2 (22nd November) and the following survey on the 6th December the net volume change was a decrease of 0.29%, significantly less than the loss observed during PX2, reflecting the reduced storm conditions and greater stability in the beach as it enters a recovery phase.

Whilst nearshore flow data are not available for the first 7 days of PX2 we can use the data collected from the ADVs during the second half to infer the conditions. From these it would be realistic to suggest strong offshore flows dominated with maximum flows generated under relative wave heights of H/h = 0.6. However, it also important to note whilst there was widespread loss across most of L1 with reference to the initial surface, accretion does occur towards the upper beach (Figure 5.28 d). The increase in the

profile at the high tide line becomes more pronounced towards the end of the survey period after day 10 as wave conditions drop considerably becoming more consistent with those experienced during PX1. During this period berm build up starts to develop at high tide to the edge of the survey area, suggesting a return to onshore-directed sediment flux which was dominant during PX1. This shift towards onshore transport is rapid and occurs as the tidal range increases allowing the build-up of the berm to take place. The development of a low tide bar feature to the northern extent of the survey area supports this shift in cross-shore transport as it is fed by the subtidal region. Owing to restricted survey areas it is not possible to quantify the rate of migration observed in this region; however, its development is evidence of onshore transport and subsequent increased 3D morphology.

The horizontal translation and subsequent residence times of the surf zone clearly plays a significant role in the development and generation of the morphologic features identified in PX1 and PX2. Chapter 4 has already identified the relative importance of tidal state and wave conditions on morphological response. During PX1 and PX2 the tidal range between spring- neap varied by 1.4m and 2m respectively. Both the rate of berm accretion and the onshore migration of the low tide bar (Figure 5.28, a and c) become more apparent as the tide range drops, however this also coincides with the arrival of small swell waves which are linked with positive sediment transport predictions in Figure 5.29. Conditions during PX2 saw large storm waves and contrasting calm conditions occurring during both the spring and neap tidal stages, which makes comparison of the tidal effect on the morphological response not possible.

5.6 Conclusions

Comparable datasets of daily intertidal 3D morphology and nearshore flow dynamics have been presented under contrasting wave climates (H_s = 0.2 – 6.2 m) for a macrotidal intermediate beach. Two field experiments were undertaken over fourteen days at PTN to investigate the dominant nearshore processes and relate these to the morphological response. To this end daily intertidal topographic surveys were undertaken and complimentary hydrodynamics were measured at MLWS. In additions Argus images were used to qualitatively identify the surfzone position throughout the measurement period.

Under small to medium wave conditions; morphological response indicates net onshore transport across the intertidal region, with the development of a high tide berm and low tide bar features. Although net flows were offshore directed, with strongest flow rates under shallow water depths, the importance of onshore transport driven by shoaling waves and swash-bore processes was significant.

Contrasting storm waves during PX2 lead to widespread loss of material across the entire intertidal region with strong offshore flows present throughout increased wave conditions (0.5 m/s^{-1}). As the surfzone width increased flow velocities peaked under deeper water depths where infragravity frequencies dominated the cross-shore flow spectra. Post-storm morphological response was characterised by early berm development in the upper beach as the tidal range increased towards springs and reduced surfzone width saw a transition to onshore directed transport driven by shoaling waves and swash processes.

Within the context of the monthly survey programme, the present intensive experiments have identified key aspects of the beach response and nearshore dynamics; 1) under energetic storm waves strong offshore-directed cross-shore flows are dominated by

infragravity frequencies; 2) post-storm recovery under small swell-dominated waves is rapid with berm development and onshore bar migration evident within tidal cycles (< 1 day); 3) accretionary phases under small swell-dominated waves lead to reduced three dimensionality through infilling of channels.

6 MODELLING 3D MORPHOLOGY WITH XBEACH

6.1 Introduction

Through long-term monitoring and the more intensive surveys presented in Chapters 4 and 5, key trends in the behaviour and response of the intertidal region at four macrotidal energetic beaches has been presented. Numerical models are a ubiquitous feature of nearshore research and are employed as a predictive tool building on local data sources to further address system dynamics. They allow the impacts of changes in natural systems to be assessed through gradual systematic shifts in forcing and domain conditions. This chapter introduces the application of the XBeach model to an intermediate-state beach (PTN), which has been shown to exhibit significant shifts in low tide morphology in response to variations in the dominant wave conditions. As well as testing the model performance a series of scenarios are undertaken to assess morphological response to varying waves, tides and beach states.

6.1.1 XBeach

XBeach is a 2D depth-averaged numerical coastal model which operates on wave-group time scales through the parameterisation of sediment transport contributions of individual waves. XBeach was developed in response to the devastating effects of hurricanes on low-lying sandy coasts and barriers in the USA. Designed to model eXtreme Beach behaviour, XBeach is a numerical model of nearshore processes optimized to calculate the time-varying storm conditions and, as a result, it incorporates the possibility of dune erosion through avalanching, overwashing and breaching for analysis of dune degradation (Roelvink et al., 2010). As an open source program the

model offers users the ability to feedback into the development of the model, and, importantly, makes it more accessible for wider applications. More detailed description of the XBeach model is available elsewhere , (e.g. McCall et al., 2010; Roelvink *et al.*, 2010) and here only a brief summary is presented.

A key characteristic of the XBeach model is the representation of waves which is handled by employing wave-group forcing derived from the time-varying wave action balance solver. This solves wave refraction, shoaling, and allows variation of wave action in x, y, time and over the directional space, and can be used to simulate the propagation, breaking and dissipation of wave groups (Roelvink *et al.*, 2010). Cross-shore and longshore flows are generated by the long-wave forcing, with a Generalised Lagrangian Mean (GLM) approach to represent the depth-averaged undertow and its affect on bed shear stress and transport. The complex nearshore sediment transport processes present in the swash and surf zone are resolved for long waves by a depth-average advection-diffusion equation computed by the Soulsby-van Rijn formulation (Soulsby, 1997). It is assumed the less dominant intra-wave sediment transport,which occurs through wave asymmetry and wave skewness, are minor compared with the mean flows and long wave contributions (Roelvink *et al.*, 2010). It can be suggested that this is a valid assumption on sandy beaches forced by energetic wave action (Russell, 1993).

The following section introduces a brief summary of the key components of the model set-up, followed by model calibration with survey data. Model validation is then presented before application of the model to test the response of different beach morphologies.

6.2 Methodology

The initial set-up of XBeach is centred around 3 work areas: (1) generation of the model domain (including grid size and blanking regions); (2) the input files (waves, tides); and (3) the model parameters. XBeach uses a coordinate system where the x-axis is shore-normal, increasing inland, while the y-axis is alongshore perpendicular positive towards the north (Figure 6.1). The grid is defined relative to the real world coordinates (xw, yw) through the origin (xori, yori) and the orientation *alfa*. The grid size can be variable in both the x and y direction; however, the grid must remain rectilinear.

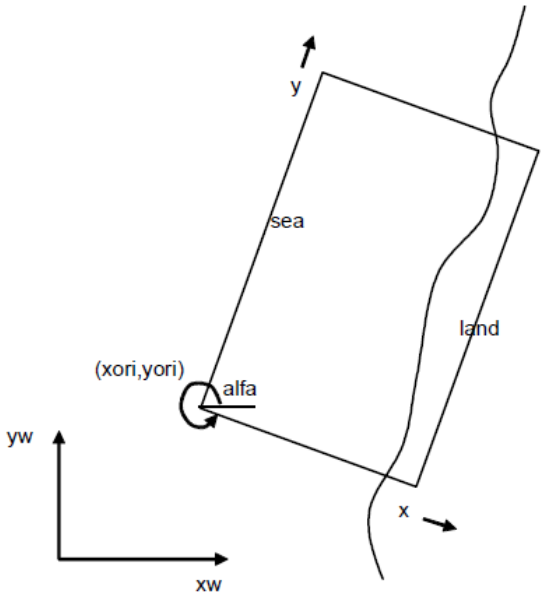

Figure 6.1– Grid orientation within XBeach

For the initial bed level a combination of intertidal survey data and nearshore bathymetry data (www.channelcoast.org) was used to create a model domain which extended ca.1000m cross-shore and ca.100m longshore with a graded grid size of 20m x 20m offshore and 10 x 20m inshore. Bathymetric data were available from July 2008, which was merged with the relevant intertidal survey data for each model run. The interval between the datasets meant a level of smoothing and interpolation was

undertaken to ensure a realistic bathymetry was used.Further discussion on this approach is given in Section 6.8, Model Performance.

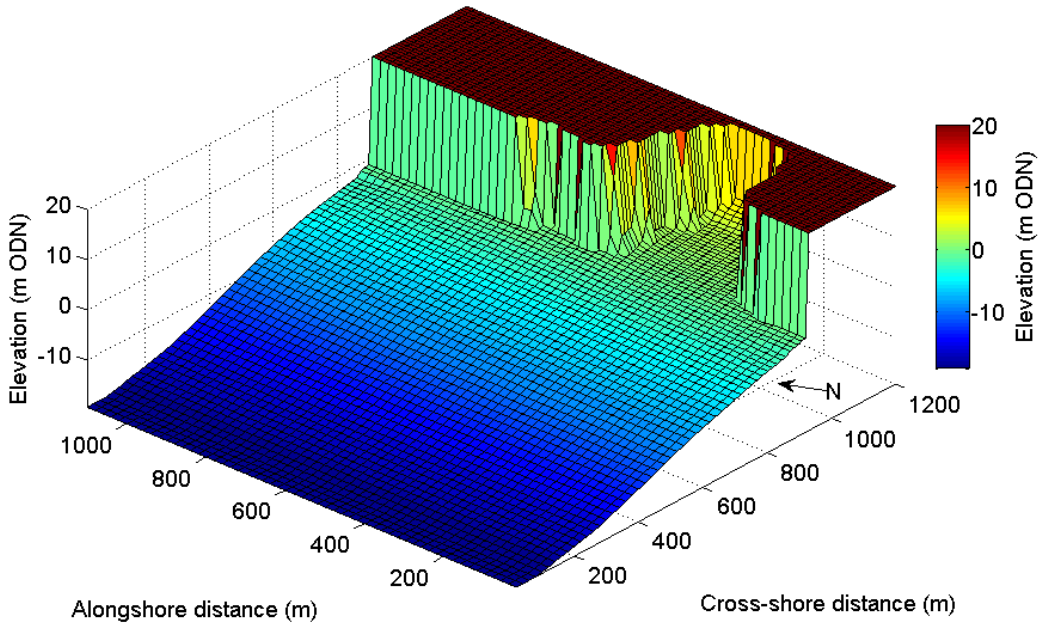

Figure 6.2– Representative planar bathymetric grid set-up for PTN with XBeach coordinate system. Raised cliff areas were blanked out during model runs.

6.2.1 Hydrodynamics

Non-stationary wave conditions were generated using wave data from the nearshore buoy located north of the survey area at PPT (Chapter 3). It should be pointed out that the model area extends deeper (ca -19m ODN) than the wave buoy (ca.-10m ODN), but it was felt that its relative position was more suitable data source than generating a new wave dataset from model/offshore sources. Wave parameters, height (*Hm0* (m)), peak period(T_p(sec)), direction (*Dir* (°)), gamma (3.3), directional spread (sprd), the duration (sec) and the wave time step (sec), are used to create time-varying wave amplitudes which provides the envelope of the wave group (Van Dongeren *et al.*, (2003), in Roelvink *et al.*(2010)).

Tide data were provided from the local tide gauge sited at PTN (Chapter 3) with input values every 30 min. While XBeach allows the user to provide more than one time-varying water level to each of the model boundaries, for the purpose of the current model a single time-varying water level across the entire boundary was applied. This approach means that tidal currents are not considered within the model.

6.2.2 Boundaries

In addition to the bathymetry, XBeach allows the user to set boundary conditions. Initially the lateral boundaries which lie perpendicular to the coastline were set as "*nueman"* boundaries which prescribe "no change" between the surface elevations/velocities. However, during early runs weak circulation cells developed and through positive feedback generated significant longshore currents not observed *in-situ*. Therefore, subsequent runs were undertaken with "*no-flux*" boundaries. However, because circulation effects remained present during longer runs, the domain was extended by 40m at each boundary with uniform gradients to reduce irregular bathymetry. The back of the beach and the cliff areas surrounding the beach site were classed as a blanking region to prevent cliff instability into the system.

6.2.3 Sediment Transport

One of the key aspects of XBeach is the morphological updating which is a primary component of the model development. A depth-averaged advection-diffusion equation to solve suspended transport is used (Reiners *et al*. (2004), in Roelvink *et al*. (2010)), while the equilibrium sediment concentration is computed using the Soulsby-van Rijn formulation (Soulsby, 1997). The model also allows for multiple sediment fractions and hard structures. However, this approach can also be computationally slow for large-

scale runs. Within XBeach the "*morfac"* parameter can be used to accelerate the timescale relative to the hydrodynamic timescale. As will be discussed further, following preliminary runs and to maintain accuracy with regard to morphological updating *morfac* was set to 2–4.

6.3 XBeach Calibration

XBeach has been extensively validated for sandy beaches through both field and lab experiments (Roelvink et al., 2009), which has resulted in a set of default values used. A two stage process of model setup was undertaken; firstly calibration, where the default values were adjusted to produce a realistic response compared with field data; secondly validation, using the final settings on further field data to test the model performance. Model calibration was undertaken using the PX1 dataset presented in Chapter 5. A period of relatively calm conditions over 7 days (Figure 6.3) was used to test the stability of the model, the computational efficiency, the different *morfac* parameters and the wave input structure. An example of the complete input file (*params.txt*) is given in Appendix 6.1.

Quantitative 2D assessment of the model performance was undertaken using the *Brier Skill Score* (Sutherland, Peet & Soulsby, 2004)

$$BSS = 1 - \frac{\sum_{i=1}^{N}(dz_{b_i meas_i} - dz_{b_i xb_i})^2}{\sum_{i=1}^{n}(dz_{b_i meas_i})^2} \qquad 6.1$$

where N is the number of grid locations, and $dz_{b,\,meas}$ and $dz_{b,\,xb}$ are the measured and model-predicted bed-level change at location i, respectively. A skill value of one indicates perfect model performance; a value of zero is the same as predicting no bathymetry change; and a negative value is worse than predicting no change. Owing to

the limited survey coverage, subtidal change was not measurable and therefore the skill computations were undertaken for the intertidal region, ignoring the alongshore extension of the model domain. While the detailed measured surface change plots are presented here, skill score analysis was undertaken using surface plots interpolated onto the model grid to facilitate direct comparison.

With comparative nearshore wave and current data, as well as intertidal morphology available (Chapter 5), the period provides an ideal assessment of the model performance for a range of user defined settings.

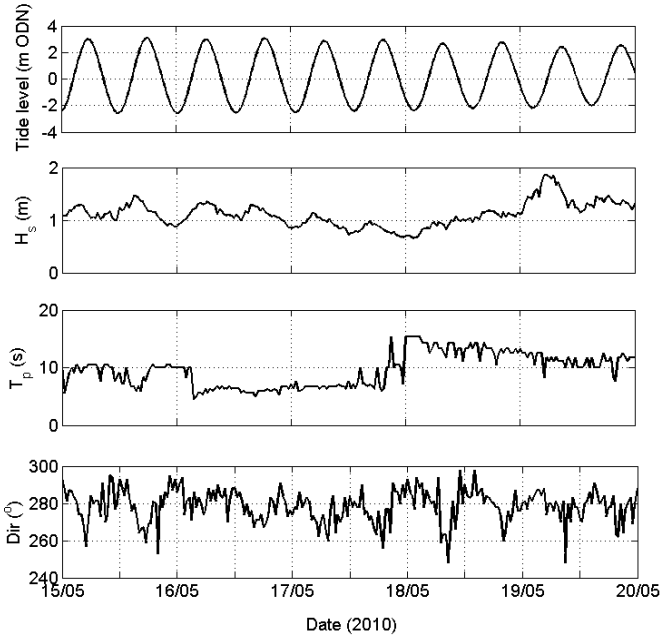

Figure 6.3– Measured hydrodynamic conditions during PX1, from the top to bottom: tidal elevation (m), significant wave height (m), peak wave period (sec) and wave direction (^{o}).

Initially, default settings were used for preliminary runs to assess the model stability – further discussion on model performance is given in Section 6.6. Early tests identified substantial flattening of the upper profile and excessive erosion dominated the intertidal response under relatively calm conditions. To reduce the level of erosion observed in the upper beach changes in the amount of wave asymmetry were made through the

facua parameter.Table 6.1 provides an overview of the common settings and any adjustments made through the calibration runs.

Table 6.1 – The main parameters and their settings used. Parameters not listed are set to default with complete details in Appendix 2.

Parameter	**Value (bold = optimum)**	**Parameter**	**Value (bold = optimum)**
nx,ny	77,54	tideloc	1
vardx	1	dtbc	4
xori, yori	0,0	wavint	5
Alfa	0	sprdthr	0.08
posdwn	-1	taper	100
thetamax, thetamin	27.5°,-27.5°	C (Chezy)	**50**,55,60
dtheta	5°	Nuh	0.15
break	3	CFL	0.7
instat	41	smag	1
facua	0.1, **0.2**, 0.3, 0.5	gamma	0.55
Rho	1025 kg/m^3	gammax	2
G	9.81 m/s^2	D50	0.00035m
Struct	1	D90	0.00050m
Morfac	2, **4,** 6,	rhos	2650 kg/m^3

Comparison of the nearshore wave height, cross-shore flows (*u*) and longshore flows (*v)* was undertaken with the co-located measured hydrodynamics during PX1 (Figure 6.4). Overall there is reasonable agreement between the measured and modelled results. Comparison of the modelled wave height is good albeit with XBeach values generally under-predicting the measured heights by ca.16%. Cross-shore flows share a similar overall shape through the tidal cycle; however, the strong onshore flows predicted for shallow conditions contrasted with the measured flows and strong onshore flows are also predicted under high tide whereas only weak onshore flows were measured (Figure 6.4). Longshore flows show the greatest variability with much stronger flows predicted than those measured and the presence of strong southerly flows (positive) which were not recorded in the field data (Figure 6.4). Longshore flows became increasingly noisy

as wave heights increased with strong fluctuations in flow direction and speed not present in the measured values.

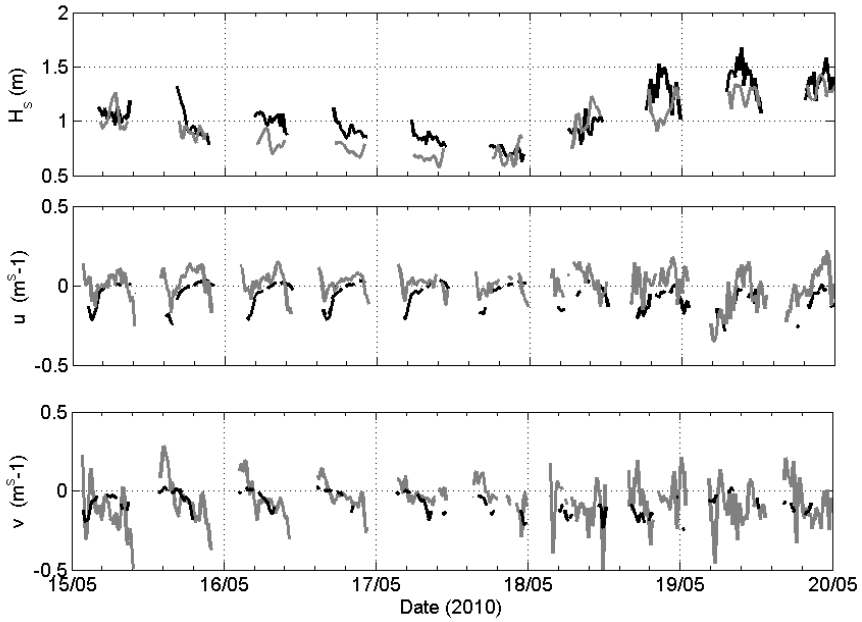

Figure 6.4– Comparison of co-located field measurements and XBeach output used for calibration, from top to bottom: wave height (BSS =0.92), cross-shore velocity (BSS = 0.33) and longshore velocity (BSS = -0.43). Black lines are field measurements; grey lines are XBeach output values. Gaps in data occur where water levels were too low for accurate measurements to be taken.

The generation of strong longshore flows was an early cause of model instability during initial runs, which was improved by defining the lateral boundaries as walls and increasing the model domain with a uniform bathymetry; however, for periods of more than 1 week unrealistic circulation patterns develop. While there are clear differences in the exact values between the measured hydrodynamics and the XBeach generated flows, the overall representation is reasonable.

Because of the restricted detail in the nearshore bathymetry, comparative analysis of the morphological response is provided for the intertidal region only (Figure 6.5). The main morphological response observed during PX1 was the development of a berm in the upper beach, infilling of channels coming off both headlands and onshore migration of the low tide bar (Figure 6.5, left panel). The morphological response generated by XBeach shows good qualitative agreement with the measurements, in particular the

infilling of the headland channels and the low tide channel are well represented. However, the response evident at the upper beach is less consistent with the measured morphology: XBeach predicted erosion in the upper profile with material deposited just below MHW, resulting in a flattening of the profile. This flattening response was also observed by Orzech *et al.*(2011), and became a focal area of disparity between model output and measured response. Quantitative assessment of the model performance gave a skill score of 0.63, which indicates the model is performing well. However, interpretation of the model output needs to be undertaken subjectively, and following numerous runs it became clear that the complexities of the steep cliff backed lower beach resulted in "edge effects", characterised by unrealistic surface change, despite the use of blanking files to restrict updating in these regions (Figure 6.5).

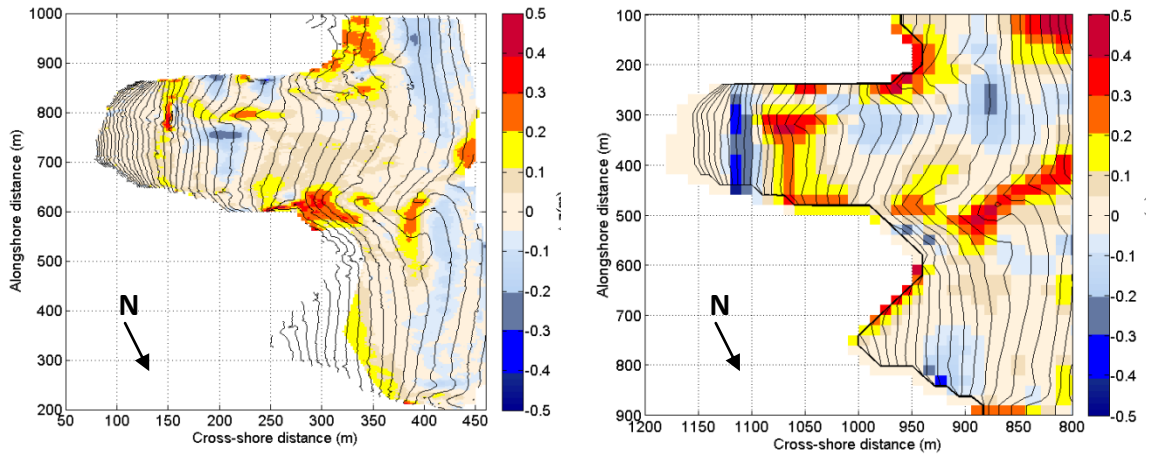

Figure 6.5– Surface change plots during PX1 with the left panel showing observed morphological change from RTK-GPS surveys and the right panel showing the XBeach predicted morphological change for the same period. Black contour lines show the initial morphology at 0.25-m intervals. Good agreement is evident in the lower beach and the in-filled channels off the headland; however, the flattening of the upper beach was not measured in the field (BSS = 0.63).

6.4 XBeach Validation

Following calibration of XBeach using conditions experienced during PX1, validation of the model was undertaken using two periods of measured change. The first was a sustained energetic period during the last week of PX2 when widespread offshore

transport occurred and both nearshore hydrodynamics and morphology were measured, the second was a brief intense storm event during October 2009, during which berm removal was observed in the upper beach.

Summary wave conditions during PX1 highlight a significant change in wave size from H_s= <1 m to a peak of H_s= 3.8 m; the peak wave period also increased from a low of 10 sec to 16sec at the storm climax, while wave approach remained steady throughout (Figure 6.6). Tidal conditions moved from neaps with a range of ca.3 m to springs with a range of ca.5 m (Figure 6.6).

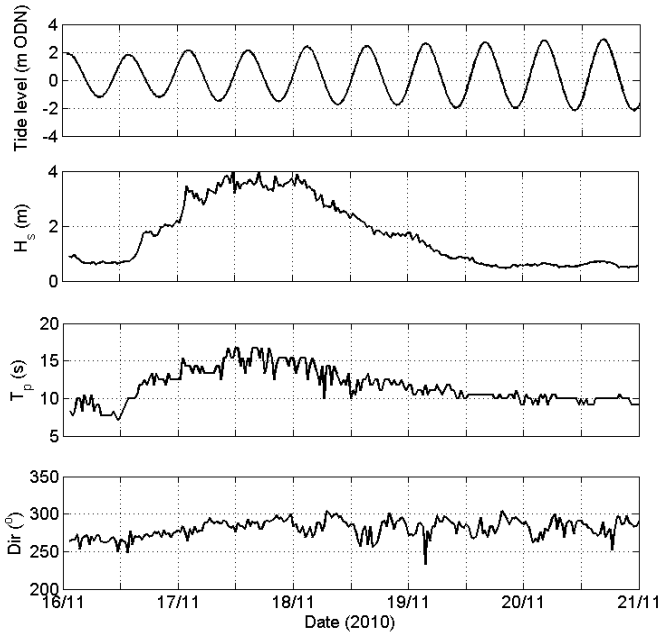

Figure 6.6– Measured hydrodynamic conditions during PX2; from the top, tidal elevation (m); significant wave height (m), peak wave period (sec), and wave direction (^{o}).

Comparison of the measured wave conditions (located at LWS) and currents with the XBeach simulated output is presented in Figure 6.7. Again, good overall agreement is observed with regards to the nearshore wave height; however, there is over-prediction during energetic conditions and under-prediction during calm waves at the end of the survey period (Figure 6.7). Cross-shore flows exhibit good agreement with the measured values under energetic conditions (both predicted and observed flows peaking

around 0.5 m s^{-1}); however, under calm waves the predicted flows become onshore-directed which differs significantly from the measured values. Longshore flows show the weakest conformity with the measured flow rates: large fluctuations under energetic waves are predicted, while strongly southern (positive) flows are predicted under small waves, both contrasting with the negligible measured longshore flows (Figure 6.7).

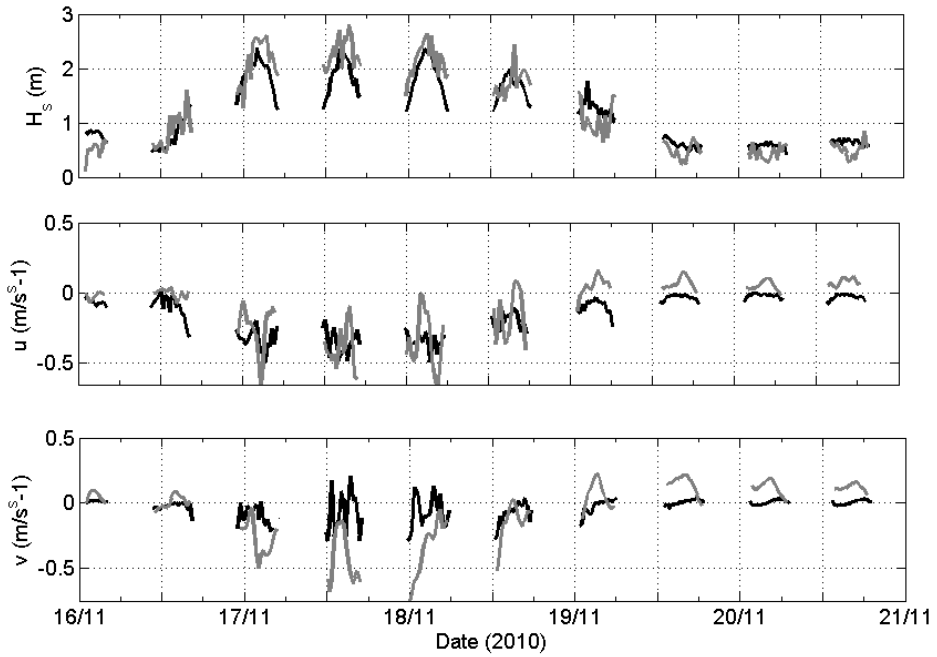

Figure 6.7– Comparison of co-located field measurements and XBeach output used for validation, from top to bottom: wave height (BSS = 0.91), cross-shore velocity (BSS = 0.60) and longshore velocity (BSS = 0.22). Black lines are field measurements; grey lines are XBeach output values. Gaps in data occur where water levels were too low for accurate measurements to be taken.

In line with the assessment of the morphological response observed during the model calibration, comparison of morphological change is undertaken for the intertidal region alone and restricted in the longshore direction by the survey coverage during PX2 (Figure 6.8). Morphological response during PX2 was characterised by widespread erosion (Chapter 5), with removal of material across much of the beach face. Small accretionary areas are present at the upper beach in response to the calm conditions during the final few days of the survey period (Figure 6.8; left panel). XBeach shows good overall agreement with the measured response with regions of sand removal

across the low tide region well represented. Again, XBeach generates excessive erosion in the upper beach and flattening of the upper profile, and this is the main cause of the negative (-0.82) BSS skill score.

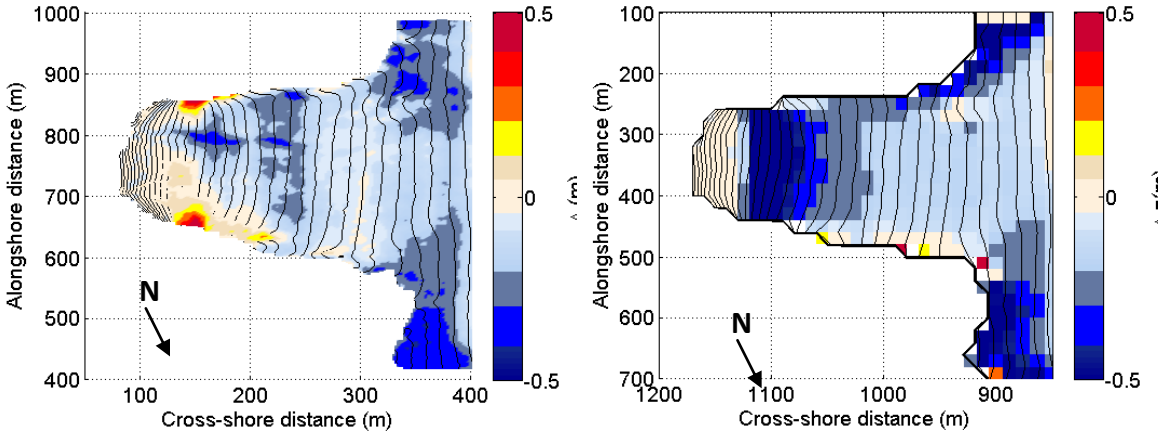

Figure 6.8– Surface change plots during PX2with the left panel showing observed morphological change from RTK-GPS surveys and the right panel showing the XBeach predicted morphological change for the same period. Black contour lines show the initial morphology at 0.25-m intervals. Good agreement is evident in the mid and lower beach where material has been removed; however, the large change in the upper beach was not measured in the field (BSS-0.82).

The second event which was used for model validation occurred in October 2009 and was characterised by a rapid increase in the significant wave height from H_s = 0.75 m to H_s= 3.76 m and a corresponding increase in the peak wave period from T_p= 10 s to T_p = 18.2s over 6 hours (Figure 6.9). The morphological surveys prior to this event identified a well-defined berm which had formed in response to the calm conditions which dominated for the preceding 7 days. This berm was rapidly removed following the increased waves, with deposition occurring in the lower upper beach and below MSL, resulting in flattening of the beach profile (Figure 6.10, left panel).

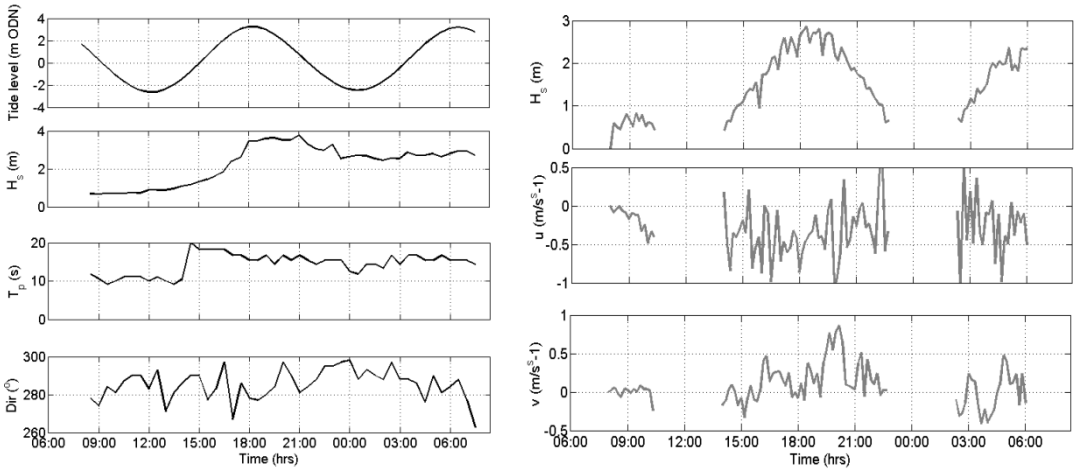

Figure 6.9 – Hydrodynamics for the October 2009 event with the left panel showing the measured hydrodynamics; from the top, tidal elevation; significant wave height (m), peak wave period (sec), and wave direction (^{o}). The right panel shows the XBeach derived nearshore flows; from the top, wave height(m), cross-shore velocity (m s^{-1}) and longshore velocity (m s^{-1}).Gaps in data occur where water levels were too low for accurate measurements to be taken.

Nearshore flow rates were not measured for this event and it was therefore not possible to compare the hydrodynamics generated by XBeach with *in-situ* values. The predicted morphological response shows good overall agreement with the observations (Figure 6.10). While there is less accretion evident across the full low tide region, deposition is evident around the southern headland as observed in the surveys. The upper beach shows much stronger agreement with removal of the berm and deposition at a similar location (Figure 6.10; right panel). However, despite the good qualitative agreement, the BBS is negative (-1.23), and this is attributed to disagreement of the exact position of the erosion and deposition in the upper beach and the lack of deposition in the low tide region.

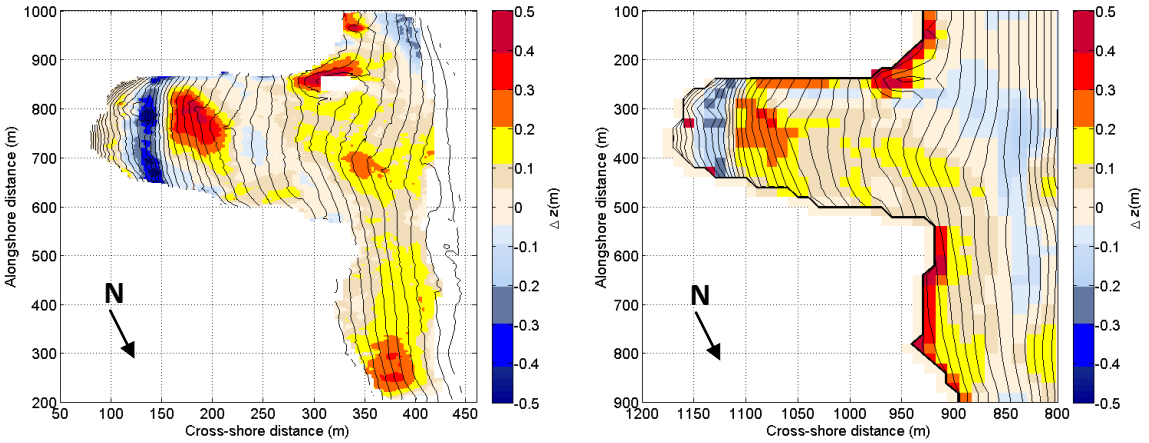

Figure 6.10– Surface change plots during the storm event in October 2009with the left panel showing observed morphological change from RTK-GPS surveys and the right panel showing the XBeach predicted morphological change for the same period. Black contour lines show the initial morphology at 0.25-m intervals. Qualitative comparison suggests overall the performance is good particularly for the upper beach (BSS -1.23). The blank square at x=300, y=860 on the measured morphology reflects rock outcrops in this region.

6.5 Application of XBeach to 3D morphology

Following validation of the model with reasonable success, the primary objective of applying XBeach to the complex morphology present at PTN is to try to simulate and replicate the observations and trends associated with storm events, onshore migration and 3D growth which have been identified in Chapter 4. Under energetic conditions, smoothing of 3D morphology was evident as material was moved offshore, while post storm recovery resulted in re-development of low tide bar/rip systems. Under sustained calm conditions onshore accretion was evident leading to increased planar states.

As discussed previously, longer term (>1 week) runs within XBeach became unstable as unrealistic flows developed, while short-term more intense periods are well represented. Following on from the validation output and consideration of the model performance as outlined above, the range of possible scenarios to be modelled was limited to focus on the intertidal response. Building on the observations in Chapter 4, the following conditions were identified to further investigate the beach response;

- *Response to initial morphology, from highly 3D to strongly planar*
- *Response to variability in wave conditions (highly energetic/calm)*
- *Tidal impact on morphological response (spring/neap range)*

Through a combination of these conditions, the morphological response of the intertidal zone is assessed with respect to the measured responses observed.

The model domain was setup using 2 distinctive morphological states: (1) a highly planar beach face and nearshore bathymetry ($\overline{CV}$ = 1.071); and (2) a highly 3D low tide region with a subtidal nearshore crescentic bar system ($\overline{CV} = 1.251$; Figure 6.11). These were generated using original intertidal survey data merged with available bathymetric surveys and smoothed accordingly.

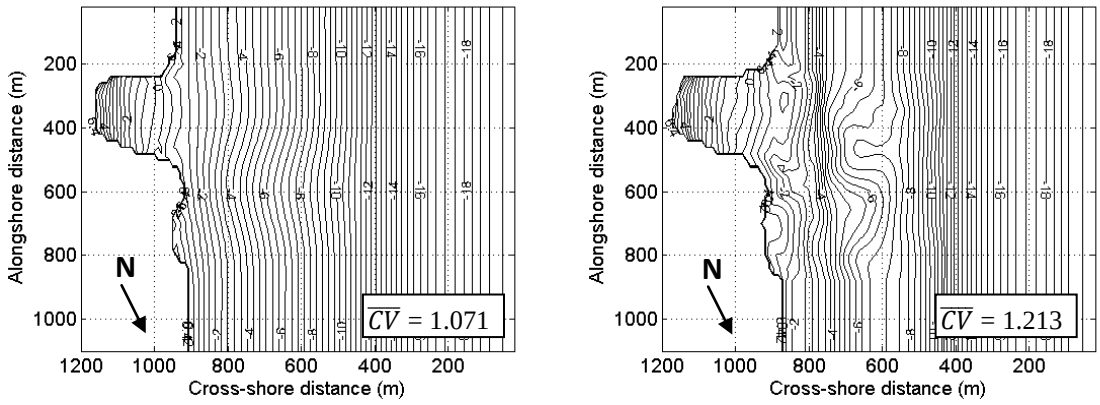

Figure 6.11 – Initial bathymetry for the model runs with left panel showing a highly planar profile and the right panelshowing a strongly 3D morphology. Both domains are generated form original survey data and merged with existing available bathymetry. The $\overline{CV}$ for each intertidal morphology is shown.

Model runs were undertaken for a 72 hr duration based on the morphological responses observed in Chapter 4. The different wave and tide conditions for the energetic/calm and neap/spring scenarios are presented in Figure 6.12. Wave approach was kept constant for both sets. For computational efficiency wave parameters were updated every 6hrs and tide data was provided at 0.5hr intervals, although XBeach interpolates onto the model time-step which is a function of the grid spacing, the water depth and the non-dimensional *CFL* parameter which was set to 0.7.

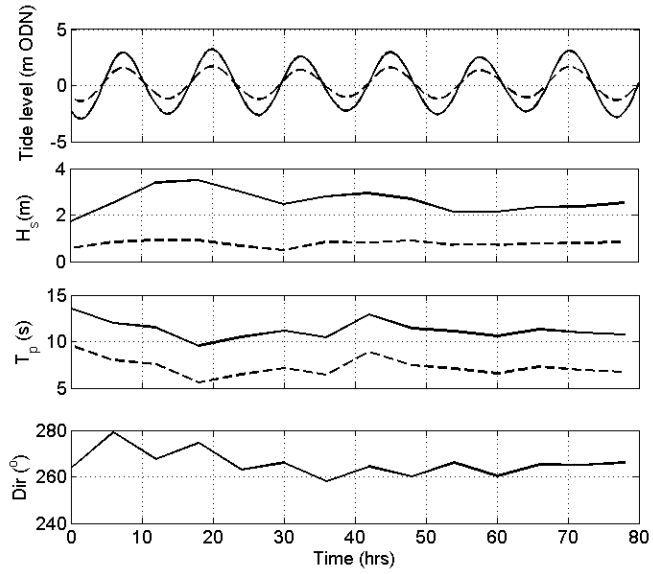

Figure 6.12 – Summary hydrodynamic conditions used for the model runs, from top to bottom: tidal elevation for springs (solid line) and neaps (dashed line); significant wave height H_s for energetic waves (solid line) and calm waves (dashed line); peak wave period T_p for energetic conditions (solid line) and calm conditions (dashed line); and wave direction *Dir*.

Assessment of the morphological response was confined to the intertidal region throughout the analysis presented. Whilst change was observed in the subtidal areas a lack of measured response from field data and the reliance on interpolated bathymetry meant discussions on any observations would be limited.

6.6 Model Results

Where the initial beach face was highly planar, under energetic conditions for both spring and neap tidal conditions, low tide deposition resulted in increased smoothing, characterised by reduced $\overline{CV}$ values of 0.05 and 0.06 respectively (Table 6.2). Overall, a net loss of material was experienced, with a slightly higher loss under spring tides. Under calm conditions, XBeach predicted a modest flattening of the profile with low

tide deposition and some loss of the upper beach, and resulted in reduced $\overline{CV}$ values by 0.04 and 0.03 under neap and spring tides, respectively (Figure 6.13).

Table 6.2 – Summary table of quantitative analysis of the morphological response during XBeach model runs

Run Set-up	Decrease Net (m^3)	Increase Net (m^3)	Net Volume change (m^3)	Initial $\overline{CV}$	Final $\overline{CV}$	$\overline{dCV}$
Planar-Neap-Energetic	-14087	9985	-4102	1.071	1.009	0.063
Planar-Spring-Energetic	-14794	10082	-4712	1.071	1.014	0.057
Planar-Neap-Calm	-4507	3607	-900	1.071	1.031	0.040
Planar-Spring-Calm	-4478	4562	85	1.071	1.040	0.031
3D-Neap-Energetic	-48181	14001	-34181	1.213	1.036	0.177
3D-Spring-Energetic	-61991	9015	-52976	1.213	1.082	0.131
3D-Neap-Calm	-10766	10172	-594	1.213	1.145	0.068
3D-Spring-Calm	-9264	9457	193.5	1.213	1.169	0.043

Under neap conditions there was a small net loss of material, while for the spring settings a net increase in intertidal sediment volume occurred (Table 6.2). Under initial 3D morphology exposed to energetic conditions, the morphological response centred on infilling of the low tide channels and smoothing of the bar systems.

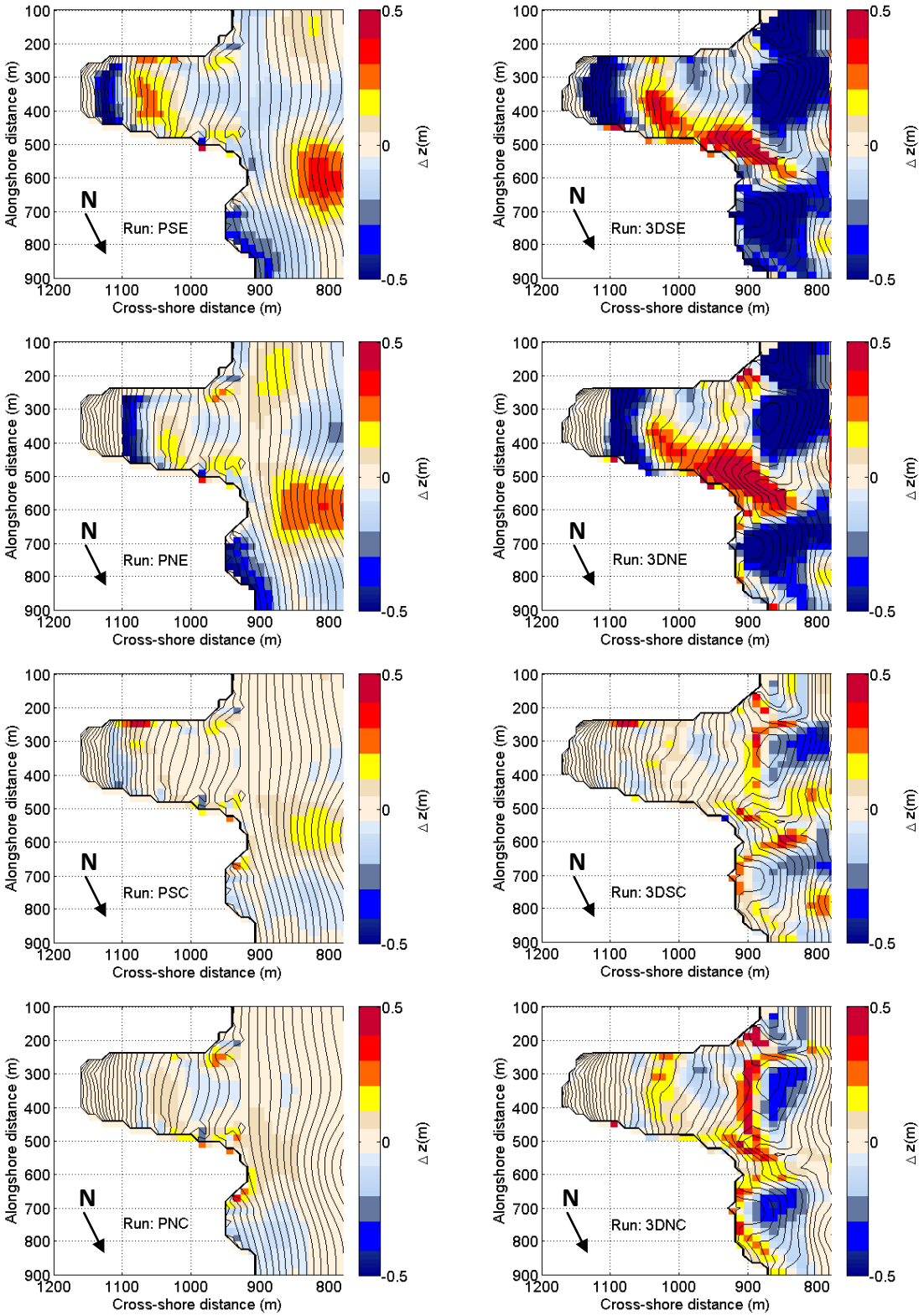

Figure 6.13 – XBeach generated output of morphological response under varying tide and wave conditions; combinations of P = planar, 3D = 3D, E = energetic, C = calm, N = neap and S = springs. Red shading = accretion, blue = erosion. The contour lines show the original morphology at the start of each model run.

For both spring and neap tides the $\overline{CV}$ reduced by 0.13 and 0.17, respectively, and the net loss was largest under spring conditions (Table 6.2). Under calm conditions, the morphological response was similarly dominated by infilling of the channels and

smoothing of the low tide region. Net loss of material occurred under neap conditions compared with a small net increase under spring tides (Figure 6.13).Building on the observations of XBeach morphological updating during model calibration and validation, for all energetic model scenarios flattening of the upper profile was observed through removal of material from the top of the beach and deposition in the mid beach (Figure 6.13).

6.7 Discussion

Quantitative assessment of model performance during validation showed reasonable agreement between nearshore wave heights and cross-shore flows; however, in all cases the longshore flows showed the weakest agreement with the measured values. Subsequently, as the morphological response is driven by the modelled hydrodynamics it is reasonable to expect that the predicted behaviour of the morphology differs from the observations, resulting in the reduced BBS values (Orzech *et al.*, 2011). While the quantitative agreement was lower than in previous XBeach applications (McCall *et al.*, 2010), qualitative evaluation of the overall response patterns was in line with the measured change and as such provides a sufficient level of confidence for qualitative assessment of the model scenarios. As discussed in the model validation and results, excessive erosion of the upper beach face was a dominant feature in model behaviour, and is likely to be a key cause of the low skill scores presented.

The primary response observed under each of the model scenarios is removal of morphological features and flattening of the existing profile. The extent of these processes is driven by: (1) the wave forcing with more energetic conditions mobilising greater amounts of sand; (2) the tidal range with larger range resulting in increased redistribution; and (3) the initial $\overline{CV}$ which dictates the level of erosion and infilling

observed. With an initial planar beach under energetic waves only small levels of smoothing were evident, with slight infilling of the rhythmic shoreline to the north of the survey area; however, under identical wave conditions the 3D beach experienced widespread redistribution of material as sediment transport resulted in removal of the intertidal bars and infilling of the channels to create a smooth beach face. Both of these responses support observations under similar storm conditions outlined in Chapter 4. Less consistent with the field observations is the response under calm conditions which exhibited net loss of material under neap and 3D scenarios, while net accretion was observed under planar and 3D spring conditions. Field surveys during PX1 saw sustained accretionary conditions under relatively calm conditions, with onshore migration of a low amplitude bar. While the infilling of the channels present in Figure 6.13, is in keeping with accretionary phase development observed at PTN, the extent of erosion present on the bars is much higher than expected, casting doubt on the model reliance under calm wave conditions.

The variability in the low tide smoothing under spring and neap conditions is also of note. For all scenarios, neap conditions resulted in a greater level of smoothing than under identical conditions with a spring tidal range. While the differences are small, consistency in the results highlights the importance of tidal range on the morphological response through the relative position of the surf zone. In field surveys a short period of medium waves during neap tides resulted in the development of highly 3D morphology (Chapter 4), from a previously rhythmic beach face; contrasting strongly with the model output.

The complex physical processes present in up-rush and backwash related transport found in the swash zone are poorly understood and a focus of more recent field studies (Austin et al., 2011; Masselink & Puleo, 2006; Miles, Butt & Russell, 2006). As such,

the ability to accurately represent these dynamics in a modelled environment as yet has not been achieved. It is therefore reasonable to suggest the excessive erosion present at the top of the beach and the lack of sustained accretion under calm conditions are a reflection on an under estimation of swash zone up-rush transport relative to the offshore-directed transport through backwash (Orzech *et al.*, 2011). Because of this, the model favours the more erosive storm-driven conditions where offshore removal is widespread and infilling of the low tide channels is observed, whereas onshore accretionary phases are poorly reproduced. While onshore flows were generated, which might suggest onshore transport should be better represented, these are depth-averaged values and so the strength of the bed return flows are not clear, unlike the field measurements.

Apart from recent work by Orzech *et al.* (2011), which has used XBeach to look at megacusps and rip currents, current applications of XBeach to macro-tidal energetic sites with a focus on the low tide morphology are not currently published. It is therefore hard to consider the present model performance with comparable studies. Our understanding of the complex processes of low tide bar/rip systems is a relatively young field; the ability to model such dynamics is younger still. Recent work on wave by wave swash analysis (Blenkinsopp et al., 2011; Turner, Russell & Butt, 2008) provides more understanding of the individual wave contributions to bed level change, yet implementation of these observations into XBeach would require parameterisation to fit with the wave-group approach adopted in XBeach.

6.8 Model Performance

It has not been the intention of this chapter to further develop or adapt the XBeach model; it has been assessed for its performance applied to 3D beach states and as a tool

in which the response of the intertidal morphology under varying forcing conditions can be explored. While the model performs reasonably well under short-term intensive periods, its application for longer-term response is limited and as such the analysis presented here has been restricted to relatively short episodes of wave forcing. Early investigations with comparison of monthly survey data identified the computationally slow and stability problems which prevented such an approach. However, a principal restriction on the model is through a lack of relevant nearshore bathymetry specific to individual scenarios. The distribution of wave breaking and subsequent generation of nearshore currents which drive sediment transport and the resulting bed updating is reliant on the bathymetry. With a highly dynamic system the complex nearshore bar system plays a crucial role in the morphological response under varying wave conditions; subsequently, in the absence of up-to-date bathymetry care has to be taken on the interpretation of model response.

Unlike previous applications of XBeach (McCall *et al.*, 2010; Orzech *et al.*, 2011), PTN is characterised by complex 3D morphologyand is backed by steep non-erosive cliffs which extend down to MLWN either side of the main beach face. The presence of these geological features is likely to be responsible for the high levels of surface change which were observed, in contrast to neighbouring cells. While these features have been shown to be controlling forces on the location and presence of rip channels (Chapter 4), it is evident further work is required for XBeach to handle flow behaviour within these regions.

6.9 Conclusions

To assess the development and stability of low tide 3D morphology at an intermediate bar/rip beach (PTN) the 2DH numerical model XBeach has been used to build on previous measured results by modelling the complex low tide morphology behaviour under a range of hydrodynamic and morphodynamic states. Using measured nearshore wave and flow conditions obtained during PX1 and representative nearshore bathymetry collected in July 2008, combined with the intertidal morphology, XBeach was calibrated through small adjustments of the input settings specifically *facua* and *C*. Validation of the model was undertaken for short (1 day) and medium length (7 day) periods and resulted in overall reasonable performance for the low tide region; however, the overall skills score for the full intertidal area was negative. Although the model hindcasts the low tide morphological response reasonably well, over-estimation of the swash-zone-induced offshore transport led to flattening of the upper profile and excessive erosion in this region - likely to be responsible for the low skill scores.

A series of eight model runs were designed to test the intertidal behaviour generated by the model in response to varying wave, tide and planar/3D morphology. Time-varying wave forcing was provided for a 72hr period with conditions updated every 6hr, tidal levels differed between neap and spring ranges, while the initial morphology was generated from measured planar and bar/rip morphology interpolated onto the available bathymetry. Initial morphology which was highly 3D, and exposed to energetic waves resulted in the greatest redistribution and net removal of material from the beach face as the beach moved towards a more planar beach state. While the overall trend presented supports measured behaviour under similar conditions, the extent and rate of change exceeds any observed response. Changes in the tidal range resulted in greater loss during spring tides – a reflection of the upper beach erosion which dominated this

region, while neap tides resulted in greater smoothing. Initial planar conditions also experienced a net loss of material and further smoothing of the beach face. Under calm conditions both 3D and planar beaches experienced infilling of channels and headland scour holes respectively; however, this appears to be attributed to smoothing of the beach face as opposed to onshore accretion.

PTN presents a complex morphological site with significant geological constraints through dominant headlands which shape the beach. XBeach has proved it is able to work reasonably well under medium (<7days) to short (<1 day) periods, especially under storm-like conditions. However, as an energetic site, the sustained removal of material forecast by XBeach does not reflect the real equilibrium of this site.

Future application to further address the complex morphodynamics associated with intermediate beaches would benefit from improved nearshore bathymetry which is likely to be the focal weak component of this present study. Such data are difficult and expensive to obtain; however, the variability in the nearshore bar system further necessitates regular data capture from this region. The handling of swash zone based transport is also a key aspect which deserves greater attention and will greatly improve the overall model performance.

7 SYNTHESIS AND CONCLUSIONS

This chapter will provide a summary of the discussions explored in the separate chapters and brings together the different components which have structured the thesis with summary results. This is followed by the overall conclusions of the thesis.

7.1 Discussion Summary

7.1.1 Inter-site Comparisons

Between February 2008 and December 2010 monthly topographic surveys were undertaken at four sites located on the north Cornish coast: Perranporth (PPT), Chapel Porth (CHP), Porthtowan (PTN) and Gwithian (GWT). Located within a 23 km stretch of coastline, the sites were exposed to similar wave and tide climates throughout the survey period. The following section compares and contrasts the different morphological responses and identifies the main trends observed at each site.

The survey area at GWT represented ca.14% of the much larger bay system which undoubtedly affected its low tide dynamics (Figure 7.1). Sheltered from northerly swells by a rocky headland, which also created a non-uniform bathymetry, the nearshore wave climate was less energetic than the other sites. The low tide morphology was characterised by a single low-amplitude bar which increased in longshore size towards the south through the survey area, from the Red River outflow, becoming more subdued over a period of months on three occasions under calm wave conditions. The exposed rock within the survey area exhibited localised scour, but had no discernable impact on the overall morphology response (Figure 7.1).

Figure 7.1 – Panoramic photographs of Gwithian; a) St Ives Bay with the location of GWT highlighted; and (b) a more detailed view of the full survey area.

The two central sites of PTN and CHP underwent similar behaviour to each other which reflects their proximity within the same headland-confined system. Periods of high rhythmicity in the low tide morphology were observed which further supports the coherence in morphodynamic response seen at both sites (Figure 7.2b).Over three separate phases the development of deep channels, incising low tide bars, was observed following large waves (H_s = >4 m) before gradual migration of the channels (to the north) and infilling occurred over a period of two-three months as wave conditions decreased (H_s = ~1.6 m).

The defining characteristic of the beaches at PTN and CHP is the presence of intertidal geology that dominates the low tide region. Backed by steep cliffs with medium-small pocket beaches exposed above MSL they exhibited the most dynamic morphology of all the sites; however, it is difficult to quantify the extent to which these factors are responsible for the generation and stability of the bar/rip morphology which was present. Although more chaotic shoreline and subtidal bar shapes were sometimes evident (Figure 7.2a), which might be attributed to the interruption of the intertidal geology by the beaches at PTN and CHP, the sustained periods of highly rhythmic shoreline and crescentic bars complicates this assessment (Figure 7.2; Backstrom, Jackson & Cooper,

2009; Enjalbert *et al.*, 2011). While the importance of geology in determining beach states and rip behaviour has been identified within recent studies (Enjalbert *et al.*, 2011; Scott, Masselink & Russell, 2011), there remains a paucity of research focused on the role of geology in influencing morphology. It is difficult to quantify geological control and it has not been the focus of this thesis; however, there is a clear demand for further comparative studies.

Figure 7.2 – Panoramic photographs of the headland confined bay where PTN and CHP are located. Photo a) shows a highly 3D low tide region at CHP compared with the less dynamic southern end, while photo b) gives an example of a highly rhythmic bay wide system connecting the two sites.

Similar observations are true for PPT which experienced corresponding levels of three dimensional (3D) growth and decay through low tide bar and rips. While definite cyclicity in the morphological response was less evident, greater variability was observed in the low tide morphology moving north through the survey area in the narrower section of the beach (Figure 7.3).

Figure 7.3 – Panoramic photograph of PPT showing the reduced beach width backed by cliffs to the north of the survey area (dashed line)

Ranging from highly dissipative to intermediate the exposure to the same wave climate is reflected by the similarities in the site-specific morphological responses outlined above; the overall trends from the sites are explored in the following section. The most immediate difference from the survey data is the variability between the subtidal and the more responsive intertidal areas. While it could be argued that the survey technique may add bias towards smaller changes in the intertidal region through more detailed regular surveys, the tide-induced cross-shore translation of the surfzone results in highly varied hydrodynamics acting across the beachface unlike the more consistent conditions for the subtidal. However, the importance of the immediate subtidal region, which acts as a sediment sink during periods of erosive conditions, was difficult to assess fully using Argus images which only provide a proxy for subtidal morphology through wave breaking. The rate of change is also a defining component of any system. Much of the work which has been done on Australian beaches has observed rapid re-setting of bar morphology under storm events followed by a return to pre-storm states over a period of days(Smit *et al.*, 2008b). For all Cornish sites similarly rapid changes in upper beach morphology (berm removal) was evident under storm conditions (October 2009); however, the system did not re-set back to pre-storm states in the same manner. Instead, a more gradual recovery occurred often resulting in changes to the low tide region. Attempts to establish a clear link with the wave forcing and the morphological response through partitioning of the wave spectrum and assessment of wave groupiness, were

confounded, in part, by the large relaxation times present due to the macrotidal range. While specific examples of the spring/neap tidal influence were not identified due to the reasons above, the importance of the tidal stage on the morphology is clear, with nearshore processes varying in response to tidal translation across the beach face. These results further highlight the significance of the antecedent bars which prescribe and feedback to the wave breaking, sediment transport and morphodynamic evolution.

7.1.2 Storm Response

At each site, accretion was observed over three years characterised by an increase in the net intertidal beach volume. The overall upward trend in beach volume was punctuated by periodic drops driven by sustained storm conditions (peak H_s = > 4 m, for > 50 hours) during more energetic winter months. Although a longer database would be needed to identify the significance of the drop in storm conditions in 2010, our dataset highlights the importance of storms in driving beach change and, as will be discussed further, the role of post-storm recovery in determining the morphological state. Hindcast wave records (Dodet, Bertin & Taborda, 2010), analysed for storm occurrence, display 15-20 year cyclicity in storm events overlain by a gradual increase in individual storm duration. The present survey period appears to fall in a stage of reduced storm events; in particular 2010 was notably calmer than the preceding two years, and this seems to be reflected in the more subdued morphological responses observed.

At PTN, CHP and PPT beach state transitions were focused between *planar*, *low tide rhythmic*, *rhythmic with channels* and *low tide bar/rip*. While there was no seasonal pattern in the morphology, a strong relationship between storm events and morphological response was present. Under storm conditions (as documented for the PX2 field experiment), strong offshore-directed flows were recorded resulting in the

significant bed level changes that occurred. Following the majority of storm events, the post-storm recovery led to the development of highly 3D low tide morphology at PTN, CHP and PPT. Where pre-storm morphology was 3D this became more subdued following offshore transport under storm conditions; however, subsequent post-storm onshore transport led to highly 3D morphology. Where the pre-storm conditions were more 2D the post-storm build up was not as extensive. This trend highlights the importance of the antecedent conditions in affecting both the removal of material and the subsequent deposition caused by alongshore variability in wave breaking and the subsequent generation of nearshore currents which drive sediment transport. While the onshore transport, and subsequent 3D increase, is believed to be primarily undertaken during the recovery phase, it is possible material from the bar connects with the shoreline during the storm conditions as suggested by Almar *et al*. (2010).

XBeach storm simulations reproduced offshore transport flows and sediment removal well; however, post-storm 3D morphological build up was not well reproduced by the model. The extent of 3D recovery is also dependant on the extent of pre-storm 3D features and their stability under storm action. If the beach face remains sufficiently 3D, under suitable accretionary post-storm swell dominated waves, increased development of these features is often observed.

While the small swell dominated recovery phase leads to a growth in the 3D morphology, continued onshore transport and mixed energy waves results in gradual smoothing of the low tide bars, in-filling of channels and a decrease in the 3D nature of the beach. Although mean nearshore flows in the surf zone remained predominantly directed offshore (as documented for the PX1 field experiment), the small swell waves result in a narrow surf zone and so the onshore transport caused by shoaling waves dominates the nearshore zone, and possibly low-energy surf zone bores. The complex

processes which surround onshore transport and the redistribution of material across the beach face are still poorly understood and subsequently difficult to model numerically (Chapter 6). Incorporation of flow velocity skewness and flow acceleration in sediment transport formulae (Chapter 5) provides some support for the morphological response observed; however, they do not fully account for the measured accretion. Despite each of the sites being exposed to an energetic wave climate (mean H_s = 1.6m), the overall net accretion which is evident in the beach volumes and the X_{MCL} suggests onshore accretionary conditions are more widespread than erosive phases. With limited sediment inputs into the northern sites (PTN, CHP and PPT), the balance between onshore and offshore sources of material is relatively restricted; therefore, the stability of the system is dependent on the frequency and intensity of storm events.

It is clear that monthly surveys lack the temporal resolution for detailed storm assessments. Where resources are available and through alternative techniques (bathymetric measurements) the interval between surveys could be reduced, yet intertidal work will remain limited by the spring-neap cycle.

7.1.3 Subtidal Bar Response

Although it is not possible to quantify the sediment flux from the subtidal to the intertidal, and vice-versa, without detailed offshore surveys; the Argus images can provide a qualitative insight into the subtidal bar dynamics. As mentioned previously, under storm conditions material is deposited within the subtidal area which is then gradually returned to the intertidal under calmer post-storm conditions. Subtidal bar analysis is only possible where cameras are located, i.e. at PPT and PTN.

Bar shape at PTN showed the greatest variability over 2.3 years with transitions from *transverse, crescentic, multibar* and *longshore bar* all evident. Reflecting the intertidal

behaviour, there was little seasonal trend in the bar movement; however, unlike the intertidal region which exhibited greater variability in morphology, the nearshore bar remained far more stable over weeks-months. The cross-shore position of the bar showed a gradual offshore migration over the 2.3 year survey period; moving ca.40 m seaward, at a pace which matched the rate of change in the momentary coastline position (X_{MCL}).

Bar behaviour at PPT lacked a clear seasonal pattern; however, storm events caused sediment to move offshore towards the bar, partially affecting the landward edge of the bar shape, followed by post-storm accretion. The bar shape remained *attached-longshore crescentic* for the majority of the survey window, alternated by shorter periods of *multi/transverse bars* dominated by rip channels. The subtidal bar on PPT exhibited similar cross-shore migration moving steadily offshore with the X_{MCL} position as the net intertidal volume increased. For both PPT and PTN, the offshore position of the bars peaked at the start of 2010. This was followed by onshore migration during which the bars became more longshore parallel and in close proximity to the shoreline (Figure 7.4).

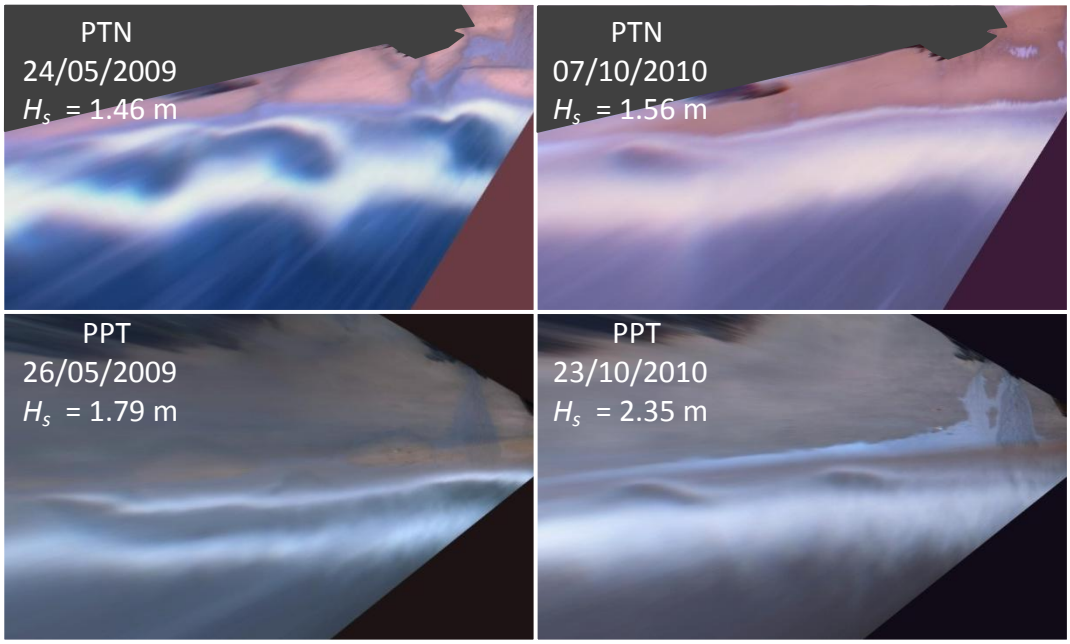

Figure 7.4 – Plan-view rectified Argus images of Porthtowan (top row) and Perranporth (bottom row) showing the change in nearshore bar shapes from the middle and end of the survey period.

Throughout the survey period the bars exhibited a range of bars types with *longshore cresecntic* predominant at both sites. While quantitative analysis of bar behaviour during storm conditions was not possible, the strong link between the intertidal and the subtidal under such conditions was apparent. Post-storm recovery was characterized by onshore transport from the subtidal resulting in highly 3D morphology in the low tide region. With the reduced number of storms in 2010 (74 hrs compared with 119 hrs and 229.5 hrs in 2008 and 2009, respectively) sustained accretion from the subtidal resulted in the decreased nearshore bar structure and growth in the net intertidal volume (Figure 7.4).

7.1.4 Morphological Results

The key morphological behaviour during the survey period reflects a strongly storm driven system which is governed by sustained high-energy events. Subsequent morphological response exhibited highly 3D recovery phases before seasonal wave conditions dominated further evolution.

Despite the inherent complexities governing the response at each of the sites, the overall behaviour has been well characterised by (Figure 7.5): (1) offshore transport occurring under sustained large waves, supporting previous field observations (Castelle et al., 2007b; Hill *et al.*, 2004; Larson & Kraus, 1994; Lee, Nicholls & Birkemeier, 1998); and (2) followed by increased 3D morphology not observed in the present literature. The gradual up-state evolution then returns and dominates resulting in the morphology becoming more 2D. This trend was observed at PTN, PPT and CHP three-four times during the survey period. The rapid post-storm 3D growth is likely to reflect non-uniform wave breaking of small swell dominated waves which promotes onshore transport. The antecedent morphology and the extent of the storm event determine the post storm low tide morphology, which in turn dictates subsequent onshore transport and deposition. Further key components discussed above include the low tide geology and the tidal stage.

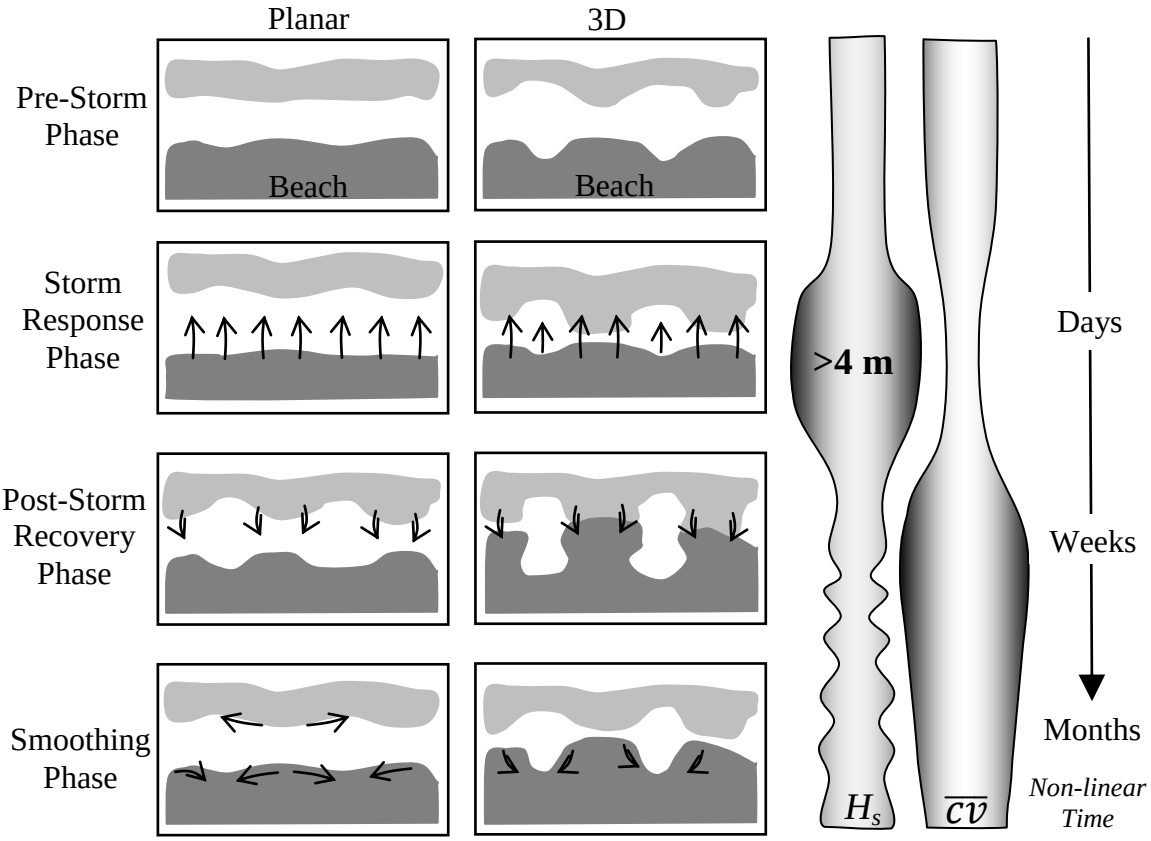

Figure 7.5 – Schematic diagram of the beach and bar response during and following a storm event. The cycle occurs over a period of two-three months following a sustained large storm, which sees material moved offshore to the subtidal bar (light shading) and returned to the intertidal (dark shading) region as the wave conditions decrease resulting in highly 3D morphology. The relative H_s and $\overline{cv}$ are indicated on the right with larger waves and increased 3D represented by wider columns. Anteceedent morphology (planar/3D) dictates the extent of morphological response during the storm event and under post storm recovery phases.

The delay to the Wave Hub deployment has allowed for continued monitoring under "normal" conditions, which has provided a greater understanding of the natural variability; however, this has also highlighted the need for greater spatial coverage to include the subtidal region. The unequivocal relationship between the intertidal and the subtidal has been explored within the previous chapters; further research would benefit from increased survey coverage, of the subtidal region, which would allow extended analysis of this relationship.

7.1.5 Hydrodynamics and XBeach

As datasets increase in temporal scope there is the opportunity to identify seasonal/annual relationships between the various components within a system. The importance of wave spectra has long been identified within coastal research. Through spectral partitioning the relative importance of swell or wind-dominated conditions has been examined. While a seasonal signal in the swell waves is present, linked with the more energetic storm conditions, the lack of a similar signal in the beach three dimensionality ($\overline{CV}$) suggests such a relationship is not as straightforward. Through more detailed analysis of specific upstate/downstate transitions, the importance of relative energy/swell conditions becomes more apparent with post-storm accretionary conditions associated with smaller swell-dominated phases (H_s=<1.5 m, T_p = >10 sec).

The response to varying tide levels is more difficult to quantify. Through intensive surveys and nearshore measurements of hydrodynamics, interpretation of the impact of tide range was not self-evident; however, as discussed above, due to relaxation time effects it is not possible to discern the spring-neap effects. The importance of the shifting surfzone and the subsequent non-stationarity of the nearshore processes acting on the bed have been discussed above; under neap conditions a reduced width of beach experiences longer exposure to these processes, which was supported by the XBeach simulations.

Throughout this thesis the role of timescales for individual components within the coastal system has become increasingly important in determining the subsequent response observed. The dataset has shown: (1) the rapid (hrs/days) response of the intertidal beach under storm conditions; (2) the short term (weeks) response of the bar/rip systems; (3) the medium term (months) seasonal response of the subtidal bars;

and (4) the long (yearly) response to the frequency and occurrence of storms on the shoreline position and beach stability. Trying to replicate these differing timescales within a numerical simulation is complex and beyond the ability of the current generation of numerical models.

XBeach was used to assess the model's ability to replicate morphological behaviour within the intertidal zone compared with observed changes. Despite limits in the model run-time stability and a lack of accurate bathymetry, restricting analysis to the intertidal region, XBeach simulations provided support for the removal of material under energetic conditions and the flattening of 3D beach morphology. However, despite the generation of onshore mean currents under calm waves, accretionary phases failed to generate the significant 3D morphology that was evident under measured post-storm recovery. XBeach parameterises sediment transport contributions on a wave group timescale; therefore, the importance of incident waves and onshore wave asymmetry is not sufficiently represented (Orzech *et al.*, 2011) and may account for the poor representation of 3D features.

7.1.6 Wave Hub Impacts

As stated in the introduction, marine renewables is a growth industry which the southwest of England is well placed to exploit. However, currently tourism is the dominant economic driver for this region and there is a need for a careful balance between development and sustainability for both of these sectors. With beaches providing a fundamental part of the regions attraction for families and surfers there is widespread interest in the future stability of these environments with regard to; wave quality; long term beach stability; and effects on nearshore hazards e.g. rips.

Understanding the likely impacts of the proposed Wave Hub development on the naturally variable nearshore wave climate is a complex task itself, further compounded by the reticence of device developers to disclose the efficiency of their WEC's. A comparison of two independent studies on the likely impact to wave conditions suggests a maximum reduction in nearshore wave heights of 6% for a fully saturated site and high attenuation of the wave field (ASR, 2007). Following deployment at the site, future monitoring would benefit highly from increased wave measurements surrounding the Wave Hub, and in the predicted shadow region to follow up on these model predictions.

Assessing the impact of reduced waves on the nearshore morphology is not straight forward and depends on a wide range of uncertainties. This thesis has presented a summary of the naturally variable morphological response from four sites most likely to fall within a shadow zone of the proposed Hub development. While their stability and response is dependent on the antecedent morphology and geological controls, the primary driver is the naturally variable local wave climate, with wave processes modulated by the tide. The nature of this system, dependent on highly variable wave conditions, prevents detailed long term forecasting of small scale (bar/rip) behaviour.

7.1.7 Wave Hub Impact Result

With limited data on the full effect of offshore devices on the local wave climate it is difficult to comprehensively assess the impact of the Wave Hub development. However, on a much broader scale the beaches likely to be affected can be classified using the dominant wave conditions, sediment characteristics and tidal range, and this concept can be used to address the likely impact of significant shifts in any or all of these inputs (Figure 7.6). Using the modeled forecast of a 6% reduction in inshore wave conditions,

all sites undergo a small shift towards more intermediate dominated systems, with planar/dissipative states less common.

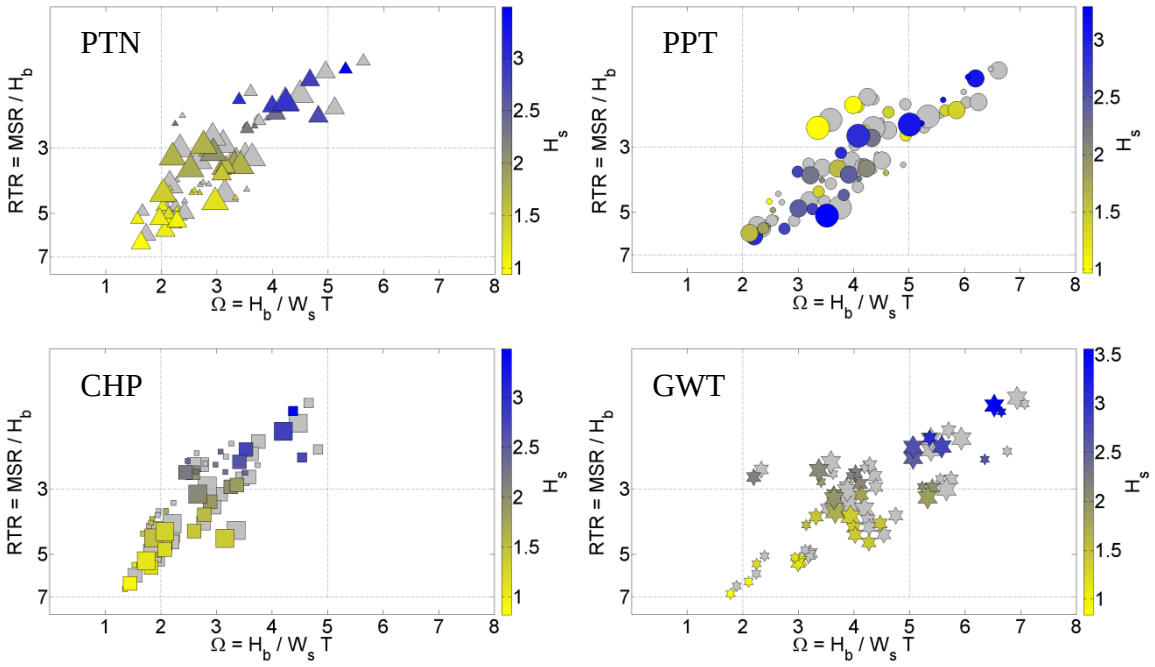

Figure 7.6 – Conceptual classification of monthly beach states as previously presented in Figure 4.9.1. Coloured symbols show relative position of states resulting from a 6% reduction in wave height compared with the measured states (shaded grey symbols). The size of the marker reflects the 3D level as derived using the $\overline{CV}$.

While this analysis does not provide detailed specifics on the nature and extent of these beach states, or the size and distribution of the nearshore bars, it does provide some context that the current variability is unlikely to vary significantly beyond the present beach classifications. In other words, the natural variability in wave conditions, or the parameter space within which the beaches exist, is too large for a 6% reduction in the wave height to cause a significant change in beach state and behaviour.

7.2 Conclusions

This thesis provides an interpretation and level of understanding of the natural variability for a highly dynamic section of coast. Through comparison of four distinctive beaches the morphological response to changing wave conditions and specific storm events has been addressed through monthly topographic surveys, remotely sensed images and in-situ measurements of hydrodynamics. As a central

component of the WHISSP project the principal aim of this study has been to provide an understanding of the baseline morphological variability and response at four sites likely to be affected by the Wave Hub. The main conclusions to be drawn from this study with reference to this aim include:

- Morphological variability is high for PTN, CHP and PPT, with beach states moving between planar to highly 3D, with little evidence of an equilibrium state. GWT stands alone as less dynamic with more subdued morphology. This is attributed to a more sheltered location of GWT and a less energetic inshore wave climate.
- Sustained high intensity storm events, with wave conditions exceeding 4 m H_s for more than ~50 hours, are catalysts for significant beach change and longer term 3D cycles: post-storm recovery results in rapid development of 3D low tide morphology which gradually smooth's over during the following months, before another significant shift in waves repeats the cycle. The storm-driven response cycles dominated over underlying seasonal patterns in wave conditions, however post-storm recovery was dependant on these conditions.
- Beach size, antecedent morphology and the intertidal geology are significant controls of the beach dynamics: links between intertidal geology and beach morphology was more evident at the smaller sites (CHP and PTN), which exhibited strong rhythmicity and stability in bar/rip behaviour, compared with the responses for the larger beaches (PPT and GWT).
- Overall inter-site response to seasonal conditions was found to be temporally and seasonally consistent with up-state and down-state shifts occurring in response to changing wave conditions.

- The four sites are in a phase of net accretion reflecting a decrease in the frequency and intensity of storm events throughout the survey period.

With reference to the longer term stability of these site in response to the Wave Hub development and a maximum likely decrease in $H_s$of 6%:

- Beach variability will remain within the current intermediate/dissipative range, with no significant shifts beyond the present observed dynamics.
- Within intermediate/dissipative range our ability to attribute a shift in the dominant morphological behaviour to offshore deployments is not presently realistic. The expected response will be an increase in more intermediate beach states, which may lead to low tide bar/rip features becoming more common.
- Without continued monitoring of the nearshore and intertidal region, supported by concurrent wave measurements as WECs are deployed, comprehensive assessment of likely future response will not be possible.

As explored in the review in Chapter 1 our broad understanding of beach behaviour and in turn their relative state can be identified and predicted relatively well: we can define beaches from reflective to dissipative with a range of intermediate states in-between. It is also possible to qualitatively describe the behaviour of these beaches in response to changes in the dominant forcing conditions, and through this describe the overall dynamics for a particular site. However, as identified above, the importance of the antecedent conditions and the role of the local geology in determining the exact response is complex. Wave conditions remain the dominant force which drives beach change, and while we are able to predict their relative behaviour through large scale climate models, fundamentally they represent a nonlinear dynamical system (also referred to as chaos). While our understanding of these processes continues to improve, the nature of such systems means that where the principle processes can be understood

(relatively) the interacting forces acting on these mean we are not yet fully able to predict the complete outcome sufficiently to reach a deterministic state. Continued research and monitoring of these sites, and principally the role of waves, antecedent conditions and geology, will provide greater confidence to predict the short and long term response; although it is unlikely the coastal system will ever be regarded as fully deterministic.

REFERENCES

Aagaard, T., Hughes, M., Moller-Sorensen, R. & Andersen, S. (2006) 'Hydrodnamics and sediment Fluxes across an Onshore Migrating Intertidal Bar', *Journal of Coastal Research*, 22 (2),pp. 247-259.

Aagaard, T., Kroon, A., Hughes, M. G. & Greenwood, B. (2008) 'Field observations of nearshore bar formation', *Earth surface processes and landforms*, 33 (7),pp. 1021-1032.

Aagaard, T., Nielsen, J. & Greenwood, B. (1998) 'Suspended sediment transport and nearshore bar formation on a shallow intermediate-state beach', *Marine Geology*, 148 (3-4),pp. 203-225.

Aagaard, T., Kroon, A., Andersen, S., Møller Sørensen, R., Quartel, S. & Vinther, N. (2005) 'Intertidal beach change during storm conditions; Egmond, The Netherlands', Marine Geology, 218 (1-4), pp. 65-80.

Aarninkhof, S. G. J., Janssen, P. C. & Plant, N. G. (1997) 'Aarninkhof et al., 1997. S.G.J. Aarninkhof, P.C. Janssen and N.G. Plant', *Coastal Dynamics Conference*. Plymouth, UK, pp. 365-374.

Aarninkhof, S. G. J., Turner, I. L., Dronkers, T. D. T., Caljouw, M. & Nipius, L. (2003) 'A video-based technique for mapping intertidal beach bathymetry', *Coastal Engineering*, 49 (4),pp. 275-289.

Almar, R., Castelle, B., Ruessink, B. G., Sénéchal, N., Bonneton, P. & Marieu, V. (2010) 'Two- and three-dimensional double-sandbar system behaviour under intense wave forcing and a meso-macro tidal range', *Continental Shelf Research*, 30 (7),pp. 781-792.

Arup (2001) Assessment of the Potential Contribution of Marinas and Watersports to Increasing Prosperity in Cornwall.Ove Arup and Partners, Bristol.

ASR (2007) *Review of Wave Hub Technical Studies: Impacts on inshore surfing beaches.* 40 pp. Available at: http://www.sas.org.uk/pr/2007/docs07/Review-of-Wave-Hub-Technical-Studies-Apr-071.pdf.

Austin, M., Masselink, G., O'Hare, T. & Russell, P. (2009a) 'Onshore sediment transport on a sandy beach under varied wave conditions: Flow velocity skewness, wave asymmetry or bed ventilation?', *Marine Geology*, 259 (1-4),pp. 86-101.

Austin, M., Scott, T., Brown, J., Brown, J., MacMahan, J., Masselink, G. & Russell, P. (2010) 'Temporal observations of rip current circulation on a macro-tidal beach', *Continental Shelf Research*, 30 (9),pp. 1149-1165.

Austin, M. J., Masselink, G., Russell, P. E., Turner, I. L. & Blenkinsopp, C. E. (2011) 'Alongshore fluid motions in the swash zone of a sandy and gravel beach', *Coastal Engineering*, 58(8), pp.690-705

Austin, M. J., Scott, T. M., Brown, J. W., Brown, J. A. & MacMahan, J. H. (2009b) 'Macrotidal Rip Curent Experiemnt: Circulation and Dynamics', Silva, C.P.d. (ed. *10th International Coastal Symposium*. Lisbon Journal of Coastal Reserach, pp. 24-28.

Backstrom, J. T., Jackson, D. W. T. & Cooper, J. A. G. (2009) 'Shoreface morphodynamics of a high-energy, steep and geologically constrained shoreline segment in Northern Ireland', *Marine Geology*, 257 (1-4),pp. 94-106.

Battiau-Queney, Y., Billet, J. F., Chaverot, S. & Lanoy-Ratel, P. (2003) 'Recent shoreline mobility and geomorphologic evolution of macrotidal sandy beaches in the north of France', *Marine Geology*, 194 (1-2),pp. 31-45.

Battjes, J. A. (1974) 'Surf Similarity', *14th International Conference of Coastal Engineerings*. ASCE, pp. 466-480.

Birkemeier, W. A., Nicholls, R. J. & Lee, G. H. (1999) 'Storms, storm groups and nearshore morphologic change', Kraus, N.C. and McDougal, W.G. eds.). 4th International Symposium on Coastal Engineering and Science of Coastal Sediment Processes. Hauppauge, Ny Jun 21-23. Amer Soc Civil Engineers, pp. 1109-1122.

Blenkinsopp, C. E., Turner, I. L., Masselink, G. & Russell, P. E. (2011) 'Swash zone sediment fluxes: Field observations', *Coastal Engineering*, 58 (1),pp. 28-44.

Bowen, A. J. & Inman, D. L. (1969) 'Rip Currents 2. Laboratory and Field Observations', Journal of Geophysical Research, 74 (23),pp. 5479-5490.

Bruun, P. (1962) 'Sea-level rise as cause of shore erosion', *American Society of Civil Engineering Proceedings*. Journal of Waterways and Harbours Division, pp. 117-130.

Buscombe, D. D. & Scott, T. M. (2008) 'The Coastal Geomorphology of North Cornwall: St Ives Head to Trevose Head'. University of Plymouth.

Castelle, B., Bonneton, P., Dupuis, H. & Sénéchal, N. (2007a) 'Double bar beach dynamics on the high-energy meso-macrotidal French Aquitanian Coast: A review', *Marine Geology*, 245 (1-4),pp. 141-159.

Castelle, B., Turner, I. L., Ruessink, B. G. & Tomlinson, R. B. (2007b) 'Impact of storms on beach erosion: Broadbeach (Gold Coast, Australia)', *9th International Coastal Symposium*. Gold Coast , Australia Journal of Coastal Research, pp. 534-539.

CISCAG (2010) Cornwall and Isles of Scilly Shoreline Management Plan Review; Sub-cells 6d, 6e,7a and 7b. Rame Head to Hartland Point, and the Isles of Scilly. Available at http://www.ciscag.org/smpindex.html

Dalrymple, R. A. & Thompson, W. W. (1977) 'Study of equilibrium beach profiles', *15th International Conference of Coastal Engineering*. Honolulu, Hawaii, pp. pp1277-1296.

Davidson, M., Huntley, D., Holman, R. & George, K. (1997) 'The Evaluation of Large-scale (km) Intertidal Beach Morphology on a Macrotidal Beach using Video Images ', *Proceedings Coastal Dynamics '97*, pp. 385-394.

Davidson, M. A., Lewis, R. P. & Turner, I. L. (2010) 'Forecasting seasonal to multi-year shoreline change', *Coastal Engineering*, 57 (6),pp. 620-629.

Dean, R. G. (1977) *Equilibrium Beach Profiles: US Atlantic and Gulf Coast Ocean.* University of Delaware, Engineering Report, (Report No. 12). Available.

Dodet, G., Bertin, X. & Taborda, R. (2010) 'Wave climate variability in the North-East Atlantic Ocean over the last six decades', *Ocean Modelling*, 31 (3-4),pp. 120-131.

Elgar, S., Gallagher, E. L. & Guza, R. T. (2001) 'Nearshore sandbar migration', Journal of Geophysical Research, 106 (C6),pp. 11623-11627.

Enjalbert, C., Castelle, B., Rihouey, D. & Dailloux, D. (2011) 'High-frequency video observation of a geologically-constrained barredbeach:La Grande Plage de Biarritz (France)', *Journal of Coastal Research*, 70-74 (64),

Gallop, S. L., Bryan, K. R. & Giovanni, C. (2009) 'Video observations of rip currents on an embayed beach', Silva, C.P.d. (ed. *International Coastal Symposium*. Lisbon Journal of Coastal Research, pp. 49-53.

Gourlay, M. R. (1968) *Beach and dune erosion tests.* Delft Hydraulics, Laboratory, Report No. M935/M936. May.

Greenwood, B. & Osborne, P. D. (1990) 'Vertical and horizontal structure in cross-shore flows: An example of undertow and wave set-up on a barred beach', *Coastal Engineering*, 14 (6),pp. 543-580.

Greenwood, B. & Osborne, P. D. (1991) 'Equilibrium slopes and cross-shore velocity asymmetries in a storm-dominated, barred nearshore system', *Marine Geology*, 96 (3-4),pp. 211-235.

Guza, R. T. & Thornton, E. B. (1985) 'Veolocity moments in the nearshore', *Journal of Waterway, Port, Coastal and Ocean Engineering*, 111(2) pp. 235-256.

Halcrow (2006) South West of England Regional Development Agency: Wave Hub Development and Design Phase Coastal Processes Study Report. Available at: http://www.wavehub.co.uk/wp-content/uploads/2011/06/Appendix-A-Coastal-Processes.pdf.

Hallermeier, R., J. (1981) 'Terminal settling velocity of commonly occuring sand grains', *Sedimentology*, 28 pp. 859-865.

Hansen, J. E. & Barnard, P. L. (2010) 'Sub-weekly to interannual variability of a high-energy shoreline', *Coastal Engineering*, 57 (11-12),pp. 959-972.

Haxel, J. H. & Holman, R. A. (2004) 'The sediment response of a dissipative beach to variations in wave climate', *Marine Geology*, 206 (1-4),pp. 73-99.

Hill, H. W., Kelley, J. T., Belknap, D. F. & Dickson, S. M. (2004) 'The effects of storms and storm-generated currents on sand beaches in Southern Maine, USA', *Marine Geology*, 210 (1-4),pp. 149-168.

Holland, K. T., Holman, R. A., Lippmann, T. C., Stanley, J. & Plant, N. (1997) 'Practical use of video imagery in nearshore oceanographic field studies', *Oceanic Engineering, IEEE Journal of*, 22 (1),pp. 81-92.

Holman, R. A. & Stanley, J. (2007) 'The history and technical capabilities of Argus', *Coastal Engineering*, 54 (6-7),pp. 477-491.

Holman, R. A., Symonds, G. Thornton, E.B., Ranasinghe, R. (2006) 'Rip spacing and persistance on an embayed beach', Journal of Geophysical Research, 111 pp. C01006.

IPCC (2007) Climate Change 2007 – Impacts, Adaptation and Vulnerability; Contribution of Working Group II to the Fourth Assessment Report of the IPCC. eds. M.L. Parry, O.F.C., J.P. Palutikof, P.J. van der Linden and C.E. and Hanson, E., Cambridge: Cambridge University Press.

Jackson, D. W. T., Cooper, J. A. G. & del Rio, L. (2005) 'Geological control of beach morphodynamic state', *Marine Geology*, 216 (4),pp. 297-314.

Jago, C. F. & Hardisty, J. (1984) 'Sedimentology and morphodynamics of a macrotidal beach, Pendine Sands, SW Wales', *Marine Geology*, 60 (1-4),pp. 123-154.

King, C. A. M. (1972) *Beaches and Coasts.* Arnold, London.

Kingston, K. S., Ruessink, B. G., van Enckevort, I. M. J. & Davidson, M. A. (2000) 'Artificial neural network correction of remotely sensed sandbar location', *Marine Geology*, 169 (1-2),pp. 137-160.

Komar, P. D. (1998) *Beach Processes and Sedimentation.* 2nd edn. Prentice-Hall, Upper Saddle River, NJ.

Komar, P. D. B. C. (1985) 'Analysis of grain-size measurements by sieving and settling-tube techniques J Sediment Petrol V54, N2, June 1984, P603-614', *International Journal of Rock Mechanics and Mining Science & Geomechanics Abstracts*, 22 (3),pp. A80-A81.

Kroon, A. & Masselink, G. (2002) 'Morphodynamics of intertidal bar morphology on a macrotidal beach under low-energy wave conditions, North Lincolnshire, England', *Marine Geology*, 190 (3-4),pp. 591-608.

Lafon, V., De Melo Apoluceno, D., Dupuis, H., Michel, D., Howa, H. & Froidefond, J. M. (2004) 'Morphodynamics of nearshore rhythmic sandbars in a mixed-energy environment (SW France): I. Mapping beach changes using visible satellite imagery', *Estuarine, Coastal and Shelf Science*, 61 (2),pp. 289-299.

Lafon, V., Dupuis, H., Butel, R., Castelle, B., Michel, D., Howa, H. & De Melo Apoluceno, D. (2005) 'Morphodynamics of nearshore rhythmic sandbars in a mixed-energy environment (SW France): 2. Physical forcing analysis', *Estuarine, Coastal and Shelf Science*, 65 (3),pp. 449-462.

Larson, M. & Kraus, N. C. (1994) 'Temporal and spatial scales of beach profile change, Duck, North Carolina', *Marine Geology*, 117 (1-4),pp. 75-94.

Lee, G.-h., Nicholls, R. J. & Birkemeier, W. A. (1998) 'Storm-driven variability of the beach-nearshore profile at Duck, North Carolina, USA, 1981-1991', *Marine Geology*, 148 (3-4),pp. 163-177.

Levoy, F., Anthony, E., Barusseau, J. P., Howa, H. & Tessier, B. (1998) 'Morphodynamics of a macrotidal ridge and runnel beach', *Comptes Rendus De L Academie Des Sciences Serie Ii Fascicule a-Sciences De La Terre Et Des Planetes*, 327 (12),pp. 811-818.

Lippmann, T. C. & Holman, R. A. (1989) 'Quantification of sand bar morphology: A video technique based on wave dissipation', Journal of Geophysical Research, 94 pp. 995-1011.

Lippmann, T. C. & Holman, R. A. (1990) 'The spatial and temproal varability of sand bar morphology', Journal of Geophysical Research, 95 (C7),pp. 11575-11590.

Longuet-Higgins, M. S. & Stewart, R. W. (1964) 'Radiation stress in water waves, a physical discussion with applications', *Deep-Sea Research*, 11 (4),pp. 529-563.

MacMahan, J. H., Thornton, E. B. & Reniers, A. J. H. M. (2006) 'Rip current review', *Coastal Engineering*, 53 (2-3),pp. 191-208.

MacMahan, J. H., Thornton, E. B., Stanton, T. P. & Reniers, A. J. H. M. (2005) 'RIPEX: Observations of a rip current system', *Marine Geology*, 218 (1-4),pp. 113-134.

Masselink, G. (1993) 'Simulating the effects of Tides on Beach Morphodynamics', *Journal of Coastal Research*, (SI 15),pp. 180-197.

Masselink, G. (2004) 'Formation and evolution of multiple intertidal bars on macrotidal beaches: application of a morphodynamic model', *Coastal Engineering*, 51 (8-9),pp. 713-730.

Masselink, G. & Anthony, E. J. (2001) 'Location and height of intertidal bars on macrotidal ridge and runnel beaches', *Earth surface processes and landforms*, 26 (7),pp. 759-774.

Masselink, G., Auger, N., Russell, P. & O'Hare, T. (2007) 'Short-term morphological change and sediment dynamics in the intertidal zone of a macrotidal beach', *Sedimentology*, 54 (1),pp. 39-53.

Masselink, G. & Hughes, M. (1998) 'Field investigation of sediment transport in the swash zone', *Continental Shelf Research*, 18 (10),pp. 1179-1199.

Masselink, G., Kroon, A. & Davidson-Arnott, R. G. D. (2006) 'Morphodynamics of intertidal bars in wave-dominated coastal settings -- A review', *Geomorphology*, 73 (1-2),pp. 33-49.

Masselink, G. & Puleo, J. A. (2006) 'Swash-zone morphodynamics', *Continental Shelf Research*, 26 (5),pp. 661-680.

Masselink, G. & Short, A. (1993) 'The effect of tide range on beach morphodynamics and morphology: A conceptual beach model', *Journal of Coastal Research*, 9 (3),pp. 785-800.

McCall, R. T., Van Thiel de Vries, J. S. M., Plant, N. G., Van Dongeren, A. R., Roelvink, J. A., Thompson, D. M. & Reniers, A. J. H. M. (2010) 'Two-dimensional time dependent hurricane overwash and erosion modeling at Santa Rosa Island', *Coastal Engineering*, 57 (7),pp. 668-683.

Mckenzie, P. (1958) 'Rip-Current Systems', *Journal of Geology*, 66 pp. 103-113.

McNinch, J. E. (2004) 'Geologic control in the nearshore: shore-oblique sandbars and shoreline erosional hotspots, Mid-Atlantic Bight, USA', *Marine Geology*, 211 (1-2),pp. 121-141.

Merefield, J. R. (1984) 'Modern cool-water beach sands of Southwest England', Journal of Sedimentary Research, 54 (2),pp. 413-424.

Miles, J., Butt, T. & Russell, P. (2006) 'Swash zone sediment dynamics: A comparison of a dissipative and an intermediate beach', *Marine Geology*, 231 (1-4),pp. 181-200.

Millar, D. L., Smith, H. C. M. & Reeve, D. E. (2007) 'Modelling analysis of the sensitivity of shoreline change to a wave farm', *Ocean Engineering*, 34 (5-6),pp. 884-901.

Min V&W, (1991). 'De Basiskustlijn, een technisch / morfologische uitwerking'. (in Dutch).

Orzech, M. D., Reniers, A. J. H. M., Thornton, E. B. & MacMahan, J. H. (2011) 'Megacusps on rip channel bathymetry: Observations and modeling', *Coastal Engineering*, In Press, Corrected Proof

Pape, L., Ruessink, B. G., Wiering, M. A. & Turner, I. L. (2007) 'Recurrent neural network modeling of nearshore sandbar behavior', *Neural Networks*, 20 (4),pp. 509-518.

Pilkey, O. H., Young, R., Riggs, S. R., Smith, A. W. S., Wu, H. & Pilkey, W. D. (1993) 'The Concept of Shoreface Profile Equilibrium: A Critical Review', *Journal of Coastal Research*, 9 (1),pp. 255-278.

Plant, N. G., Holland, K., T. & Puleo, J. A. (2008) 'Application of quadratic loess filters to bathymetric interpolation', Unpublished. Naval Research Lab, pp.37

Plant, N. G. & Holman, R. A. (1997) 'Intertidal beach profile estimation using video images', *Marine Geology*, 140 (1-2),pp. 1-24.

Price, T.D., Rutten,J. and Ruessink,B.G. (2011) 'Coupled behaviour within a double sandbar system'. Journal of Coastal Research, SI 64, pp. 125-129.

Puleo, J. A., Holland, K. T., Plant, N. G., Slinn, D. N. & Hanes, D. M. (2003) 'Fluid acceleration effects on suspended sediment transport in the swash zone', *J. Geophys. Res.*, 108 (C11),pp. 3350.

Ranasinghe, R., Symonds, G., Black, K. & Holman, R. (2004) 'Morphodynamics of intermediate beaches: a video imaging and numerical modelling study', *Coastal Engineering*, 51 (7),pp. 629-655.

Reichmüth, B. & Anthony, E. J. (2007) 'Tidal influence on the intertidal bar morphology of two contrasting macrotidal beaches', *Geomorphology*, 90 (1-2),pp. 101-114.

Roelvink, D., Reniers, A., van Dongeren, A., van Thiel de Vries, J., McCall, R. & Lescinski, J. (2009) 'Modelling storm impacts on beaches, dunes and barrier islands', *Coastal Engineering*, 56 (11-12),pp. 1133-1152.

Roelvink, D., Reniers, A. J. H. M., Van Dongeren, A., Van Thiel de Vries, J., Lescinski, J. & McCall, R. (2010) 'XBeach Model Description and Manual', *Unesco-IHE Institute for Water Education, Deltares and Delft University of Technology*, 6

Roelvink, J. A. & Stive, M. J. F. (1989) 'Bar-generating cross-shore flow mechanisms on a beach', *Journal of Geophysical Research*, 94(C4) pp. 4785-4800.

Ruggiero, P., Kaminsky, G. M., Gelfenbaum, G. & Voigt, B. (2005) 'Seasonal to Interannual Morphodynamics along a High-Energy Dissipative Littoral Cell', *Journal of Coastal Research*, 21 (3),pp. 553-578.

Russell, P. E. (1993) 'Mechanisms for beach erosion during storms.', *Continental Shelf Research*, 13 pp. 1243-1265.

Russell, P. E. & Huntley, D. A. (1999) 'A Cross-Shore Transport "Shape Function" for High Energy Beaches', *Journal of Coastal Research*, 15 (1),pp. 198-205

Schlax, M. G. & Chelton, D. B. (1992) 'Frequency domain diagnostics for linear smoothers', *Journal of the American Statistical Association*, 87 (420),pp. 1070-1081.

Scott, T. M. (2009) *Beach Morphodynamics and associated hazards in the UK*. University of Plymouth. Unpublished Thesis.

Scott, T. M., Masselink, G. & Russell, P. (2011) 'Morphodynamic characteristics and classification of beaches in England and Wales', *Marine Geology*, 268 (1-4) pp.1-20

Scott, T. M., Russell, P. E., Masselink, G., Wooler, A. & Short, A. (2007) 'Beach rescue statistics and their relation to nearshore morphology and hazards: a case study for south-west England', *9th International Coastal Symposium* Gold Coast, Australia 16-20 April. CERF.

Sénéchal, N., Gouriou, T., Castelle, B., Parisot, J. P., Capo, S., Bujan, S. & Howa, H. (2009) 'Morphodynamic response of a meso- to macro-tidal intermediate beach based on a long-term data set', *Geomorphology*, 107 (3-4),pp. 263-274.

Shepard, F. P., Emery, K. O. & La Fond, E. C. (1941) 'Rip Currents : A process of geological importance', *Journal of Geology*, XLIX pp. 337-369.

Short, A. D. (1987) 'A note on the controls of beach type and change, with S.E. Australian examples', *Journal of Coastal Research*, 3 pp. 387-395.

Short, A. D. (1996) 'The role of wave height, period, slope, tide range and embaymentisation in beach classifications: a review', *revista Chilena de Historia Natural*, 69 pp. 589-604.

Short, A. D., Editor (1999) *Handbook of beach and shoreface morphodynamics.*ISBN: 978-0-471-96570-1, pp.392

Short, A. D. & Hesp, P. A. (1982) 'Wave, beach and dune interactions in southerstern Australia', *Marine Geology*, 48 pp. 259-284.

Smit, M. W. J., Reniers, A. J. H. M., Ruessink, B. G. & Roelvink, J. A. (2008a) 'The morphological response of a nearshore double sandbar system to constant wave forcing', *Coastal Engineering*, 55 (10),pp. 761-770.

Smit, M. W. J., Reniers, A. J. H. M., Symonds, G. & Ruessink, B. G. (2008b) 'Morphodynamic modelling of up-state and down-state transitions at Palm beach, NSW, Australia', Smith, J.M. (ed. *Coastal Engineering*. Hamburg World Scientific, pp. 2437-2445.

Soulsby, R. L. (1997) Dynamics of marine sands: a manual for practical applications. Thomas Telford.

Stockdon, H. F. & Holman, R. A. (2000) 'Estimation of wave phase speed and nearshore bathymmetry from video imagery', *Journal of Geophysical Research*, 105 (C9),pp. 22015-22033.

Sutherland, J., Peet, A. H. & Soulsby, R. L. (2004) 'Evaluating the performance of morphological models', *Coastal Engineering*, 51 (8-9),pp. 917-939.

Thornton, E. B., Humiston, R. T. & Birkemeier, W. (1996) 'Bar/trough generation on a natural beach', *Journal of Geophysical Research,*, 101(C5) pp. 12097-12110.

Trimble (2003) Real-Time Kinematic Surveying, Training Guide. Available.

Turner, I. L., Russell, P. E. & Butt, T. (2008) 'Measurement of wave-by-wave bed-levels in the swash zone', *Coastal Engineering*, 55 (12),pp. 1237-1242.

Turner, I. L., Whyte, D., Ruessink, B. G. & Ranasinghe, R. (2007) 'Observations of rip spacing, persistence and mobility at a long, straight coastline', *Marine Geology*, 236 (3-4),pp. 209-221.

UKMO (2011) 'MIDAS Land Surface Stations data (1853-current) '. *NCAS British Atmospheric Data Centre*. Available at:

http://badc.nerc.ac.uk/view/badc.nerc.ac.uk__ATOM__dataent_ukmo-midas

van Enckevort, I. M. J. & Ruessink, B. G. (2001) 'Effects of hydrodynamics and bathymmetry on video estimates of nearshore sandbar position.', *Journal of Geophysical Research,*, 106 pp. 16969-16979.

van Koningsveld, M. & Mulder, J. P. M. (2004) 'Sustainable Coastal Policy Developments in The Netherlands. A Systematic Approach Revealed', *Journal of Coastal Research*, 20 (2),pp. 375-385.

Woodroffe, C. D. (2003) *Coasts, form, process and evolution.* Cambridge University Press.

Wright, L. D. & Short, A. D. (1984) 'Morphodynamic variability of surf zones and beaches: A synthesis', *Marine Geology*, 56 (1-4),pp. 93-118.

Wright, L. D., Short, A. D., Boon I, J. D., Hayden, B., Kimball, S. & List, J. H. (1987) 'The morphodynamic effects of incident wave groupiness and tide range on an energetic beach', *Marine Geology*, 74 (1-2),pp. 1-20.

Wright, L. D., Short, A. D. & Green, M. O. (1985) 'Short-term changes in the morphodynamic states of beaches and surf zones: An empirical predictive model', *Marine Geology*, 62 (3-4),pp. 339-364.

APPENDIX 1 – SUMMARY OF DATA AVAILABLE FROM THE DWR AT PPT.

File	Parameters	Application
*.csv Summary parameters •	*Hs*, *Tp*, *Tz*, *Hmax*, Dir, Spread,	•
*.spt Spectrum file, a list of 64 frequency records.	Frequency (Hz), Normalised Power Spectral Density (m^2/Hz) (PSD), Direction, Spread, Skewness, Kurtosis	Frequency spacing is 0.005 Hz up to 0.1 Hz, and 0.01 Hz beyond.
*.raw List of displacements	• heave, north, west	Displacements in cm

Initial quality control on the summary parameters supplied in the *.csv files are undertaken by CCO and include:

1. Out of Range data
2. Rate of change (spikes)
3. T_p "jumps"

Flag = 0 All data pass

Flag = 1 Either $H_s$or $T_z$fail, so all data fail

Flag = 2 T_p fail + derivatives

Flag = 3 Dir fail + derivatives

Flag = 4 Spread fail + derivatives

Flag = 5 $T_p >= 2 * T_z$

APPENDIX 2 – EXAMPLE PARAMS.TXT FILE USED FOR XBEACH SIMULATIONS

Grid input

==========

nx = 77

ny = 54

vardx = 1

xfile = xfileApr.grd

yfile = yfileApr.grd

depfile = bathy_Apr.dep

xori=0

yori=0

alfa = 0

posdwn = -1

struct = 1

ne_layer = blank_Apr.dep

Wave input

==========

gamma = 0.55

gammax = 2

n = 10.

rho = 1025

g = 9.81

thetamin = -27.5

thetamax = 27.5

dtheta = 5.

wci = 0

break = 3

instat = 41

facua = 0.1

bcfile=wave_Apr_e.txt

rt=172800
dtbc=4
wavint=5
sprdthr=0.08
taper=100
nspr=0
facua = 0.15

flow input
==========
tideloc = 1

zs0file=tideAprN.dat

C=55
eps=0.005
umin=0.0

tstart= 0
tintg = 600
tintm = 3600
tstop = 302400

CFL = 0.7
Nuh = 0.15
smag = 1
smax = 0.8

Boundary conditions
==========
Front = 1
back = 2

left = 1
right = 1

Sediment input
==========
D50 = 0.00035
D90 = 0.00050
rhos = 2650

Morphologic updating
==========
morphology = 1
morfac = 4
morfacopt = 1
sourcesink = 0
sedtrans = 1

Output
==========
nglobalvar = 7
zs
zb
zb0
H
ue
ve
zs0

nmeanvar = 3
H
ue
ve

APPENDIX 3 – FIRST AUTHOR PAPERS

3D BEACH RESPONSE TO ENERGETIC WAVE CLIMATE, CORNWALL, UK

TIM POATE[1], MARTIN AUSTIN[1], PAUL RUSSELL[1], GERD MASSELINK[1], KEN KINGSTON[1]

1. *School of Marine Science and Engineering, University of Plymouth, Drake Circus, Plymouth, Devon, PL4 8AA, UK. timothy.poate@plymouth.ac.uk.*

Abstract: Intertidal GPS surveys were carried out on four high-wave energy macrotidal beaches on the north coast of Cornwall, UK, for 31 months between February 2008 and June 2010. These beaches sit at a mophodynamic classification boundary between dissipative and intermediate beach states, the latter typically characterised by varying degrees of three-dimensional (3D) low tide bar/rip morphology. Through a simple measure of 3D we identify the importance of storm events on the dominant beach features. The results suggest that low tide bar/rip morphology typically develops in a three stage process: (1) high-energy wave conditions cause widespread erosion across the beachface as material is moved offshore; (2) low-energy swell-dominated conditions bring sediment back onshore; and (3) growth in 3D features around the low tide level as redistribution of nearshore sediment occurs. This approach provides new understanding of the accretionary response rates of boundary beach states which exhibit dissipative/intermediate characteristics.

Introduction

There is global growth in the need for, and research into, marine renewables, which in the UK has led to a pioneering experimental wave farm ('Wave Hub') being installed 20 km off the north coast of Cornwall. This development provides a unique opportunity for the assessment of any impacts on the beaches in the lee of the wave farm due to shadow affects caused by the Wave Farm, Millar *et al* (2007). Concern over the impact on beach stability and surfing wave conditions has provoked great public interest in offshore energy extraction. Although there have been several medium to longer term (>1 year) studies into the behaviour of high-wave energy/macrotidal environments e.g. (Jago and Hardisty, 1984; Reichmüth and Anthony, 2007), as well as more intensive short term studies (Masselink *et al.*, 2007), these dataset focus on single 2D profile analysis. More recent work by Ruggiero *et al*. (2005) and Hansen and Barnard (2010) has utilised longer 3D datasets (~5yrs) to assess seasonal variability for more energetic mesotidal sites, yet with a focus on larger scale shoreline response and beach management. There remains an obvious paucity of consistent, detailed 3D morphological data from energetic macrotidal sites.

In this paper we use 31 monthly real time kinematic (RTK) GPS surveys at four high-wave energy, macrotidal beaches. In terms of their morphodynamics, these beaches are located at the transition between intermediate and dissipative beach

states according to the classification of Wright *et al.*, (1985). To increase the temporal resolution of the morphological data set, ARGUS images are used to establish morphological variability during survey intervals (Holman and Stanley, 2007).

Beaches at the intermediate/dissipative beach state boundary exhibit quasi-seasonal low tide bar/rip systems which are of significant interest to beach users in terms of surfing and as potential hazards (Scott *et al.*, 2007). The sensitivity of such beach states to small shifts in wave conditions makes them ideal sites for assessment of equilibrium morphology. The presented data set is first used to identify annual/seasonal patterns in individual beach response and the coastal system as a whole. Secondly, a quantitative measure of low tide 3D morphology is used to characterise significant shifts in beach dynamics in response to the dominant wave conditions.

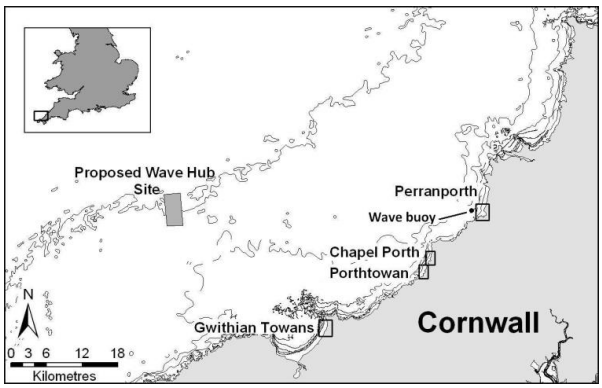

Fig 1. Location of four study sites (Gwithian, Porthtowan, Chapel Porth and Perranporth), inshore wave buoy (1 km offshore) and Wave Hub (16 km offshore) on the North Cornish coast, England.

The four sites shown in Figure 1 lie within a 23-km stretch along the North Cornish coast. The coastline is macrotidal (mean spring tidal range 6.1 m) and is exposed to a highly energetic wave climate (mean offshore H_s = 1.6 m; H_{10} = 2.6 m) of both North Atlantic swell and local wind-generated seas producing a dominant westerly wave direction (Poate *et al.*, 2009). Each of the beaches detailed below has a W-NW orientation exposed to the prevailing wave approach. Table 1 gives a summary of the four sites and further details can be found in Poate *et al.*, (2009).

Table 1. Summary of site details

Site	Alongshore (m)	Cross shore (m)	D_{50}	w_s (cm/s)	Lower beach slope tanβ
Perranporth (PPT)	1200	500	0.35	0.038	0.012
Porthtowan (PTN	800	400	0.38	0.049	0.015
Chapelporth (CHP)	600	400	0.38	0.058	0.015
Gwithian (GWT)	700	350	0.25	0.037	0.013

Data set and Methods of Analysis

Intertidal beach morphology was mapped during the lowest spring tide every month over 31 months from February 2008 to June 2010. 3D surface morphology was surveyed using RTK-GPS mounted on an all terrain vehicle (ATV), allowing for rapid data collection over a wide area. Data collection was undertaken in a grid pattern with lines spaced 5–20 m depending on the terrain and dominant morphological features. On two beaches (PTN and PPT) ARGUS video sites were established to provide half hourly "image products" consisting of a single snapshot image, a time-exposure image and a variance image (Holman and Stanley, 2007; Poate *et al.*, 2009).

3D Classification

Identification of beach state or beach type (e.g., Low Tide Bar/Rip; Masselink and Short (1993)), relies on the presence or absence of intertidal morphological features, such as bars and rip channels. Beaches at the boundary between dissipative and intermediate beach states can display either smooth planar 2D beach faces or well-defined 3D channels and bar patterns respectively. The ability to quantify these characteristics is a fundamental aspect of this paper. Here, we present a measure by which a relative level of 3D is assigned to each survey. Although 3D implies a volumetric component, in our approach we are concerned with the surface shape and intuitively the term 3D is adopted as a measure of the morphological features present. In order to assign a 3D value to each survey, contour lines were extracted between 0.2m ODN (mean sea level) and -2.4m ODN (0.2m above low water springs) at 0.2m intervals. A "curl value" *CV* was then computed using the ratio of total contour length and straight line length of the contour:

$$CV = \frac{CL}{CS} \tag{1}$$

where *CL* is the total contour length and *CS* is the straight distance from the start to the end point of the contour. For each survey the significant $\overline{CV}$ was computed by averaging the highest one third of the *CV* values. In addition, the

contour standard deviation (CSTD) was computed using the same contours extracted and the top third of the contours with the highest individual standard deviations were used to compute the $\overline{CSTD}$.

To ensure the automatic routines were a realistic representation of the conditions presented in a surface elevation map, the opinions of relevant researchers within this field was sought to verify the results. Following the same approach as Ranasinghe *et al.,* (2004), 10 "experts" were asked to rank the monthly surveys for levels of 3D on a scale of 0–100 providing a direct comparison of the automatic 3D classification methods. To facilitate assessment the results were first standardised before cross-correlation analysis using a Pearson linear correlation co-efficient showed the relationship between the $\overline{CV}$ and the expert values had a p-value of <0.002, whereas the $\overline{CSTD}$ had a p-value of <0.009, showing they both exhibit a significant correlation. The relative shifts in the 3D parameters each month are crucial for identifying trends in morphological response. Comparison of the expert values with the $\overline{CV}$ and $\overline{CSTD}$ showed both had 80% agreement with the relative shifts in 3D morphology, however $\overline{CV}$ followed more closely. Following this assessment of the contour extraction techniques, $\overline{CV}$ is adopted within this paper as an indication of morphological variability.

The dimensionless fall velocity Ω is used here to indicate the monthly beach state:

$$\Omega = H_{\mathrm{b}}/(w_{\mathrm{s}}T_p) \tag{2}$$

where H_{b} is the breaker height, T_p is the significant peak period and w_{s} is the mean fall velocity of the beach sand. The beach state exhibited through the monthly surveys reflects the beach response to the antecedent processes. The hydrodynamic conditions experienced during the inter-survey period are of most relevance in understanding the observed beach state. Following Wright *et al.,* (1985; 1987), the conditions dominant in the period since the previous survey were computed. A weighted mean value $\bar{\bar{\Omega}}$ was calculated according to:

$$\bar{\bar{\Omega}} = \left[\sum_{j=1}^{D} 10^{-j/\phi}\right]^{-1} \sum_{j=1}^{D}\left(\Omega_j 10^{j/\phi}\right) \tag{3}$$

where j = 1 on the day just preceding the intertidal survey and $j = D$ on D days prior to the survey. The parameter ϕ defines the rate of memory decay, where ϕ days prior to the survey the weighting factor will decrease to 10%. Wright *et al.,* (1985) found the best fit using ϕ = 10 which was also adopted here, and D = number of days since the previous survey.

Hydrodynamic Data

Tidal elevations were recorded using self-logging RBR pressure recorders (TWR 2050) mounted at fixed locations at PPT and PTN. Nearshore directional wave data is provided from the Channel Coastal Observatory (*www.channelcoast.org*) Datawell Mk III directional wave rider situated in approximately 10 m water depth, 1 km west of Perranporth (Figure 1). The buoy was deployed in December 2006. Full wave statistics and raw time series have been used for further spectral analysis, including bimodality and wave groupiness.

A wave groupiness factor *GF* was calculated following Wright *et al.,* (1987) based on the groupiness time series g_t generated by low pass filtering the modulus of the water surface elevation time series (reduced to zero mean and scaling the result with a factor of $\pi/4$):

$$GF = \frac{\sqrt{2\sigma_g}}{\bar{g}_t} \tag{4}$$

where σ_g is the standard deviation of g_t and $\bar{g}_t$ is the mean of g_t. This provides a *GF* with a range of 0 to 1, where 1 represents highly grouped waves and 0 represents a sea state with no clear variability in wave amplitude. With raw heave data available from the wave buoys since December 2006, *GF* was calculated for each 17-min sampling period. This provided over 4000 values during the survey period. These were then averaged to produce a daily time series $\overline{\overline{GF}}$.

Spectral partitioning was undertaken to quantify the relative importance of low-frequency (swell) and high-frequency (wind) components in the nearshore wave climate. Wave spectra were computed for each 17-min survey period from the wave buoy, allowing set criteria to be used to determine the energy contained within the various frequencies. The Datawell directional Waverider spectra provides 64 spectral frequencies with frequency spacing of 0.005 Hz up to 0.1 Hz, and 0.01 Hz beyond.

The spectra are chacteristically bi-modal and were split using the spectral trough between the longer period swell and shorter period wind-waves (e.g. Figure 2). While set thresholds work in the majority of cases (e.g., partition at 0.1Hz), the growth and decay in swell events required peaks to be tracked as they move through the spectrum.

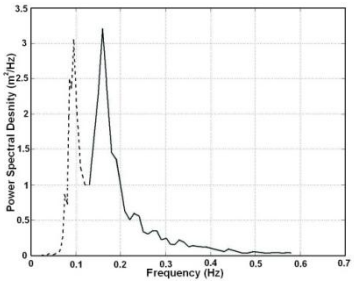

Fig 2. Example of spectral partitioning computed from the Perranporth Datawell Directional Waverider. The dashed line indicates a predominant low frequency (swell) component, while the black line identifies the high frequency (wind) waves.

The best approach was found by first identifying the location of the spectral peaks and using these to identify the biggest trough where the partition could be made (Figure 2).

Results and Analysis

Hydrodynamics

The monitoring program established in early 2008 was designed to assess the long-term site-specific and region-wide shoreline trends, as well as identify the morphological variability, response and behavior of smaller nearshore features, such as bars and rips. In the winter preceding the first survey, several storm events occurred, and after one month of observations the largest wave heights of the survey period were recorded (H_s = 7.5 m). This resulted in poor survey coverage limiting data analysis for this month. Summary wave statistics are presented in Figure 3 and show a strong seasonality in the wave height (Figure 3a) with a distinct increase in the frequency of H_s > 3m during the winter months, while the summer experiences H_s < 1–2 m.

Similar trends are evident in the wave period, where the general trend is an increased period during the winter (Figure 3b). Wave direction is increasingly W-SW during the summer, yet distinctive northerly events are relatively frequent in 2010 (Figure 3c). The percentage swell component of the wave spectra (Figure 3d) shows more temporal variance, although swell dominates during the energetic periods in January 2009 and November 2009. This trend is reflected in the groupiness factor which shows similar peaks during these energetic conditions (e.g. Dec 2009).

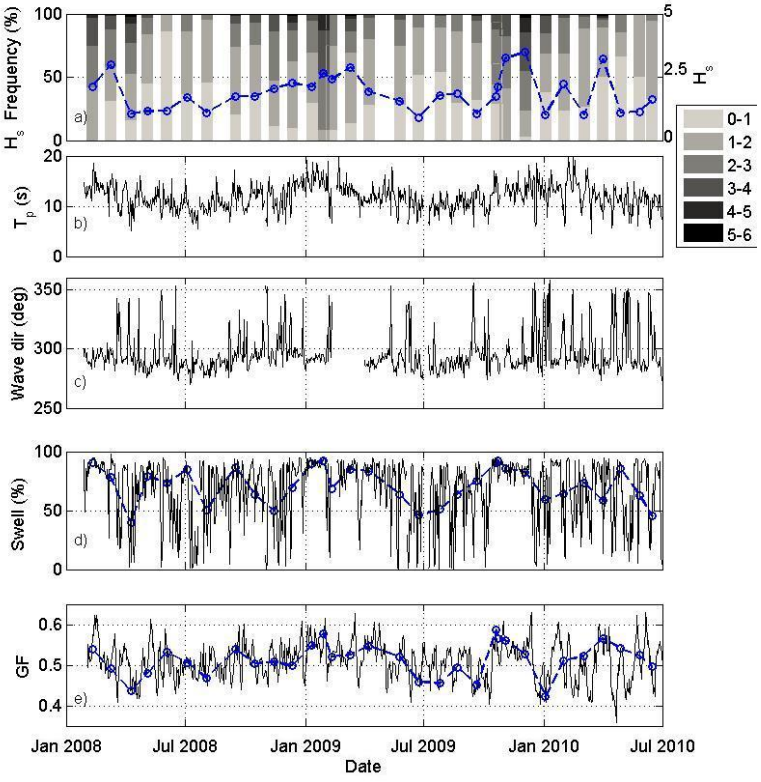

Fig 3. Summary wave conditions; from top panel, a) stacked histogram of occurrence of H_s during intra-survey periods, light shading indicates small H_s, and solid line shows mean weighted H_s for same period; b) T_p (s); c) Wave direction (˚)- data gap due to buoy error; d) Percentage swell component of wave spectra (%), dashed line shows survey interval average; e) Groupiness Factor, dashed lines shows weighted mean *GF* for survey interval ($\overline{\overline{GF}}$).

Morphology

Figure 4 provides a summary of the morphological conditions with the top panel providing a reference of the hydrodynamics. Intertidal beach volume was calculated for each site over a defined control region. The overall trend is a steady increase in net beach volume, which equates to 0.5m, 0.3m, 0.3m and 0.9m of accretion at PTN, PPT, GWT and CHP (Figure 4b). This growth is punctuated by two periods of widespread erosion at all sites during January 2009 and October/November 2009, (vertical boxes).

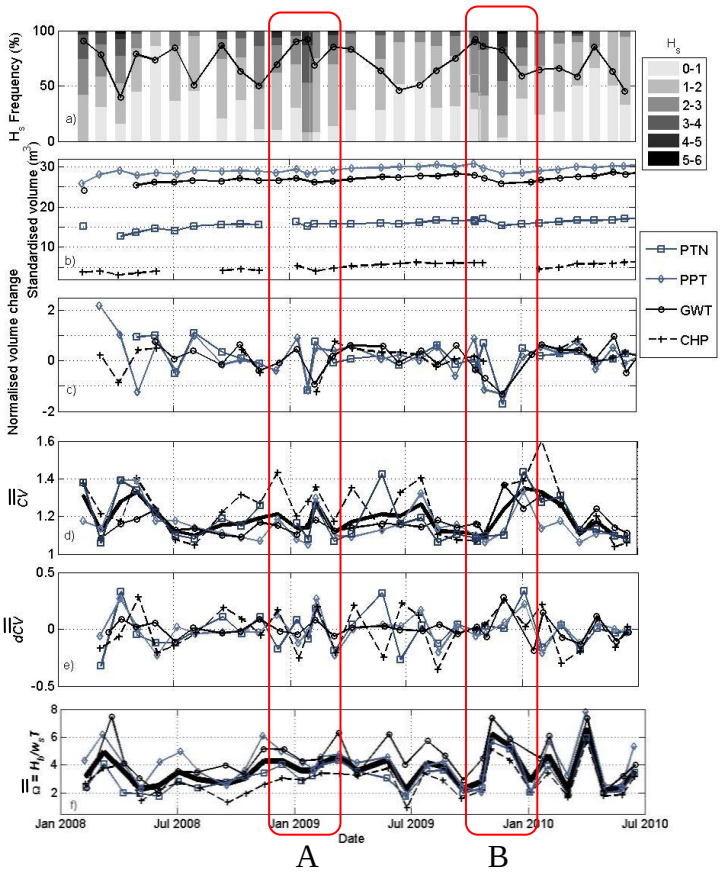

Fig 4. Morphological summary, from the top panel; a) Percentage frequency occurrence of significant wave height during survey intervals, with percentage swell component of spectral energy (solid line); b) Standardised volume for each of the sites (missing data due to poor survey coverage); c) Normalised volume change between monthly surveys; d) $\overline{\overline{CV}}$ for each site and average (thick solid line); e) Difference in $\overline{\overline{CV}}$ values for each site; f) Weighted dimensionless fall velocity ($\overline{\overline{\Omega}}$) for all sites and the average value (thick solid line). Vertical boxes A and B highlight erosive periods followed by 3D conditions for all beaches.

These periods of sand removal provide some indication of an annual pattern with overall volumes staying within a small envelop of change. Monthly change in volume is shown in Figure 4c). Aside from the first few months, in general there is good coherence between the beach volumetric changes at the different sites.

Figure 4d) and e) show $\overline{\overline{CV}}$ values from all sites and the change in $\overline{\overline{CV}}$ between surveys $d\overline{\overline{CV}}$ which provide some indication of the relative shifts in the lower

beach dynamics. From Figure 4d), two distinct periods can be identified that are characterised by increased 3D: February 2009 and January 2010. Figure 4f) shows the dimensionless fall velocity $\bar{\bar{\Omega}}$ calculated for each site, smaller values of which are associated with more intermediate beaches. A salient point from these plots is the removal of material from the beach face which precedes these periods of increased 3D morphological variability.

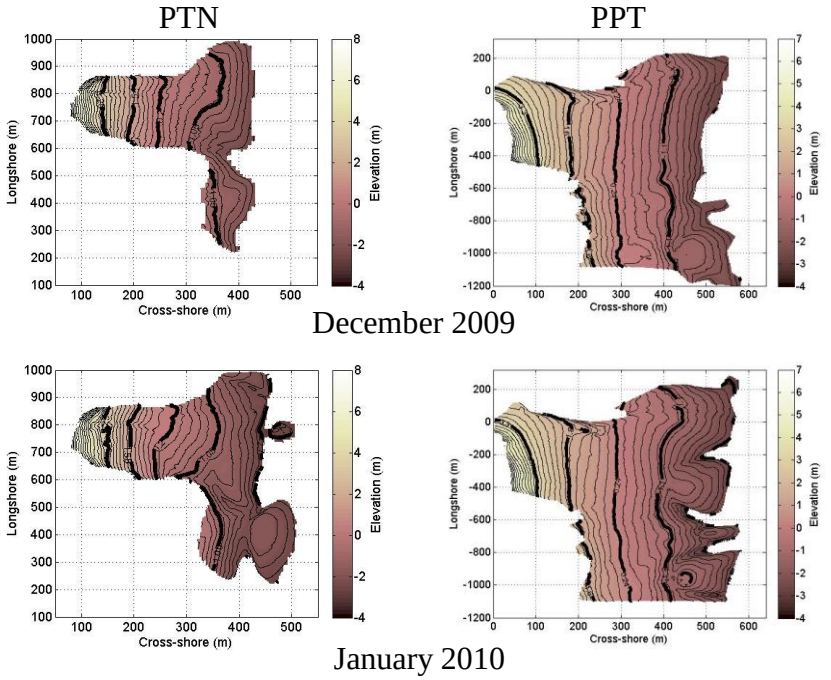

Fig 5. Surface elevation maps for PTN (left side) and PPT (right side) between December 2009 and January 2010.

Whilst monthly survey data clearly the seasonal shifts in beach dynamics, the temporal resolution is too coarse to identify patterns using monthly-weighted hydrodynamics. To identify a closer link between the dominant hydrodynamics and the beach response it is useful to examine some of the more defined periods of change identified in Figure 4. GWT has exhibited little evidence of sustained low tide bar/rip features, and CHP experiences significant fluctuation in survey area due to the size of the beach, this makes PTN and PPT best suited to analyse further as they exhibit similar response characteristics and consistent survey areas allows good comparisons to be made.

Figure 5 shows the extension of the low tide region at PTN and PPT between December 2009 (maximum erosion) and January 2010 (maximum 3D), which

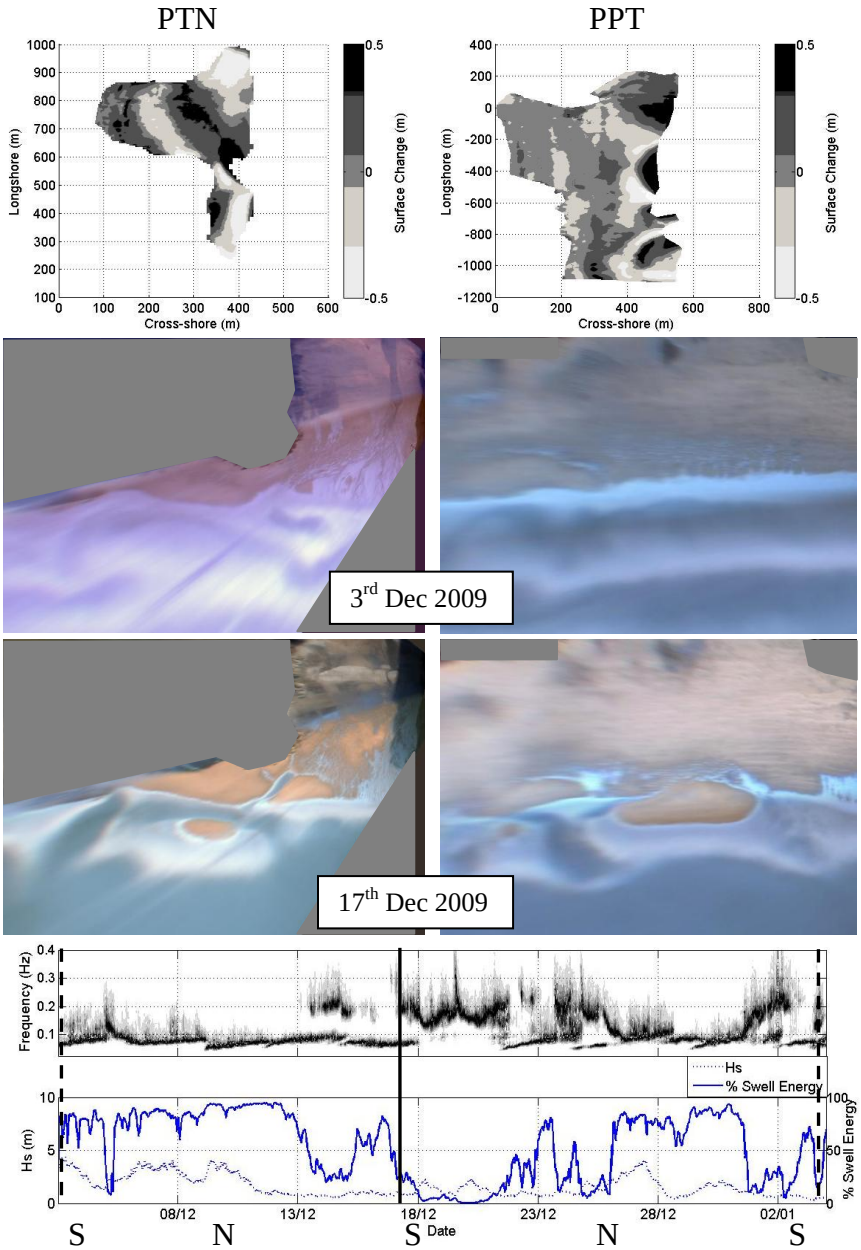

Fig 6. Summary plot for PTN (left side and PPT right side); from the top panel, surface plot showing beach elevation change between December 2009 and January 2010; ARGUS rectified images (grey patches indicate land/low quality); normalised frequency distribution during survey interval, H_s (dashed line) and percentage swell component (solid line). Dashed vertical line indicates survey dates, solid vertical line indicates bar exposure in ARGUS images, S/N show spring and neap tides.

was also evident at CHP (not shown). The surface elevation plots show the development of strongly 3D low tide morphology as nearshore bars evident offshore in ARGUS images become welded to the intertidal region. This transition follows the removal of beach material across the whole beach face for both sites, which took place between November and December 2009 (Figure 4c, box B).

Figure 6 demonstrates that the change in 3D morphology is due to a redistribution of sediment across the intertidal beach, on PTN (Figure 6a), two distinct zones of accretion and erosion in the upper and lower sections of the beach are evident. While on PPT (Figure 6b) there is limited evidence of upper beach accretion, yet the sediments at the lower beach were redistributed resulting in bar features. Figure 6e) shows wave forcing over the corresponding period and illustrates the dominance of long-period swell conditions during neap tides for the first part of the inter-survey periods, combined with large H_s. ARGUS images collected during spring tide conditions on the 17th December (vertical line in Figure 6e) show the lower bar-rip morphology already in place suggesting, little change occurred during the remaining two weeks when the wave spectrum appears more broad-banded.

Figure 7, box A, shows the significant removal which took place during energetic conditions between January and February 2009, which was followed by an increase in the low tide 3D. Again we see two distinct regions of erosion and accretion taking place at PTN, and clear redistribution of material in the lower region of the beach at PPT (Figure 7b).Throughout most of the interval between the January and February surveys the beaches experienced large swell dominated conditions resulting in the observed drop in volume (Figure 4c).

Discussion

The frequency and concurrence of highly 3D beach states is a function of all aspects of nearshore processes, including hydrodynamic forcing, sediment inputs to the system and the antecedent conditions. An attempt to link the morphological response to the variability and extent of these system drivers, whilst also incorporating the relative importance of each component over time provides a complex task. Although a simple approach to characterize the morphological state has been adopted the hydrodynamic conditions cannot be treated as such, which makes the interpretation of responsive periods more multifarious.

The nature and extent of the growth in bar features is dependent on the antecedent conditions, in particular the sub-tidal sediment supply which feeds the onshore movement of material. Through individual analysis, specific shifts

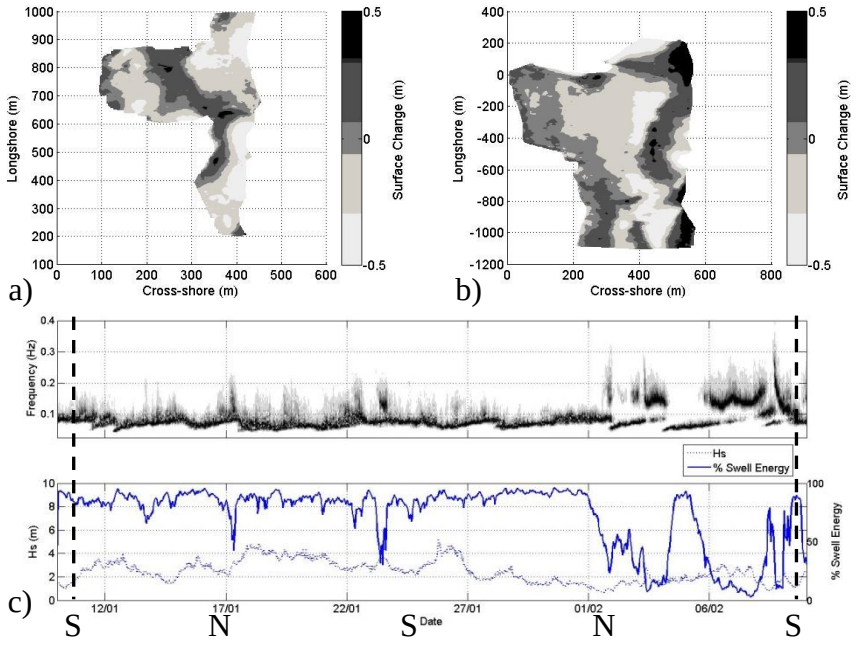

Fig 7. Surface plot showing beach elevation for a) PTN and b) PPT between January 2009 and February 2009, c) from the top, normalised frequency distribution during survey interval, H_s (dashed line) and percentage swell component (solid line). Dashed vertical line indicates survey dates, S/N show spring and neap tides.

in the morphology can be interpreted on a case-by-case basis. Using Figures 6 and 7 it is suggested that the development of low tide bar/rip morphology is dependent on removal of sediment providing a source within the nearshore sub-tidal region, supporting the accretionary cycle outlined by Wright and Short, (1984).

Large waves combined with neap tides ensure the breakpoint is situated just beyond MLWS, providing the perfect depositional source for onshore transport under reduced conditions. The data presented here supports this concept, with the initial driver coming from a significant period of increased conditions which acts to accelerate the offshore deposition. Under suitable wave conditions (low-energy swell) the development of defined bar/rip channels can occur within weeks of widespread sediment loss. Their stability is then determined by the dominant conditions, if swell conditions continue sustained onshore movement further combined with the macrotidal range acts to smooth out these features.

Conclusions

Monthly survey data from four high-energy macrotidal sites over 31 months have been presented. The temporal variability of the nearshore 3D bar/rip morphology is expressed using a simple curl value ($\overline{\overline{CV}}$) based on contour length which effectively identifies periods of increased low tide morphological variability, i.e. bar/rip channels. This approach allows the frequency and occurrence of these periods to be assessed and linked with the prevailing hydrodynamics, highlighting strongly 3D morphology during February 2009 and January 2010. These events can be broken down into 3 stages: (1) the onset of high-energy swell-dominated conditions which cause widespread erosion across the beach face as material is moved offshore; (2) a period of low-energy swell-dominated conditions which bring sediment back onshore; and (3) growth in 3D features around the low tide level as redistribution of nearshore sediment occurs.

Overall we conclude that the beach morphology exhibits seasonal variation to wave conditions while 3D periods are more event-driven. With just over 2 years of observations the dataset is only short term however it is intended further data will help develop our understanding of this complex system. Through developments in the application of ARGUS images it is hoped the temporal resolution of the 3D periods will be increased. In addition complexities in the nearshore sediment distributions will be further addressed, which form the key link to the onshore morphological variability.

References

Hansen, J.E. and Barnard, P.L., 2010. Sub-weekly to interannual variability of a high-energy shoreline. *Coastal Engineering*, 57(11-12), 959-972.

Holman, R.A. and Stanley, J., 2007. The history and technical capabilities of Argus. *Coastal Engineering*, 54(6-7), 477-491.

Jago, C.F. and Hardisty, J., 1984. Sedimentology and morphodynamics of a macrotidal beach, Pendine Sands, SW Wales. *Marine Geology*, 60(1-4), 123-154.

Masselink, G.,Auger, N.,Russell, P. and O'hare, T., 2007. Short-term morphological change and sediment dynamics in the intertidal zone of a macrotidal beach. *Sedimentology*, 54(1), 39-53.

Masselink, G. and Short, A., 1993. The effect of tide range on beach morphodynamics and morphology: A conceptual beach model.

Journal of Coastal Research, 9(3), 785-800.

Millar, D.L.,Smith, H.C.M. and Reeve, D.E., 2007. Modelling analysis of the sensitivity of shoreline change to a wave farm. *Ocean Engineering*, 34(5-6), 884-901.

Poate, T.G.,Kingston, K.S.,Masselink, G. and Russell, P., 2009. Response of high-energy, macrotidal beaches to seasonal changes in wave conditions: examples from North Cornwall, UK. CAR (ed.). *10th International Coastal Symposium*. (Lisbon, Portugal, Journal of Coastal Research, SI 56), pp. 747-751.

Ranasinghe, R.,Symonds, G.,Black, K. and Holman, R., 2004. Morphodynamics of intermediate beaches: a video imaging and numerical modelling study. *Coastal Engineering*, 51(7), 629-655.

Reichmüth, B. and Anthony, E.J., 2007. Tidal influence on the intertidal bar morphology of two contrasting macrotidal beaches. *Geomorphology*, 90(1-2), 101-114.

Ruggiero, P.,Kaminsky, G.M.,Gelfenbaum, G. and Voigt, B., 2005. Seasonal to Interannual Morphodynamics along a High-Energy Dissipative Littoral Cell. *Journal of Coastal Research*, 21(3), 553-578.

Scott, T.M.,Russell, P.E.,Masselink, G.,Wooler, A. and Short, A., 2007 Beach rescue statistics and their relation to nearshore morphology and hazards: a case study for south-west England. *9th International Coastal Symposium* (Gold Coast, Australia, CERF),

Wright, L.D. and Short, A.D., 1984. Morphodynamic variability of surf zones and beaches: A synthesis. *Marine Geology*, 56(1-4), 93-118.

Wright, L.D.,Short, A.D.,Boon I, J.D.,Hayden, B.,Kimball, S. and List, J.H., 1987. The morphodynamic effects of incident wave groupiness and tide range on an energetic beach. *Marine Geology*, 74(1-2), 1-20.

Wright, L.D.,Short, A.D. and Green, M.O., 1985. Short-term changes in the morphodynamic states of beaches and surf zones: An empirical predictive model. *Marine Geology*, 62(3-4), 339-364.

Journal of Coastal Research	SI 56	pg - pg	ICS2009 (Proceedings)	Portugal	ISSN

Response of high-energy, macrotidal beaches to seasonal changes in wave conditions: examples from North Cornwall, UK

T. Poate†, K. Kingston†, G. Masselink∞, and P. Russell†

†School of Ocean, Earth and Environmental Sciences, University of Plymouth, Plymouth, PL4 8AA, UK
Timothy.poate@plymouth.ac.uk

∞ School of Geography University of Plymouth PL4 8AA UK

ABSTRACT

T. Poate, K. Kingston, G. Masselink, and P. Russell., 2009. Response of high-energy, macrotidal beaches to seasonal changes in wave conditions: examples from North Cornwall, UK. Journal of Coastal Research, SI 56 (Proceedings of the 10th International Coastal Symposium), pg – pg. Lisbon, Portugal, ISBN

An experimental wave farm ('Wave Hub') will be installed 20 km off the north coast of Cornwall in 2010. To assess its potential impacts on the nearshore wave climate and beach morphology, an extensive beach monitoring programme has been established. This paper will discuss some preliminary results with specific emphasis on the seasonal morphological response. The North coast of Cornwall is exposed to spring tidal ranges of 5–6 m and a 10% exceedance significant wave height of over 3 m, producing a highly energetic environment. Described as intermediate-dissipative, the beaches exhibit boundary classification features with dominant low tide bar/rip morphology. The sensitivity of such beach types to small variations in seasonal wave conditions can lead to changes in the morphological response of these beach systems which has implications for beach safety during high visitor periods. Seasonal and storm-induced morphological responses are presented for four high-energy, macrotidal beaches. Monthly 3D beach morphology was mapped using differential GPS (DGPS), and supplemented at two sites using daily ARGUS video images. In addition, nearshore wave conditions and tidal data have been combined to provide comprehensive storm and sea-level analysis. Seasonal trends are evident for all sites with clear low water bar morphology dominant in early spring. During summer wave conditions, rip currents are prevalent within the defined bar features prior to onshore migration of bars produces 2D beach profiles with pronounced berm growth.

ADITIONAL INDEX WORDS: *Macrotidal, morphology, rip currents, bars, Cornwall*

INTRODUCTION

Most studies of nearshore morphodynamics have focused on micro-mesotidal environments over a range of spatial and temporal scales, fewer comparable studies exist for macrotidal settings (JAGO and HARDISTY, 1984; BATTIAU-QUENEY *et al.*, 2003; MASSELINK *et al.*, 2007; REICHMÜTH and ANTHONY, 2007), whilst long term research on high energy macrotidal coastlines are rarer still. The importance of short term beach response to hydrodynamic conditions is clear and such studies have done much to further our understanding of coastal processes and as such help advance model capabilities. There is, however, a growing need to be able to extend beyond monthly, seasonal and annual shoreline response, to be able to assess long terms shifts in climate variability and the impacts these have on the coastline.

Exposure to energetic wave conditions responsible for driving sediment transport results in rapid profile response seen most noticeably on micro-mesotidal beaches (KOMAR, 1998). The presence of a large tidal range forces the transitions of morphodynamic zones across the shore face resulting in morphological features being suppressed (SHORT, 1996). The complex dynamics exhibited through more subtle cross shore and longshore morphological change requires 3D analysis over a wide spatial extent to promote understanding of such systems as a whole.

The proposed development of an offshore wave farm (Wave Hub, www.wavehub.co.uk) has provided the opportunity for a long-term monitoring programme to be established to assess changes to the nearshore morphology resulting from any sheltering effects caused by the Wave Hub. The unique location, nature and timescale of this project allows for a thorough analysis of the present environment as well as subsequent changes observed. Model analysis of the impact on the local wave field suggests wave attenuation will decrease linearly with increased wave transmission, with a maximum reduction in wave height of < 5%, in the direct shadow of the Wave Hub, (MILLAR *et al.*, 2007). It is suggested little change in the wave period will occur, however no assessment of the energy distribution across the wave field is given.

This paper presents results from the first year of the monitoring programme which was designed to provide sufficient temporal and spatial resolution to assess the morphological response to a possible change in the local wave climate. To achieve this, four sites were identified with reference to MILLAR *et al.*, (2007), to be those expected to experience the greatest shadow effects caused by the Wave Hub installation.

Firstly, a brief overview of the sites and monitoring techniques are introduced before the methodology adopted for further analysis is presented. The paper then goes on to explore the annual conditions and the seasonal morphological response in both 2D profile evolution and 3D bar migration exhibited at the sites.

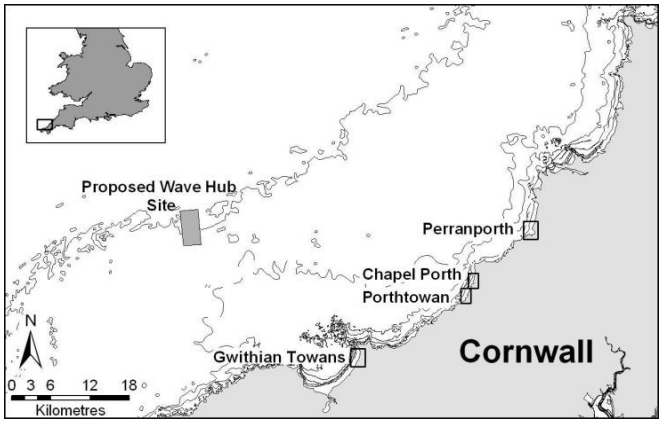

Figure 1. Map showing the location of proposed Wave Hub and the survey sites.

Site Description

The four sites shown in Figure 1 lie within a 23 km stretch along the North Cornish coast. This is a strongly macrotidal coastline (mean spring tidal range 6.1m) exposed to a highly energetic wave climate (mean offshore H_s 1.6m) of both local wind-generated seas and North Atlantic swell (DAVIDSON, 1997). Each of the beaches detailed below has an W-NW orientation ensuring they are exposed to the dominant wave approach.

Perranporth (PPT) forms the largest survey area with a cross shore intertidal region of 500m and a longshore extent of 1.2 km (the beach extends 3.5 km alongshore, exposed when the tide drops below mean sea level of 0.24m Ordnance Datum Newlyn). The wide highly dissipative beach has a low tide beach gradient of $\tan\beta\approx0.012$, composed of medium sand (D_{50}=0.35). Relatively featureless throughout the intertidal region, a well developed bar system interspaced with rip channels is exposed at spring low water (DAVIDSON, 1997).

To the south the two central sites, Chapel Porth (CHP) and Porthtowan (PTN) are in close proximity and connected at spring low tide forming a 1.6 km headland confined beach. Similar morphology is present at each site with steep cliffs flanking the relatively narrow upper beach, while the open lower beach (~75m cross shore by 400-600m longshore) exhibits strong bar/rip features (Figure 2). CHP and PTN are the smallest sites, yet exhibit the most dynamics in bar movement and profile shape. Sediment distribution across the lower slope ($\tan\beta\approx0.015$) consists of medium sand (D_{50}=0.38) whereas the upper beach ($\tan\beta\approx0.05$) shows a mix of gravel and sand with exposed boulders during periods of offshore sand movement.

Forming the northern extent of St Ives Bay, which extends for 5km at low tide, Gwithian Towans (GWT) consists of a wide sandy bay backed with ancient dune systems. The beach is ~700m longshore by ~350m cross shore with a gently sloping ($\tan\beta\approx0.013$) profile composed of well sorted medium sand (D_{50}=0.25). Similar to PPT, GWT reveals a relatively featureless intertidal region, however initial shallow bar formations are exposed at spring low water. The upper 75m of beach has a more pronounced profile shape ($\tan\beta\approx0.06$), with mixed sand and gravel often forming large cuspate berm morphology following periods of increased wave conditions.

METHODOLOGY

Wave and Tide Data

Wave climate data have been collected courtesy of the Channel Coastal Observatory (www.channelcoast.org) Datawell directional Waverider Mk-III buoy, which is deployed off Perranporth in ~10m Chart Datum (CD). The buoy was deployed in December 2006 and records for 30 minutes at 3.84 Hz, before transmitting at a reduced sampling frequency of 1.28 Hz to the shore station. Full wave statistics are available from the buoy. Tidal elevations prior to September 2008 have been generated using model predictions with a high level of accuracy (+/-0.2m). Self-logging RBR Ltd pressure recorders (TWR 2050) were installed in mid-September 2008 logging at 2 Hz with a 2-min averaging period every 15-min. Mounted at fixed locations at PPT and PTN these provide tidal information for all but spring low water when the instruments become exposed. Tidal harmonics are then used to infill missing data to provide a full tidal cycle.

Topographic Data

Topographic surveys have been undertaken using real time kinematic (RTK) global positioning system (GPS) at each site during the lowest spring tide each month. Where possible, specific storm events have been recorded to assess the recovery rate for the beaches; these comprise pre- and post-storm surveys at nominated sites. Surveys are conducted using an all terrain vehicle (ATV) with the RTK GPS receiver mounted on the front of the vehicle, allowing high resolution (5cm) rapid surveys to be completed. Survey areas naturally varied between sites from 400-500m in the cross shore to 800-1200m in the longshore. Where possible a regular grid of longshore and cross-shore lines at 5-15m spacing was sampled. Measuring at 5 Hz this technique allows reliable measurements to be taken at up to 10ms^{-1} (HAXEL and HOLMAN, 2004). The topographic data was transformed with rotation and translation onto a local coordinate system which was in common with the grid used by the video data.

Video Data

Effective use of video imaging of the nearshore can provide an additional tool to supplement the monthly topographic surveys. The following approach provides a cost effective method to evaluating the long term large scale changes in beach morphology (DAVIDSON, 1997).

At PTN an ARGUS system consisting of 4 cameras covering

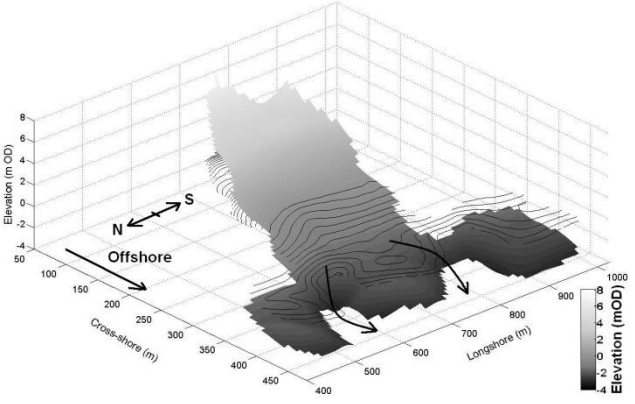

Figure 2. Surface morphology for 4th May 2008 at Porthtowan. Elevation is reference Ordnance Datum Newlyn. Dominant rip locations are indicated with arrows.

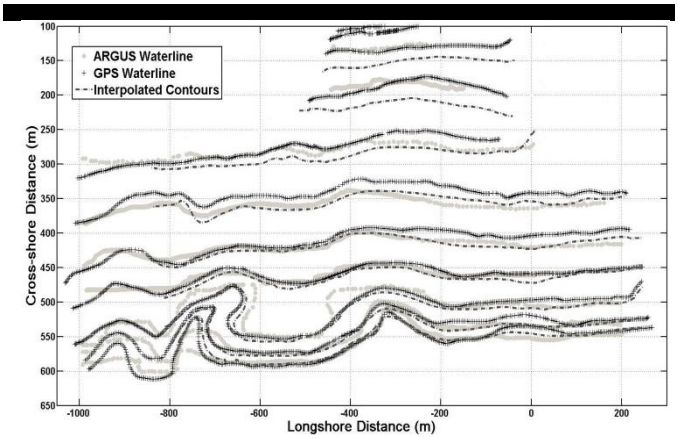

Figure 3. Comparison of automated and manual waterline detection using merged ARGUS images from Perranporth 17/09/2008, GPS waterlines recorded in situ and extracted contours of the same elevation from the interpolated surface generated from the full survey.

the full intertidal beach and offshore bar/rip system was installed in September 2008. An existing site at PPT (2 cameras) which was first established in 1993 (DAVIDSON, 1997), has been re-established following replacement cameras in 2006. Both sites provide half hourly digital "image products" consisting of a single snapshot image, a time-exposure image and a variance image (HOLMAN and STANLEY, 2007). Of principal interest for this study are the 10 min time exposure (timex) images which allow the identification of the waterline at the beach-face (PLANT and HOLMAN, 1997). Using local tide data these positions mark an approximate elevation contour which when combined can be used to determine the intertidal bathymetry, (PLANT and HOLMAN, 1997; MADSEN and PLANT, 2001).

The identification of the waterline can be done using various techniques (PLANT and HOLMAN, 1997). For PPT a combination of manual and automatic detection was employed, utilising variations in the colour criterion between wet and dry sand, as developed by AARNINKHOF *et al.*, (2003). This technique was found to be the most effective when applied during the flood tide to maximise the wet/dry difference. To increase the spatial extent of data across the wide intertidal zone, waterlines from 2 days of consistent wave conditions were used to map a single surface. Due to the exposure of bar features at spring low tide, video mapping was concentrated on these periods, providing bi-monthly surface plots.

To provide analysis and interpretation of the surface data over time both video-derived and GPS surface points were fixed to a grid in a local coordinate system. Interpolation of the gridded data was achieved using the Loess filter technique after PLANT *et al*., (2002), which provides various length scales and smoothing scales to be applied which allow sufficient resolution for the large scale 3D features to be mapped.

RESULTS

Methodology

The extraction of 2D cross sectional profiles of the beach surface provides an established means to identify nearshore bathymetric change. This paper is concerned with the large scale 3D morphological features which cannot be sufficiently tracked using such profiles (SEDRATI and ANTHONY, 2007), however, confidence in the ability of the survey technique to accurately represent 2D change is vital. To address potential errors caused by the interpolation technique, analysis of individual cross shore profile lines was undertaken for a 2D profile at PTN. Comparison was made of the surface profile extracted from the loess interpolation, the measured surface using the RTK GPS mounted on the ATV, and the profile measured on foot with a pole mounted RTK GPS. Vertical difference was found to range between 0.02-0.08m, with overall profile shape well reported. Variance of this extent was regarded to be sufficiently low to ensure confidence in the interpolation technique for further analysis.

The accuracy of ARGUS interpolated surfaces is reliant on tidal data and waterline position (DAVIDSON, 1997). Prior to September 2008, tidal information for PPT has been provided by a tidal model. Subsequent image analysis has been undertaken using tidal data obtained from the self-logging pressure sensors, which are also corrected for atmospheric pressure. The influence of run up and setup on the waterline positions was addressed by analysing days where the mean H_s was < 1m, thereby reducing the need for an offset to be applied. To assess the accuracy of the shoreline detection approach, and to identify the need for a horizontal offset, a comparison of waterlines picked from geo-rectified merged images and those measured using RTK GPS was undertaken (Figure 3). Using the extracted contours from the interpolated survey data we can also assess the ability of the technique to accurately represent the morphology compared to full-scale surveys. Of greatest interest to the present study is the level of consistency in contour lines at low water. Figure 3 shows that for the low tide region bar morphology is well represented. Moving up the beach greater variance between the methods is evident, although again the overall morphology is preserved.

Comparison of the interpolated 3D surfaces using ARGUS waterlines with a full RTK GPS survey, show a mean difference of 0.15m with a standard deviation of 0.16m. Whilst such variance is significant, the ability to represent the major morphological landforms is of greatest importance and evident in Figure 3. Therefore the application of ARGUS derived surfaces is restricted to large scale landform behaviour, not 2D profile extraction.

Morphology

Table 1 provides a synopsis of the wave conditions experienced between surveys, this shows an extended winter 2007/2008 with mean H_s for March above 2.0m following on from 2.3m for December 2007 and January 2008 (not shown). February showed a slight drop to 1.7m H_s down on 2.4m in 2007. Summer conditions during May-July remained below 1.2m H_s, before rising between 1.5-2.0m from August-November.

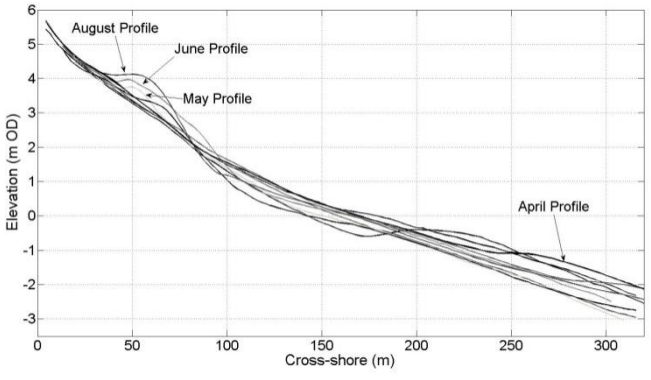

Figure 4. Typical profile shapes for Porthtowan, showing berm growth during summer conditions and bar presence in April.

Table 1: Wave climate with surface change as percent of beach area (shaded values indicate accretion is dominant).

	Wave Climate between surveys		Surface Accretion (% of area)			
	H_s (m)	T_p (sec)	PPT	PTN	CHP	GWT
Feb-Mar	1.77	11.83	**93**	**56**	42	1
Mar-Apr	2.06	12.73	**85**	12	12	**97**
Apr-May	1.27	10.54	17	42	**67**	**65**
May-June	0.72	10.12	**60**	**85**	**75**	**81**
June-July	1.32	9.96	**58**	23	**58**	**61**
July-Aug	1.11	9.38	**78**	**92**	**98**	**65**
Aug-Sep	1.61	8.14	**54**	**67**	15	32
Sep-Oct	1.44	9.65	36	45	**62**	**90**
Oct-Nov	2.05	10.23	42	**55**	36	28
Nov-Dec	1.99	10.68	**53**	27	29	27

In line with the annual wave conditions we can identify similar trends in the overall surface morphology. At the start of the survey period we see greatest contrast between the sites following a sustained month of increased wave conditions during March. Surveys at the start of April show extensive erosion across 88% of the survey areas at PTN and CHP (Table 1). Significantly 42% and 32% respectively of this was a difference of >0.5m. Conversely both PPT and GWT experienced widespread accretion during the same period, with 85% and 97% of the survey areas showing an increase in elevation. During May-July all the sites experienced levels of accretion taking place for more than 50% surface area. PTN is the only exception between June and July, with a marked drop over 77% of the surface, 11% of which was >0.5m.

Most pronounced profile response is evident at PTN. Figure 4 shows profiles for each survey which clearly displays berm growth during the summer months, in particular the calm conditions during May leading to 85% accretion across the beach, particularly in the formation of a defined berm. The drop shown between June and July represents a slight smoothing of the berm caused by an increase in wave conditions (1.32m). Long period (T_p) large wave conditions during the March survey prevented identification of bar formations at PTN, however the April surveys clearly show low water bar morphology which remain in May (Figure 2).

Figure 5 further builds on the 2D annual trends, showing a comparison of the seasonal 3D surface with the annual mean surface for PTN. Following the energetic winter conditions which produced surface elevations above the mean surface, removal takes place into the spring, although restrictions with the March survey limit the low water comparison. More clearly represented is the build up of sand during the summer conditions at the upper shore-face forming a pronounced berm. Less obvious are the defined bar features which are clear in Figure 2, although the shape of the beach surveys gives an indication of their prominence which is gradually smoothed over the summer months. As the autumn increase in mean H_s occurs we see a build up of sand in the lower shore-face and above the high water spring line (Figure 5), as bar systems become more defined and the berm is removed.

Similar trends in bar formation were also exhibited at CHP, although the nature of the site resulted in inconsistency in survey areas limiting further comparison. Bar movement at PPT is less defined; onshore migration of bar features is evident through the summer months, although the development of a berm feature is not apparent. GWT exhibited the least dynamic response in overall morphology with no distinct bar formations evident at the start of the survey period or throughout.

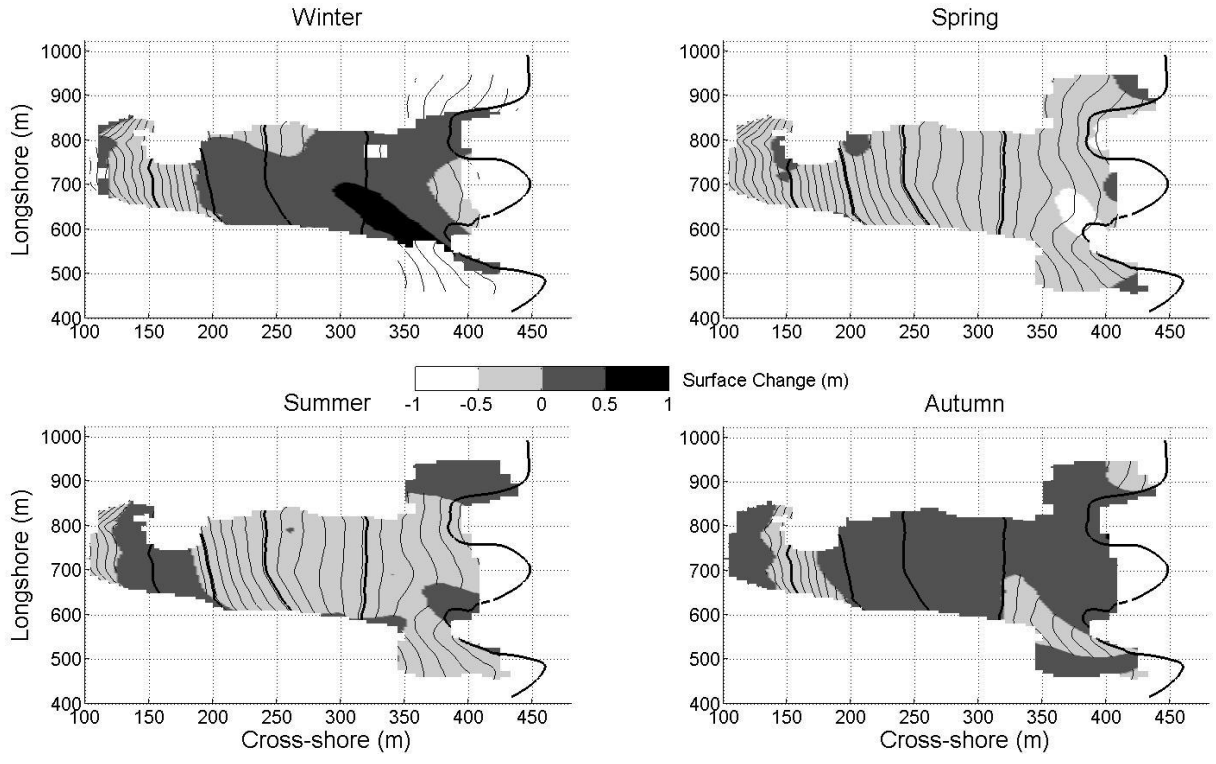

Figure 5. Morphology at PTN, showing difference between seasonal mean surface and annual mean surface (light contour lines). Dark shading reflects accretion above the annual mean, whereas light shading beneath the contours shows sediment removal. Contour lines in bold indicate High Water Springs, High Water Neaps, Mean Sea Level, Low Water Neaps and Low Water Springs.

DISCUSSION

The morphology witnessed at PTN follows a clear pattern in response to the seasonal change in wave climate. Winter bar features are maintained well into the start of May, despite substantial berm formation also evident. Sustained summer wave conditions gradually leads to smoothing of bar features and onshore migration resulting in increased accretion at the upper slope (KOMAR, 1998). Although further hydrodynamic measurements would be required it is suggested that the narrow low tide region which is backed by cliffs, experiences offshore directed flows which act to maintain the incised channels either side of the of the central bank (Figure 2). Whilst onshore transport occurs during sustained calm conditions the headland return flows help to maintain bar features throughout the year. The difference in response observed at PPT is representative of a more dissipative beach with a far greater intertidal region. Less confined and more widespread transient bar formation is evident. Although bar characteristics are less defined onshore migration during the summer period is also evident, however a corresponding berm feature is not present. With wave records obtained offshore at PPT the variation in wave conditions experienced at GWT (23 km to the south) is unclear. Nearshore bathymetry for the region (Figure 1) shows the extension of the depth contours extending out in the vicinity of St Ives Bay as well as rocky shallows which form Godrevy Point to the north.

The monthly surface change shown in Table 1 highlights the different nature and extent of response for each of the sites. PTN and CHP form the central sites closest to the intermediate/dissipative boundary classification and they also exhibit greater variability in the grain size composition than PPT and GWT. Although beyond the scope of the present paper such factors clearly require further investigation with regard to profile response and bar morphology.

CONCLUSION

Preliminary results from 11 months of monitoring have been presented from four macrotidal highly energetic beaches exposed to similar wave conditions. Ranging from highly dissipative to boundary dissipative/intermediate beach types, morphological response has been identified and is consistent with previous studies (MASSELINK *et al.*, 2006). The modulation in response identified at PPT and GWT reflects the wide intertidal region and extensive longshore sediment source, whereas the headland confined sites at PTN and CHP show far greater dynamics.

An effective methodology has been presented incorporating ARGUS imagery which allows the interpolation of beach contours from waterlines. Combined with monthly RTK GPS surveys the movement of large scale features is tracked during spring tidal cycles. Further ARGUS applications will include nearshore current studies to address the findings presented. The importance of 3D dynamics is clear, however the means by which observations are extrapolated into seasonal trends based on wave conditions is less defined. The dynamics of the low tide region and the ability to monitor this area requires further attention to better match the upper beach response. There are many aspects of this project which will benefit from an extended data series which will allow more in-depth statistical analysis and understanding to be made. Of principal interest is the application of recent ARGUS images at PTN, the need for improved wave transformation into GWT and more detailed spectral analysis with regard to nearshore bathymetry.

LITERATURE CITED

AARNINKHOF, S.G.J.; TURNER, I.L.; DRONKERS, T.D.T.; CALJOUW, M. and NIPIUS, L., 2003. A video-based technique for mapping intertidal beach bathymetry. *Coastal Engineering*, 49(4), 275-289.

BATTIAU-QUENEY, Y.; BILLET, J.F.; CHAVEROT, S. and LANOY-RATEL, P., 2003. Recent shoreline mobility and geomorphologic evolution of macrotidal sandy beaches in the north of France. *Marine Geology*, 194(1-2), 31-45.

DAVIDSON, M., HUNTLEY, D., HOLMAN, R., GEORGE, K., 1997. The Evaluation of Large-scale (km) Intertidal Beach Morphology on a Macrotidal Beach using Video Images. *Proceedings Coastal Dynamics '97,*, 385-394.

HAXEL, J.H. and HOLMAN, R.A., 2004. The sediment response of a dissipative beach to variations in wave climate. *Marine Geology*, 206(1-4), 73-99.

HOLMAN, R.A. and STANLEY, J., 2007. The history and technical capabilities of Argus. *Coastal Engineering*, 54(6-7), 477-491.

JAGO, C.F. and HARDISTY, J., 1984. Sedimentology and morphodynamics of a macrotidal beach, Pendine Sands, SW Wales. *Marine Geology*, 60(1-4), 123-154.

KOMAR, P.D., 1998. *Beach Processes and Sedimentation.* (2nd ed.) Prentice-Hall, Upper Saddle River, NJ, 544 p.

MADSEN, A.J. and PLANT, N.G., 2001. Intertidal beach slope predictions compared to field data. *Marine Geology*, 173(1-4), 121-139.

MASSELINK, G.; AUGER, N.; RUSSELL, P. and O'HARE, T., 2007. Short-term morphological change and sediment dynamics in the intertidal zone of a macrotidal beach. *Sedimentology*, 54(1), 39-53.

MASSELINK, G.; KROON, A. and DAVIDSON-ARNOTT, R.G.D., 2006. Morphodynamics of intertidal bars in wave-dominated coastal settings -- A review. *Geomorphology*, 73(1-2), 33-49.

MILLAR, D.L.; SMITH, H.C.M. and REEVE, D.E., 2007. Modelling analysis of the sensitivity of shoreline change to a wave farm. *Ocean Engineering*, 34(5-6), 884-901.

PLANT, N.G.; HOLLAND, K.T. and PULEO, J.A., 2002. Analysis of the scale of errors in nearshore bathymetric data. *Marine Geology*, 191(1-2), 71-86.

PLANT, N.G. and HOLMAN, R.A., 1997. Intertidal beach profile estimation using video images. *Marine Geology*, 140(1-2), 1-24.

REICHMÜTH, B. and ANTHONY, E.J., 2007. Tidal influence on the intertidal bar morphology of two contrasting macrotidal beaches. *Geomorphology*, 90(1-2), 101-114.

SEDRATI, M. and ANTHONY, E.J., 2007. Storm-generated morphological change and longshore sand transport in the intertidal zone of a multi-barred macrotidal beach. *Marine Geology*, 244(1-4), 209-229.

SHORT, A.D., 1996. The role of wave height, period, slope, tide range and embaymentisation in beach classifications: a review. *Revista Chilena de Historia Natural*, 69, 589-604.

ACKNOWLEDGEMENTS

The authors wish to acknowledge the South West Regional Development Agency and PRIMaRE for the funding and support to undertake this research. Further thanks go to Dr. Martin Austin for advice and comments as well as all field surveys and Peter Ganderton for the ARGUS Installations and field support.